Development of methods for modulating binding protein affinity

Reiersen, Herald

Award date:
2000

Awarding institution:
University of Bath

Development of Methods For Modulating Binding Protein Affinity

Submitted by Herald Reiersen

for the degree of

Doctor of Philosophy

Department of Biology and Biochemistry

University of Bath

March 25, 2000

ProQuest LLC
789 East Eisenhower Parkway
P.O. Box 1346
Ann Arbor, MI 48106-1346

Abstract

Development of Methods For Modulating Binding Protein Affinity.

Herald Reiersen

PhD Thesis

March 2000

Polymers (VPGVG)n of the elastic vascular wall protein, elastin, exhibit an inverse temperature transition where, as temperature rises, the polymer collapses from an extended chain to a β-spiral structure with three VPGVG units per turn, each pentamer adopting a type II β-turn conformation. Results obtained by thermodynamic fitting of circular dichroic (CD) spectroscopy melting data of short elastin peptides suggest that this conformational change is an intrinsic property of the individual pentameric sequences, rather than a global, co-operative effect of many pentamers within the β-spiral structure.

The effect of trifluoroethanol (TFE) on these peptides further supports a model in which TFE-micelles locally chaperone the folding by providing a mobile matrix for assisted non-polar side-chain side-chain interactions.

A short elastin sequence was also inserted into a globular protein in order to obtain a temperature responsive switch. The original type I β-turn of a two-helical minidomain version of the three helix staphylococcal Protein A domain, previously shown to retain the Fc binding properties of protein A, was replaced with a GVPGVG β-turn. These unstructured 'elastin mutants' exhibited a much lower stability than the wild-type domains. However, although the starting binding affinity towards Fc was lower than the wild-type, it exhibited a 21-fold improvement in affinity when the temperature was raised from 5° C to +37° C. The wild-type sequences lost their structure and/or binding affinity for Fc over the same temperature range. Analysis of the mutant minidomain structures by CD

suggests that the increased affinity was correlated with the formation of a temperature induced type I β-turn. In addition, the minidomain mutant exhibited similar behaviour in sodium sulphate to that exhibited in TFE and in response to temperature.

This demonstrates that when inserted into a stable globular protein, short elastin sequences have the ability to modify local structure, and activity, by operating as temperature modulated switches.

Some of the work described in the thesis has already been published, is under consideration, or being prepared for publication.

1. Reiersen, H., Rees, A. R., Korsnes, L. K. Allosteric antibodies. (1997) *International patent application* **PCT/GB98/02602.**

2. Reiersen, H., Clarke, A. R., & Rees, A. R (1998). Short Elastin-like Peptides Exhibit the Same Temperature-induced Structural Transitions as Elastin Polymers: Implications for Protein Engineering. *J. Mol. Biol.* ***283***, 255-264.

3. Reiersen, H., & Rees, A. R. (1999). An Engineered Minidomain Containing an Elastin Turn Exhibits a Reversible Temperature-induced IgG Binding. *Biochemistry 38(45)*, 14897-14905.

4. Reiersen, H., & Rees, A. R. (2000). Trifluoroethanol May Form a Mobile Matrix for Assisted Hydrophobic Interactions Between Peptide Side-chains. (to be submitted).

5. Reiersen, H. & Rees, A. R. (2000). Sodium Sulphate Refolds and Reactivates a Globular IgG-binding Minidomain With a Short Elastin Polymer β-turn. (to be submitted).

6. Reiersen, H. & Rees, A. R. (2000). The Hunchback and His Neighbours: Proline as an Environmental Modulator. (to be submitted).

Acknowledgements

I thank Professor Anthony R. Rees for his enthusiasm and interest in elastin which has given me three interesting years here in Bath leading to this PhD-thesis. I also thank Research Manager Lars Korsnes at Dynal A/S (Oslo, Norway) and Professor Florian Rüker at the University of Agricultural Sciences (Vienna, Austria) for good discussions. I am also grateful to Dr. Anthony R. Clarke at the Department of Biochemistry, School of Medical Sciences, University of Bristol, for introducing me to their Circular Dichroism-machine and fruitful discussions on thermodynamics. I further acknowledge the other members of Professor Rees', Dr. Cox's and Professor Rüker's laboratories for introducing me into various fields of molecular biology. I especially thank Dr. Pnina Dauber-Osguthorpe for revealing the art of molecular modelling and Dr. Stephen M. J. Searle for helping me with Unix. In addition, I was given a good hands-on introduction to solid phase peptide synthesis by Mrs. Sue Phillips and Dr. Richard Kinsman, and I also thank Mr. Chris Cryer for recording ESP/MS spectra and Dr. Graham Bloomberg at School of Medical Sciences, University of Bristol for amino acid analysis. Dr. Guiliano Siligardi at Kings College, London is acknowledged for help in reproducing some of the CD-spectra. The thermodynamic interpretation was further supported with helpful comments by Dr Alexei Finkelstein. I also gratefully acknowledge Mrs. A. K. Lindgaard and Mrs. H. T. Trømborg at Dynal Core Tech. R & D for start-up help with BIAcoreX^{TM} and BIAcore2000^{TM} measurements.

A very special thank you to my Margareth for supporting and giving me the chance to come to Bath to study for a PhD. I further apologise to my sons Oliver and Mathias for the extra hours spent in the laboratory, and to their Norwegian grandparents and family who wanted to see them more frequently. In addition, thank you to my friends Drs. Carl-Gunnar Fossdal, Pravin Sharma and Diep Dzung for an excellent time back in Norway discussing science, philosophy and chess.

This work was supported by grants from The Research Council of Norway (grant no. 110859/410) and DYNAL A/S, Oslo, Norway.

Abbreviations

AD	-	Alzheimer's disease
Boc	-	butyloxycarbonyl
BP	-	binding protein
BSE	-	bovine spongiform encephalopathy
CD34	-	cluster determining no. 34
CD	-	circular dichroism
CDR	-	complementarity determining region
CJD	-	Creutzfeldt-Jacob's disease
CM	-	carboxy methylated
CTD	-	C-terminal domain
DIEA	-	*N,N*-diisopropylethylamine
DMF	-	*N,N*-dimethylformamide
DNA	-	dioxyribonucleic acid
ds	-	double stranded
EDC	-	N-ethyl-N'-[(dimethylamino)propyl]carbodiimide
ESI	-	electrospray ionisation
ESI-MS	-	electrospray ionisation mass spectrometry
Fmoc	-	9-fluorenylmethyloxycarbonyl
Fn	-	fibronectin
gp	-	glycoprotein
GMP	-	good manufacturing practice
HA	-	hemaglutinin
HBS	-	hepes buffered saline
HD	-	Huntingtons's disease
HF	-	hydrogen fluoride
HFIP	-	hexafluoro-2-proanol or hexafluoro-iso-proanol
HIV	-	human immunodeficiency virus
H*iv*	-	S-α-hydroxyvaleric acid
HOBt	-	1-hydroxybenzotriazole hydrate
HPLC	-	high performance liquid chromatography

HPRG	-	histidine-proline-rich glycoprotein
HSA	-	human serum albumin
Hsp	-	heat shock protein
IFC	-	integrated μ-fluidic cartridge
Ig	-	immunoglobulin
LED	-	light-emitting diode
MDL	-	method definition language
MRE	-	mean residual ellipticity, $[\theta]_M$
MS	-	mass spectrometry
MW	-	molecular weight
NHS	-	N-Hydroxysuccinimide
NIPAA	-	N-isopropyl acrylamide
NMR	-	nuclear magnetic resonance
Opfp	-	pentafluorophenyl ester
ORD	-	optical rotary dispersion
P_I	-	polyproline I
P_{II}	-	polyproline II
P20	-	Polysorbate 20
PAGE	-	polyacrylamide gel electrophoresis
PAL	-	5-(4-aminomethyl-3,5-dimethoxyphenoxy)valeric acid
PEG	-	polyethylene glycol
Pfp	-	pentafluorophenyl
PHF	-	paired helical wound filament
Pol	-	polymerase
PS	-	polystyrene
RF	-	release factor
RNA	-	ribonucleic acid
RU	-	resonance unit
SDS	-	sodium dodecyl sulphate
SH	-	src homology
SpA	-	Staphylococcal protein A
SPPS	-	solid phase peptide synthesis

SPR	-	surface plasmon resonance
SPW	-	surface plasma wave
src	-	sarcoma
tBoc	-	*tert*-butyloxycarbonyl
TFII	-	transcription factor II
TFA	-	trifluoroacetic acid
TFE	-	trifluoroethanol
T_M	-	transition temperature midpoint.
TMAO	-	trimethylamine N-oxide
TNF	-	tumour necrosis factor
tof	-	time of flight
TRAP	-	thrombospondin-related anonymous protein
UV	-	ultraviolet

Contents

Part I - Theory and Background

Part II - Experimental section

B Herald Reiersen and Anthony Rees (1999) *An Engineered Minidomain Containing an Elastin Turn Exhibits a Reversible Temperature-induced IgG Binding. Biochemistry* **38**(45), 14897-14905

List of Figures

List of Tables

Part I

Theory and Background

NOTE: The following three chapters constitute a review of various aspects of the field and, in addition, contain some original ideas/hypotheses of the author.

Chapter 1. Introduction

1.1 Regulation of Protein Activity and Affinity.

Proteins are biological polymers synthesised by covalently linking amino acid monomers through peptide bonds. This primary structure is chosen from 21 different amino acid residues encoded by the gene, and it may also be post-translationally modified. The chemistry of each residue and its sequential context determine its position in the final folded three-dimensional structure of the protein. Noncovalent forces such as dispersion forces, electrostatic interactions, hydrogen bonds and hydrophobic effects determine and dictate folding towards the final structure of a protein. Each residue has a propensity for forming a certain secondary structure as helix, sheet or turn through its backbone interactions with other residues. However, in some cases the periodicity of polar/nonpolar residues within a specific secondary structure, rather then intra-residual propensity, is more important (Xiong *et al.*, 1995). This is seen in the mutant Arc repressor where a β-strand is transformed to an α-helix by slightly altering the residue periodicity involving just two residues (Cordes *et al.*, 1999). Other sequences, 'chameleons', may also adopt different secondary structures depending on neighbour residues even though they have the same primary structure (Mezei, 1998; Minor Jr. & Kim, 1996). A protein can also be transformed into a complete new fold by changing 50 % of its original sequence (Dalal *et al.*, 1997). In addition, the interfacial contacts within tertiary and quaternary structures, and the exact aqueous composition of the milieu may influence sequences towards a certain secondary structure preference.

The main active function of proteins, excluding those proteins not serve a structural or motor role in tissues or muscles, is to bind or chemically transform ligands such as proteins, DNA, RNA, sugars, lipids, metals, ions, gases, or other small molecules. Covalent or non-covalent interactions between ligands and a protein may be transient or permanent, and may be regulative or catalytic. Enzymes bind substrates and convert them to other molecules. The activity of

enzymes can also be positively and negatively regulated by binding of other ligands, either in the active site or at other sites. Inhibitors turn off activity, and bound cofactors such as metals help to stabilise the protein against degradation and to confer specific chemical activities. Regulation of affinity may often involve a conformational change in the target protein.

Engineering switches into the primary structure of a protein in order to turn its function on or off, is a challenging task. The ultimate goal of such studies should be to create a molecular switch which can respond to an external stimuli without reducing the overall activity of the protein. A specific and sensitive all-or-none switch-like behaviour in a small protein is more difficult to obtain relative to a smooth transition. Switch-like responses are ideally found in transitions which produce no intermediates (Ferrell, 1998). One way of changing the activity of a protein may be to insert a sequence which undergoes a large reversible plastic deformation (change of topology) in a protein upon a stimulus (Noguti & Gō, 1989a). There are several reports where proline-rich sequences are involved in large structural transitions, and these may offer an excellent tool to engineer transitions into proteins. Interspersed into a polypeptide chain, prolines give the chain a flexibility which minimises the energetic cost of folding into other structures (Frankel, 1992) and, due to the restricted conformations of the side-chain, proline-rich repeats can only adopt certain well defined helical structures.

1.2 The Structure and Conformations of Proline

If there is one single residue in proteins that is very different from all other amino acids, yet is very important in the binding and function of proteins, it is proline. It is frequently found in repeats responsible for such functions as muscle contraction and in signalling pathways. This small residue is unique in that its backbone resembles that of a hunchback, with its propyl side-chain binding back to the amide nitrogen forming a five-membered pyrrolidine ring - the only naturally found N-substituted residue. It is in fact this property that makes this residue suitable for binding to signalling domains such as the Src homology 3 (SH3) and WW domains (Nguyen *et al.*, 1998).

1.2.1 The Structure of Proline

The pyrrolidine ring of proline allows only a limited number of conformations for this residue. Its restricted torsion angle ϕ, for the N-C^{α} bond, varies little from about -63° while ψ , for the C^{α}-C bond, can vary between -35° (α region) and +150° (β region) (MacArthur & Thornton, 1991) (Figure 1.1).

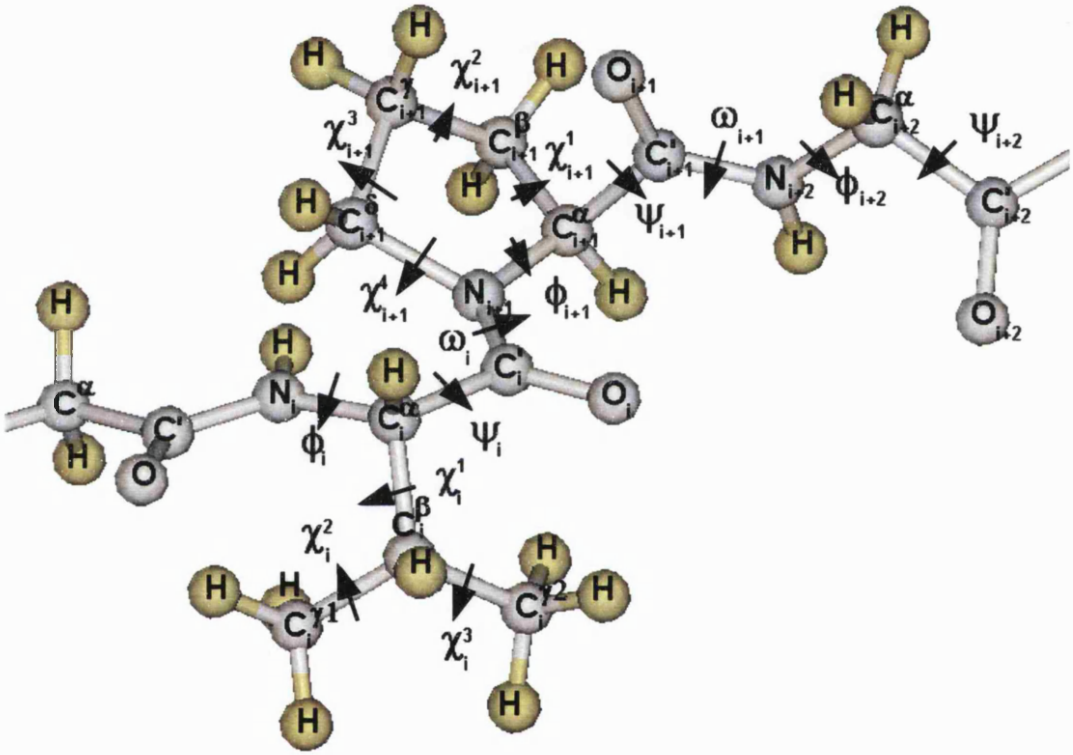

Figure 1.1 The Definition of Dihedral Angles of a Proline Sequence.

The figure shows the nomenclature of a proline residue in a valyl-prolyl-glycidyl sequence respectively denoted i to i+2. The torsion angles are: $\omega_i = 0$ for C^{α}_i - C'_i *cis* to N_{i+1}-C^{α}_{i+1};

$\Psi_i = 0$ for C^{α}_i - N_i *trans* to C'_i - O_i;

$\phi_i = 0$ for C^{α}_i - C'_i *trans* to N_i - H_i; (or *cis* to C'_{i-1} - N_i)

and $\chi^1_i = 0$ for C^{α}_i - N_i *cis* to C^{β}_i - C^{γ}_i (Creighton, 1984).

The arrows indicate rotation towards positive angles (clockwise rotation viewed from the N-terminal side of the bond).

The conformation of proline is largely determined by the preceding residue, X, in X-Pro. Where X is hydrophobic or X-Pro is a cis bond (dihedral angle ω (C_X-N_{Pro}) = 0°) the ψ-angle sits at ~ +150° (β-region). About 56 % of prolines are in the β-region. A similar shift in the dihedral angles has also been found for the X-Pro with a trans bond (ω = 180°) where the ϕ-angles becomes more negative (around -76° to -86°) and ψ has a more positive value in the α-region (+1°). These two states avoid the steric repulsion between H-C^{α}_X and C_{pro} and between C^{α}_X and O_{pro}, respectively. On average *cis* has a frequency of only 5-6 % relative to *trans* for X-Pro residues (MacArthur & Thornton, 1991). *Cis*-bonds are found more frequently in protein structures when X is an aromatic residue (Tyr, 10-19 %), and less frequently when X is a valine (around 2.7%) or other β-branched hydrophobic residues (MacArthur & Thornton, 1991; Reimer *et al.*, 1998). Proline also limits the conformational space (in ψ) for the residue X due to clashes between $^{\delta}CH_{2Pro}$ and C^{β}_X or NH_X. Thus X has a theoretical 90 % preference for the β-region, although surprisingly only 13 % of prolines are found in β-strands compared to 26 % in helices. Its imino acid cannot donate a H-bond and thus it is disfavoured in both α-helices and a β-strands. It is equally likely to be found within the first helix-turn or at the edge strands of a β-sheet (MacArthur & Thornton, 1991, and references herein).

1.2.2 Prolines in α-helices and β-sheets

The frequency with proline which occurs within α-helices argues that it cannot be a pure α-helix breaker. There is now evidence suggesting that C^{δ} atoms of prolines are involved as C^{δ}_i-H $\cdots$ $O_{i-3/i-4}$ hydrogen bond donors while the carbonyl oxygen of the preceding turn of the helix acts as an acceptor (Chakrabarti & Chakrabarti, 1998). Depending on where the acceptor is O_{i-3} or O_{i-4} it may respectively increase the kink of the helix from 13° to 25°. When prolines are in the middle of the helix sequence, the preceding residue is mainly hydrophobic (MacArthur & Thornton, 1991). This may help to stabilise the proline in the more favourable UP ring pucker conformation where C^{γ} protrudes from the

pyrrolidine ring plane *trans* to the carbonyl group (Chakrabarti & Chakrabarti, 1998). It remains to be tested if alternative H-bond patterns also exist for prolines inside β-sheets. If not, in addition to its α-helix favouring ϕ-angles, it may explain the higher frequency of prolines inside helices relative to β-strands. The α-helical structure of membrane peptides is unaffected by inserted prolines (Li *et al.*, 1996). In this context, the lowered dielectric inside membranes may stabilise the intrahelical C^{δ}_{Pro}-H $\cdots$ $O_{i-3/i-4}$ H-bond relative to water. By strategically inserting prolines into membrane helices it is now possible to modulate both their geometry, stability and activity (Nilsson & von Heijne, 1998; Zhang *et al.*, 1999).

In contrast, irrespective of the environment, prolines melt β-sheet structures (Li *et al.*, 1996). Interestingly, this has been demonstrated by incorporating prolines into Alzheimer's amyloid peptides having the effect of completely dissolving the insoluble β-sheet core of the fibrils and preventing further aggregation (Moriarty & Raleigh, 1999; Wood *et al.*, 1995).

1.2.3 Prolines in Turns

The frequency of prolines in loops, random-coils and turn-regions of proteins (61 %) is much higher than in helices and sheets (MacArthur & Thornton, 1991). There have been different classifications of β-turns which define a reversal of the polypeptide chain. The first β-turns (type I, I', II, II', III, and III') were identified in a tetra-peptide by Venkatachalam (1968) (Table 1.1). The type III/III' turns are a subgroup of type I/I' β-turns, and this group has been pooled with type I/II' turns (Richardson, 1981). A distance definition of turns (C^{α}_{i} - C^{α}_{i+4} less than 7Å) was made by Chou and Fasman (1977). However, the 1← 4 H-bond often found in β-turns between NH_{i+3} and O_i, is insufficient to define a β-turn (Chou & Fasman, 1977; Dyson *et al.*, 1988; Zimmerman & Scheraga, 1977). The latest classification by Hutchinson & Thornton (1994) now includes nine types of β-turns (I, I', II, II', VIa1, VIa2, VIb, VIII and IV) defined by a variation of ϕ and ψ dihedral angles, in which type IV is the most frequent (35 %). It is the type I or II turns (Table 1.1) that have a high proportion of prolines. Especially frequent in proline turns is the

Pro-Gly sequence (MacArthur & Thornton, 1991; Wilmot & Thornton, 1988). This dipeptide sequence has a 88 % preference for type II β-turns relative to type I turns and is very stable (Yang *et al.*, 1996).

Table 1.1. Comparison of Some Secondary Structure Elements Identified in Proteins.

	Backbone Dihedral Angle values (°)				
2° structure	ϕ_{i+1}	ψ_{i+1}	ϕ_{i+2}	ψ_{i+2}	Ramachandran nomenclatature[c]
β-sheet (P)	-119	+113	-119	+113	β_P
β-sheet (A)	-139	+135	-139	+135	β_A
α-helix (R)	-57	-47	-57	-47	α_R
α-helix (L)	+57	+47	+57	+47	α_L
3_{10}-helix (R)	-49	-26	-49	-26	3_{10}
Poly-L-Proline I (R)	-78	+149	-78	+149	P_I
Poly-L-Proline II (L)	-78	+149	-78	+149	P_{II}
Collagen (L)	-51	+153	-51	+153	C
Type I β-turn	-60 ± 30	-30 ± 30	-90 ± 30	0 ± 45[b]	$\alpha_R \rightarrow \alpha_R$
Type I' β-turn	+60 ± 30	+30 ± 30	+90 ± 30	0 ± 45[b]	$\alpha_L \rightarrow \gamma$
Type II β-turn	-60 ± 30	+120 ± 30	+80 ± 30	0 ± 45[b]	$\beta \rightarrow \alpha_L$
Type II' β-turn	+60 ± 30	-120 ± 30	-80 ± 30	0 ± 45[b]	$\varepsilon \rightarrow \alpha_R$
Type III β-turn	-60 ± 30	-30 ± 30	-60 ± 30	-30 ± 45[b]	$\alpha_R \rightarrow \alpha_R$

The data for helices and sheets are adapted from Creighton (1984) and for turns from Venkatachalam (1968). R = Right-handed; L = Left-handed; P = parallel; A = Anti-parallel. The right-handed poly-L-proline I has *cis* peptide bonds. [a]Wilmot and Thornton (1990) have found that ψ_{i+2}-values in β-turns vary more than the other dihedral angles. [c]Thornton *et al.* (1988).

Type II β-turns turns along with the N-terminal regions of helices are the most soluble segments of proteins (Robert & Ho, 1995), which is a little surprising for the PG sequence that is uncharged and not particularly hydrophilic. However, the ϕ-dihedral angle of proline restricts the number of turns that it can occupy. The

difference between β-turn I and II is a 180° flip between ψ_{i+1} and ϕ_{i+2} (Table 1.1), and the I' and II' represent the backbone mirror-image conformations of respectively I and II. The latter have a left-handed twist while type I' and II' conformations are right-hand twisted and are more likely to be found in the invariably right-hand twisted anti-parallel β-sheets (Mattos *et al.*, 1994; Sibanda & Thornton, 1985).

Sequences which include stacking of aromatic (X) and proline rings form a type VI turn and have a high proportion of the cis form (Yao *et al.*, 1994). By substituting proline with α-methylproline it was possible to stabilise a type I β-turn in a NPNA-motif, and the ψ-angles for the prolines were rather unrestricted (Nanzer *et al.*, 1997). That 58 % of β-turns have residues that participate in another β-turn (Hutchinson & Thornton, 1994) suggests that a switch between different types of β-turns may be possible, as was found from a 2.2 ns molecular dynamics simulation of a pentapeptide in water (Tobias *et al.*, 1991), or that they may be able to form larger super-secondary helical structures. The torsion angles for some of the secondary structures are not far away from β-turns. The 3_{10}-helix and the α-helix are very close in conformation to the type I β-turn, and the type III β-turn is in fact one turn of the 3_{10}-helix.

1.2.4 The Poly-L-Proline Helix and Other Proline-rich Helices.

The most frequent helical conformation associated with prolines is a left-handed poly-L-proline II helix (P_{II}, Table 1.1) and is very common in globular proteins (Adzhubei & Sternberg, 1993). It has about three residues per turn (n), typically $(Pro\text{-}X\text{-}X)_n$, as is illustrated by the collagen helix (n = -3.3). However, if the peptide group is in *cis*-confirmation it will form a poly-proline I helix which is right-handed (n = +3.0) with the side-chains pointing perpendicularly out from the P_{II}-helix. In proteins the helices are mostly located on the surface, stabilised by backbone hydrogen-bonding to water-molecules, and can bridge other helical regions (α-helices and 3_{10}-helices). The P_{II}-conformation has a geometry and flexibility of dihedral angles with no intramolecular H-bonds which easily allows

structural transitions into other 2° structures (Sreerama & Woody, 1999), and may explain why other unordered peptides tend to occupy this conformational space (Sreerama & Woody, 1994). Interestingly, the right-hand twisted anti-parallel β-sheet is geometrically related to left-handed polyproline II and collagen helices through carbonyl-carbonyl interactions (Maccallum *et al.*, 1995). The term β-helix according to Adzhubei & Sternberg's definitions covers both those with β-structure H-bonds (β-ladders) and those without this structure (unladdered β-helix) (Adzhubei & Sternberg, 1993). A small change in the ϕ,ψ-angles change from -75°,145° to -120°,135° can easily facilitate a transition from a P_{II} helix to a β-helix. There are many examples in nature where proline can occupy different helical structures, and proline is often repeated alone or in a context with other residues. These are reviewed in chapter 2.

1.3 Protein A

One of the cell surface proteins on the bacterium *Staphylococcus aureus,* Protein A (SpA), is an example of a tandem penta-repeat domain structure involved in binding of some classes of mammalian antibodies, especially IgG Fc (Richman *et al.*, 1982). Approximately one in three people have this bacterium in the nose and on the skin, causing acute infections and food poisoning when it is inappropriately translocated (e.g. in an open wound). The in vivo function of this 57 kDa surface membrane protein is still not understood although 95 % of bacteria from human isolates express SpA (Goward *et al.*, 1993). The homology between each of the five solvent-exposed ~58 residue repeats varies between 64 and 90 %, with each domain more similar to its neighbour than to distant domains (Nilsson *et al.*, 1987; Uhlén *et al.*, 1984). The designation of the repeats from the solvent exposed N-terminus is E, D, A, B, and C, based on the chronology of their discovery (Uhlén *et al.*, 1984). The spacer Xr region near the C-terminus and the cell-wall consists of octamer-repeats, while another part of this region (Xc) attaches the protein to the cell-wall (Guss *et al.*, 1984) (Figure 1.2).

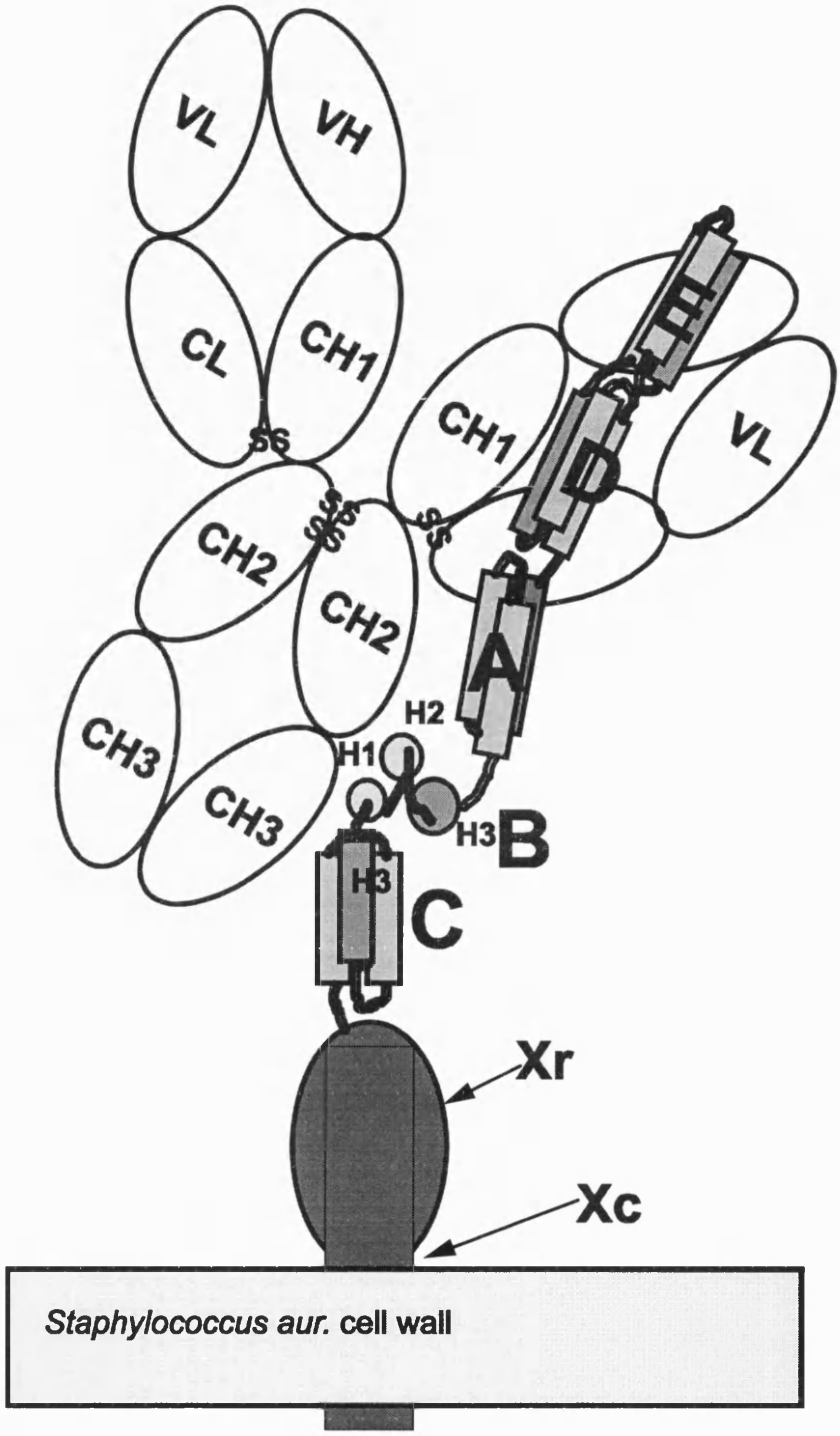

Figure 1.2 Schematic Representation of the Different Domains in Protein A on the Surface of *Staphylococcus aureus*.

The different domains E-D-A-B-C-X of the Protein A are shown and their interaction with an IgG molecule (Guss *et al.*, 1984; Uhlén *et al.*, 1984).

A number of NMR-structures of domains B and E and the synthetic Z-domain (designed for high-level protein expression, (Nilsson *et al.*, 1987)) have now verified that each repeat forms an antiparallel three-helix bundle (Figure 1.3) (Gouda *et al.*, 1992; Jendeberg *et al.*, 1996; Starovasnik *et al.*, 1996; Tashiro *et al.*, 1997; Tashiro & Montelione, 1995).

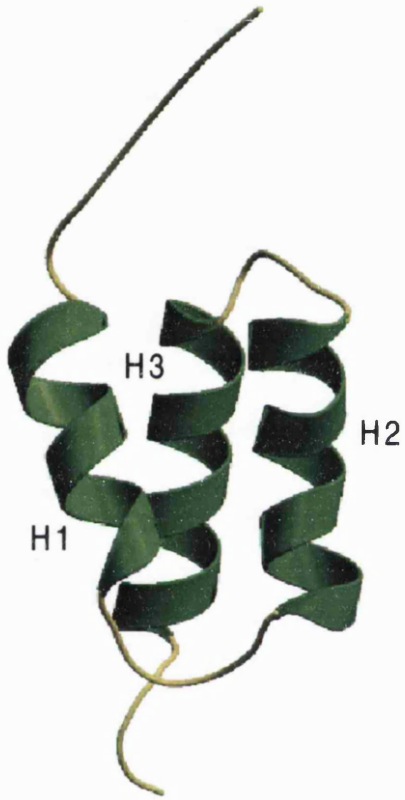

Figure 1.3 Energy Minimised and Averaged NMR-structure of the B-domain of Protein A.

The triple-helical structure of the B-domain is displayed (Gouda *et al.*, 1992). H1 is the N-terminal helix. Helices H2 and H3 are also shown. The structure 1BDD was displayed by MOLSCRIPT (Kraulis, 1991). The primary structure is ADNKFNKEQQNAFYEILHLPNLNEEQRNGFIQSLKDDPSQSANLLAEAKKLNDAQAPK (58 residues) with helices H1, H2 and H3 underlined.

Immobilised Protein A is a well-known method for purification of antibodies, such as IgGs from dog, pig, human and rabbit. The human subclasses IgG1, IgG2 and IgG4 bind strongly, while IgG3 does not bind at all. Likewise, the mouse

IgG2a and IgG2b bind well, but mouse IgG1 and IgG3 bind poorly (Hermanson *et al.*, 1992).

All of the protein A domains bind to human Fc of IgG and also to Fab with lower affinity (Jansson *et al.*, 1998; Moks *et al.*, 1986; Roben *et al.*, 1995). Although all domains can bind to Fc, there is only room for two IgG-molecules per five-domain Protein A (Langone *et al.*, 1978). The initial 2.8 Å resolution x-ray structure of the B-domain in complex with the Fc of IgG (Deisenhofer, 1981) suggested eleven residues on the two antiparallel SpA helices (helix 1, H1, and helix 2, H2) in the binding to Fc to the CH_2 and CH_3 domains (**H1**: F6, Q10, Q11, N12, F14, Y15, L18; **H2**: N29, I32, Q33 and K36). The x-ray structure, however, did not resolve the position of the third helix, later verified by NMR (Figure 1.4). Recent data from NMR hydrogen-deuterium exchange experiments of the binding of the B-domain to Fc has however revealed that only nine residues are responsible for binding: **H1:** F14, Y15, E16, L18 and H19, and **H2:** N29, Q33, L35 and K36 (Gouda *et al.*, 1998). Other data have also suggested that the packing of the three helices is unchanged upon binding to Fc (Gouda *et al.*, 1998; Tashiro *et al.*, 1997), and that the surface of the Z-domain engaged in binding involves the same residues as the B-domain (Cedergren *et al.*, 1993; Jendeberg *et al.*, 1995).

SpA binds to Fab of the V_H3 subfamily (human IgG, IgM, IgA and IgE). The D and E domains are important for the Fab-binding, although all of the domains bind more or less strongly to Fab. (Ibrahim, 1993; Jansson *et al.*, 1998; Ljungberg *et al.*, 1993; Roben *et al.*, 1995). There is a different binding-site on the D-domain of SpA for Fab relative to Fc-binding (Roben *et al.*, 1995). For the binding to Fab by the E-domain (to V_H only), it involves residues on the helix 2 and helix 3 face, which are negatively charged with a central hydrophobic patch. The Fc-binding, however, incorporates residues from helix 1 and helix 2 displaying a hydrophobic face with two positive charges (Starovasnik *et al.*, 1999). There may be several epitopes on human Fab of IgG1 (V_H3) that can bind to Protein A (Starovasnik *et al.*, 1999). Framework regions 1 and 3 and a sequence of CDR2 may be involved (Hillson *et al.*, 1993; Potter *et al.*, 1996; Randen *et al.*, 1993).

Figure 1.4 X-Ray Structure of the B-domain of Protein A in Complex with Fc of Human IgG. The 2.8 Å resolution x-ray structure of the B-domain in complex with the Fc of IgG (Deisenhofer, 1981) displays the two antiparallel SpA helices that bind to the Fc between CH_2 and CH_3 domains. Later the third helix in this domain (H3) has been solved by NMR which was not resolved in the X-ray structure (Gouda *et al.*, 1992; Jendeberg *et al.*, 1996; Starovasnik *et al.*, 1996; Tashiro *et al.*, 1997; Tashiro & Montelione, 1995). The MOLSCRIPT representation (Kraulis, 1991) is of structure 1FC2.

The stability of Protein A is exceptionally good. The Z-domain can be boiled without any loss of activity after cooling (Nord *et al.*, 1995 and reference therein). Previous attempts to minimise the three-helical domain in protein A to two helices have been made with a resulting loss of stability and affinity (Jansson *et al.*, 1989). Stabilising a minimised protein A as a fusion protein to a scFv lowered the affinity

by 10 to 100,000 fold, and revealed that the region corresponding to the helix 3 was very important to preserve affinity/stability (Huston, 1992). Recently, the Z-domain has been minimised to 34-38 residues retaining most of its affinity towards the Fc-portion of human IgG. Braisted & Wells (1996) removed the third helix by carrying out selective mutagenesis by phage display technology (Figure 1.5).

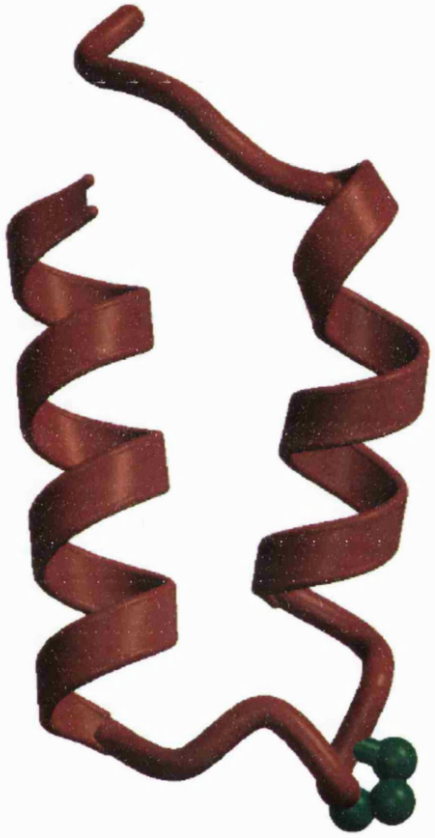

Figure 1.5 NMR Structure of a Minidomain Evolved from the B-domain of Protein A. The MOLSCRIPT structure (Kraulis, 1991) of 1ZDB displays an averaged and energy-minimised structure of the antiparallel 38-residue α-helical minidomain Z38 (Starovasnik *et al.*, 1997) evolved by phage display technology from the B-domain of protein A (Braisted & Wells, 1996). The proline-residue in the type I β-turn is shown in green. The primary structure is AVAQSFNMQQQRRFYEALHDPNLNEEQRNAKIKSIRDD, with helices underlined.

By displaying protein A on the coat protein gene III of the phage M13 (bacterial virus), the target sequence (59-residues = 177 nucleotides) is incorporated into the genome of the phage and will thus evolve in the bacteria (*E. coli* XL-1 Blue) over time. This allows for selection (panning) of binding to

human IgG1 from a very large library of phage. To remodel protein A, its DNA-sequence from the selected phages is selectively (or randomly) changed and reintroduced into the phage for further panning (Barbas III, 1995; Braisted & Wells, 1996). For remodelling protein A Braisted & Wells (1996) first changed the exposed hydrophobic residues in helix 1 and 2 that interact with the helix 3 (Leu-20 and Phe-31 were randomly reselected as Asp 20 and Lys-31). After panning for activity, a second round of random mutagenesis of five residues was performed on the best selectant from the first round in order to remove/repack the hydrophobic core between helix 1 and 2. The best candidate was further mutated to improve its IgG-binding. The correlation between structure and affinity was clearly seen since the α-helicity increased with increasing affinity. The new structure Z38 (38 residues) consisted only of two anti-parallel α-helices connected by a single type I β-turn (Starovasnik *et al.*, 1997). However, the initial structure was quite unstable so five residues were removed from the N-terminus of Z38 and a disulfide bond was introduced connecting the ends of both helices. This improved the affinity for human IgG1 from 185 nM for the open double helical form to 20 nM for the S-S linked helices, with an additional 40° C improvement in stability. The affinity for the S-S form is very close to the affinity of the Z-domain (15 nM) (Starovasnik *et al.*, 1997). The structure of the selected S-S minidomain (Z34C, 34 residues) is also similar to its mother helices 1 and 2 from the Z-domain (Figure 1.6). The residues on the B-domain previously found to be involved in Fc-binding are also quite conserved in the minidomains. They contain exactly the same residues on helix 1 suggested by Gouda *et al.* (1998) to participate in binding of the B-domain on the basis of NMR hydrogen-deuterium exchange experiments. However, on helix 2 there are the following mutations Q33K, L35I and K36R (Braisted & Wells, 1996) in which the mutation Q33K is more serious than the others.

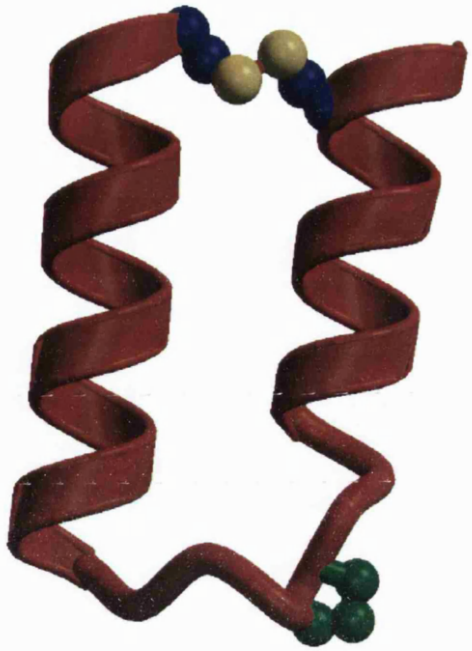

Figure 1.6 NMR Structure of a Disulphide Stabilised Minidomain Z34C Evolved From the B-domain of Protein A. The averaged and energy-minimised NMR structure, 1ZDD, is displayed in MOLSCRIPT (Kraulis, 1991). The two antiparallel α-helices in the minidomain are stabilised by a disulphide bond (Starovasnik *et al.*, 1997). The primary structure of 1ZDD (helices are underlined): FNMQCQRRFYEALHDPNLNEEQRNAKIKSIRDDC. The cysteines are labelled bold in text and blue/yellow in the figure.

Protein A is often used as an affinity-handle fusion protein in order to purify a target protein (Nilsson & Abrahmsén, 1990). There is currently no inexpensive, simple and gentle *in situ* method to purify isolated and unstable proteins, although competitive elution, lowering pH and adding salt or other chemicals may provide some solutions. The short two-helical minidomain by Braisted & Wells (1996) is an excellent model on which to base a re-design based on natural protein conformational switches found in some proteins. If successful, it should be possible to obtain a mutant protein which would provide an inexpensive and gentle elution procedure.

1.4 Solvent Induced Structural Transitions Within Proteins.

As a method of studying natural transitions within secondary structure elements in proteins, chemicals such as trifluoroethanol (TFE) and sodium dodecyl sulphate (SDS) have been used to promote or provoke formation of, or switches between, secondary structures. Typically, TFE induces α-helices while SDS induces β-sheet at non-micellar concentrations and α-helices at micellar concentrations (Sönnichsen *et al.*, 1992; Waterhous & Johnson, 1994). An investigation of an unordered peptide structure using these solvents may thus reveal hidden structural propensities. TFE has also been shown to modify an existing secondary structure in proteins (Jayaraman *et al.*, 1996; Narhi *et al.*, 1996a). Also polyols, alcohols, salts, sulphates or detergents have been shown to induce secondary structures (Bello, 1993; Lee *et al.*, 1993; Uversky *et al.*, 1998a; Wille *et al.*, 1996; Zhang *et al.*, 1995a). In the cells there is also a natural osmolyte, trimethylamine N-oxide (TMAO), that can restore the activity of some protein by dehydrating charged sites (Tseng *et al.*, 1999). This suggests that water may disrupt or prevent some natural structural transitions.

1.5 The Structure of Water in Protein Solvation.

Water plays an important role in specifying contacts between amino acid residues by reducing their mutual polar, ionic and H-bond interactions, and by promoting hydrophobic interactions proposed to be a driving force for the folding of proteins (Dill, 1990). Due to its two hydrogen-atoms and the two 'lone-pair' electrons on oxygen contributing to the dipole moment and the polarity (33 % ionic character), water can form H-bonds and electrostatic charge-dipole interactions. In bulk liquid at 25° C ninety percent of OH-groups are H-bonded, and each molecule has on average 3.45 H-bonds separated by a distance of 2.9 Å, though displacements are very rapid (pico-second) and random. Water can, in addition, form intermolecular structures such as ice and can also dissolve other polar and ionic molecules. The classic view is that charged groups are rapidly hydrated by water forming a hydration shell with 'structure' which largely reduces other charge-charge

interactions of the solvated molecule. These interactions are entropically driven due to the release of water-molecules at higher temperatures (Collins & Washabaugh, 1985; Creighton, 1984). An alternative explanation is that water molecules generate an osmotic barrier by entropically pushing water molecules back to interacting macromolecular surfaces preventing contact without involving structured water. The array of surface associated water molecules largely dictates if interacting surfaces are attractive or repulsive due to the dipole-dipole repulsions of the immobilised water molecules (Israelachvili & Wennerström, 1996).

There are many reports on structural ordered water or even clathrate structures around peptide groups. Some ice nucleator proteins and alcohols have a structure that orders water molecules on their surfaces and thus limits supercooling (Gavish *et al.*, 1990; Wolber & Warren, 1989). In addition, water structure on hydrophobic groups has been detected both by crystallography and by computer simulation. In the x-ray structure of crambin, pentagonal arrangements of water molecules on a leucine side-chain were detected. Pentagons are characteristic for clathrate structures of water with few higher polygon structures observed (Head-Gordon, 1995; Teeter, 1984). The cryogenic x-ray structure of β-trypsin has identified hydration water aggregates with tetragonal and pentagonal structures on hydrophobic residues (Nakasako, 1999). However, hydrophobic regions may also have water hexagons and larger polygons with reduced H-bonding back to bulk solvent (Head-Gordon, 1995). During a computer simulation of the peptide mellitin in water, clathrate-like hydration shells were detected on protruding convex hydrophobic surfaces while flat surfaces had more fluctuating structures (Cheng & Rossky, 1998). By a combination of small angle scattering measurements and molecular dynamics simulations a hydrophobic amino acid was found to affect the structure of several water layers (Pertsemlidis *et al.*, 1996, 1999). All these results suggest that water is somehow structured surrounding hydrophobic groups. The structures may however be a snapshot of a very mobile water layer. In addition water is involved in structural transitions in proteins.

1.6 The Role of Water in Transitions in Proteins.

Water molecules around hydrophobic groups in proteins are more structured than in the bulk phase and thus make an entropic contribution to the energy of folding or burial of these groups. There is also a substantial number of water molecules on these that are completely lost by heating or folding (Urry *et al.*, 1997). However, negative charged residues as Asp and Glu have a large population of surface water molecules relative to their surface areas (Kuhn *et al.*, 1993; Nakasako *et al.*, 1999), and they bind water stronger than the hydrophobic residues (Urry *et al.*, 1997). In addition, water molecules are particularly frequent at the N-termini of helices and in type II β-turns (Robert & Ho, 1995). It has been argued that type II β-turns may be found in a less-structured environment and the water thus contributes to their stabilisation. Thus, the 'affinity' of the different residues and sequences towards water molecules clearly dictates the folding and the final structure of the protein.

Some exposed and hydrophobically hydrated surface areas may induce cold denaturation of a protein. In these cases the water at lower temperatures destabilises the structure, and structure/activity is regained by heating (Antonino *et al.*, 1991). There are also some examples on proteins that have water molecules in their cavities, and the water molecules may be 'frozen' with a low entropy or they may be more disordered (Yu *et al.*, 1999; Zhang & Hermans, 1996). The entropic cost of burying a structural water molecule may be compensated by an increased flexibility (and destabilisation) of the protein (Fischer & Verma, 1999). However, the molten globule state, proposed to have an increased intramolecular solvation, surprisingly has near native structure solvation properties (Denisov *et al.*, 1999). The molten globule states with reduced or no tertiary contacts may be quite compact with respect to the diffusion of water. The mobility of the protein may also prevent water accessing the core, as was found for solvent shielding of the helix backbone by mobile hydrophobic residues (Luo & Baldwin, 1999).

On the other hand, surface water molecules have been proposed to form large extended H-bonded networks to stabilise proteins, either by bridging secondary structures (Nakasako, 1999), by linking subunits and the structure of the active centre of an enzyme (Nakasako *et al.*, 1999), or by bridging antigen bound

to antibody (Bhat *et al.*, 1994). From crystal structures it has also been shown that structural water can stabilise secondary structures such as α-helices and loops by cross-linking important H-bonds (Harpaz *et al.*, 1994; Nugent *et al.*, 1996). These proteins may be destabilised through perturbations of the water network.

In addition to providing both stabilising and destabilising interactions with proteins, water may participate in specific transitions between different secondary structures. It may promote the transition between type I β-turns and helices (Perczel *et al.*, 1992; Sundaralingam & Sekharudu, 1989) through external H-bonds to the backbone carbonyl and amide, or internal in an α-helix contributing to a bridging 5→1 H-bond. The three-centre H-bond structure (4→1 and 5→H_2O→1) involving water stabilises different types of β-turns (type I, II or III), and may fold into an 4→1 α-helix (stabilised by water) or to a 5→H_2O→1 open turn (β strand). Based on results from Raman spectroscopy at room temperature and the above findings, it has been proposed that water molecules may promote flickering transitions (on the picosecond time scale) between α-helices, β-structures and poly-L-proline II helices in unordered proteins and in loop-regions for molten globule-like proteins (Barron *et al.*, 1997). A similar water catalysed transition where parallel gramidicine dimers are redirected into anti-parallel orientation via destabilising an existing H-bond structure and reforming new H-bonds, has recently been proposed (Xu & Cross, 1999). There are also several examples where the binding and the release of water molecules induces or is a consequence of large conformational changes in a protein. For example, the release of about 20 water molecules promotes the formation of the photoactivated state of rhodopsin (Mitchell & Litman, 1999). Again, by manipulating the solvent conditions it is possible to refold poly(L-lysine) to either α-helix or to the less hydrated β-sheet (Chiou *et al.*, 1992).

1.7 Elastin, The Hydrophobic Muscle Motor.

As demonstrated in the previous section, water molecules bound to hydrophobic interfaces are structurally ordered. Transitions which involve melting of 'clathrate-like' water structures near hydrophobic groups can thus increase hydrophobic interactions and the entropy of bulk water. This is also proposed to be a driving force for protein function, assembly, stability and folding (Dill, 1990; Nakasako, 1999), and suggested by Urry (1988a, b, 1993, *et al.* 1997) to contribute to folding or conformational changes in elastin.

The elastin protein is found in different vertebrates although there is also some sequence similarity for mussel byssus (Coyne *et al.*, 1997). In mammals it is mainly found in the yellow connective tissue in lungs and walls of large blood vessels and especially in aorta where fibrous elastin forms 5-6 μm fibres of the precursor protein tropoelastin (Sandberg *et al.*, 1969; Smith *et al.*, 1968; Urry, 1984). It is an essential component of the arteries since mice that lack elastin die of obstructive arterial disease (Li *et al.*, 1998).

Elastin is composed of repeating hydrophobic monomers, the most frequent sequence being (VPGVG)n where n is as large as 50 in a single molecule (Sandberg *et al.*, 1985; Yeh *et al.*, 1987). Synthetic polymers of (VPGVG)n where n = 150 are soluble in water at all temperatures below 25° C, but above this temperature they undergo a phase transition to a viscoelastic state called coacervate, with 50 % water and 50 % peptide by mass (Urry, 1993). This transition is reversible and is dependent on protein concentration. The binding of water molecules to hydrophobic parts of the protein is an exothermic process (Blokzijl & Engberts, 1993; Privalov, 1992), and an increase in added heat above a certain transition temperature leads to a release of associated water and intensified intra- and intermolecular hydrophobic interactions. For elastin this added heat disrupts the elongated, less ordered hydrophobically hydrated structure, and the polymer contracts via an intramolecular process (Urry, 1993; Urry *et al.*, 1998). Several observations have verified that increased temperature induces an intramolecular structural transition.

The linear sequences (from a single peptide to polymers) and a cyclic conformation of three VPGVG repeats were studied by NMR or X-ray crystallography, and the conclusion from all these studies was the same. Each VPGVG-repeat forms a repetitive type II β-turn, which folds into a right-handed β-spiral with 2.7 to 2.8 VPGVG-repeats per turn and a translation of 3.2 to 3.5 Å per pentamer, or an axial rise of 9.45 Å per turn. Hydrogen bonds are only found within each turn ($Val_4NH \rightarrow Val_1CO$; $Val_1NH \rightarrow Val_4CO$ and a weaker $Gly_3NH \rightarrow Gly_5CO$) and not along the axis as described for other helices (e.g. α-helix), and the peptide bonds are all-*trans*. The latter hydrogen bond involving glycines has been described as a γ-turn as demonstrated in the hexapeptide VAPGVG (Khaled *et al.*, 1976; Renugopalakrishnan *et al.*, 1978a). Each turn also has paired valyl side chains with intramolecular and interturn hydrophobic associations that facilitate the folding and stabilisation of the structure, and additionally provide a lipophilic ridge along the water-filled β-spiral which can interact with other spirals. The diameter of each helix is 15-17 Å, and three β-spirals form a supersecondary intermolecular twisted filament, about 50 Å in diameter (Cook *et al.*, 1980; Long *et al.*, 1980; Ruben *et al.*, 1991; Urry, 1984; Urry & Long, 1976; Urry *et al.*, 1981, 1983; Venkatachalam & Urry, 1981; Volpin *et al.*, 1976; Wasserman & Salemme, 1990). From molecular dynamics studies of a 90-residue model segment of VPGVG-repeats it has been shown that by an extension to its low-temperature form, the diameter across the β-helix axis decreases to about 10-12 Å and the pitch increases from 8.7 to 15.2 Å (Figure 1.7). However, by raising temperature the β-helix contracts (up to 130 %) with an expansion of its helical diameter to 15-17 Å (Chang & Urry, 1988; Ruben *et al.*, 1991; Wasserman & Salemme, 1990).

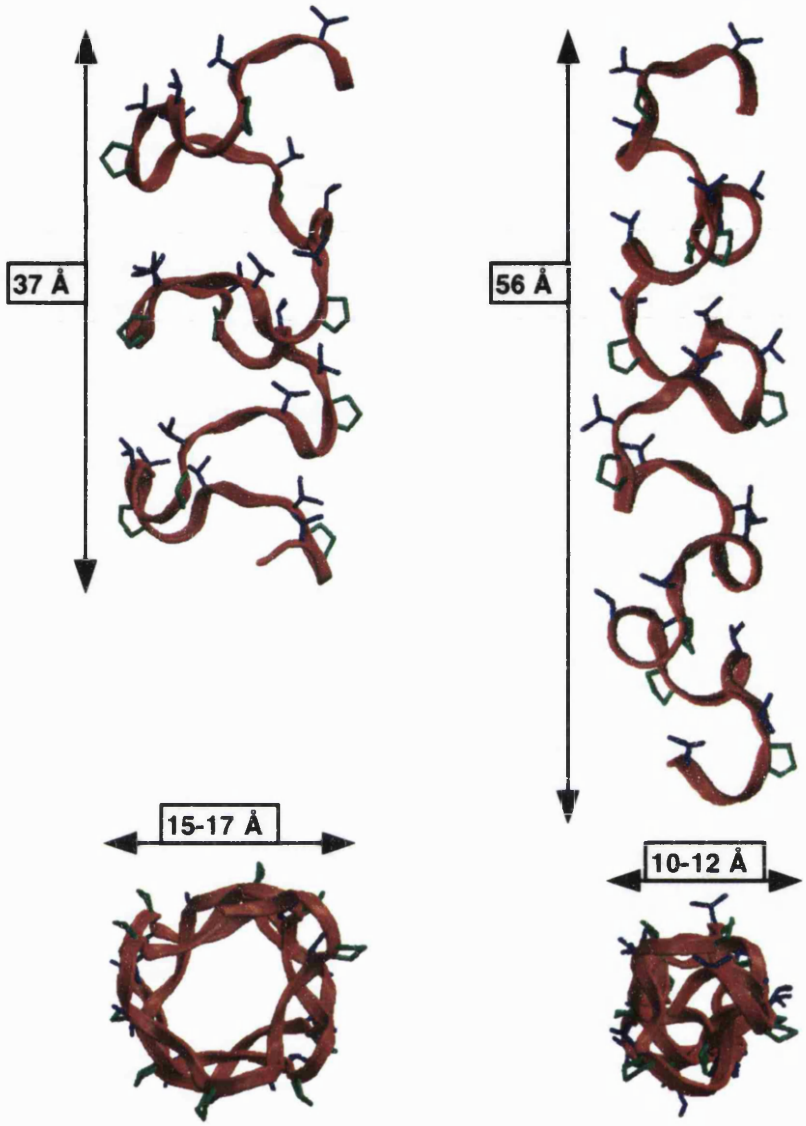

Figure 1.7 Molecular Models of a Short Elastin Pentamer Repeat Sequence.

A short VPGVG repeat helix was constructed based on the dihedral angles for the contracted (left-hand side) and expanded (right-hand side) forms of the peptide, extracted from the average Φ and Ψ angles in a published molecular dynamics simulation of $(VPGVG)_{18}$ in relaxed and stretched forms (Wasserman & Salemme, 1990). The MOLSCRIPT figures (Kraulis, 1991) display prolines in green while valines are in blue.

The energy that drives the reaction has been proposed to originate from either the solvent entropy (by libration of hydrophobically hydrated water molecules) or

from the reduction of librational entropy in each pentameric segment (Urry, 1984, 1988b). The latter model proposes that the Val^4-Gly^5-Val^1 segment of the contracted (relaxed) protein linking successive β-turns, exhibits low-frequency rocking motions. For the relaxed structure, a correlated counterrotation of ψ_i and ϕ_{i+1} dihedral angles (crank-like motion) across the central bonds of the VGV-segment was observed with large-amplitude torsional oscillating motions (Chang & Urry, 1988; Urry, 1988a,b; Wasserman & Salemme, 1990). By fixing all pentamers but one, the initially large RMS-variation of the dihedral angles of the VGV-segment, or the internal chain dynamics, is decreased upon stretching. Thus, the contraction of the polymer may be driven by librational entropy. However, the importance of hydrophobically hydrated water molecules in these transitions has also been stressed, and there is a good correlation between temperature for loss of these water molecules, residue hydrophobicity and transition temperature for the inverse folding (Urry *et al.*, 1997, 1998). It may well be that hydrophobic hydration is responsible for initiating and driving the folding of the β-helix, while the librational entropy dominates in later stages of the transition (Gosline, 1978; Gray *et al.*, 1973).

By varying amino acid composition, X, and content in the polymer (VPGXG)n, it is possible (theoretically) to manipulate the transition temperatures for reversible β-spiral folding from -130° C to +1000° C (extrapolated). These data also provide a hydrophobicity scale for all amino acid residues. Similar manipulations of transition temperature for folding can be obtained by reversible phosphorylation and other covalent modification, electrochemical or chemical reduction of a prosthetic group attached to the polymer, by changing solvent composition, increasing pressure, and by irradiating a chromophore (Urry, 1993). All of the manipulations will affect the water solvated structure of the polymer, and reversibly reduce its length by more than 50 per cent. The elastin polymer is capable of lifting a mass of more than 1000 times its dry mass, performing work and producing motion. The energy involved for a transition within one monomer, VPGVG, is reported to be around 2.0 kcal/mol (Chang & Urry, 1988).

The elastin sequences have excellent biocompatibility and cells do not bind to the elastin cross-linked matrix. Thus, it may be used to prevent post-operative adhesions, e.g. to artificial hearts. It is also a potential drug delivery and controlled

pesticide vehicle. Additionally, the polymer has been proposed to be a controllable docking site for enzymes, as a molecular energy transducer, or a superabsorbent (Urry, 1993; Urry *et al.*, 1993). The polymer can be cloned, expressed and harvested from *E. coli* cells or from tobacco plants. In *E. coli* it is expressed as a fusion protein to glutathione-S-transferase, or just as a large single polymer with up to 250 repeats of GVGVP (Guda *et al.*, 1995; McPherson *et al.*, 1992; McPherson *et al.*, 1996; Zhang *et al.*, 1995b). In these cases the purification is simple, based on successive heating/cooling cycles of the protein. A flanking elastin-like sequence has also recently been demonstrated as a tag for thermally-responsive purification of recombinant proteins (Meyer & Chilkoti, 1999).

1.8 Design and Production of Globular Proteins With Elastin Sequences.

Engineering switches into the primary structure of globular proteins is a challenging design goal in which sequences from the muscle polymer elastin may offer a novel way to modulate activity. De novo design of proteins have so far been tried on α-helix bundles, some β-sheet designs and on metalloproteins (Blundell, 1994; Bryson *et al.*, 1995; DeGrado *et al.*, 1999; Quinn *et al.*, 1994).. However, in order to design elastin sequences in the context of other structural elements such as helices and sheets, is also important to test whether single pentameric VPGVG repeats exhibit the same properties as a large elastomeric polymer. If this is the case, even very short sequences can be inserted into globular protein to modulate the structure. A very promising model system to test elastin β-turn sequences is a minidomain of Protein A of *Staphylococcus aureus,* which binds to the Fc-region of mammalian IgG. (Braisted & Wells, 1996). The structure consists of only two α-helices connected by a single type I β-turn, which can easily be replaced by an elastin turn. Previously, sequences up to 14 residues have been inserted into an enzyme without dramatically changing its function (Starzyk *et al.*, 1989), while an existing α-helix within T4 lysozyme was tandemly repeated, exhibiting just a extension of its original helical structure (Sagermann *et al.*, 1999).

However, the elastin sequence might very well adopt different structures as found for 'chameleon' sequences (Mezei, 1998; Minor Jr. & Kim, 1996), in order to repack some of its hydrophobic residues. Alternatively, larger elastin repeat sequences might be inserted into solvent exposed loops (El Hawrani *et al.*, 1994), for example inter-domain linking regions. The ultimate prize would be to construct a novel globular protein with a specified function which responds and folds into a desired structure at a specified temperature.

Chapter 2. The Hunchback and His Neighbours: Proline as an Environmental Modulator.

Proline as reviewed in chapter 1.2 has some special structural properties that influence the structure and stability of other neighbouring amino acid sequences. As already mentioned for elastin, it is very much responsible for the defined β-helical structure which leads to its remarkable biological properties (chapter 1.7). Here, its role in modulating the biological activity and affinity of other proteins when it is inserted into their sequences is discussed.

2.1 Proline as a Stress Modulator.

The amino acid has been reported to stabilise cells during intracellular or extracellular stress. Prolines improve the salt and freezing tolerance of *E.coli* when they are inserted as a short fusion linker, GPGPAGPGP, in the β-glucuronidase. It also increases the intracellular proline concentration and the expression yield of the enzyme *in vivo* (Bülow & Mosbach, 1991). An increased free proline accumulation has also been recorded on other external stress responses (e.g. temperature extremes, salinisation, metals toxicity, UV-irradiation, hyperosmosity and nutrient deficiency) in plants. However, bi-products during proline synthesis and degradation may be more important to counteract stress than increased proline concentration (Hare & Cress, 1997).

2.2 Prolines Affect Folding and Stability of Proteins.

Several observations on the effects of prolines on the stability and folding of proteins have been reported. The turns in proteins have been suggested to initiate protein folding (Perczel *et al.*, 1992; Rose, 1978; Zimmerman & Scheraga, 1977), and the eight prolines in the loops and turns connecting the β-sheets of the fibronectin type III module may very well be responsible for its very rapid

refolding relative to the generally observed slow formation of β-sheets influenced by its prolyl cis-trans isomerisation rate (Plaxco *et al.*, 1996, and references herein). However, *cis-trans* isomerisation of surface residues in a flexible loop, in contrast to more non-mobile regions, may not affect the overall stability and the folding kinetics of the protein (Ikura *et al.*, 1997). The unfavourable strain and isomerisation rate may sometimes be improved by replacing the prolines by other residues, or by adding neighbouring glycines (Ikura *et al.*, 1997; Nakamura *et al.*, 1997; Ueda *et al.*, 1993). There are several reports which describe increased thermostability of globular proteins by inserting prolines into the first turn of an α-helix, or into β-turn and loop regions (Bogin *et al.*, 1998; Nakamura *et al.*, 1997; Ueda *et al.*, 1993). For membrane proteins proline insertions even in the middle of the α-helix may improve their thermostability (Li *et al.*, 1996). Generally, replacing target residues by prolines, glycines with other residues, or deleting residues, lowers the conformational entropy for the unfolded protein and stabilises the folded state. In a comparative analysis the thermophilic proteins are generally found to be shorter than their mesophilic homologues, and with a higher frequency of deleted exposed loops (Thompson & Eisenberg, 1999, and references herein).

2.3 The Biological Role of Poly-L-Proline Helices.

An extensive review by Williamson has shown that several globular proteins, in addition to collagen, may carry a poly-L-proline II helix (chapter 1.2.4). In these cases the P_{II}-helix may function as a stiff 'sticky arm' which facilitates association with other proteins (Frankel, 1992; Schleif, 1999; Williamson, 1994). Sometimes the arm may be unordered with some flexibility and folds into a structure upon binding. For other proline-rich sequences they may even form a functional moiety, the entropic bristle domain - which is a time-averaged region for a flexible chain (Hoh, 1998).

There are important groups of signalling modules which bind proline-rich ligands adopting a P_{II}-conformation. The Src-homology-3 protein domains (SH3) bind proteins with a proline-rich sequence containing the consensus PXXP (Yu *et*

al., 1994), and the WW-domains likewise bind to PPXY sequences, where X is any amino acid and Y is Tyrosine (Macias *et al.*, 1996). The structures of two other proline-rich ligand binding modules profilin and EVH1, which are involved in regulation and dynamics of the cytoskeleton, have recently been solved (Fedorov *et al.*, 1999; Mahoney *et al.*, 1999). Both bind proline-rich sequences in a P_{II} helical conformation. Other proteins carrying proline-rich ligands for these ubiquitous binding domains are exemplified by the PPXY ligand for the WW domain. This has been found on Gag proteins of retroviruses which are important for virus assembly, on sodium channel proteins, interleukin receptors, formins (proteins associated with murine limb and kidney development) and on serine/threonine kinases (Einbond & Sudol, 1996). However, the WW-domain of the murine formin binding protein FBP21 which is a spliceosome-associated protein, binds to a proline, glycine and methionine rich motif, PXXGMXPP (Bedford *et al.*, 1998). Moreover, some WW-domains bind to proline-rich ligands containing phosphoserine or phosphothreonine preceding a proline residue (pSer-Pro or pThr-Pro). For these ligands phosphorylation may be an important on/off regulation of binding through reduced cis-trans isomerisation rate of pSer-Pro and pThr-Pro bonds (Lu *et al.*, 1999b). This may suggest a structural transition between Poly-L-Proline II and Poly-L-Proline I helices regulated by phosphorylation.

SH3 and WW are both small β-sheet modules, respectively about 70 and 38 residues (Macias *et al.*, 1996; Musacchio *et al.*, 1994). The proline ligand in the P_{II}-conformation interdigitates by van der Waals interactions with the aromatic residues in the binding pocket of these proteins, and at least for profilin, SH3 and ENV1 the ligand also associates through H-bonds with carbonyl oxygens and donor groups on the aromatic residues (Fedorov *et al.*, 1999). For SH3 and WW domains the $^{\delta}CH_2$-N group of proline is responsible for the specificity. The low affinity (K_d = 1-200 μM) relative to antibodies can be 100-fold improved by replacing prolines with other artificial N-substituted residues (Nguyen *et al.*, 1998). It may be expected that N-substitution on ligands can also affect other proline-rich ligand binding protein such as EVH1 and profilin (Fedorov *et al.*, 1999; Mahoney *et al.*, 1999). Williamson (1994) has suggested that the low affinity for interaction between proline rich repeat proteins and their ligands may

be compensated by having tandem repeats, i.e. by improving their 'avidity'. This is now illustrated for profilin which can bind very long repeat stretches of proline (10-15 residues) and having a submicromolar dissociation constant (Mahoney *et al.*, 1999). However, at least for the signalling domains the low affinity may also be important to bind multiple related ligands. Both SH3 domains and profilin can bind their ligand in two different backbone polarities which reflects the pseudo-two-fold symmetry for the P_{II} helices of these ligands (PXXP, P_{10}) (Feng *et al.*, 1994; Lim *et al.*, 1994; Mahoney *et al.*, 1999; Yu *et al.*, 1994). Moreover, that SH3 and WW modules can compete for their proline-rich ligands (Alexandropoulos *et al.*, 1995; Chan *et al.*, 1996; Chen & Sudol, 1995) may have a regulatory function, and by specifying flanking residues for these ligands the binding domains can increase their fidelity (Feng *et al.*, 1994; Lim *et al.*, 1994; Yu *et al.*, 1994).

The number of different signalling domains is steadily increasing - in 1997 it was more than 30 (Bork *et al.*, 1997). A recently example is the novel CD2 binding protein CD2BP2 which binds to two tandem repeats of the PPPPGHR sequence, separated by a SQAPSHR linker (Freund *et al.*, 1999; Nishizawa *et al.*, 1998). Its binding surface, the GYF domain, has a maximal length of about 25 Å. This suggests that the proline-rich ligand must accommodate a different conformation than a P_{II}-helix (Freund *et al.*, 1999). A positive identification of P_{II}-helices in globular proteins has however been found for the C-terminal fragments of histones (Makarov *et al.*, 1992), for the hydroxyproline-rich plant glycoproteins extensins, arabionogalactan-proteins and solaneous lectins (Sommer-Knudsen *et al.*, 1998), and for the a proline, serine and threonine-rich tandem repeat sequence of the human salivary mucin glycoprotein MG2 (Antonyraj *et al.*, 1998). By contrast, the proline, glutamine and glycine-rich tandem repeat from mouse salivary proline-rich protein MP5 had an unordered conformation (Murray & Williamson, 1994). Surprisingly, glycine is more destabilising in P_{II}-helices than in α-helices, β-ladders and 3_{10}-helices (Adzhubei & Sternberg, 1993). This argues that a large class of proline and glycine-rich repeats and without the $(PXX)_n$-repeat motif found in collagen, could be classified into other secondary structures.

2.4 Prolines Form Alternative Helical Structures.

There are several reports on different 2° structures formed by proline-rich repeats or sequences. Most of them have been found or proposed to form helical secondary structures in which 1 to 4 proline-repeats generate one turn of the helix. Recently, the NMR structure of a 22 residue peptide TPPI from the replication arrest protein Tus was solved in TFE. TPP1 is a penta-repeat sequence where a proline is either preceded or followed by a basic residue. Its structure is a left-handed helix with 5.56 residues per turn and a solvent accessible channel making it look like a pipe, hence the name: the proline pipe helix (Butcher *et al.*, 1996). This amphiphilic helix has intramolecular hydrogen bonds only on one side of the helix, which also has the shallowest pitch relative to the prolines and its neighbours on the opposite side. It may fit perfectly into the major groove of B-DNA with its basic residues facing the DNA backbone phosphate groups. The x-ray structure of the tus protein has now been solved. The corresponding TPPI peptide segment within its complex with DNA is surprisingly not helical but is composed of short β-stands separated by proline-initiated loops (Kamada *et al.*, 1996). This illustrates the importance of solvent conditions or the context of the local sequence on the global structure of short peptide sequences. However, it may also suggest that the tus protein undergoes large conformational changes upon binding to DNA (Kamada *et al.*, 1996), and that the TPPI-segment may have undergone changes also. Alternatively, it may be able to bind to other DNA-sequences by adopting a different (e.g. helical) fold.

The RNA polymerase II has a C-terminal domain (CTD) which is a tandem repeat of the proline-rich sequence (SPTSPSY)n, where n = 17-52, depending on the organism. The CTD is essential for cellular functions such as transcription and splicing (Corden & Patturajan, 1997). Hyperphosphorylation of CTD switches the polymerase from PolIIA to PolIIO and may be essential for the polymerase to start transcription and for an efficient elongation. In addition, it is a signal for ubiquitination of the RNA polymerase II large subunit (Mitsui & Sharp, 1999). There are many CTD-associated proteins that has been discovered which include a cis-trans peptidyl-prolyl isomerase that may modulate the structure of the CTD (Corden & Patturajan, 1997). Phosphorylation of serines at the proposed SPTS

and SPSY turns (Cagas & Corden, 1995) may change the cis-trans isomerisation status to facilitate a transition to a more extended P_I or P_{II} helical conformation (Zhang & Corden, 1991). As far as the author knows the exact structure of the CTD of RNA polymerase II has still not been solved, although its domain was identified as a conformationally mobile region by electron crystallography (Meredith *et al.*, 1996). However, there are several models based on NMR and CD data which have been proposed. Cagas & Corden (1995) have suggested that the eight proline-rich heptamer repeats form a right-handed β-spiral (Urry, 1993), and that each repeat folds independently of the others. The spiral has a diameter of about 9Å with proposed recurring type I β-turns for the SPTS and SPSY regions. Nishi *et al.* (1995) have, alternatively, proposed a β-helix which is left handed. It was also possible to stabilise the repeats into overlapping type II β-turns by replacing serine and threonine in the PS and PT turns with glycines or D-alanine (Dobbins *et al.*, 1996). Glycosylation of the threonine in a short peptide covering one of the tandem repeats also induced a turn-like structure (Simanek *et al.*, 1998).

A similar proline motif has been recognised in the transcription factor from the *Drosophila K10* gene product which contains the octapeptide, SPNQQQHP, repeated eight times (Suzuki *et al.*, 1994). The 'SPXX' motif also has a strong tendency to form a turn involving the side-chain of serine (Suzuki & Yagi, 1991), and in addition to its occurrence in the CTD of RNA-polymerase II, it is also found as a DNA binding motif in histones (Suzuki, 1989).

Models based on energy minimisation of different proline rich tandem repeats from rhodopsin, synaptophysin, synexin, gliadin, hordein, gluten and RNA polymerase II have been suggested by Matsushima *et al.* (1990). The tandem repeats vary from 5-9 residues, and it is suggested that they all form β-turn helices with about three repeats per turn (15-27 residues). In this system the helix model for RNA polymerase II was very different from the model by Cagas & Corden (1995). However, there are several observations that support the view that some proline-rich sequences or tandem repeats form helical structures other than the poly-L-proline type.

The elasticity of the wheat gluten protein, glutenin, is responsible for the bouncy viscoelasticy of kneaded dough during bread-baking (Wrigley, 1996). The central elastic glutenin repeat domain consists of $(PGQGQQ)_n$,

$(GYYPTSP/LQQ)_n$ and $(GQQ)_n$. Scanning tunnelling microscopy of the wheat gluten protein reveals that it forms a spiral supersecondary structure with β-turns (Miles *et al.*, 1991). The prolamin storage protein from hordeins of barley has similar tri-, hexa- and nonapeptide repeats as found in glutenin, and a representative peptide (TTVSPHQGQQTTVSPHQG) displays a type I/III β-turn CD spectrum in 90 % TFE (Halford *et al.*, 1992).

The longest single-chain polypeptide reported (about 27,000 residues) is the muscle sarcomere protein called titin or connectin (Labeit & Kolmerer, 1995; Maruyama, 1997). It consists of tandem repeat domains of fibronectin-III (FnIII), immunoglobulin (Ig) regions and elastic PEVK-domains rich in prolines, glutamates, valines and lysines. The elasticity of titin, in relaxed striated muscle, derives from the entropy of unfolding of the β-strands in Ig and FnIII modules and from extension of the PEVK region. The latter may involve both entropic and enthalpic processes (Linke *et al.*, 1996, 1998; Tskhovrebova *et al.*, 1997). It has also been suggested that the PEVK repeats may fold into a large cylindrical structure with a diameter corresponding to the Ig flanking regions (Linke *et al.*, 1996; Nave *et al.*, 1989).

Another muscle protein with proline-rich repeats is elastin. This viscoelastic protein is found in vascular cell walls and several repeating sequences have been described for the elastin precursor protein, tropoelastin. The most frequent repeat (up to 50 times) is the pentapeptide VPGVG (Sandberg *et al.*, 1985; Yeh *et al.*, 1987). The polymer contracts by increasing temperature to an ordered right-handed β-spiral with about three VPGVG units, each forming a type II β-turn, per turn of the spiral (Urry, 1988a,b). By contraction, the diameter of the spiral is increasing from 12Å to 16Å while its length is 55 % shorter (Ruben *et al.*, 1991; Wasserman & Salemme, 1990). The spiral has a pitch about 10Å per turn with all-trans peptide bonds (Wasserman & Salemme, 1990). The driving force for this inverse temperature induced transition is a dehydration of hydrophobic valines side-chains which is entropically driven (Chapter 1.7).

The spider dragline silk has proline, glycine and glutamine rich repeats (GPGGQGPYGPG)n, (GGYGPGS)n and (GPGQQ)n, where n = 1 to 8. It is stiff, strong and tough to break, and it may well form complex helical secondary structures (Guerette *et al.*, 1996). The collagen from mussel byssus have flanking

sequence motifs with resemblance to both elastin and spider dragline silk. It is composed of bulky hydrophobic residues along with proline and glycine, and contains the repeat motif (XXXPG)n, where n is between 6-12 (Coyne *et al.*, 1997).

2.5 The Pathology of Prolines.

Proline repeats or stretches are also found in proteins associated with diseases such as Alzheimer's disease (AD), Huntington's disease (HD) and Creutzfeldt-Jacob's disease (CJD) in humans. Alzheimer's disease is progressive towards neuronal and glia alteration, synaptic loss and dementia (Selkoe, 1999). Polymerisation and deposition of the 40-residue β-peptide Aβ into a β-sheet fibril structure, is important for the pathogenesis of AD. Neurofibrillary tangles of paired, helically wound filaments (PHF, about 10 nm) are found in Alzheimer's brain, and with tau, a microtubule associated protein, as a subunit. Tau is normally a very soluble cytoplasmic protein, but in PHF it is hyperphosphorylated, long, stiff, inactive and insoluble (Hagestedt *et al.*, 1989; Selkoe, 1999). The hydrophilic tau proteins are proline and glycine-rich forming a triple-stranded left-helical superhelix $(tau)_3$ with a diameter about 20 Å (each chain about 10 Å), and can stretch and contract by more than 300 % with very little 2° structure (Lichtenberg *et al.*, 1988; Ruben *et al.*, 1991). However, hyperphosphorylated tau may exhibit an extended left-handed poly-L-proline helical structure (Uversky *et al.*, 1998b). Recently, a prolyl isomerase, Pin1, has been shown to restore the function of hyperphosphorylated tau so that it can bind microtubules *in vitro,* suggesting that depletion of Pin1 to tau in PHF may contribute to neuronal death (Lu *et al.*, 1999a). Again, it is the pS/T sites preceding prolines that are the substrate. On the other hand, the natural occurring osmolyte trimethylamine N-oxide (TMAO) has also been shown to restore the activity of hyperphosphorylated tau without involving cis-trans isomerisation, suggesting that dehydration of charged sites restores it function (Tseng *et al.*, 1999). This is well correlated with the observations that tau undergoes an inverse temperature transition as elastin does. (Ruben *et al.*, 1991; Urry, 1988a,b). For elastin it is the dehydration of

hydrophobic groups that drives the reaction. For tau it is probably the dehydration of charged groups that restores (and refolds) it.

Huntington's disease is another neurodegenerative disease that involves repeat structures in the protein huntingtin. The expansion of glutamine-repeats initiates the pathology involving precipitation of huntingtin as insoluble fibres in the brain (Perutz, 1999). There is a 50-residue long proline-rich region (with stretches of proline-repeats) just after the glutamine repeat in hungtintin with unknown function (MacDonald *et al.*, 1993), and this region may very well affect the secondary structure of the glutamine repeats.

Mutant cell surface prion proteins are implicated in several neurodegenerative diseases such Creutzfeldt-Jacob disease (CJD), scrapie and bovine spongiform encephalopathy (BSE, 'mad cow disease'). Although little is known about the function of normal prions, the are nevertheless important for normal cellular development (Kuwahara *et al.*, 1999). In contrast to Alzheimer's disease, the prion diseases can either be inherited within the species or be transmitted across the species barrier. The conformational change that transform the ~ 250 residue wild-type cellular prions, PrP^{C}, to the disease-causing isoform, PrP^{Sc}, is either caused by a somatic mutation (for inherited diseases) or by replication by a transmissible form (Cohen & Prusiner, 1998). There is a structural change from α-helices (PrP^{C}) to β-sheets (PrP^{Sc}) which further aggregate into rod-shaped molecules and initiate the pathogenesis of prion-diseases.

Recently, the 48-residue N-terminal repeat of prions has been suggested to play a part in both the function of the wild-type prion and in the onset of the aggregation (Brown *et al.*, 1997; Liu & Lindquist, 1999; Marcotte & Eisenberg, 1999; Prince & Gunson, 1998; Stöckel *et al.*, 1998; Viles *et al.*, 1999). (The C-terminal end of prions is attached to membrane by a glycoinositol phopholipid (GPI) anchor (Cohen & Prusiner, 1998)). Mammalian prions have a very conserved octamer PHGGGWGQ repeated 6 times while avian prions have a hexamer N/QPGYPH repeated 6-9 times (Wopfner *et al.*, 1999). In yeast [PSI^{+}]-cells the translation release factor subunit Sup35 of eRF3, unrelated to prions, has an imperfect nonamer PQGGTQQYN repeated five times (Liu & Lindquist, 1999). All of these aggregating proteins surprisingly have the same length of repeat - about 45 residues. However, by increasing the length of the repeat in the

Sup35 protein the aggregation process was increased relative to wild-type Sup 35 (Liu & Lindquist, 1999). For mammalian prions the octapeptide repeat binds Cu(II) both *in vivo* and *in vitro* (Brown *et al.*, 1997; Hornshaw *et al.*, 1995; Miura *et al.*, 1996; Prince & Gunson, 1998; Stöckel *et al.*, 1998). Binding of Cu^{2+} to the octarepeat of a PrP^{c} isoform transforms the α-helical prion to a β-sheet structure with aggregating properties. Metal-induced aggregation of Alzheimers's Aβ-peptide has also been shown (Bush *et al.*, 1994). The octarepeats have been suggested to have a role in storage and supply of copper to the brain (Stöckel *et al.*, 1998). However, the chicken prions do not bind copper and their hexa-repeats are more unstructured in the presence of copper (Hornshaw *et al.*, 1995; Marcotte & Eisenberg, 1999). Likewise, the transition of prions into a β-sheet aggregate upon Cu^{2+} complexation is difficult to ascribe to a native function. The repeat segments of the mammalian prions are flexible and unordered without metals (Cohen & Prusiner, 1998), but by adding Cu^{2+} (at pH > 6) the octarepeats transform into a type II β-turn structure (Viles *et al.*, 1999). Previously, these had been found to induce an α-helical structure (Miura *et al.*, 1996). In chicken prions the repeats are not flexible but rather constrained, suggesting a different structure (Marcotte & Eisenberg, 1999).

The proposal by the author is that the respective N-terminal repeats form a helical structure that may interact with other proteins, as has been suggested for CTD of RNA polymerase II and for elastin. Several proline-rich repeats and regions, including CTD, associate with other cellular proteins. The WW and SH3 signalling domains utilise proline-aromatic interactions by association, indicating a role for the conserved aromatic residues in the prion repeats. The binding of copper may induce a structure in the octamers of the mammalian prions that is important for association with other proteins. In this context, the binding of Ca^{2+} helps to direct correct folding of the ligand-binding repeat of low-density lipoprotein receptor (Atkins *et al.*, 1998). The pre prion-structure may already be induced upon association with other proteins for avian prions. Saturation of all copper sites in the repeats may also be a signal for 'empty' copper proteins (or for other regulatory proteins) that can dock onto a folded helical repeat structure and harvest the metal (and thus prevent self-aggregation of prions). It is however unlikely (due to aggregation) that the prions bind copper just for storage. This

may be clarified by a molecular model of the repeats in order to find recognition motifs, or by a search for possible proteins that can interact with the N-terminal repeats at different concentrations of copper. Synexin (annexin VII) from *Dictyostelium discodeum* which binds, fuses and forms ion channels in membranes upon Ca(II) binding, has also a N-terminal unordered $(GYPPQQ)_n$ repeat (n = 12-16) that is the site for post-translational modifications and for association with other proteins (Liemann *et al.*, 1997, and references herein).

Some repeat structures of surface proteins also have proline stretches that interact with other cells and molecules. This has been shown, for example, in adhesins from *Streptococcus pyogenes* (Talay *et al.*, 1994) and in the yeast pathogen *Candida galbrata* (Cormack *et al.*, 1999), both of which adhere to human epithelial cells. The adhesion molecule thrombospondin-related anonymous protein (TRAP) from the *Plasmodium* sporozoite has a conserved acidic N/P-rich repeat region (Templeton & Kaslow, 1997). Likewise, the circumsporozoite surface proteins with a (NANP) repeat may fold into a recurring type I β-turn helical structure by hydrophobic packing of prolines from the first and third repeat against each other (Nanzer *et al.*, 1997). The NP-turns may also be stabilised in one conformation by hydrogen bonds between the Asn side-chain and the back-bone (Wilson & Finlay, 1997). The surface repeats from parasites may in addition contribute to immune evasion within the host (McKean *et al.*, 1997). The glycosylated repeats (EP)n and (GPEET)n on the surface of the protozoan parasite *Trypanosoma brucei*, may form extended rod-like structures (Roditi *et al.*, 1989; Treumann *et al.*, 1997). Surface proteins of another parasite, *Leishmania major,* have aspartate-rich heptamer repeats with one proline (McKean *et al.*, 1997) which are related to the peptidoglycan binding domain of protein A from *Staphylococcus aureus* (Smith & Rangarajan, 1995). Helical repeats adopted by parasites may have a function to camouflage its active part by forming extended solvent exposed regions. A helical conformation may also help to create a large surface area for docking of ligands (Williamson, 1994). Alternatively, if the repeat contains an 'active' domain with binding properties, it may help to increase the avidity for the ligand of the molecule.

The ubiquitous functions of proline have here been described. It plays an active role in affinity, folding, stability and transitions in proteins due to its unique

structure and influence it has on its neighbour residues. The proline may be accommodated into α-helices, it helps to dissolve β-fibre aggregates and it may increase intracellular metabolic rates upon stress responses. It can influence structures of proteins by accepting different neighbour residues. By itself it forms two different helices, poly-L-proline I and II. The number of unique structures of prolines repeated in context with other residues (preferably glycines and glutamines) has already revealed different alternative helices, and thus discovering new proline-rich secondary structures will not be surprising. It also plays an active part in binding and affinity of important signalling domains such as WW and SH3 domains due to its unique geometry and chemistry, and it is likewise involved with neurodegenerative diseases such as Alzheimer, Huntington and prion-related diseases.

As discussed above there are several possible secondary structures for proline-rich repeats. An anomalous migration (false increased MW) of proline-rich proteins in SDS-PAGE also suggests that they either adopt a conformation which lowers the amount of SDS that can bind to the protein, or they form rod-like structures that have a different migration on SDS-gels (Noelken *et al.*, 1981; Robson *et al.*, 1997; Suñé *et al.*, 1997). The x-ray structure of the virulence (adhesion) factor P.69 pertactin from *Bordella pertussis* containing two repeats $(GGXXP)_5$ and $(PQP)_5$, reveals a large 16-stranded parallel β-helix (Emsley *et al.*, 1996). Here the proline repeats are rather unstructured loops that interact with other proteins.

Chapter 3. Transitions in Proteins.

3.1 Natural Conformational Transitions Found in Globular Proteins.

The ability of a globular protein to response to different stimuli has evolved as a function of its role in the environment. Switches are dependent on parameters such as location in cells, external stimuli by temperature, pressure and radiation and the availability for other ligands. Structural switches and transitions that control activities of proteins thus involve different mechanisms.

3.1.1 Covalent Modification Versus Conformation and Activity.

The covalent modification of the polypeptide chain is a very common mechanism of regulation. Phosphorylation and dephosphorylation of tyrosine, serine, threonine and histidine residues are frequent regulatory switches involving e.g. enzymes in glycogen metabolism and the citric acid cycle.

Phosphorylation blocks access of substrate to the active site of *E.coli* isocitrate dehydrogenase (Stroud, 1991). For glycogen phosphorylase both the mammalian and the yeast enzymes are activated by phosphorylation, but the mechanisms differ - the new ionic interactions from phosphate groups pull the mammalian enzyme subunits together (Barford & Johnson, 1989; Johnson & Barford, 1994; Sprang *et al.*, 1988). The yeast enzyme, however, refolds its rather unstructured N-terminal region and creates a new hydrophobic α-helical cluster at the subunit-subunit interface (Lin *et al.*, 1996). The very soluble cytoplasmic microtubule associated protein, tau, is normally a very soluble, but upon phosphorylation it becomes long, stiff, inactive and insoluble. (Hagestedt *et al.*, 1989; Selkoe, 1999).

Some other post-translational covalent modifications of proteins, which are also suggested to be reversible or irreversible regulatory switches, are acylations (Linder *et al.*, 1993; McIlhinney, 1990; McLaughlin & Aderem, 1995),

ADP-ribosylations (Burnette, 1994; Pappenheimer Jr., 1977), methylations (Sakashita *et al.*, 1994), amidations (Bradbury & Smyth, 1991; McIntire *et al.*, 1998; Robinson & Robinson, 1991) and adenylations. For example, adenylation or deadenylation of a tyrosine group in glutamine synthetase controls the activity of the enzyme (Stadtman & Ginsburg, 1974), and the Ada protein (a DNA repair protein) in *Escherichia coli* is regulated by methylation (Sakashita *et al.*, 1994).

The proteolytic cleavage of proenzymes may also be regarded as a switch. This is found for serine proteases such as trypsin, chymotrypsin and elastase, and involves a partial autoproteolytic cleavage of their proenzymes, which enables them to become active at a specific location (Creighton, 1984). A large conformational change is found for serpins (*ser*ine *p*rotease *in*hibitor) following the progress from the native state to the inhibitor state and further to the cleaved state. A 15-residue solvent exposed loop is cleaved and inserted as an extra antiparallel β-strand in the serpin separating the cleaved ends by about 70 Å (Bruch *et al.*, 1988; Gettins & Harten, 1988; Mourey *et al.*, 1993). This 'spring-loaded' mechanism is driven by the improved stability of the cleaved form and the ordering of structures (Carell *et al.*, 1991).

3.1.2 Binding of Ligand Moves Tertiary and Quaternary Structures.

Examples of structural transitions in proteins induced by non-covalent binding to other ligands are numerous. These may involve interactions with other proteins, sugars, DNA, RNA, metals, substrates and other smaller ligands. Several allosterically regulated proteins such as haemoglobin, aspartate transcarbomyolase and glycogen phosphorylase exhibit large changes in conformation at the tertiary and quaternary level upon ligand binding, as has been previously well reviewed in the literature.

The catalytic mechanisms of enzymes often have conformational changes with movements of hinges, loops and domains upon substrate binding. Close packing of polypeptide regions (usually helices) produce shear motions between domains (Lesk & Chothia, 1984) while more open conformations allows hinge movements and closures (Gerstein & Chothia, 1991; Gerstein *et al.*, 1993, 1994;

Lesk & Chothia, 1988). Thus, hinge motions involve large changes in local main-chain dihedral angles while shear motions have correspondingly small changes spread over several residues. Antibodies may also have structural conformational changes upon antigen binding (Stanfield & Wilson, 1994), and even a 30° elbow bending between the variable and constant domains has been reported (Sotriffer *et al.*, 1998). The apolipophorin III (apoLp-III) is a helix bundle with six antiparallel helices, and two of the helices (helix 3 and 4) move away from the bundle by exposure to lipoproteins (hinge movement). There is a short linker helix (PDVEKE) between helix 3 and 4 with its valine initiating the interaction to the lipoprotein (Narayanaswami *et al.*, 1999).

Displacement of some tertiary structure upon ligand binding may also have a regulatory function. The Src tyrosine kinases are involved in signal transduction where the N-terminal SH3 and SH2 regulatory domains are connected via a linker to the catalytic domain and the C-terminal regulatory tail with a tyrosine residue. Phosphorylation of this tyrosine reduces the activity of the kinase because the phosphotyrosine folds back and binds to the SH2-domain. The SH3-domain binds to proline-rich substrates in a poly-L-proline II (P_{II}) helix conformation. Surprisingly, the linker region between the SH2 domain and the catalytic domain, almost free for prolines, folds back and intercalates with the SH3 ligand-binding site in a P_{II} helix conformation by non-specific hydrophobic interactions. In this way only specific proline-rich ligands with high affinity may compete with the linker and bind to the SH3-domain, suggesting structural movements upon binding (Williams *et al.*, 1998). This type of autoregulatory sequences directed at the active site have in addition also been reported for proteins kinases, protein phophatases, proteinases, metabolic enzymes and transport receptors (Kobe & Kemp, 1999).

3.1.3 Binding of Ligand Refolds and Induces Secondary Structures.

Some proteins also induce or refold their secondary structures when they bind ligands. There are two regulatory gene products in the synthesis of flagellum proteins to *Salmonella typhimurium* and *E. coli* which interact. FliA encodes the

alternative transcription factor σ^{28}, and FlgM which is an anti-sigma factor, inhibits σ^{28}. The C-terminal end of FlgM induces structure when it associates with σ^{28} (Daughdrill *et al.*, 1997). Upon binding to dsDNA lysine and alanine-rich peptides assume an α-helical conformation from unordered structure (Johnson *et al.*, 1994). The same structure was also folded by an activation domain of herpes simplex virus VP16 when it finds its partner: $hTAF_{II}31$, the human TFIID TATA box-binding protein-associated factor (Uesugi *et al.*, 1997). Some other unordered DNA-binding peptides of RecA form, however, β-structures and filaments when interacting with DNA (Wang *et al.*, 1998). Certain peptides from the HIV surface glycoprotein gp120 (Graf von Stosch *et al.*, 1995b; Reed & Kinzel, 1991) undergo a trifluoroethanol-induced switch from β-sheet to a 3_{10}-helix. This seems to be controlled by a LPCR tetrad plus a tryptophan residue in the neighbourhood of the sequence (Graf von Stosch *et al.*, 1995a, b; Reed & Kinzel, 1993). This switch or conformational change in gp120 is important for HIV to bind to CD4, and an axial hydrophobic helical patch may associate with the CD4-receptor (Graf von Stosch et al., 1995a). The conformational changes in gp120 following CD4 docking may allow it to further interact with the HIV co-receptor CCR-5 (Trkola *et al.*, 1996; Wu *et al.*, 1996).

3.1.4 Metals Expose, Regulate and Refold.

The calcium-binding protein calmodulin and also other muscle regulatory proteins, are Ca(II) activated. Similarly, the calcium-binding protein S100b in human brain has also an EF-hand as calmodulin. For both calmodulin and S100b the metal exposes a buried methionine rich hydrophobic patch or surface which interacts with other proteins (da Silva & Reinach, 1991; Ikura, 1996; Smith *et al.*, 1996). Moreover, the helical protein recoverin, a calcium-sensor in retinal rod cells, undergoes major conformational changes upon associating with the metal. In its absence, it is a cytosolic protein sequestering its amino-terminal myristoyl group in a deep hydrophobic pocket in the N-terminal domain, clamped by residues from three of its four EF-hands. Calcium coordination releases the myristoyl group to bind to membranes by melting eight residues of the N-terminal

helix forming a mobile arm which swings out in solution, and also by rotating the N-terminal domain by 45° relative to the C-terminal. At the same time, it exposes several hydrophobic residues (Ames *et al.*, 1997). In addition to all these large tertiary structural changes, calcium also induces cis-trans isomerisation of a peptide bond in a mannose-binding lectin (Ng & Weis, 1998). Changes in secondary structure upon metal binding are better illustrated by the bacterial chemotaxis regulator protein CheY. By magnesium coordination the protein unfolds a turn of an α-helix displacing residues by up to 10 Å, extends a β-strand, and forms a new β-turn (Bellsolell *et al.*, 1994). A folding of type II β-turns upon copper-coordination has in addition been detected for the N-terminal octarepeat sequences in the prion proteins (Viles *et al.*, 1999). Binding of a sodium ion to thrombin allosterically activates the enzyme. The metal site lies 15 Å away from the active site (Di Cera *et al.*, 1995), and metal binding may induce burial of a large cluster of ordered water molecules also shown by the large and negative change in heat capacity (Guinto & Di Cera, 1996).

3.1.5 Turn on the Light for Transition.

A light-switch is described for the halobacterial rhodopsin seven helix-bundle membrane protein. This is a light-driven proton (or chloride) pump. The chromophore 13-*trans*-retinal is covalently linked to Lys 216 in the middle of the helix bundle, exposed on the extracellular side of the bacteria. Upon absorption of light it isomerises to *cis*-retinal and is moving into the cytoplasmic side of the bacteria. Although the detailed mechanism is still unclear, the correlated transport of ions across the membrane may however be kinetically independent of this switch. A re-isomerisation to *trans*-retinal may be induced by ion-binding or further irradiation (Haupts *et al.*, 1997; Mukohata *et al.*, 1999). A bacterial enzyme nitrile hydratase (EC 4.2.1.84) hydrating nitrile compounds to amides: $RCN + H_2O \rightarrow RCONH_2$ (Kobayashi & Shimizu, 1998) is also activated by photo-irradiation. Inactivation of the enzyme during aerobic incubation in the dark involves binding of NO which coordinates the catalytic non-heme iron. However,

this gas-molecule is released by irradiation and the activity is restored (Nagashima *et al.*, 1998; Tsujimura *et al.*, 1997).

3.1.6 When Transitions Turn Basic or Get Sour.

The influenza virus contains an elongated transmembrane glycoprotein on the surface called hemaglutinin (HA), which can help the virus to fuse with host cells at pH 5. At this pH there is a conformational change in one of the long helices (deprotonation of multiple Asp-residues) with a ~25 residue hydrophobic segment moving 100 Å from the inside of the protein to the top of the molecule, and this part may interact with the host cell surface (Bullough *et al.*, 1994; Carr & Kim, 1993; Oas & Endow, 1994).

pH-transition in proteins often involve pH-sensitive residues as histidines which have a pKa about 6.2, in the physiological range. The repeat pentapeptide structure $([H/P]\text{-}[H/P]PHG)_{15}$ in the histidine-proline-rich glycoprotein (HPRG) has a conformational change below pH 6 which modulates its affinity for heparin and glycosamineglycans through a conformational change. It has been described as a physiological pH-sensor. (Borza *et al.*, 1996; Borza & Morgan, 1998). Some transcription factors are also regulated by pH. (HX)n-repeats are found in some eukaryotic transcription factors (Janknecht *et al.*, 1991), and there is an alkaline activation of *Aspergillus nidulans* PacC zinc finger transcription factor (Tilburn *et al.*, 1995).

Changes in pH also switch the conformation of some secondary structures. The tumour necrosis factor-α (TNF-α) looses its tertiary structure and converts β-sheets into α-helices upon lowering pH below 4, with an increase in surface hydrophobicity and cytolytic activity (Narhi *et al.*, 1996a). The helices may insert them into membranes forming a sodium ion channel (Baldwin *et al.*, 1996). The pH-stability of enzymes also involves structural transitions. The glycinamide ribonucleotide transformylase has a transformation from ordered loop-helix to a disordered loop close to its active site by lowering pH to 3.5 (Su *et al.*, 1998).

3.1.7 Putting the Heat on Transitions.

Most mesophilic proteins denaturate and aggregate upon raising the temperature. However, temperature induced transitions have been reported for heat shock proteins and proteins that are either thermostable or thermosensitive. The abundant molecular chaperone Hsp90 can suppress aggregation of unfolded proteins and promote refolding (Buchner, 1999). The C-terminal regions of the protein associate with each other forming a dimer, and by increasing the temperature they fold into a closed conformation bringing the N-terminal domains in close proximity (Maruya *et al.*, 1999). α-crystallin which is the major protein of eye lens displays a chaperone activity and irreversibly exposes hydrophobic surfaces at elevated temperatures (Das & Surewicz, 1995). Moreover, a lac repressor protein is modified by inserting a large proline rich transcriptional activation domain from herpes simplex virus viron protein 16 (VP16) which also has been shown to form helix by binding to another protein (Uesugi *et al.*, 1997) . The engineered repressor protein is temperature sensitive compared to the wild type and activates expression at +32° C and not +39.5° C (Baim *et al.*, 1991). At the other end of the temperature scale, the trimer propylamine transferase from the extreme thermophilic archeabacterium *Sulfolubus solfataricus* has a temperature induced molecular switch inducing increased structure and activity around 45° C, and thus turning on thermostability (Facchiano *et al.*, 1992).

3.1.8 Transforming into Pathologic Proteins.

When switch sites in proteins are no longer under control or new binding sites are formed by mutation, they may induce different diseases in their hosts. At the quaternary structural level this can be illustrated by sickle-cell anaemia. The haemoglobin molecule undergoes a specific Glu → Val surface mutation, opening up a new hydrophobic site which leads to aggregation of multiple protein molecules (Baudin-Chich *et al.*, 1990; Wishner *et al.*, 1975).

For secondary structure transitions, the prion molecule and amyloid fibrils are examples of proteins which aggregate due to generation increased β-sheet

structures (Soto *et al.*, 1995; Zhang *et al.*, 1995a). These structures have an interstrand H-bonding and more extensive side-chain side-chain interactions relative to the intrastrand H-bonds in α-helices, which make them more susceptible to aggregation. The transformation of α to β structure may be due to exposed hydrophobic regions as illustrated by α-helices with hydrophobic groups attached to the N-termini (Takahashi *et al.*, 1998). Protein precipitation is also suggested to be important in the etiology of glutamine expansion diseases as for Huntington's disease (deposition of huntingtin) and for other neurodegenerative diseases (Kakizuka, 1998; Perutz, 1999). The transition into β-stranded aggregates or into polar zippers/transglutaminated deposits for respectively prions/amyloid proteins and huntintin, may proceed through different mechanisms (Cohen & Prusiner, 1998; Green, 1993; Perutz *et al.*, 1994; Selkoe, 1999). Transglutamination has been shown to be involved in Huntington's disease (Karpuj *et al.*, 1999). However, this did not form the cross-β-like amyloid-like fibres that has been seen for huntingtin fragments suggested for the polar zipper model (Perutz, 1999; Scherzinger *et al.*, 1999). For amyloid diseases the aggregation of antiparallel β-strands may either process through a cross-β-sheet conformation, or through supercoiled β-helical protofibrils (Blake & Serpell, 1996; Lazo & Downing, 1998). Prion deposits stain with congo red similarly as for amyloid suggesting an ordered aggregate (Prusiner *et al.*, 1983). In contrast to Alzheimer's disease, the prions can also be transmitted across the species barrier. Domain-swapping where one β-strand in a prion-molecule displaces a corresponding β-strand in the next prion-molecule has been suggested as a mechanism by Cohen and Prusiner (1998). And recently, an N-terminal repeat sequence has been proposed to play a part in the α-helix to β-sheet transition (Stöckel *et al.*, 1998). The induction of β-strand structure in prions relative to amyloid proteins differs in folding. The conversion of human prion protein into its infective form goes through a highly unfolded state (Hosszu *et al.*, 1999), although the scrapie prion protein and amyloid deposits have been found to process through intermediate(s) with large contents of secondary structure, unstable or none tertiary interactions, and an exposed hydrophobic surface. All of these features

are characteristic of a molten-globule like state (Booth *et al.*, 1997; Kayed *et al.*, 1999; Safar *et al.*, 1994).

3.2 Engineering Switches that Control Function of Proteins.

The recent developments in combinatorial selection strategies have made it possible to evolve proteins with new binding affinities on different structural frameworks (Smith, 1998). There is a trend towards optimising or engineering new functions of single monomeric proteins, or by reducing the size or topology of larger existing binders and enzymes. Of note are the antibody-like scaffolds of cytotoxic T-lymphocyte associated protein-4 (CTLA-4), the fibronectin type III domain and lipocalin which have recently been optimised for presentation (Beste *et al.*, 1999; Koide *et al.*, 1998; Nuttall *et al.*, 1999). Different mini-protein motifs have been rational designed as reviewed by Imperiali and Ottesen (1999). Recent examples on downsizing domains include the three-helical protein A to two helices (Braisted & Wells, 1996), the selection for antigen-binding by the isolated V_H-domain of antibodies (Reiter *et al.*, 1999), and the reduction of the α-helical enzyme chorismate mutase to half its size (MacBeath *et al.*, 1998). The α/β-barrel of an enzyme has been used as a scaffold to evolve a new enzymatic activity by redesign of loop regions (Altamirano *et al.*, 2000). In addition, computerised design from screening combinatorial libraries of possible side-chain rotamer conformations through a dead-end algorithm, have shown that is it possible to redesigning a structure from a fold (Dahiyat & Mayo, 1997). This approach has successfully been utilised to engineer a thermophile Protein G by improving its stability by 4.3 kcal mol^{-1} at 50° C (Malakaukas & Mayo, 1998). However, to the author's knowledge these novel methods for selection have not been utilised for evolving novel switch-properties or transitions in proteins. Generally, switches that already exist in globular proteins have been reengineered into a different protein context.

3.2.1 Engineered Metal Switches.

Metal switches have been inserted into different proteins. By adding or removing the metal it is possible to regulate the function of the engineered protein. A recombinant exotoxin, α-hemolysin, from *Staphylococcus aureus* has been made with histidines in the middle of a central loop important for function, enabling it to turn off pore activity by binding Zn^{2+} ions and switch it on again by removing zinc (Walker *et al.*, 1994). Similar switches have been engineered into different enzymes' active sites providing metallo regulated inhibition (Corey & Schultz, 1989; Higaki *et al.*, 1992), and also into antibodies regulating antigen binding (Rees *et al.*, 1994).

The metal binding can also be introduced in order to form a secondary structure. By inserting a calcium-bind loop from calmodulin in the N-terminal to a short α-helix it is possible to use the metal to fold the α-helix (Siedlecka *et al.*, 1999). A similar induced folding is also found by engineering a metal-binding site direct into disulfide-linked α-helical coiled-coil dipeptide through γ-carboxyglutamic acid residues. These are extra strong metal chelators but they also destabilise the helices through their charge repulsion (Kohn *et al.*, 1998). However, the energetic cost of desolvating intrahelical negatively charged groups upon helix-folding is the proposed mechanism behind reversible coil-coil (leucine-zipper) destabilisation, obtained via an engineered threonine phosphorylation site (Szilàk *et al.*, 1997). It is also possible to change the oligomerisation of an engineered leucine zipper GCN4 through reversible binding of small hydrophobic ligands. By adding cyclohexane or benzene to GCN4, the energetically unfavourable packing of three stands was stabilised and induced the dimer to trimer transition (Gonzalez Jr. *et al.*, 1996).

3.2.2 Photo Switches - Covalent Modification Does the Trick.

There are described several engineered photoswitchable peptides offering a transition to another secondary structure by illuminating the sample at a specific wavelength. Willner & Rubin (1996) have reviewed the different switches. By

inserting large photoisomerisable groups as spiropyran and azobenzene into peptides as poly(L-glutamic acid) or poly(L-lysine), switches between α-helix to coil or β-sheet to α-helix transitions can be induced by irradiation. For azobenzene the photo induced *cis*-structure is more hydrophilic than the planar *trans*. Inserted into proteins such switches control a reversible binding and dissociation of an antibody to a *trans*-azobenzene modified antigen (Harada *et al.*, 1991). Azobenzene and spiropyran derivatives have also been utilised for photostimulation of enzymes such as papain, phospholipase A_2, α-chymotrypsin and amylases. In addition, these principles have been transferred to sensor and computers (Willner & Rubin, 1996).

3.2.3 Temperature-switches can be Created by Manipulation of Residue Hydrophobicity.

By attaching hydrophobic fluorescence groups on glutamic acids residues in a synthetic peptide, it was possible to generate a temperature induced α-helix to 3_{10}-helix transition (Hungerford *et al.*, 1996). On the other hand, similar temperature induced secondary structures transition can also be engineered from its primary sequence alone. A synthetic peptide with periodic prolines interspersed with hydrophobic and ionic residues, forms an α-helix structure and oligomerises with rising temperature, while it is unordered at low temperatures (Kitakuni *et al.*, 1993, 1994). This temperature induced α-helix folding (or cold-denaturation) can also occur intramolecularly as was shown by a similar leucine and lysine-rich peptide with prolines (Lacassie *et al.*, 1996). There are also other proline-rich peptides and proteins that undergo this type of temperature transition. The VPGVG repeat sequences of elastin form a β-spiral formed by recurring type II β-turns stabilised by hydrophobic interactions as discussed previously in Chapter 1.

In some cases engineered residue hydrophobicity can temperature stabilise existing turns without significantly altering the amino acid composition. The replacement of proline by (S)-α-methylproline in the tandemly repeated NPNA tetrapeptide motif in *Plasmodium falciparum* provided exactly this (Bisang *et al.*,

1995). The temperature induced switch from β-sheet to α-helix transition has recently been described in an engineered 16-residue peptide (Zhang & Rich, 1997). These peptides were alanine-rich alternating with either lysine and glutamate or aspartate and arginine forming a β-sheet self complementary structure with repeating negative or positive residues.

By the use of a hydrophobic synthetic polymer, NIPAA (N-isopropyl acrylamide), which contracts in response to temperature, a novel method of modulating activity to streptavidin was found. A cysteine residue close to the biotin binding site in the protein acted as an anchor site for grafting NIPAA. By increasing temperature above 32° C the synthetic polymer contracted and blocked the binding site of biotin (Stayton *et al.*, 1995).

3.2.4 Ionisation of Charged Residues Provides Possible pH-switches.

The β-sheet → helix transition described by Zhang & Rich (1997) can also be induced by lowering pH, but only very low pH-values (pH 1-2) are able to induce α-helix. The authors have suggested that inserted into a globular protein the sequence may be a powerful structural switch. In this context the sequence does not always need to be replaced to make a pH-switch in a protein. By modifying tyrosine residues by tetranitromethane in the active centre of an antibody, it is possible to generate a pH-dependent switch for binding to antigens. This generates 3-nitrotyrosin which lowers the pKa for the hydroxyl group of tyrosine to around 7 (Tawfik *et al.*, 1994). Such pH sensitive switches can be utilised to induce or melt secondary structures as with, for example, the insertion of γ-carboxyglutamic acids into α-helices. The negative charges of these groups are helix-destabilising at pH-values above their pKa, but by lowering the pH to below 5 (below the pKa of the acids), the helices fold again (Kohn *et al.*, 1998). Generally, negative charges have a destabilising effect on the protein structure, as seen from Urry's scale of temperature induced folding of synthetic hydrophobic elastin polymers (Urry, 1993). Here a phosphoryl group on a serine residue increases this transition temperature by the amazing (extrapolated) value of 1000° C.

The large number of examples on natural transitions in proteins have only partly been exploited to engineer new switches in proteins. However, more advanced switches based on binding of small ligands in order to generate a predictable allosteric modulation of proteins is complex. On the other hand, by the use of the selection combinatorial chemistries that are available today it should be possible to select for novel binders that can turn on/off activity as a function of environmental parameters such as temperature, pH and solvent composition. Additionally, it should likewise be possible to evolve novel allosterically regulated enzymes and binding proteins.

Chapter 4. Scope and Aims of the Thesis.

The synthetic elastin polymer with VPGVG-repeats, e.g. from 10-50, forms a contractile spring which responds to different physical and chemical parameters (Chapter 1.7). It is desirable to test whether it is possible to transfer the general biophysical properties of large elastin sequences into smaller molecules (less than 10 repeats). The fine-tuned transitions of elastin could make the contractile sequences of this polymer a very promising tool for introducing tuneable transitions in globular proteins. The energy involved could be employed to form a controllable switch-site structure that could turn on or off activity or affinity respectively for enzymes and binding proteins. In this thesis the author describes investigation into the behaviour of elastin-like peptides of different lengths (8-35 residues) produced by solid phase peptide synthesis (SPSS). In order to compare the biophysical differences between the short peptides and the longer elastin polymer, peptides with protected or free N- and C-termini were synthesised to study the effect of charge on structure. In addition, the composition within short VPGVG-peptides was also varied. The effects of solubility, temperature, pH and trifluoroethanol were tested on the short peptides by circular dichroism. A short elastin sequence was modelled into the two-helical minidomain of Protein A (Chapter 1.3). Here, the objective was to test if it is possible to generate a temperature-controlled switch that can turn on or off IgG-binding within a mild temperature range (4° to 40° C). The small minidomain was synthesised by SPSS and examined by temperature controlled circular dichroism and surface plasmon resonance spectroscopy.

The first part of this thesis (Chapters 1 to 3) reviews various aspects of elastin biological and biophysical behaviour, discusses the peculiar characteristics of proline in certain sequence environments and reviews the current state of knowledge of natural and engineered transitions in proteins. In the second part (Chapter 4 to 9) the experimental work referred to above is described. The conclusions of these studies and suggestions for further work are described in Chapter 10.

Part II

Experimental Section

5. General Materials and Methods.

5.1 Chemicals.

Reagent grade Fmoc and pentafluorophenyl activated amino acids (Fmoc-Gly-OPfp, Fmoc-L-Val-Opfp (Figure 5.1), Fmoc-Pro-OPfp, Fmoc-L-Glu(OtBu)-OPfp, Fmoc-L-Ile-OPfp, Fmoc-L-Leu-OPfp, Fmoc-L-Lys(Boc)-OPfp) and Fmoc-PEG-PS resins (Perseptive Biosystems) were used for peptide synthesis. *trans*-Androsterone and Dioxane were obtained from Fluka. Acetic Anhydride and Methanol were of peptide synthesis grade and were from Applied Biosystems (Perkin Elmer). Anisole, thioanisole (both 99 % pure) and 1,2-ethanedithiol (+90 % pure) were purchased from Aldrich Chemical Corp. TFA (Biochemical grade) was from Fluorochem. Ltd, and Acetonitrile Far UV (HPLC solvent grade) was obtained from Fisons Scientific Equipment , UK.

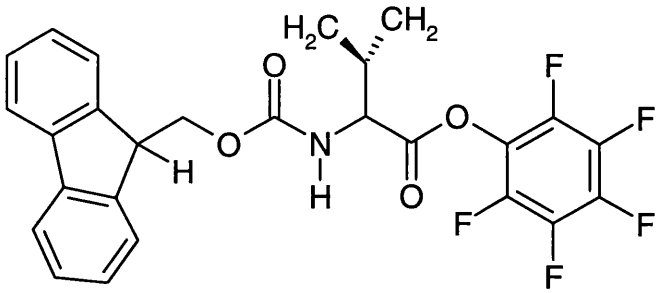

Fmoc-Val-OPfp

Figure 5.1 Structure of Fmoc-Val-Opfp.

5.2 Peptide Synthesis and Purification.

5.2.1 Solid Phase Peptide Synthesis (SPPS).

The pioneering work of Merrifield on the use of a solid phase in peptide synthesis (Merrifield 1963, 1997) has now made it possible to rapidly synthesise peptides and smaller proteins at a rate of 10-15 amino acid residues per hour (Miranda & Alewood, 1999). The concept of SPPS is a combination of previous established solution chemistries plus the anchoring of the C-terminus of the growing peptide chain through a handle to an insoluble solid support. The C → N direction of synthesis prevents racemization of the peptide, and its immobilisation facilitates the use of and efficient removal of excess reagents, and automation of the whole process (Bayer, 1991). For each cycle the N-terminus of the immobilised peptide is deprotected, neutralised and coupled to the next N-protected residue (Merrifield, 1997), and the final peptide is cleaved, side-chain deprotected and purified. Merrifield utilised N_{α}-*tert*-butyloxycarbonyl (Boc) protected amino acids using graduated acidolysis. The Boc group is removed by the moderately strong acid trifluoroacetic acid (TFA) while side-chain deprotection and cleavage from the resin were obtained by hydrogen fluoride (HF) or other strong acids (Bayer, 1991; Merrifield, 1997). A mild alternative method is the TFA-stable N_{α}-9-fluorenylmethyloxycarbonyl (Fmoc) group which can be removed from the amino acid by a secondary base (Figure 5.2), e.g. 20 % piperidine in dimethylformamide (DMF). Fmoc chemistry permits the use of TFA-labile side-chain protection and attachment to solid phase, giving a milder deprotection protocol (Carpino & Han, 1970; Wellings & Atherton, 1997).

5.2.2 Solid Phase and Coupling Chemistry.

Peptides in this study were synthesised by a continuous-flow automatic method on a MilliGen/Biosearch 9050 PepSynthesizer (Millipore, Bedford, MA).

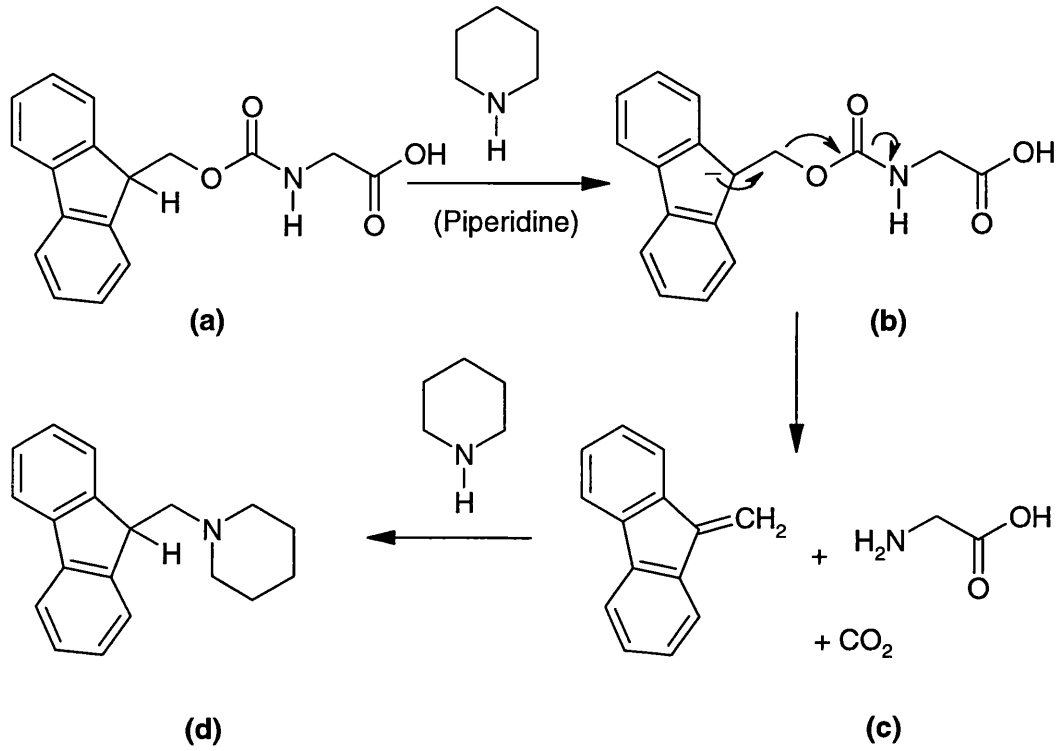

Figure 5.2 Mechanism for Deprotection of Fmoc-glycine by Piperidine.
(adapted from (MilliGen/Biosearch, 1990)). The base-labile Fmoc groups is removed by beta-elimination with the secondary amine piperidine.

A graft copolymer solid support of 1 % cross-linked polystyrene (PS) and polyethylene glycol (PEG), providing stability and similar swelling in different solvents, was used (Bayer, 1991). The mild orthogonal Fmoc chemistry was implemented, and thus the Fmoc-PAL-PEG-PS or Fmoc-Gly-PEG-PS resins were used in this study (Figure 5.3). The first resin with the PAL handle (5-(4-aminomethyl-3,5-dimethoxyphenoxy)valeric acid) produces an amidated C-terminal peptide after cleavage in TFA, while the second resin already incorporates the last residue in the peptide giving a free C-terminus (Wellings & Atherton, 1997). The resins (approx. 1 g - equivalent to 0.1 mmol scale) were swelled in 40 ml fresh DMF for 60-90 minutes and then packed in a column. The amino acids were purchased as preactivated pentafluorophenyl esters and N_{α}-protected with Fmoc (Fmoc-X-Opfp; Figure 5.1), and a four-fold molar excess (0.4 mmol) was utilised for each coupling. The OPfp esters coupling rate is

improved by adding 1-hydroxybenzotriazole-solution (HOBt; 1-2 equivalents; Figure 5.4) (Albericio & Carpino, 1997; Atherton *et al.*, 1988b; Hudson, 1990). An HOBt-solution was made by dissolving 5 g HOBt, 25 mg acid violet 17 (AV17, dye indicator), and 66 µl diisopropylethylamine (DIEA) in 100 ml DMF. DIEA will form an ionic pair with the dye in solution.

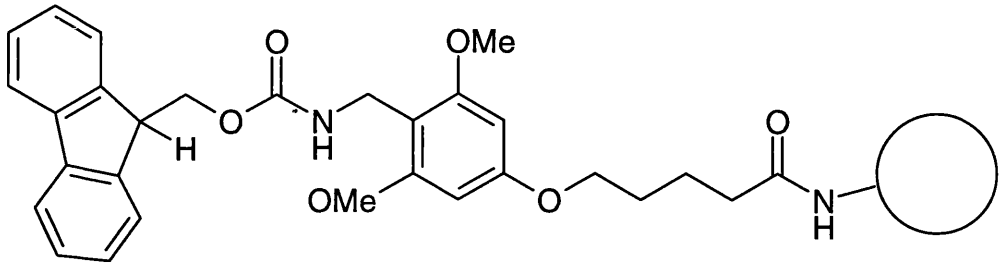

Fmoc-PAL-linker-solid support

Figure 5.3 Structural Representation of Fmoc-PAL-linker Resin.
The PAL handle (5-(4-aminomethyl-3,5-dimethoxyphenoxy)valeric acid) provides an amidated C-terminus for the peptide after cleavage in TFA. (adapted from (MilliGen/Biosearch, 1990)).

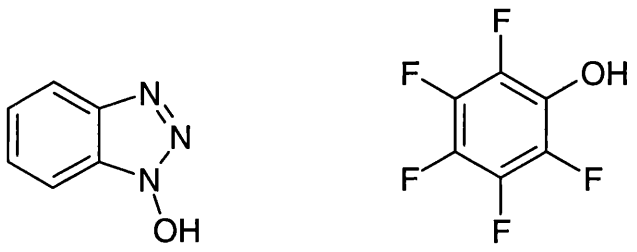

HOBt **HOPfp**

Figure 5.4 Structures of HOBt (1-hydroxybenzotriazole) and HOPfP (penta-fluorophenol). Adapted from (Albericio & Carpino, 1997).

5.2.3 Continuous-flow Automatic SPPS and its Detection.

The MilliGen/Biosearch 9050 peptide synthesiser was prepared for synthesis by topping up containers with DMF, 20 % (v/v) piperidine in DMF and HOBt-solution, and purging these with N_2. Likewise, the columns with resins were mounted and washed in DMF, and the synthesis module was programmed.

The synthesis was started by deprotecting the Fmoc group from the resin using a 7-minute column wash with 20 % piperidine in DMF and then flushing it for 12 minutes with DMF. The amino-acids were dissolved in HOBt-solution (with dye and DIEA) by forty five 10-second cycles of nitrogen purging, and recirculated through the resin-packed column for at least 30 minutes and up to 3 hours if required (Figure 5.5) Finally, the column was washed again with DMF for 8 minutes to remove the excess of Fmoc-X-OPfp amino acids before the cycle started again. The flow rate during synthesis was 5 ml/min (MilliGen/Biosearch, 1990). Coupling efficiency was followed continuously by recording the absorbance at 544 nm for the AV17 dye. This indicator binds to the Fmoc deprotected N_α-terminal of the peptide through its negative charged sulphite-group (there is a 20 fold molar excess of N-termini relative to DIEA in solution), and is displaced as acylation proceeds. It is also possible to monitor the decreasing Fmoc amino acid concentration at 300 nm as it is coupled to the immobilised peptide. However, by using OPfp-esters this measurement may be disturbed (Atherton *et al.*, 1988a). Generally, a 95 % yield was required for each step. Calibration points (empty amino acid vials) were inserted during synthesis (one every 10 amino acid residue). The first amino acid (Gly) required more than 12 hours of coupling to Fmoc-PAL-PEG-PS due to the slow coupling kinetics. The remaining amino acids were coupled with standard chemistry and protocols as described by the manufacturer, typically an 89-minute cycle per amino acid. After synthesis the Fmoc protection was removed with 20 % piperidine in DMF, and some of the peptides were then acetylated at their N-termini with acetic anhydride in DMF.

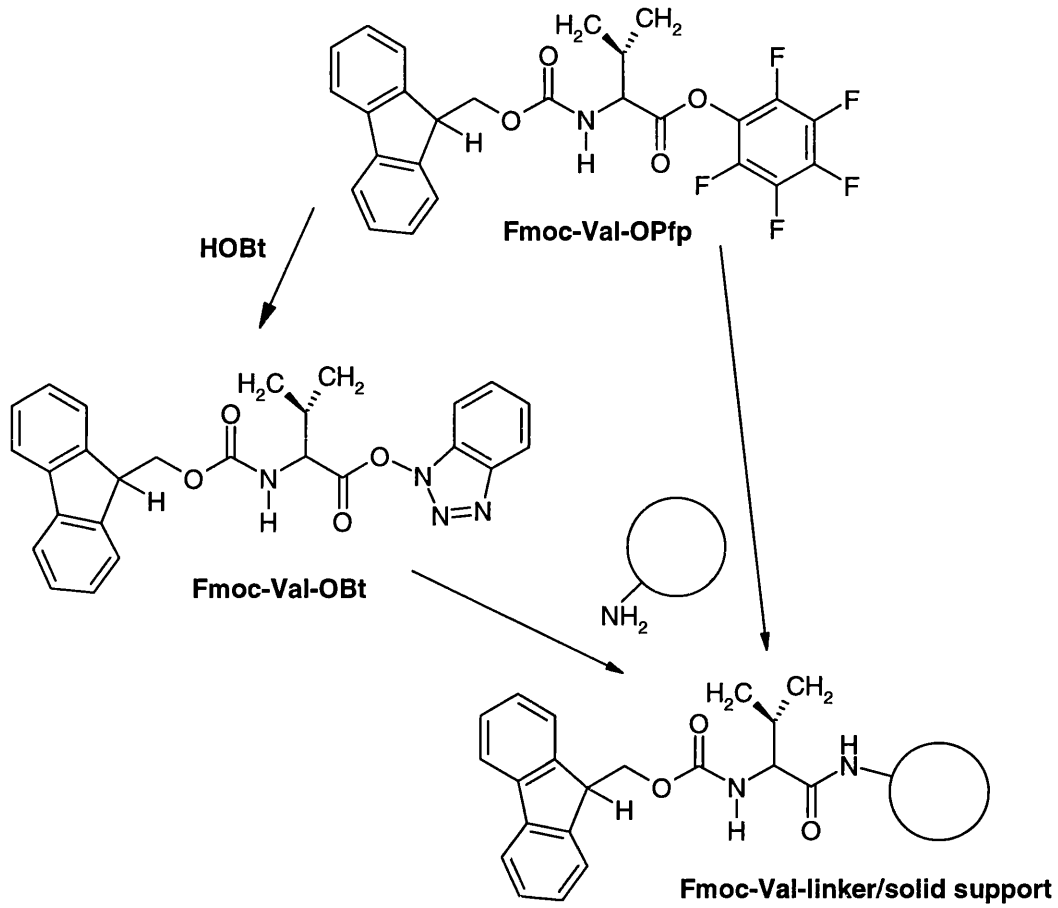

Figure 5.5 Coupling of Fmoc-protected and Opfp-activated Valine on a Solid Support. (adapted from (MilliGen/Biosearch, 1990)).

5.2.4 Trifluoroacetic Acid Cleavage and Deprotection of Resin-bound Peptides.

The resin was washed successively with dichloromethane, methanol, diethylether and then dried using N_2. The dry weight of the resin was then measured as an indicator of the success of the synthesis, and peptides were further cleaved from the resin in a TFA-mixture. TFA induces a reactive pool of carbocations or sulfonyls on the cleaved protecting groups of the side-chains and on the linker which can easily covalently modify residues (Guy & Fields, 1997). Peptides were cleaved from the resin and deprotected by a treatment with TFA containing the

scavengers 5 % (v/v) thioanisole, 3 % 1,2-ethanedithiol and 2 % anisole (reagent R; Albericio *et al.*, 1990) for 4-6 hours at 20° C. One ml of reagent R was added per 50 mg resin in a 5 ml glass vial stored in a safety cabinet. The pipette tips for the scavengers were ejected into a bleach-filled tube. However, the scavengers could strictly have been omitted since there were no arginine, cysteine, methionine, tryptophan or tyrosin residues, which are more easily destroyed by reactive species (Wellings & Atherton, 1997).

The efficiency of deprotection was tested by sampling 200 µl cleavage mixture every 2nd hour for analytical HPLC. The sample was transferred into a 5 ml Pyrex^{TM} tube and diluted 20 times (to 4 ml) with petrol ether. A small yellow blob appeared in the bottom of the tube. The glass was rotated slowly and petrol ether was poured off. The procedure was repeated, and 2 ml diethyl ether was carefully added after two washes and the yellowish blob formed a white precipitate which was dried under N_2. The solubility was screened by dissolving the peptide in 4.5 % (v/v) acetonitrile in 0.1 % (v/v) glass-distilled TFA in water (HPLC running buffer), and further tested for cleavage efficiency.

After cleavage of the large batch of peptide-resin in reagent R it was transferred to a vacuum glass-filter and washed stepwise with several pipette volumes of TFA (10 ml) over a 250 ml flask. The cleaved peptides were further washed stepwise by adding a 10-fold volume excess of petrol ether and swirling the peptide-oil bottom layer well. Petrol ether was added until the solution turned blank and was then gently poured off. The peptide was precipitated by slowly pouring diethylether into the flask covering the whole surface. The white peptide solid was N_2-dried and dissolved in 10-20 ml deionised water and lyophilised. Where the recovery of peptide was low the pooled ether washes were evaporated in a safety cabinet over 1-3 days. If crystals were detected, they were dissolved in HPLC running buffer, rotary evaporated and further washed/precipitated with ethers.

5.2.5 High Performance Liquid Chromatography (HPLC) of Peptides.

Different side products are very common during SPPS, and even for a 95 % yield in every step the maximal purity of a normal 25-mer peptide is only about 28 % (0.95^{25}). The introduction of HPLC in the 1970s was an important development for rapid purification of peptides. The columns and pumps are constructed to deliver and maintain a very high pressure which facilitates the use of very fine column particles (the average diameter or mesh size between 3 to 10 μm), and thus the system has a very good resolution. Smaller particles give better resolution. However, in reverse phase HPLC the peptides are separated by their hydrophobic interactions with the packing material inside the column (the stationary phase). Ideally, an orthogonal separation method should be performed in tandem (capillary zone electrophoresis, ionic exchange or size exclusion chromatography) (Bayer, 1991; Skoog *et al.*, 1988; Wellings & Atherton, 1997).

In this study where the peptides have few or no ionic groups and a very large hydrophobic composition, reverse phase HPLC was utilised. The 0.1 % TFA-solution for HPLC was prepared from glass distilled TFA and deionised water, and the acetonitrile solution was of high purity with low UV-absorption. All solutions were filtered and purged with Helium before and during the HPLC run.

5.2.6 Preparative HPLC of Crude Peptides.

Large scale purification using HPLC (Waters 490E Programmable Multiwave length detector and Waters 600E system controller) at 20° C was performed using a shallower gradient elution. For peptides A-H a gradient of 13.5 to 22.5 % acetonitrile in 0.1 % TFA over 90 min was applied. The crude peptides, which were dissolved in HPLC running buffer at a concentration of 2 mg/ml and filtrated through a 0.22 μm filter, were chromatographed at 10 ml min^{-1} from a preparative 240 x 24 mm Vydac C_{18} column (10 μm mesh) with detection at 214 nm (Winkler *et al.*, 1985) and then lyophilised.

5.3 Peptide Characterisation

5.3.1 Analytical HPLC of Crude and Purified Peptides.

The crude peptides from the TFA-cleavage and the purified fractions from the preparative HPLC, were analysed on an analytical HPLC: LKB Bromma 2157 Autosampler (driven by high pressure N_2), 2140 Rapid Spectral Detector Unit, 2150 Pump and 2152 HPLC controller units. A linear gradient of 4.5 - 54 % acetonitrile in 0.1 % TFA over 91 minutes was used for each peptide at +20° C on a C_{18} column (Vydac; 250 x 5 mm; 10 µm mesh). Peptides A-O were detected at 214 nm (Winkler *et al.*, 1985) and eluted (0.7 ml min^{-1}) as follows A-H: 18-20.5 % acetonitrile, and I-O: 29-36 % acetonitrile.

5.3.2 Electrospray Ionisation (ESI) Mass Spectrometry.

The latest developments within mass spectrometry (MS) have made it possible to routinely analyse the masses of peptide and very large proteins with more than 99.99 % precision (Burdick & Stults, 1997; Mann & Wilm, 1995). For electrospray ionisation mass spectrometry (ESI-MS) a needle that is kept at high electric potential, sprays the peptides as small charged droplets at atmospheric pressure. The droplets shrink by evaporation of their carrier solvent using a hot counter-current of inert gas until the charge repulsions are stronger than the forces that maintain the droplet, and peptide ions migrate to the high vacuum inside the mass spectrometer. For proteins, protons and other cations produce positive peptide ions with multiple charges that are fragmented by gas molecules within the mass spectrometer. The method of analysis is thus very mild and can be utilised for example, to map regions on the three-dimensional structure of proteins (Mann & Wilm, 1995). Sodium adducts are common, and lead to multiple peaks whose masses differ by +23 u. The final output is a distribution of mass-to-charge ratio (m/z) depending on fragmentation. Intensities of the peaks with different

molecular masses may also be used to quantify ratios of related contaminant peptides (Burdick & Stults, 1997).

The purified peptides in this study were prepared at a concentration of 10-20 ng peptide per µl sample in a volume of 2 ml of 1:1 water/methanol with 1.0 % acetic acid, and analysed by Mr. Chris Cryer (Department of Chemistry, University of Bath) using electrospray mass spectrometry (VG Autospec with VG Analytical Electrospray).

5.3.3 Amino Acid Analysis.

A well-established method for characterising and quantifying the amino acid composition of peptides and proteins is to hydrolyse the primary structure by splitting the peptide bonds in 6 M HCl at 110° C (or 5 M NaOH). Acid hydrolysis may partly destroy serine, threonine, methionine and tyrosine residues, deaminate glutamine and asparagine, and completely destroy cysteine and tryptophan. Valine, isoleucine and leucine residues may be incompletely liberated (Blackburn, 1968; Ozols, 1990). The free amino acids are derivatised, separated on reverse-phase HPLC and detected.

Quantitative amino acid analysis was carried out by Dr. Bloomberg (University of Bristol). Samples were hydrolysed in HCl and 0.1 % (v/v) phenol at 110° C for 24 hours under N_2-gas and then freeze dried, dissolved in citrate buffer pH 2.2, and analysed on a Pharmacia AlphaPlus II amino acid analyser.

5.4 Circular Dichroism Spectroscopy

Circular dichroism (CD) is a well-established method for the study of secondary structures of proteins and other biomolecules. It is also used to study ligand-binding interactions or other conformational transitions in biomolecules, e.g. protein folding (Johnson Jr., 1985; Woody, 1995). There is a strong correlation between secondary structural data collected by CD and by NMR (Lee & Cao, 1996). Nevertheless, structural measurement of oligopeptides and proteins by CD

can only be reliably analysed by comparison with libraries of CD spectra on known structures. The reduced accuracy of calculated CD-spectra has made it difficult to obtain a theoretically consistent prediction of different protein structures (Manning *et al.*, 1988) . However, by using library information, there are now more than 10 different computer programs that can estimate the amount of secondary structure in a protein based on its CD-spectrum (Greenfield, 1996).

5.4.1 Circular Dichroic Light.

Light comprises oscillating electric and magnetic field waves with mutually perpendicular magnetic (**H**) and electric (**E**) field vectors rotating about the direction of propagation. Plane-polarised light only allows the electric field vector and its propagation vector to rotate in a single plane. Circular dichroic light utilises two perpendicular plane-polarised monochromatic electromagnetic waves of equal maximum amplitude, and their respective electric vectors, **E1** and **E2**, which are retarded by a quarter of a wavelength (i.e. 90°) relative to each other. The tip of the resultant **E** vector will rotate in either a left or right helical path following the propagation vector, forming either left ($\mathbf{E_L}$) or right ($\mathbf{E_R}$) circularly polarised light. If the right and left circularly polarised waves with similar magnitudes are superimposed they form plane-polarised light. Optical rotary dispersion (ORD) is generated when the biomolecules rotate the planes of polarised light due to differences in velocity of propagation of $\mathbf{E_R}$ and $\mathbf{E_L}$. However, circular dichroism is a result of biomolecules in an asymmetric environment *absorbing* different amounts of left or right circularly polarised light. In this situation the $\mathbf{E_R}$ and $\mathbf{E_L}$ vectors have different "magnitudes". This is manifested by an elliptical polarisation of light (Figure 5.6), and the ellipticity is defined as $\tan^{-1}$ of the b/a ratio (elliptic minor axis/elliptic major axis), $\theta = \tan^{-1}(b/a)$ (Freifelder, 1982). As the light propagates, it forms an elliptical screw helix. The ellipticity is related to absorption (A) through the relation $\theta = 32.98\ \Delta A$, where θ is in degrees. Likewise, by using Beer-Lamberts law, $A = \varepsilon cl$ (c = molar concentration and l = sample cell thickness) and the molar extinction coefficient for absorption of left (ε_L) and right (ε_R) polarised light, ΔA can be

expressed as $\Delta A = \Delta\varepsilon lc$, where $\Delta\varepsilon = \varepsilon_L - \varepsilon_R$ ($\Delta\varepsilon$ is called circular dichroism). The molar ellipticity, $[\theta]$, is thus $[\theta] = 100\ \theta\ l^{-1}\ c^{-1} = 3298\ \Delta\varepsilon$ (and is expressed as deg $cm^2\ dmol^{-1}$) (Woody, 1995).

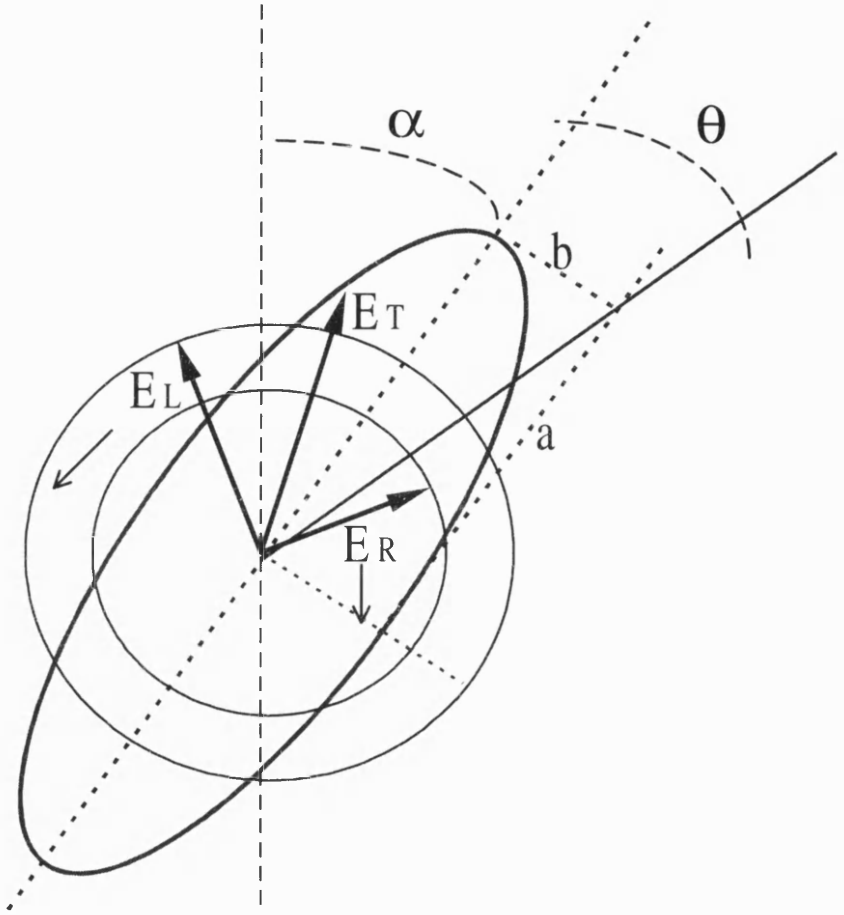

Figure 5.6 Combination of Left and Right Circularly Polarised Light Produces Elliptical Polarisation of Light. Adapted from (Freifelder, 1982). Here, the molecule absorbs more of *right* than *left* circular polarised light and the net resultant electric vector $\mathbf{E_T}$ forms an elliptical polarised light propagating out of the plane (towards the observer) while rotating in the clockwise direction due to that the angular velocity of $\mathbf{E_L}$ is retarded more than $\mathbf{E_R}$ (rotation angle α is towards right) The circular dichroism ($\Delta\varepsilon$) in this case is negative ($\Delta\varepsilon = (\varepsilon_L - \varepsilon_R) < 0$ and here its ellipticity θ is $\tan^{-1}(b/a)$.

5.4.2 Circular Dichroism and Proteins.

Electromagnetic absorption of circularly polarised light in proteins mainly involves the peptide bond (although aromatic residues and disulphide bonds also contribute to the spectra). The different electronic transitions in the amide chromophore are dependent on the energy of the photons, and the structural alignment of the absorbing chromophores with their different extinction coefficients, in the context of their asymmetrically distributed neighbouring monomers, projects the secondary structure as a CD spectrum (Johnson Jr., 1985). In CD spectroscopy of polypeptides, at wavelengths above 180 nm it is chiefly the electrons of multiple bonds in delocalised π-orbitals and of n-orbitals on heteroatoms with lone pair electrons, that participate in transitions. The σ orbitals of the single bonds are very strong and are only perturbed at shorter wavelengths (130-175 nm). Upon absorption of light there is often an electronic transition to the antibonding orbitals σ^* and π^*. The symmetrical σ^* orbital has a node point between the atoms involved in binding, and the π^* orbital has a similar node along the axis of the bond. There are predominantly two CD transitions (n-π^* and π-π^*) in the peptide bond that project the secondary structure of its peptide chain. The n-π^* transition often has the lowest energy and a small molar extinction coefficients, ε = 100 M^{-1} cm^{-1}, because the orbitals do not overlap in space. It is observed at 210-240 nm. The π-π^* transition in peptide bonds with a larger extinction coefficient around 7000 M^{-1} cm^{-1} exhibits an absorption band below 200 nm (Woody, 1995). In α-helices this transition also exhibits a couplet negative band around 208 nm (Figure 5.7a) (Johnson Jr., 1985). For this structure the n-π^* transition around 220 nm and π-π^* at 190 nm are polarised perpendicular to the helix axis, while the π-π^* transition at 208 nm is parallel to the helix axis.

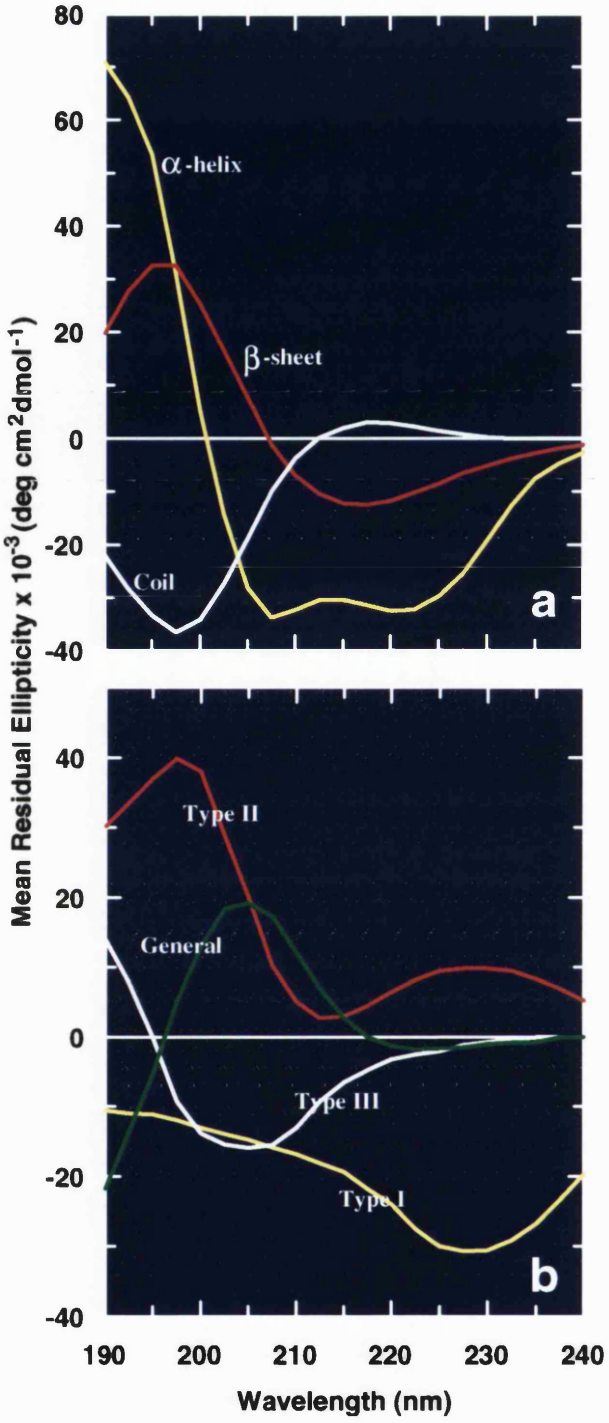

Figure 5.7 Model CD-spectra for Some Secondary Structures.

The figures are adapted from Reed & Reed (1997). Panel **a)** illustrates spectra of α-helix, β-sheet and the unordered structure (coil), while in panel **b)** the different types of β-turn (type I, type II, type III and general type) are shown. General β-turn is a mixture of type I, type II and type III β-turns.

In β-sheets the associated π-π* transition about 200 nm is polarised parallel to the backbone (Johnson Jr., 1985). n-σ* CD transitions are found in S-S bridges in

proteins absorbing between 240-360 nm (Woody, 1995) due to an intrinsic Cotton effect from its own chiral chromophore.

The aromatic residues phenylalanine. tyrosine and tryptophan may also affect CD spectra due to their π-π^* transitions. These much weaker induced transitions around 250-310 nm provide information about tertiary and quaternary structure of the protein. The different spectra for some other secondary structures are given in Figure 5.7b (Johnson Jr., 1985; Reed & Reed, 1997; Woody, 1995). The type II β-turn that is characteristic for the elastin monomer and polymer is different to that is illustrated in Figure 5.7b. It has a negative band below 200 nm, a positive maximum around 205-210 nm and a local minimum around 220-240 nm (class B spectrum) (Urry *et al.*, 1974, 1985, 1986; Woody, 1995). Related helical structures, as for the proline pipe helix, may also produce CD-spectra which resemble type C spectra for a type I/III β-turn (Butcher *et al.*, 1996; Nedved *et al.*, 1994; Woody, 1995). The CD-spectra of polyproline II helices and unordered peptides are very similar. Both project a negative band around 200 nm, a positive band at 215 nm and a weak negative band at 230 nm (Sreerama & Woody, 1994).

5.4.3 Practical Circular Dichoism

The secondary structure of the peptides was analysed by recording CD spectra on a Jobin-Yvon Model CD6 Dichrograph (Instruments S.A. UK Ltd., Stanmore, UK). The instrument has a spectral range of 180-800 nm. The reproducibility is ± 0.1 nm below 500 nm, and the wavelength is accurate within ± 0.5 nm below 200 nm and within ± 0.1 nm between 200-300 nm (Instruments, 1990). The plane-polarised light passes through an electrooptic modulator with an alternating electric field generating respectively left and right polarised light from the single 250 W Xenon light source.

The instrument was iso-andosterone calibrated according to the manufacturers instructions: The monochromator position was set at 304 nm, and 1.25 mg/ml iso-andosterone in dioxane was placed in a 1.0 cm quartz cuvette and scanned using 2 nm bandwidth, 0.1 s integration time and an increment of 0.2 nm. The intensity should read 1.425e-2 ΔA. The instrument was further temperature

controlled (water cooled with a flow rate of 6-12 liter/min) and N_2 purged (flow rate of 9 liter/min) during analysis (Johnson Jr., 1990).

The peptides were dissolved in sterile filtered (0.22 μm) solutions prior to analysis. Spectra were recorded from 190 nm up to 260 nm with a step resolution of 0.5 nm (2.0 nm bandwidth) using an integration time of 1-5 seconds. The average of 4 to 15 runs were smoothed using the Sabitzky-Golay algorithm in the Dichrograph Software version 1.1. This algorithm reduces the differences in intensities of the neighbouring peaks by taking a sliding average of the values, and thus reduces the statistical background noise while keeping major features (Instruments, 1990).

Temperature CD scans were performed by a stepwise increase in temperature, from +1° C and up, using a five minute equilibration time. The cuvette temperature was measured with a Fluke 51 K/J digital thermometer. The melting of the minidomains was monitored by integrating the molar ellipticity at 222 nm and 260 nm at each temperature for 10 seconds. The average of 3-6 measurements at each wavelength was used. The peptide stock concentrations (in deionised water) were determined by quantitative amino acid analysis. Data points at each wavelength were expressed as mean residual ellipticity ([θ], deg cm^2 $dmol^{-1}$) by dividing the measured molar ellipticity by the number of residues in the peptide.

5.5 Surface Plasmon Resonance Spectroscopy.

Interaction kinetics between an immobilised ligand and its analytes, e.g. an antibody and an antigen, can be obtained by using surface plasmon resonance (SPR) spectroscopy. The BIAcoreX and BIAcore2000 systems from Biosensor AB provide efficient systems for studying real time interactions without labelling of proteins. The BIAcore2000 is robotised and only needs to be programmed in MDL (method definition language) to operate. Kinetics is measured on an immobilised ligand on a hydrogel covered (usually ~100 nm carboxymethylated dextran) gold surfaced (~50 nm) microchip. The integrated microfluidic cartridge (IFC) provides a precisely controllable and rapidly changeable flow rate of analyte and buffer over the sensor chip surface. The syringe pumps deliver accurately

flow rates down to 1 µl min^{-1}. On the other side of the sensor chip is a prism which detects changes in refractive index when ligands and analytes bind to the surface (Figure 5.8).

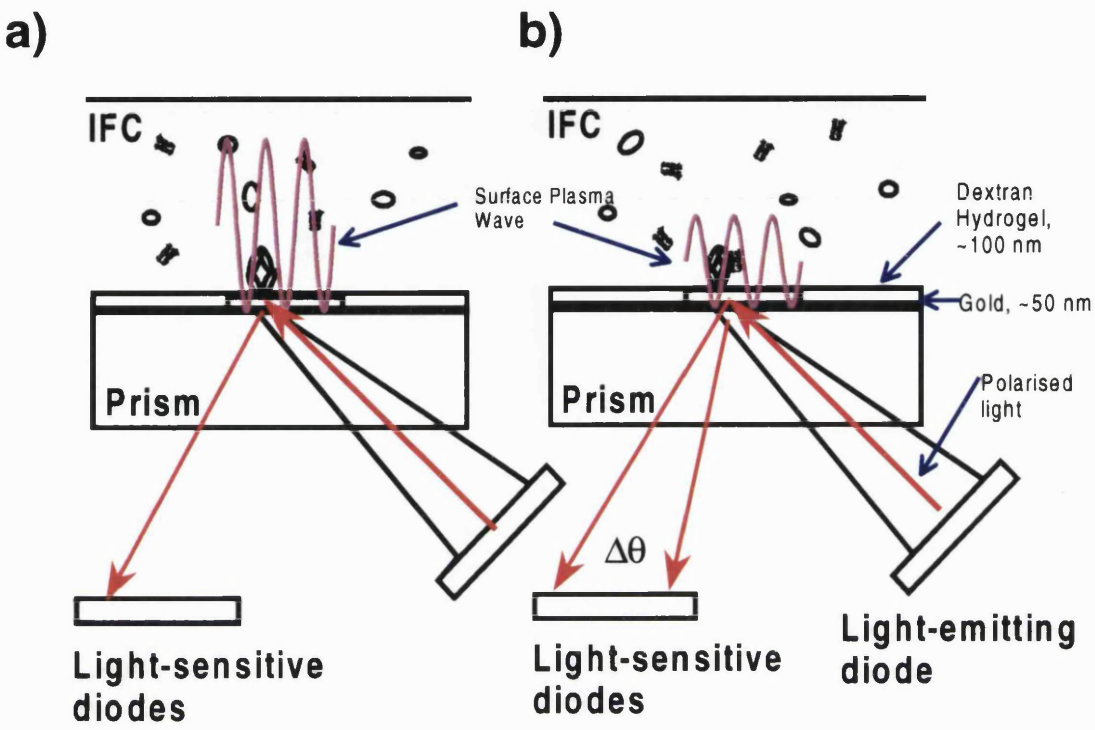

Figure 5.8 BIAcore Surface Plasmon Resonance Detection of a Binding Event.

The panel a) of figure illustrates a ligand (here Fc of IgG) immobilised on a gold surfaced sensor chip *before* it binds its analyte (a two-helical Protein A minidomain) flowing through the chip in the integrated microfluidic cartridge (IFC). Polarised light form the LED source is focused on the gold surface in a fixed range of incident angles and the reflected beam from the surface with immobilised Fc is recorded on light-sensitive diodes. When the ligand binds its analyte from bulk phase (panel b: immobilised Fc binds the SpA minidomain), the resonance angle is slightly changed ($\Delta\theta$). The angle of the optical wave (polarised light) has changed after interrogating the surface plasma wave. A continuous plot of the binding signal as a function of time gives a sensorgram recorded in real time as a binding event (Homola *et al.*, 1999; Canziani *et al.*, 1999). The sizes and proportions of proteins, surface plasma wave, polarised light, and the chip are not related.

Surface plasmon resonance is a charge-density wave which is generated at the interface between the gold surface and the solvent that have dielectric constants with opposite signs (Homola *et al.*, 1999). In the BIAcore instruments the surface plasma wave (SPW) is generated by irradiation of the gold surface by a totally

reflected polarised light at either a certain wavelength, frequency or angle, energetically matching the SPW (resonant exitation). This evanescent electromagnetic field penetrates about 25 nm into the gold surface and about 160-400 nm into the medium (Figure 5.8), and the SPW can probe all molecules interacting with this metal (Homola *et al.*, 1999). The length of propagation is only about 20-50 μm so analysis has to be focussed just on that area which is exited by light. The total detection area for SPR in the BIAcore systems is 0.224 mm^2. When analytes bind to the surface, the local refrative index increases. This leads to an altered refraction of the polarised light and also in an increased angle of absorbance maximum of plasmon electrons (Canziani *et al.*, 1999).

Light from a near-infrared light-emitting diode (LED) is transmitted through the prism and focused on the gold surface in a fixed range of incident angles. The reflected beam is monitored by a fixed linear array of light-sensitive diodes exhibiting an angular resolution of about 0.001 $\Delta\theta$ (Figure 5.8) and a refractive index resolution at 10^{-5} , or a mass change of 10 pg/mm^2 (Canziani *et al.*, 1999). The computer determines the angle of minimum reflection (SPR-angle), which is recorded in real time at 160 Hz (measurements/s) (Biosensor, 1996). BIAcore2000 simultaneously detects the refractive indices on four different surfaces with a very low noise (0.3 resonance units (RU) per minute) and thus can control the effects of the bulk solution (Biosensor, 1996). This makes it possible to monitor very small and low affinity binders, and an analyte of 180 Da can be detected with an affinity constant (Ka) of 50 μM (Karlsson & Ståhlberg, 1995). The SPR-response is proportional to the surface concentration and mass of the interacting analyte. For proteins, one RU is corresponding to one pg of analyte per mm^2 or 10 mg/liter (Stenberg *et al.*, 1991). The temperature can be controlled down to 0.003 °C min^{-1} and the range for BIAcore2000 is from +4° to +40°C which limits the use of the instrument for studying temperature induced unfolding. Here the author has employed the BIAcore instrument for measuring the kinetics of small Protein A minidomains towards immobilised Fc as a function of temperature.

The rate of change of the BIAcore response R(t) or R (which is detected in RU) as a function of time, dR/dt, can be utilised to study kinetics. However, the detector response is also a sum of analyte binding, buffer and the baseline level

which have to be subtracted from the raw data: $R_{binding} = R_{detector} - R_{baseline} - R_{buffer}$ (Karlsson & Ståhlberg, 1995).

5.5.1 Evaluation of BIAcore Data.

Generally, the one-component binding event A + B = AB can be described by the kinetic constants k_{on}, the rate per second for the formation of AB, and k_{off}, the rate ($M\ s^{-1}$) for dissociation of AB into A + B. The rate of change of R as a function of time is thus (Karlsson *et al.*, 1991; O'Shannesey *et al.*, 1993):

$$d[AB]/dt = dR/dt = k_{on}\,[A][B] - k_{off}\,[AB] \tag{5.1}$$

$$dR/dt = k_{on} \times C_A \times [R_{max} - R(t)] - k_{off} \times R(t) \tag{5.2}$$

$$R(t) = R_{eq}\,[1 - \exp(-k_{obs} \times (t-t_0))] \tag{5.3a}$$

where

$$k_{obs} = k_{on} \times C_A - k_{off} \tag{5.3b}$$

C_A is the constant concentration of analyte, A, injected. R_{max} is proportional to the total concentration of immobilised B, and $[R_{max} - R(t)]$ is proportional to free B. t_0 is the injection time and R_{eq} is the steady state response when $dR/dt = 0$.

In this study the k_{on} and k_{off} values were fitted by evaluating the sensorgram data using the BIAevaluation 2.1 software (Biosensor AB) on a 133 MHz Pentium I computer (Dell Dimension XPS P133s). First the response curves were subtracted from the bulk effect curves and all the baselines were adjusted according to the software manual (Biosensor AB, 1995). Two different models were used, and the best fit was evaluated by plotting residuals. By nonlinear fitting of two exponentials, the two-component association phase for the model:

$$2 \text{ minidomains} + \text{Fc561} + \text{Fc561*} \leftrightarrow \text{minidomain-Fc561} + \text{minidomain-Fc561*} \quad (5.4)$$

(Fc561 and Fc561* are two independent epitopes on Fc561), was found from equation 5.5,

$$R = R_A(1 - \exp(-ks_A\, t)) + R_B(1 - \exp(-ks_B\, t)) \quad (5.5)$$

where R is the response at time, t, and R_A and R_B are steady state response levels for the two events. In order to determine the on-rates, the fitted values for ks_A and ks_B were plotted against mini-domain concentration C. By using the relations $ks_A = k_{onA}C + k_{offA}$ and $ks_B = k_{onB}C + k_{offB}$ the k_{on}-rates for the parallel associations were found from the slope of a linear fit of ks_A or ks_B against C. The k_{on} - rate which had its largest value, i.e. the fastest rate-constant (k_{onA} extracted from ks_A), was used for further calculation. The off-rates were determined for the two component interaction (parallel dissociation of two complexes) from the following:

$$R = R_D \exp(-k_{offA}\, t) + R_E \exp(-k_{offB}\, t) \quad (5.6)$$

R_D and R_E are the contributions of each component to the total response at the start of dissociation. However, only the fitted k_{offA} and k_{offB} were further used by specifying the start of dissociation at $t = t_0$. Again, the k_{off} - rate which had its largest value, i.e. the fastest off-rate (k_{offA}), was used for further calculation. The dissociation constants were determined from the relation $K_D = k_{off}/k_{on}$.

5.6 Molecular Modelling.

Modelling and analysis were performed on Silicon Graphics Indy or Hewlett Packard Apollo (series 700) computers using Insight II 95.0 Molecular Modelling and Discover 2.9.0 programs (Biosym/MSI, San Diego).

Chapter 6. Short Elastin-like Peptides Exhibit the Same Temperature Induced Structural Transitions as Elastin Polymers: Implications for Protein Engineering[1].

6.1 Introduction

Elasticity of the vascular cell wall is mediated by polymeric peptide sequences that are capable of undergoing viscoelastic transitions. Several repeating sequences have been described for the elastin precursor protein, tropoelastin. In order of their frequency of occurrence they are the pentapeptide VPGVG, the hexapeptide APGVGV, the nonapeptide VPGFGVGAG and the tetrapeptide VPGG (Sandberg *et al.*, 1985; Yeh *et al.*, 1987). In elastin, the most frequent pentapeptide sequence, VPGVG, recurs up to 50 times in a single molecule. Synthetic polymers of (VPGVG)n where n can be as high as 150, are soluble in water below 25° C but above 25° C undergo a phase transition to a viscoelastic state consisting of about 50% peptide and 50% water by mass. This transition is accompanied by a contraction to less than one half the extended length of the polymer releasing sufficient energy in the process to lift a mass 1000 times the mass of the polymer itself (Urry, 1993). The presently accepted mechanism of this contraction involves a transition from an extended state at temperatures below the transition temperature, T_M, to an ordered β-spiral above the T_M with three VPGVG units, each forming a type II β-turn, per turn of the spiral (Urry, 1988a,b). This is a rare example of an inverse temperature transition during which a protein becomes more ordered at the higher temperature. The transition and the structural features of the ordered, higher-temperature form have been studied by CD (Urry *et al.*, 1985), NMR (Renugopalakrishnan *et al.*, 1978b), and x-ray crystallography (Cook *et al.*, 1980 - studied a cyclic trirepeat of VPGVG). These physical studies are consistent with the proposed type II β-turn in which the collapse to the spiral state is driven by dehydration of the hydrophobic valine side-chains. The temperature at which

[1] Note. This chapter contains additional material to that published by Reiersen *et al.* (1998) attached in appendix..

this transition occurs can be manipulated by varying the composition of the polymer (VPGXG)n and the T_M depends both on the nature of residue X and the value of n. In addition, T_M has been shown to be sensitive to pH, ionic strength, pressure and covalent modifications such as phosphorylation (Urry, 1993).

Despite extensive characterisation of such polymers the minimum viscoelastic unit has not been defined. In particular, the relative contributions to the viscoelastic state of the intrinsic propensity of VPGVG units to form type II β-turns, and any co-operative interactions between the β-spiral turns (n = 3), have not been determined.

In this study we examine the thermodynamic behaviour of single and multiple units of the VPGVG sequence using CD to monitor the previously well characterised formation of the type II β-turn structure, and we demonstrate that the polymer behaviour surprisingly can be reproduced by a single VPGVG unit. This has opened up the exciting possibility of engineering temperature and pH switch sequences of non-disruptive lengths into existing proteins.

6.2 Materials and Methods

6.2.1 Peptide Synthesis and Purification.

Peptides were synthesised with solid-phase Fmoc chemistry and purified on reverse phase HPLC as described in chapter 5.2. The purified peptides were characterised by HPLC, electrospray ionisation mass spectrometry and amino acid analysis (chapter 5.3).

6.2.2 Circular Dichroism Studies.

CD spectra were recorded on a Jobin-Yvon Model CD6 Dichrograph Instrument as described in chapter 5.4.

6.2.3 Thermodynamic Analysis.

The free energy of the transition into the folded form at higher temperatures was fitted to a macroscopic, reversible, two-state model (equation (6.1) below) using the observed CD-data, $[\theta]^{obs}$ and temperature, T:

$$\Delta G_{U\rightarrow F} = -RT \ln[([\theta]^{obs} - [\theta]^{U})/([\theta]^{F} - [\theta]^{obs})] \quad (6.1)$$

The endpoints for the transition (high temperature folded form, $[\theta]^{F}$, and low temperature unfolded form $[\theta]^{U}$) together with Δ H and Δ S, were initially fitted using equations (6.2) and (6.3), or equations (6.2) and (6.4) for the 18- 28 mer peptides. Equation (6.4) takes into account the slope effect (m) and off-axis adjustment (off) for transitions which have a slope in the pre- and postfolding base lines.

$$\Delta G_{U\rightarrow F} = \Delta H_{U\rightarrow F} - T\Delta S_{U\rightarrow F} \quad (6.2)$$

$$[\theta]^{obs} = ([\theta]^{U} + [\theta]^{F} \times \exp-(\Delta G_{U\rightarrow F}/RT))/(1 + \exp-(\Delta G_{U\rightarrow F}/RT)) \quad (6.3)$$

$$[\theta]^{obs} = ([\theta]^{U} + [\theta]^{F} \times \exp-(\Delta G_{U\rightarrow F}/RT))/ (1 + \exp-(\Delta G_{U\rightarrow F}/RT)) + m \times T + off \quad (6.4)$$

The data were further analysed using Grafit software (Leatherbarrow, 1989), and van't Hoff plots were constructed (plot of lnK *versus* 1/T where $K = ([\theta]^{obs} - [\theta]^{U})/([\theta]^{F} - [\theta]^{obs})$ utilising the data from CD, $[\theta]^{obs}$, and the previously fitted endpoints for transition, $[\theta]^{U}$ and $[\theta]^{F}$. In some cases where the inital free fit gave a lower linear correlation coefficient ($r < |-0.90$ to $-0.93|$) for the van't Hoff plot, the data were refitted using the initial fitted values for endpoints and starting points and fixing either $[\theta]^{U}$ or $[\theta]^{F}$, or both $[\theta]^{U}$ and $[\theta]^{F}$. This resulted in correlation coefficients closer to -1. A new fit of ΔH and ΔS was found from equations (6.2)-(6.4) by fixing $[\theta]^{U}$ and $[\theta]^{F}$ from the best vant't Hoff plot. The transition temperature, T_m, for all peptides was calculated using the relation $T_m = \Delta H/\Delta S$.

6.3 Results

6.3.1 Design of Short Elastin Peptides.

In this study short elastin peptides were designed to test the effect of sequence variations on the conformational transitions observed. Of specific interest was the effects of charge adjacent to the elastomeric units, studied using both uncapped peptides at various pH values and capped peptides carrying N-acetylation or C-amidation, or both. In these short peptides, the effect of adding an extra glycine at the N-termini of 8-mers was also investigated (Figure 6.1, A-H).

A:	*H*-GVG(VPGVG)-NH_2	**E:**	Ac-GVG(VPGVG)-NH_2
B:	*H*-GVG(VPGVG)-*OH*	**F:**	Ac-GVG(VPGVG)-*OH*
C:	*H*-*G*GVG(VPGVG)-NH_2	**G:**	Ac-*G*GVG(VPGVG)-NH_2
D:	*H*-*G*GVG(VPGVG)-*OH*	**H:**	Ac-*G*GVG(VPGVG)-*OH*
I:	Ac-GVG(VPGVG)(VPGVG)(VPGVG)*ILG*-NH_2		
J:	Ac-G*KL*(VPGVG)(VPGVG)(VPGVG)*ILG*-NH_2		
K:	Ac-G*KL*(VPGVG)(VPG*E*G)(VPGVG)*ILG*-NH_2		
L:	Ac-GVG(VPGVG)(VPGVG)(VPGVG)-NH_2		
M:	Ac-GVG(VPGVG)(VPGVG)(VPGVG)*L*-NH_2		
N:	Ac-GVG(VPGVG)(VPGVG)(VPGVG)*IL*-NH_2		
O:	Ac-GVG(VPGVG)(VPGVG)(VPGVG)(VPGVG)(VPGVG)-NH_2		

Figure 6.1 Sequences of Short Homologous Elastin Based Peptides.

Sequences of short elastin peptides with different composition were synthesised by solid-phase Fmoc chemistry (chapter 5.2). Deviations from the sequence Ac-GVG(VPGVG)n-NH_2 (n = 1, 3, 5) are shown in red. Ac-, acetyl; -NH_2, amide.

In order to test if there was any correlation between the number of elastomeric (-VPGVG-) units present and the T_M for turn formation, we also synthesised an 18-mer peptide (3 VPGVG units) and a 28-mer peptide (5 VPGVG units) (Figure 6.1, L,O). To measure the influence on T_M of increased hydrophobicity adjacent to the elastomeric unit, additional leucine and isoleucine residues were introduced stepwise at the C-terminus of the 18-mer peptides (Figure 6.1, I-K,M,N). The effects of internal charged residues adjacent to, or within, the elastomeric

sequences were also studied. In one design a lysine flanked by a leucine was placed close to the N-terminus (Figure 6.1, J) while in a second design a glutamic acid residue was also added replacing one of the two valines of an elastomeric unit (Figure 6.1, K).

6.3.2 Peptide Synthesis and Characterisation.

The peptide synthesis was completed with more than 95 % efficiency at each step. The masses of the resin before and after synthesis were compared (Table 6.1).

Table 6.1 Estimating Potential Yield of Crude Peptides by Comparing Resin Masses.

Peptide	Mass of resin with peptide *after* synthesis	Initial theoretical mass Of resin *before* synthesis[1]	Peptide yield on resin[2]
A	0.165 g	0.208 g	No
B	0.122 g	0.156 g	No
C	0.188 g	0.208 g	No
D	0.130 g	0.156 g	No
E	0.220 g	0.208 g	12 mg
F	0.161 g	0.156 g	5 mg
G	0.191 g	0.208 g	No
H	0.160 g	0.156 g	4 mg
I	1.006 g	0.833 g	173 mg
J	1.030 g	0.833 g	197 mg
K	1.036 g	0.833 g	203 mg
L	0.975 g	0.833 g	142 mg
M	0.982 g	0.833 g	149 mg
N	1.000 g	0.833 g	167 mg
O	1.095 g	0.833 g	262 mg

[1]For the short peptides A-H: initially 0.1 mmol of PAL-PEG-PS (0.12 mmol/g) or 0.833 g and 0.625 g of Gly-PEG-PS (0.160 mmol/g) were used to synthesise GVGVPGVG. Then half of each resin was continued incorporating an extra glycine (**G**GVGVPGVG). Finally, each resin (now with GVGVPGVG and GGVGVPGVG peptides) was again split into two parts, one to be acetylated and the other not. This gives a theoretical start amount of resin as described above.

[2]The peptide yield on the resin was calculated by subtracting the theoretical dry resin mass without peptide before synthesis from the dry mass of resin after peptide synthesis.

As Table 6.1 illustrates, the final masses of resins for the short peptides A-H were less than at the start of synthesis. This may have been due to inaccurate initial weighing, or loss of resin during division (as described in Table 6.1) and preparation steps. In addition, the very low molecular masses of the short peptides (around 500 Da) do not contribute much to increased resin-mass. The possibility exists that there was a failure in chain elongation, although the large increase in masses of the resins after synthesis of the longer similar peptides I-O using same chemistry, make this improbable. Aliquots of resin with peptides were trial cleaved and deprotected from their resins and sampled by analytical HPLC. For peptides D and E, 50 mg of resin was added to 1 ml of reagent R with scavengers, and aliquots of supernatant were washed into ethers after each 2nd hour (Chapter 5.2.4). The peptides were completely dissolved in 4.5 % (v/v) acetonitrile in 0.1 % TFA in water. This verified that the hydrophobic peptides were soluble in near aqueous solution, observed for all the peptides in this study. On analytical HPLC, a major peak was detected at 214 nm for D and E eluting at 18.9 % acetonitrile in 0.1 % TFE (Table 6.2). This is in contrast to the negative yield obtained by weighing the resins (Table 6.1).

Table 6.2 Cleavage Time of Peptides From Resins - Small Scale Trials.

Peptide	HPLC eluted at 214 nm (%, v/v acetonitrile in 0.1 % TFE)	Major HPLC peak height (in a.u. of $A_{215\ nm}$) after: 2 hours	4 hours	6 hours
D	18.9 %	0.20	0.24	0.25
E	18.9 %	0.65	>0.8	>0.8
I	33.3 %	0.71	>0.8	>0.8
J	32.4 %	0.75	>0.8	>0.8
K	30.6 %	0.76	>0.8	>0.8

The peaks of D and E (and also the longer peptides I-K which additionally contain protecting groups on lysine and glutamic acid) increased in height with increasing cleavage time and plateaued after 4 hours (Table 6.2). Another test to study the effect of deprotection/cleavage without scavengers was implemented for

peptide G. Mixture R with scavengers was replaced with 90 % (v/v) TFE in water. However, cleavage in TFE/water alone gave a much lower yield than reagent R after 4 hours incubation (comparing HPLC peaks). A minimum time of four hours of cleavage in reagent R was thus implemented for all the elastin peptides.

After cleavage/deprotection the peptides were purified on preparative HPLC as described in chapter 5.2.6 and fractions were analysed as described on chapter 5.2. The yields of the purified peptides are presented in Table 6.3.

Table 6.3 Peptide Yields After Deprotection and HPLC-purification.

Peptide	Crude peptide (mass of resin)	Peptide yield after purification (mass of crude peptide)	Yield (%) (pure/crude peptides)
A	17.4 mg (0.165 g)	12.0 mg (17.4 mg)	69
B	6.9 mg (0.122 g)	3.0 mg (6.9 mg)	43
C	19.8 mg (0.188 g)	14.2 mg (19.8 mg)	72
D	2.5 mg (0.079 g)	0.9 mg (2.5 mg)	36
E	14.5 mg (0.169 g)	8.4 mg (14.5 mg)	58
F	7.8 mg (0.162 g)	2.5 mg (7.8 mg)	32
G	19.4 mg (0.171 g)	15.4 mg (19.4 mg)	79
H	11.1 mg (0.160g)	6.9 mg (11.1 mg)	62
I	224.9 mg (0.956 g)	76.5 mg (100.6 mg)	76
J	243.3 mg (0.980 g)	83.0 mg (100.0 mg)	83
K	241.3 mg (0.986 g)	83.7 mg (100.0 mg)	84
L	197.5 mg (0.975 g)	75.4 mg (100.0 mg)	75
M	186.8 mg (0.982 g)	76.1 mg (100.0 mg)	76
N	208.4 mg (1.000 g)	82.4 mg (100.0 mg)	82
O	281.1 mg (1.095 g)	86.6 mg (100.0 mg)	87

The yield of the purification was much better when purifying more than 15 mg of peptide (yield: 70-80 %) than for small quantities of 2-8 mg of peptides (yield: 30-40 %) (Table 6.3).

Fractions from preparative HPLC were analysed on analytical HPLC and identified as single peaks, pooled, freeze dried and submitted for electrospray ionisation mass spectrometry (chapter 5.3.2). The m/z ratio for all peptides are given in Table 6.4.

Table 6.4 Electrospray Ionisation Mass Spectrometry of Purified Peptides.

Peptide	Calculated mass of peptide (Da)	ESI-MS mass (m/z)- average mass in bold script
A	639.4	**639.2** - 640.1(100 %) - 300.9 (10 %) - 339.4 (15 %).
B	640.3	**640.3** - 641.4 (100 %) - 301.1 (10 %) - 340.1 (18 %).
C	696.4	**696.0** - 697.2 (100 %) - 300.9 (15 %) - 367.9 (22 %).
D	697.5	**697.3** - 698.4 (100 %) - 301.1 (20 %) - 368.6 (25%).
E	682.4	**681.0** - 682.1 (100 %) - 360.5 (50 %) - 701.1 (20 %) - 1364.0 (8 %) - 1383.5 (7 %).
F	682.2	**682.3** - 683.4 (100 %) - 301.1 (40 %) - 361.1 (90 %) - 702.4 (20 %) - 721.3 (22 %).
G	738.4	**738.0** - 739.2 (100 %) - 300.9 (30 %) - 388.9 (90%) - 758.2 (15 %).
H	739.4	**739.1** - 740.2 (100 %) - 389.4 (95 %) - 300.9 (80%) - 759.2 (20 %) - 778.3 (20 %).
I	1785.2	**1784.2** - 1784.1 (1+; H; 60 %) - 912.0 (2+; K + H; 95 %) 904.0 (2+;Na + H;15 %) - 893.0 (2+;H) - 924.5 (2+; 904.1 Na + K; 20 %) - 1822.1 (1+; K; 95%) - 1807.1(1+; Na;15%).
J	1870.3	**1870.2** - 1869.5 (1+; H, 50 %) - 1891.5 (1+; Na; 15 %) - 1907.6 (1+; K; 95 %) - 1922.2 (2+; Na + Na; 10 %) - 1932.6 (2+; Na + K; 20 %) -935.6 (2+; H; 60 %) - 946.6 (2+; Na + H; 20 %) - 954.6 (2+; K + H; 30 %) - 636.7 (3+; K + 2H; 95 %) - 645.0 (3+; Na + K + H; 15 %).
K	1900.3	**1899.0** - 1899.3 (1+; H; 85 %) - 1922.3 (1+; Na; 13 %)- 1937.2 (1+; K; 95 %) - 1962.4 (2+; Na + K; 20 %) - 950.6 (2+; 2H; 95 %) - 969.6 (2+; K + H; 20 %) - 960.1 (2+; Na + H; 10 %) - 646.7 (3+; K + 2H; 95 %) - 655.0 (3+; K + Na + H; 20 %).
L	1501.8	**1499.9** - 1500.5 (1+; H; 100 %) - 1538.6 (1+; K; 75 %) - 1522.6 (1+; Na; 15 %) - 769.8 (2+; K + H; 95 %) - 750.8 (2+; 2H; 80 %) - (2+; Na + H; 15 %) - 781.8 (2+; Na + K; 15 %).
M	1614.9	**1612.9** - 1613.7 (1+; H; 70 %) - 1635.7 (1+; Na; 15 %) - 1651.7 (1+; K; 95 %) - 826.3 (2+; K + H; 95 %) - 807.3 (2+; 2H; 85 %) - 818.3 (2+; Na + H; 20 %) - 838.9 (2+; Na + K; 15 %).
N	1728.1	**1726.0** - 1726.8 (1+; H; 95 %) - 1748.6 (1+; Na; 55 %) - 1764.7 (1+; K; 95 %) - 864.4 (2+; 2H; 95 %) - 883.3 (2+; K + H; 75 %) - 893.9 (2+: Na + K; 15 %).

Table 6.4 continues on the next page.

Table 6.4 continued.

Peptide	Calculated mass of peptide (Da)	ESI-MS mass (m/z)- average mass in bold script
O	2320.8	**2321.3** - 2319.7 (1+; H; 60 %) - 2341.8 (1+; Na; 15 %) - 2357.7 (1+; K; 70 %) - 2381.6 (2+; Na + K; 15 %) - 2401.7 (2+; K + K; 95 %) - 1160.5 (2+; 2H; 95 %) - 1180.4 (2+; K + H; 85 %) - 1193.4 (2+; K + Na; 20 %) - 774.2 (3+; 3H; 60 %) - 787.0 (3+; K + 2H; 75 %) - 600.1 (4+; 2K + 2H; 40 %) - 409.2 (6+;2Na + 2K + 2H;40 %) - 301.2 (8+; 2K + 6H; 95%).

The major peaks (> 10 % intensity) from the m/z spectra are reported. The percentage given in parentheses for each mass is the relative intensity to each other. For peptides I-O ionisation patterns are suggested for the observed peaks. The average peptide mass reported in bold script was calculated from the different m/z - spectra.

The expected molecular masses were obtained for all 15 peptides synthesised. Other major peaks were also detected, but these were only due to adducts formed with potassium (mass 39.0) and sodium ions (mass 23.0) under the ionisation process (Burdick & Stults, 1997). The mass of peptide A (639.4 Da) can be verified from the $[\text{peptide A} + H]^+$ of 640.1 Da by subtracting the proton giving 639.1 Da, and also from adding the fragmented species 300.9 + 339.3. Likewise, peptide F (682.2 Da) was identified by $[\text{peptide F} + H]^+$ of 683.4 Da and the fragmented species of 361.1 Da which is $[\text{peptide F} + K^+ + H^+]^{2+}/2 = 361.1$ Da. The species of 721.2 Da is formed by $[\text{peptide F} + K^+]^+$ alone = 721.2 and the 702.4 Da peak possibly represents the $[2\text{x peptide F} + K^+ + H^+]^{2+}/2$ adduct = 702.2 Da. Double peptide masses from adducts were positively identified for peptide E. The masses for the longer peptides can similarly be found alone or as sodium or potassium adducts, and proposed ionisations are suggested in Table 6.4.

Quantitative amino acid analysis was also carried out from stock solutions of peptides in deionised water (chapter 5.3.3), originally prepared for circular dichroic experiments, and the results are described in Table 6.5.

Table 6.5 Amino Acid Analysis of Elastin Peptides.

Peptide	Amino acid composition: amino acid type, experimental value [expected composition].
A	Pro, 0.94 [1]; Gly 4.04 [4]; Val, 2.44 [3].
B	Pro, 1.05 [1]; Gly, 4.22 [4]; Val, 2.53 [3].
C	Pro, 0.92 [1]; Gly, 5.31 [5]; Val, 2.67 [3].
D	Pro, 0.90 [1]; Gly, 5.15 [5]; Val, 2.54 [3].
E	Pro, 0.95 [1]; Gly, 4.29 [4]; Val, 2.63 [3].
F	Pro, 0.88 [1]; Gly, 4.36 [4]; Val, 2.65 [3].
G	Pro, 1.01 [1]; Gly, 5.20 [5]; Val, 2.66 [3].
H	Pro, 0.95 [1]; Gly, 5.06 [5]; Val, 2.53 [3].
I	Pro, 3.74 [3]; Gly, 8.24 [9]; Val, 5.68 [7]; Ile, 1.13 [1]; Leu, 1.27 [1].
J	Pro, 3.52 [3]; Gly, 7.39 [8]; Val, 4.84 [6]; Ile, 1.03 [1]; Leu, 2.24 [2]; Lys, 1.21 [1].
K	Pro, 3.25 [3]; Gly, 7.98 [8]; Val, 4.32 [5]; Ile, 0.88 [1]; Leu, 1.97 [2]; Lys, 1.09 [1]; Glu, 1.17 [1].
L	Pro, 3.80 [3]; Gly, 7.65 [8]; Val, 5.66 [7].
M	Pro, 3.43 [3]; Gly, 6.96 [8]; Val, 5.06 [7];Leu, 1.25 [1].
N	Pro, 3.53 [3]; Gly, 7.80 [8]; Val, 5.87 [7];Ile, 1.03 [1]; Leu, 1.19 [1].
O	Pro, 5.82 [5]; Gly, 12.22 [12]; Val, 9.13 [11].

The values are the median of two independent amino acid analyses.

The amino acid analysis mainly verified the composition of the peptides. However, the values for valines in all peptides were less than expected. It is well known that sequences containing valine are very difficult to completely hydrolyse in just 24 hours at 110° C, and for these sequences it may be necessary to increase hydrolysis time to 72 hours (Blackburn, 1968; Ozols, 1990). The C-terminal and N-terminal residues Lys, Ile, and Leu in peptides I-K, M and N display their expected composition, acting as 'internal controls' of the amino acid analysis, and strongly suggest that the composition is from a single species.

6.3.3 CD Analysis of Peptides.

The raw CD spectra of the short elastin peptides were very noisy, and it was necessary to lower the noise by sampling data from repeated scans (as described in chapter 5.4). Figure 6.2 displays the noise level from a repetitive scan of the short

peptide E before and after smoothing the data using the Savitzky-Golay algorithm[2] (chapter 5.4.3). This smoothing algorithm was used for all scans to reduce noise.

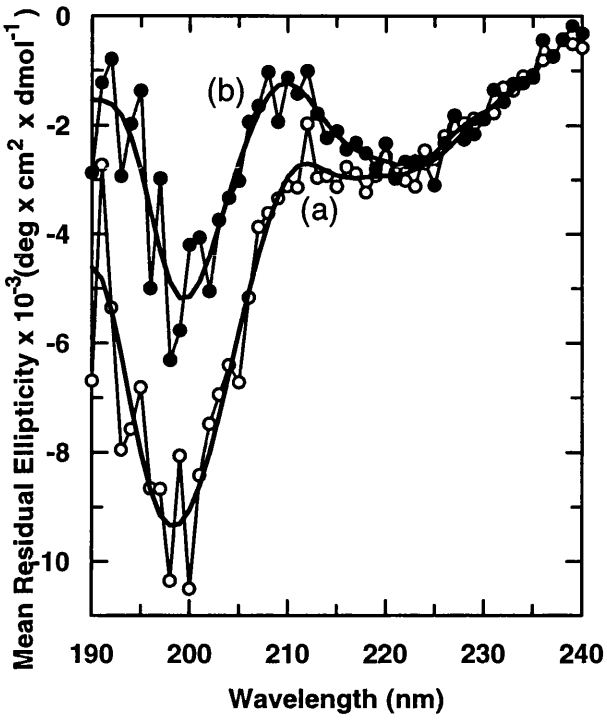

Figure 6.2 Raw and Smoothed Data of Peptide E.

Peptide E (38.7 μM) in 10 mM borate buffer pH 9.5 was scanned at (a) +5.7° C and at (b) 57.8° C in a 0.2 cm quartz cuvette. The raw data (open and closed circles) are the average of 5 scans (integrated for 1s at each wavelength, slit 2.0) , and were smoothed using Savitzky-Golay algorithm of the Jobin-Yvon software (bold line).

CD spectra of the 9-mer peptide D at various temperatures are shown in Fig 6.3a. For comparison, spectra of the 18-mer peptide L are shown in Figure 6.3b. All other short and longer peptides showed a similar CD profile. The global minimum varied slightly with pH but was typically within the range 198-200 nm - as has been previously found for unordered peptides (Woody, 1995). For the short peptides at +1° C the minimum mean residual ellipticity was -7,000 to -10,000 deg cm^2 dmol^{-1} compared to -40,000 deg cm^2 dmol^{-1} for an ideal random coil. This is within the same range (-5,000 to -16,000 deg cm^2 dmol^{-1}) previously seen for the longer (VPGG)n and the (VPGVG)n elastin polymers (Urry *et al.*, 1986; Urry *et*

[2] The Savitzky-Golay algoritm fits the data to a polynomial function.

al., 1985). The corresponding values for the 18-21-mer peptides (I-O) were -17,000 to -19,000 deg cm^2 $dmol^{-1}$. This suggests, somewhat surprisingly, that the shorter peptides are less disordered at low temperatures than the longer peptides. The MRE values of the short peptides are in fact within the range expected from an equimolar mixture of random coil and type II β-turns (Perczel *et al.*, 1993).

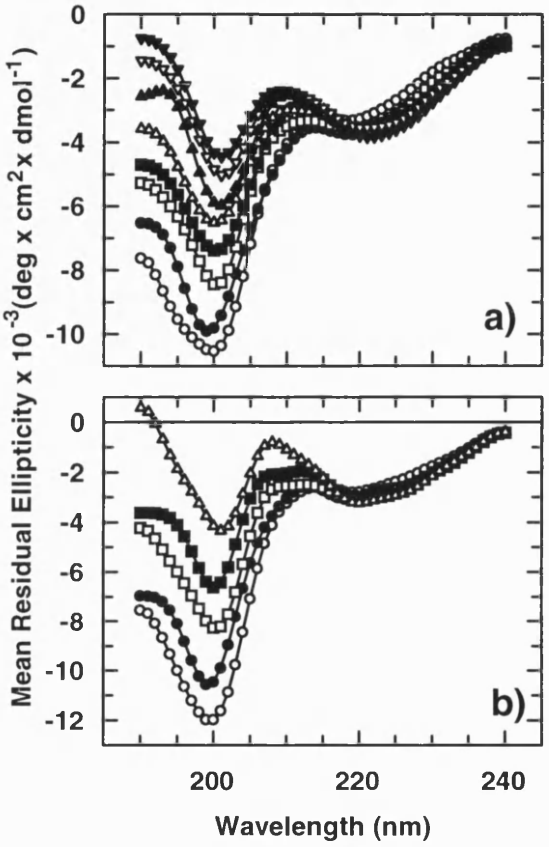

Figure 6.3 CD Wavelength Scans of Peptides D and L at Different Temperatures.

The peptides were scanned in 10 mM phosphate buffer (pH 7.0). **a)** Peptide D (49.1μM) was recorded at (-○-), 1.1° C; (-●-), 15.4° C; (-□-), 25.0° C; (-■-), 34.5° C; (-△-), 43.8° C; (-▲-), 53.0° C; (-▽-), 63.0° C; and (-▼-), 81.5° C. **b)** Peptide L (20.7μM) was scanned at 1.3° C (-○-); 15.4° C (-●-); 34.0° C (-□-); 48.4° C (-■-); and 76.6° C (-△-).

For all peptides, the CD amplitudes at 195-205 nm decreased with increasing temperature, with a smaller decrease in amplitude at 206-212 nm. A positive peak in this latter region is characteristic of type II β-turns (Perczel *et al.*, 1993; Urry *et*

al., 1985; Woody, 1995). A near isodichroic point around 218 nm was found for the short peptides in the reported transition. This was seen both for the effect of increasing concentrations of TFE (data not shown, but see chapter 7, Figure 7.1) which induces a type II β-turn, and for the temperature effect described in Figure 6.3a and b. A near isodichroic point for melting of the larger elastin polymer has previously been detected by Urry (1988a) around 220 nm. However, some peptides showed little change in position of minima/maxima when the temperature is varied and the spectroscopic changes in these are dominated by changes in intensity. For peptide K, which has the most heterogeneous composition (Figures 6.1 and 6.4), an increase in amplitude at 210-230 nm was observed with a local minimum at 222 nm (with an approximate isodichroic point around 208 nm). These were also found at higher temperatures for some short peptides with the N-terminal GGVG sequence (see Figure 6.1, C,D and G). These spectra resemble class C-spectra associated with helical or type I/III β-turn structures (Figure 6.4).

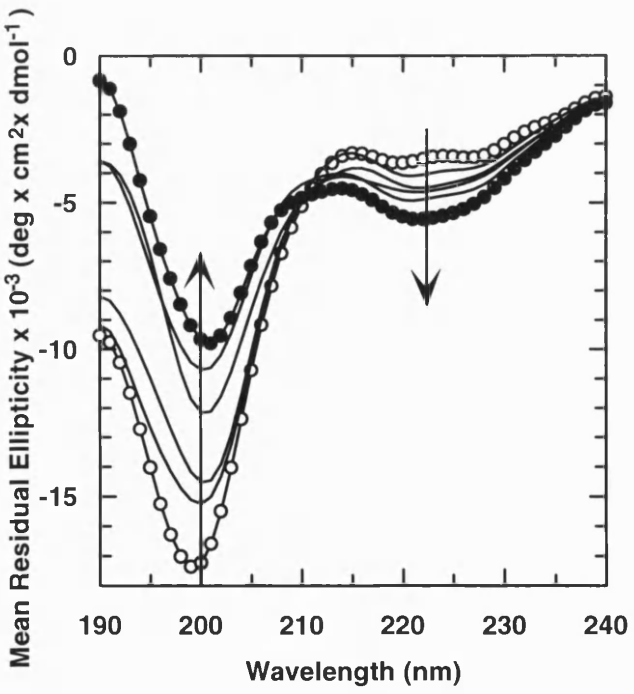

Figure 6.4 CD-wavelength Scans of Peptide K at Different Temperatures.

Peptide K (16.2 μM) in 10 mM phosphate buffer pH 7.0 was scanned in a 0.2 cm quartz cuvette by increasing temperature from 10.8° C (—o—) via 20.1° C, 29.4° C, 48.4° C and 62.2° C until 76.6° C (—●—) in the direction of the arrow. Each spectrum is the average of 10 scans integrated for 1 s at each wavelength.

The transition curves of the short peptides D, E, H in phosphate buffer, peptides C, D and G in different buffers, and for the longer peptides J, L and N at pH 7 are shown in Figure 6.5 a to c.

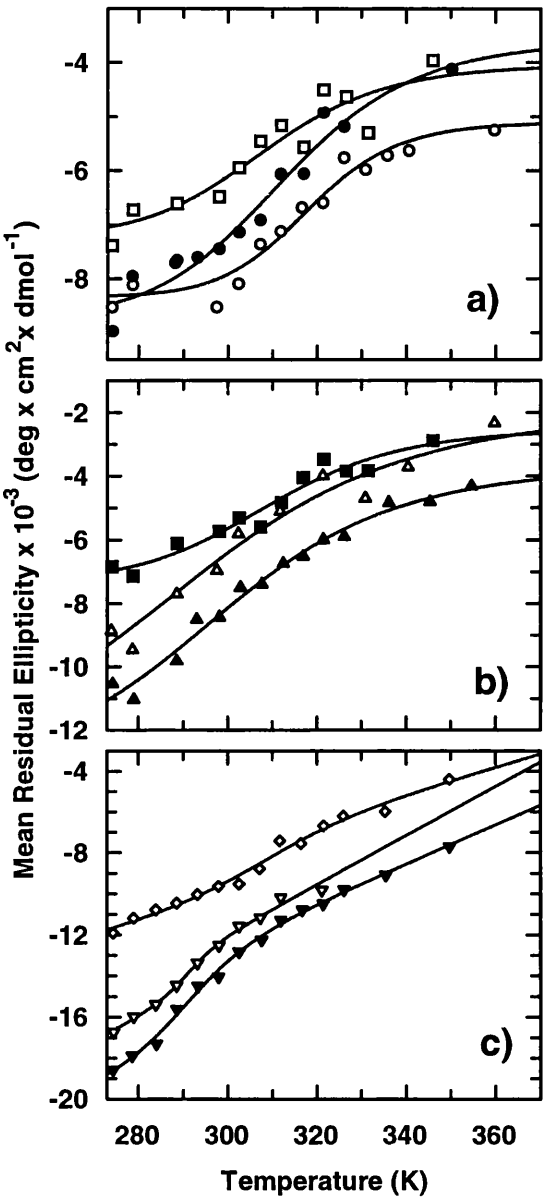

Figure 6.5 Melting of Short and Long Elastin Peptides.

The 8- or 9-mer peptides C (37.1 μM), D (49.1 μM), E (38.5 μM), G (41.8 μM) and H (31.3 μM) and the longer peptides J (16.4 μM), L (20.7 μM) and N (17.9 μM) were scanned from 190-240/260 at different temperatures in 10 mM acetate or borate buffers (panel **a**), or in 10 mM phosphate buffer (panels **b** and **c**), and the mean residual ellipticity at or close to 200 nm was plotted versus temperature. van't Hoff fits are also shown.

Figure legend continues next page.

Figure 6.5 continued.

The 8- or 9-mer peptides C (37.1 μM), D (49.1 μM), E (38.5 μM), G (41.8 μM) and H (31.3 μM) and the longer **(a)** Melting of the 9 mer peptides C (○ , at 201 nm, pH 4.0), D (● , at 200 nm, pH 9.5) and G (□ , at 201 nm, pH 9.5); **(b)** Melting of the 8-9 mer peptides H (■ , 202 nm), E (▲ , 199 nm) and D (▲ , 200 nm); **(c)** Melting of the 18-21 mer peptides N (▽), J (▼) and L (◇) at 199 nm.

The start of the transition was initially fitted for each melting curve, although well defined transitions were obtained for the majority of peptides. The transition range for all the 8/9-mer peptides (A-H) was 3-5,000 MRE units increasing to 5-10,000 for the longer peptides I-O (Figure 6.5). These values are similar to those reported for the longer elastin polytetrapeptide (VPGG)n, though a little lower than for the polypentapeptide (VPGVG)n which undergoes a change of 16,000 MRE units during a transition (Urry et al., 1985, 1986).

6.3.4 Thermodynamic Analysis.

In order to obtain thermodynamic data from the melting curves, a selection of short and longer peptides (C, E, L and N) were tested for reversibility by incubation for 30 minutes at +70° C and then rapid cooling to +20° C. All were found to be fully reversible (Figure 6.6a). The concentration dependence was also tested on peptide L (18-mer) and on the most hydrophobic short peptide E (8-mer) at two different temperatures (Figure 6.6bc). In all cases ellipticities were found, within the limit of experimental error, to be independent of peptide concentration over this temperature range. This observation shows that the temperature-induced formation of the β-turn is due to intramolecular interactions rather than intermolecular associations. The melting curves reported here were obtained at peptide concentrations 10-20 times lower than the maximum concentrations shown in Figure 6.6c (around 18 μM for the longer peptides and below 50 μM for the shorter peptides).

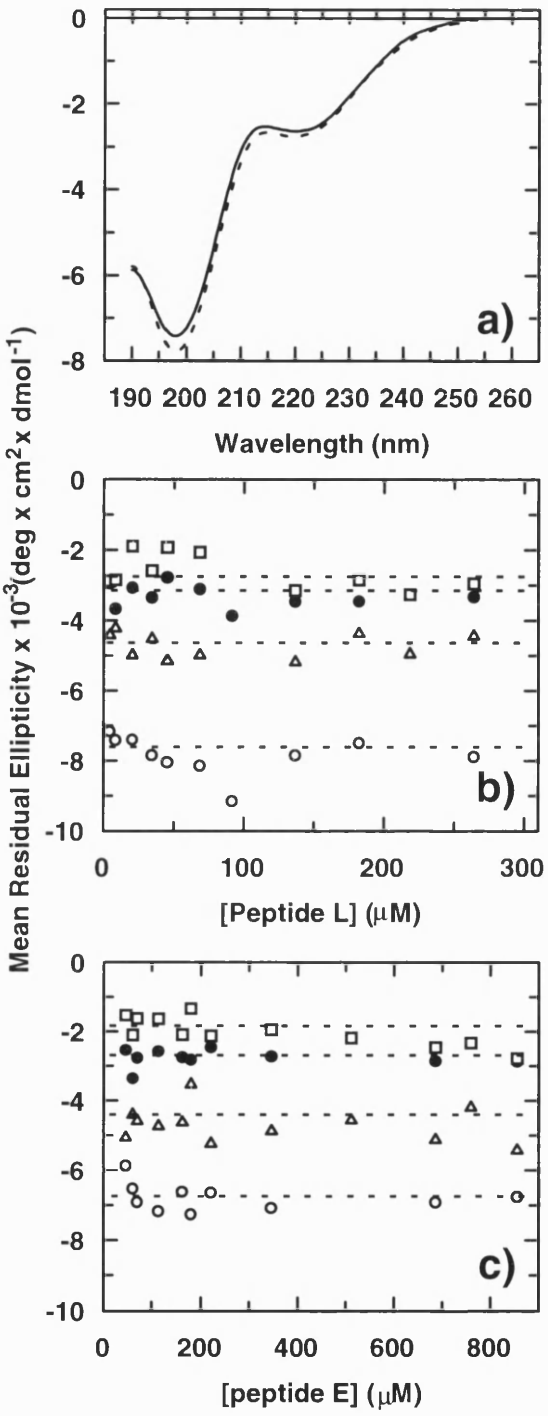

Figure 6.6 Test of Reversibility and Concentration Dependence at pH 7.0.

a) Scans of the 18-mer peptide L (91 μM in 10 mM phosphate buffer; 0.5 mm cuvette; spacing 0.5 nm; four scans each with one second integration time) at 20.6° C before heating (——) and after incubation at 70° C for 30 minutes with rapid cooling back to 20.6° C (- - - -). The concentration-dependence of MRE is shown in **b** and **c**. The concentration of peptide L was varied from 4.6 μM to 264 μM **(b)** using different quartz cuvettes (0.5 mm, 2 mm and 10 mm), and similarly the 8-mer peptide E was varied between 45 μM and 855 μM **(c)**. The variation of mean residual ellipticity for peptide L at 15.5° C or peptide E at 15.6° C (at 199 nm, ○ ; and at 210 nm, ●) and for peptide L at 62.5° C or peptide E at 48.3° C (at 199 nm, △ ; and at 210 nm, □) is shown.

Data were fitted to van't Hoff plots and were linear. Where a low signal-to-noise ratio in the CD-measurements resulted in a larger spread of data, a better fit was obtained by fixing one or both endpoints for the transition (Figure 6.7).

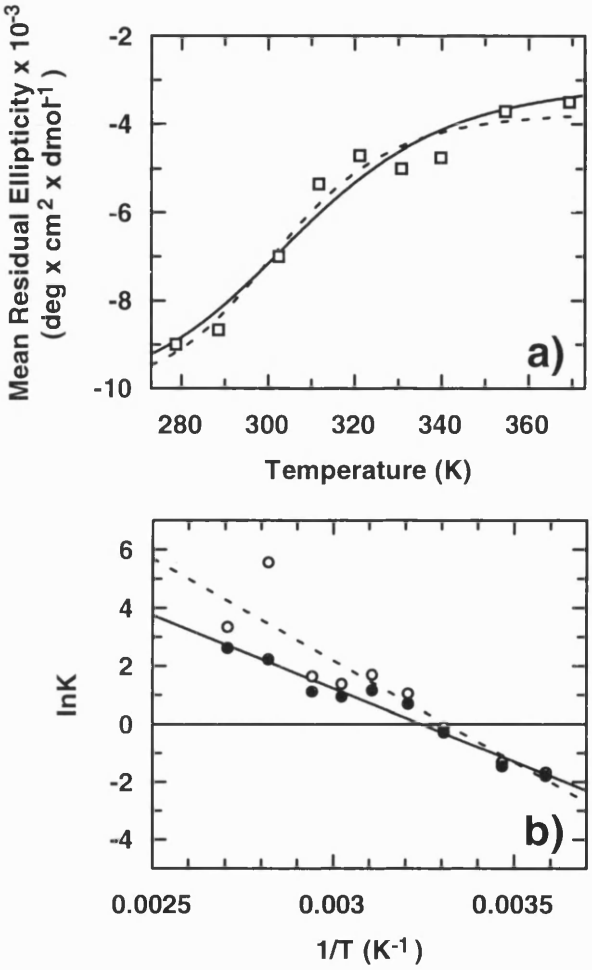

Figure 6.7 Fitting of the Melting Curve of Peptide B in 10 mM Phosphate Buffer pH 7.0.

The CD-data at 199 nm (□) were fitted to a macroscopic, reversible, two-state model by optimising the linearity of the correlated van't Hoff plot. By using the fitted endpoints for the transition, $[\theta]^F$ and $[\theta]^U$, from the initial model (panel **(a)**, - - - -) the corresponding van't Hoff plot was constructed (panel **(b)**, ○ , - - - -) and gave a linear correlation coefficient (r) of -0.91. After fixing $[q]^F$, the correlation coefficient for the van't Hoff plot improved to -0.98. The data with the correlation line (● , ———) and its corresponding fit for data of MRE against temperature with fixed $[q]^F$ (———) are respectively shown in panel **(b)** and panel **(a)**.

Energies from fits. Model with free $[\theta]^F$ and $[\theta]^U$ (- - - -): $\Delta H = 13.7 \pm 6.6$, $\Delta S = 0.045 \pm 0.021$; Model with fixed $[\theta]^F$ (———) : $\Delta H = 10.4 \pm 1.4$, $\Delta S + 0.034 \pm 0.004$.

Fitting of the CD data to the van't Hoff equation allowed calculation of ΔH, ΔS and T_M-values for the transitions of most peptides. However, due to the uncertainty of the start of the transition for some short peptides (Fig 6.5 b) only those with well defined transition curves are reported (Table 6.6). It was not possible to determine melting temperatures for two of the longer peptides, K and O.

Table 6.6 Thermodynamic Values for Thermal Transitions in Elastin Peptides.

Peptide	pH	T_M (° C)	$\Delta H_{U\rightarrow F}$ (kcal mol^{-1})	$\Delta S_{U\rightarrow F}$ (kcal $mol^{-1} K^{-1}$)
A	7.0	41	11.0 ± 2.7	0.035 ± 0.009
B	9.5	35	14.9 ± 4.9	0.048 ± 0.016
C	4.0	45	20.0 ± 2.9	0.063 ± 0.009
D	9.5	40	13.0 ± 4.8	0.042 ± 0.016
G	9.5	35	13.7 ± 2.8	0.047 ± 0.009
H	9.5	47	14.4 ± 2.3	0.045 ± 0.007
I	7.0	20	26.0 ± 10.6	0.089 ± 0.036
J	7.0	18	25.3 ± 2.5	0.087 ± 0.009
L	7.0	37	18.9 ± 4.7	0.061 ± 0.015
M	7.0	14	15.9 ± 10.7	0.055 ± 0.036
N	7.0	17	12.1 ± 2.4	0.042 ± 0.008

Peptides A - H (8- and 9-mers) at their specific pH-values were chosen because these melting curves had a well defined transition (Figure 3a). The longer 18- to 21 mer peptides (I - N) were fitted with free endpoints, $\Delta H_{U\rightarrow F}$ and $\Delta S_{U\rightarrow F}$ only specifying the slope of the pre- and post-transition curves.

All peptides studied exhibited a positive ΔH and ΔS, supporting the model of an entropy-driven folding transition. The ΔH and ΔS values for the 8/9-mer and 21-mer peptides (Table 6.6) were closely similar, suggesting that each VPGVG repeat behaves as a thermodynamically independent unit (see Discussion).

Melting temperatures for short peptides which had N and C termini in the same state were well correlated (Table 6.7 and Figure 6.8). Acetylation of α-amino or amidation of α-carboxy groups (or both) lowered the transition temperatures by an average of 13° C for both 8- and 9-mers compared to free N- and/or C-termini. However, there were no significant differences in melting temperatures for peptides where the terminal charges differed in sign (Table 6.7,

compare peptide A and B at pH 4 *versus* B and F at pH 9.5 for the 8-mers, and peptide C and D at pH 4 *versus* D and H at pH 9.5 for the 9-mers), indicating that the presence of either one or the other charge had a similar effect on the structural transition for the short peptides.

Table 6.7 Melting Temperatures for Transitions in Short Elastin peptides.

Peptide	pH 4.0	pH 7.0	pH 9.5
A	35	41	30
B	40	34	35
C	45	37	24
D	39	27	40
E	22	21	20
F	23	34	39
G	33	26	35
H	26	36	47

The MRE for each peptide was followed at one wavelength for each pH and plotted against temperature. Dependent of buffer, pH and type of peptide, this was ranging from 197-202 nm. Values were obtained by fitting data to van't Hoff equation with $\Delta Cp = 0$ allowing initially ΔH, ΔS and endpoints for transition to float. T_M was found from the relation $\Delta H/\Delta S$.

The melting temperatures for the peptides at pH 7.0 were lowered compared to those with 'high T_M' values (Figure 6.8), and the effect was larger for the 9-mer peptides compared to the 8-mers. This suggests that there may be an additive stabilising effect through N-C-terminal interactions; the lower melting temperatures found for some of the smaller 8-mers compared to the larger 18-mer may be explained by this.

The presence of an extra glycine at the N-termini of the smaller peptides increased the melting temperatures by about 6° for both 'low T_M' and 'high T_M' peptides (Figure 6.8). An opposite effect was seen by the addition of a hydrophobic residue (or residues) near the C-terminus, which resulted in a lowering of the melting temperature by 20-23° C (compare peptide L with M and N, Table 6.6).

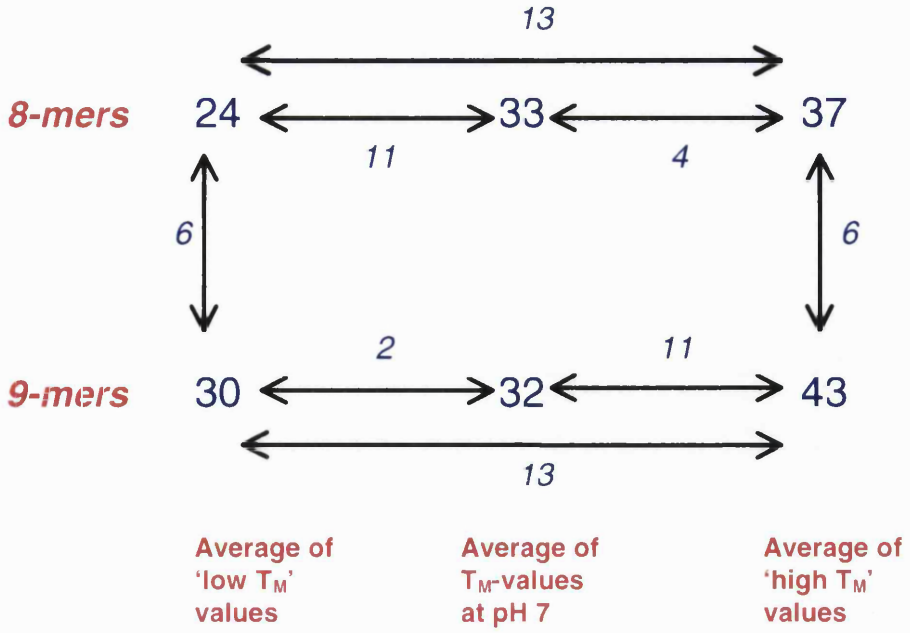

Figure 6.8 Average Melting Temperatures for Thermal Transitions of 8- and 9-mer Elastin Peptides.

The large numbers represent the average of T_M values (° C) for the 8-mers (peptide A, B, E and F) and 9-mers (peptide C, D, G and H) from Table 1. The 'low T_M' value is the average of the lowest melting temperatures (°C) at pH 4.0 or pH 9.5 for peptide A and F (or C and H for the 9-mer) and at pH 4 and 9.5 for peptide E (G for the 9-mer) - the pH-value which gives an uncharged molecule. Similarly, the 'high T_M' value represents the average of high T_M values for peptide A and F (C and H), and at both pH 4 and pH 9.5 for peptide B (D for the 9-mer), the pH-value which gives a charged molecule. The smaller numbers in italics represent the difference between average T_M values.

Peptide K, a 21-mer containing a glutamic acid replacement in the central VPGVG unit, was more disordered at lower temperatures than the other peptides (MRE value of -20,000 deg cm^2 $dmol^{-1}$ at 1.4°C; see (Perczel *et al.*, 1993; Urry *et al.*, 1985), and thermodynamic analysis was also not possible. Thermodynamic data were obtained however with peptide J, which has the same residue insertions at the N- and C-termini as peptide K but lacks the internal glutamic acid. Interestingly, in this peptide the presence of a charged lysine did not elevate the melting temperature, probably due to the more dominant hydrophobic effect of an adjacent leucine (compare I with J, Table 6.6).

6.3.5 Effects of SDS and TFE.

The effects of the detergent SDS were tested on the short (B,E and G) and the longer (K, L, N and O) peptides. For 8- and 9-mers micellar SDS (25 mM) induced an increase in MRE at 210 nm for both peptides, and for the 8-mers this was also observed in non-micellar (2 mM) SDS (Figure 6.9a).

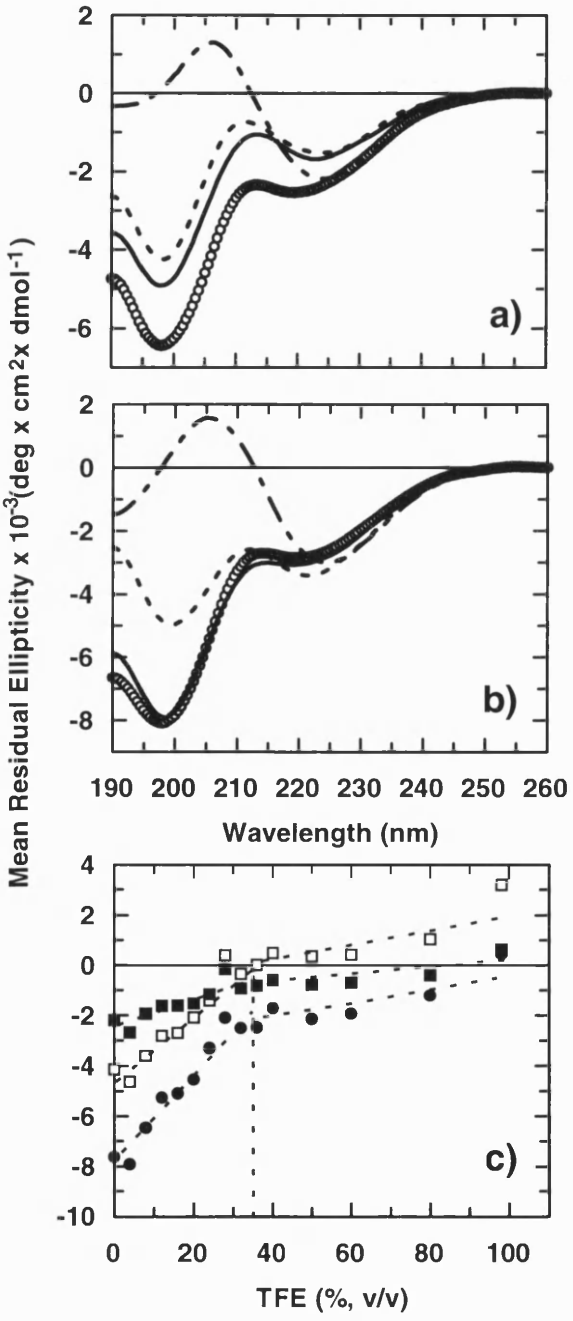

Figure 6.9 Effect of SDS and TFE on Peptides E and L. *(legend continues next page)*

Figure 6.9 continued.

a) Peptide E (218 μM) and **(b)** peptide L (91 μM) were scanned in water (-o-), in 2 mM SDS (———), in 25 mM SDS (- - - -), and in 87 % (v/v) TFE (— - —) at 20.5° C using 0.5 mm quartz cuvettes (4 scans; 0.5 nm spacing; 1 sec integration time). **(c)** Peptide L (20.7 μM) was also tested at different concentrations of TFE at 15.7° C in a 2 mm cuvette, and the variation of mean residual ellipticity versus TFE concentration at 198 nm (●), at 206 nm (□) and at 213 nm (■) is shown.

For the longer peptides this effect was only seen with micellar SDS (Figure 6.9b). The increase in MRE at 200 nm and the more gradual increase at 206-212 nm, characteristic of a transition to a type II β-turn (Perczel *et al.*, 1993; Urry *et al.*, 1985; Woody, 1995), indicated that all peptides were becoming more ordered in the presence of SDS.

Induction of the type II β-turn was more pronounced in 87-92 % (v/v) TFE than in SDS for the 8-, 9-, 18- and 28-mer peptides (Figure 6.9a,b). For peptide L, the concentration of TFE was varied from 0-97 %, and at about 35 % TFE the gradients of the MRE's at 198 nm, 206 nm and 213 nm versus TFE concentration shifted markedly, suggesting the presence of a structural transition (Figure 6.9c).

6.4 Discussion

All of the peptides studied here exhibited an increase in MRE at 195-205 nm and at 206-212 nm, a signature of type II β-turn formation, with increasing temperature, supporting the notion that the folding of these sequences is a consequence of hydrophobic interactions which are driven by positive entropies of dehydration (Privalov & Makhatadze, 1993). The type of turn structure formed is critically dependent on both the flanking sequences and the solvent conditions. At low temperature (~0° C) the short peptides showed evidence of partial structure, as has been seen with the larger polymers (Urry *et al.*, 1985, 1986). In addition, most peptides showed an increase in MRE at 210 nm, typical of type II β-turn formation in VPGVG polymers (Urry et al., 1985). Evidence for the formation of type I/III β-turns (MRE increase at 210-230nm) was seen in the CD-spectra of some peptides at high temperatures, suggesting that an equilibrium of different β-turn populations

may exist for many of these sequences. Peptides having a GGVG N-terminal region (C,D,G and H in this study) are thought to preferentially adopt the type II' β-turn (Broch *et al.*, 1996). Interconversion between type I and type II β-turns has been estimated to require +0.2 to -1.7 kcal mol^{-1} (Yang *et al.*, 1996, and references herein), a small enough change to be affected by flanking sequences or buffer composition (TFE, SDS, etc.). Previous crystallographic studies on the linear pentapeptide Boc-VPGVG-OMe (Ayato *et al.*, 1980) showed the absence of any β-turn structure while the structure of a cyclic decapeptide analogue of VPGVG exhibited a type III turn for one VPGVG unit followed by a type I turn for the second unit (Bhandary *et al.*, 1990). Here it has been clearly demonstrated that, when suitable flanking sequences are present, the VPGVG monomer is able to form the identical type II β-turn structure (within the discrimination capacity of CD) to that formed by the elastin-like polymer (VPGVG)n. It has also confirmed that, when particular types of flanking residue are present, the transition temperature can be altered in the same direction as seen for the polymers (Urry, 1993). For example, the addition of extra hydrophobic residues adjacent to the VPGVG turn sequence lowered the melting temperature by up to 20° C and an additional glycine increased T_M by 6° C. It seems quite remarkable that these large temperature effects could be produced by adding a single residue (compare the 8-mers versus 9-mers (Figure 6.8) and peptides L and M, Table 6.6), although when multiple additions were made the effect was not necessarily additive (compare peptides M and N, Table 6.6). Further, when a charged residue was inserted in the presence of these additional hydrophobic residues, the expected increase in melting temperature was not seen (compare peptides I and J, Table 6.6). This suggests that the melting temperature for an elastomeric sequence flanked by different non-elastomeric residues may be found by averaging the balance of hydrophobic and hydrophilic residues in the flanking regions.

The dramatic effect of charged residues on T_M is illustrated by the behaviour of the shorter peptides. A net charge at either the N- or C-terminus increased the melting temperature by as much as 20° C (compare peptides C and H at pH 4 and 9.5, Table 6.6). The thermodynamic effect of charged groups at the termini is likely to derive from an increased stability of the water shell surrounding the peptide.

For the amidated and acetylated VPGVG peptides of different lengths (peptides E and L) transition temperatures varied from those observed for the much longer VPGVG polymers (Luan *et al.*, 1990; Urry *et al.*, 1985).

The effect of SDS on short elastin-sequences supports the hydrophobic collapse model of stabilisation. In this study, low concentrations of SDS (up to 25mM) induced β-turn formation (Figure 6.9a). If SDS is able to bridge the two valines spanning each side (*cis*-face) of the PG-turn, it would disrupt their hydration and facilitate the closer interaction necessary for induction of a type II β-turn. Models extracted from an MD simulation of longer elastin peptides (Wasserman & Salemme, 1990) of a single GVGVPGVG unit in both the extended and contracted states (Figure 6.10), predict that the distance between the two valines in the high temperature form is approximately 2 Å shorter than in the low-temperature form.

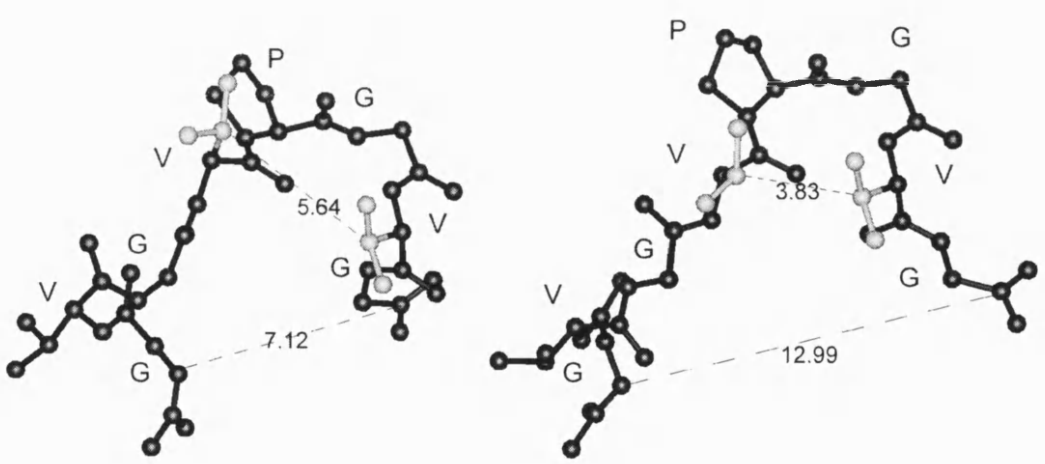

Figure 6.10 Molecular Models of Peptide Ac-GVGVPGVG-NH_2 in Expanded and Contracted Conformations.

Dihedral angles for the expanded and contracted form of the peptide in this study were extracted from the average Φ and Ψ angles in a published molecular dynamics simulation of $(VPGVG)_{18}$ in relaxed and stretched forms (Wasserman & Salemme, 1990). At the left is shown the low-temperature expanded form and the right the high-temperature contracted form. The distances between the valine C_β atoms and N- and the C-termini are shown.

The larger effect of SDS on the longer peptides (more than one VPGVG monomer) is consistent with the shielding hypothesis. The effects of TFE, studied on peptide L (Figure 6.9c), are consistent with a hydrophobic model of β-turn formation at high temperature. The largest effect was seen below 35 % TFE, where hydrophobic interactions within the peptide are likely to be important. Since the total free energy is lower for the TFE/water mixture than for water alone, the preferred form for the TFE-mixture will be where the valine side-chains are closely packed. Bodkin & Goodfellow (1996) have discussed this as a general model for TFE-induced folding of secondary structures. Above 30 % TFE the electrostatic interactions become more dominant, reflected by the more reluctant formation of type II β-turn structures. However, an alternative mechanism for TFE is proposed in chapter 7.

This study has demonstrated that short, elastin-like peptides can undergo the identical structural transitions that have been observed in neutral and modified elastomeric polymers. In elastin polymers, $(VPGVG)_n$, the identical pentamer sequences all contribute to form a beta-spiral with type II turns (Pro^2-Gly^3 with a Val^1 C=O $\cdots$ H-N Val^4 hydrogen bond). Intramolecular hydrophobic contacts are thought to drive the transition within this spiral (Urry, 1988a). However, the only stabilising hydrogen bonds reside within each of the monomers, VPGVG. Even so, it is plausible that formation of the spiral is a cooperative transition, driven by hydrophobic collapse and stabilised by intra-pentamer H-bonds. No evidence for such a cooperative effect was seen here. The ΔH and ΔS values for an 8-mer (1 VPGVG unit) and an 18-mer (3 VPGVG units) are the same indicating that a 'cooperative unit' does not exceed one repeat. The contribution of configurational entropy to the total entropy on going from an 8-mer to an 18-mer can be shown to be minimal; the difference in conformational entropy, ΔS_{conf}, between the number of states for the relaxed (764) and extended (58) conformations of a single VPGVG peptide has been calculated to be 1.024 cal mol^{-1} K^{-1} per residue (one entropic unit per residue). The increased conformational entropy change between an 8-mer and an 18-mer would then be just 0.010 kcal mol^{-1} K^{-1}, assuming the entropy derives from internal chain dynamics without random chain networks (Urry, 1988a). This shows that ΔS through the transition (Table 6.6) cannot be balanced by such small increases in ΔS_{conf} as the chain length increases.

These results lead to the intriguing possibility of engineering short, elastin-like peptide sequences into globular proteins. The presence of an elastic switch within a structurally sensitive region of a protein would enable the triggering of an "allosteric" response to temperature or pH (Noguti & Gö, 1989a,b). Is this energetically feasible? The free energy change for the transition of the VPGVG-containing 8- mer (peptide B, pH 9.5) from 0° to 60° was -2.9 kcal mol^{-1}, more than enough energy to fuel such a change. If several of these VPGVG switches are incorporated into a stable protein, they may be able not only to affect binding by an allosteric effect, but also to change the overall stability of a protein. The stability of a single-chain antibody is around 10 kcal mol^{-1} (Jäger & Plückthun, 1999) which equals the energy for three VPGVG-elements. Similarly, the energy for a H-bond is between 3-6 kcal/mol (Creighton, 1984).

Where such elastomeric sequences are introduced into enzymes or binding proteins this will offer a novel method for modulating their activities, thermostabilities or -labilities. Ultimately, such sequences will undoubtedly find use in the *de novo* design of proteins.

Chapter 7. Trifluoroethanol May Form a Mobile Matrix for Assisted Hydrophobic Interactions Between Peptide Side-chains[1].

7.1 Introduction.

During the last decade there have been a large number of observations on the effect of trifluoroethanol on peptides and proteins. TFE has been shown to induce and stabilise α-helices in sequences with intrinsic helical propensity (Sönnichsen *et al.*, 1992), and to induce β-turns, β-hairpins (Graf von Stosch *et al.*, 1995a; Searle *et al.*, 1996; Sönnichsen *et al.*, 1992) and also β-strands (Lu *et al.*, 1984; Martenson *et al.*, 1985). It can also promote switching between different secondary structures, generally from β-sheet to an α-helical structure (Kuwata *et al.*, 1998; Narhi *et al.*, 1996b; Yang *et al.*, 1994; Zhang *et al.*, 1995a). A transition to a 3_{10}-helix has also been reported for a β-sheet peptide (Graf von Stosch *et al.*, 1995a). It is implicit that intra and inter molecular side-chain interactions must play an import role in solvent induced secondary structures in proteins (Li & Deber, 1993; Zhong & Johnson, 1992). Understanding the underlying mechanisms of these induced transitions is important for elucidation of folding pathways, but particularly for *de novo* design of proteins.

Several models explaining the effects of TFE on secondary structures have been proposed. The two contrasting views are either that TFE directly associates with the folded peptide chain (Bodkin & Goodfellow, 1996; Hirota *et al.*, 1998; Jasanoff & Fersht, 1994; Rajan & Balaram, 1996) or it destabilises the unstructured form of the peptide (Cammers-Goodwin *et al.*, 1996, and references herein). Figure 7.1 illustrates the model proposed by Bodkin & Goodfellow (1996).

[1] This chapter has been submitted for publication.

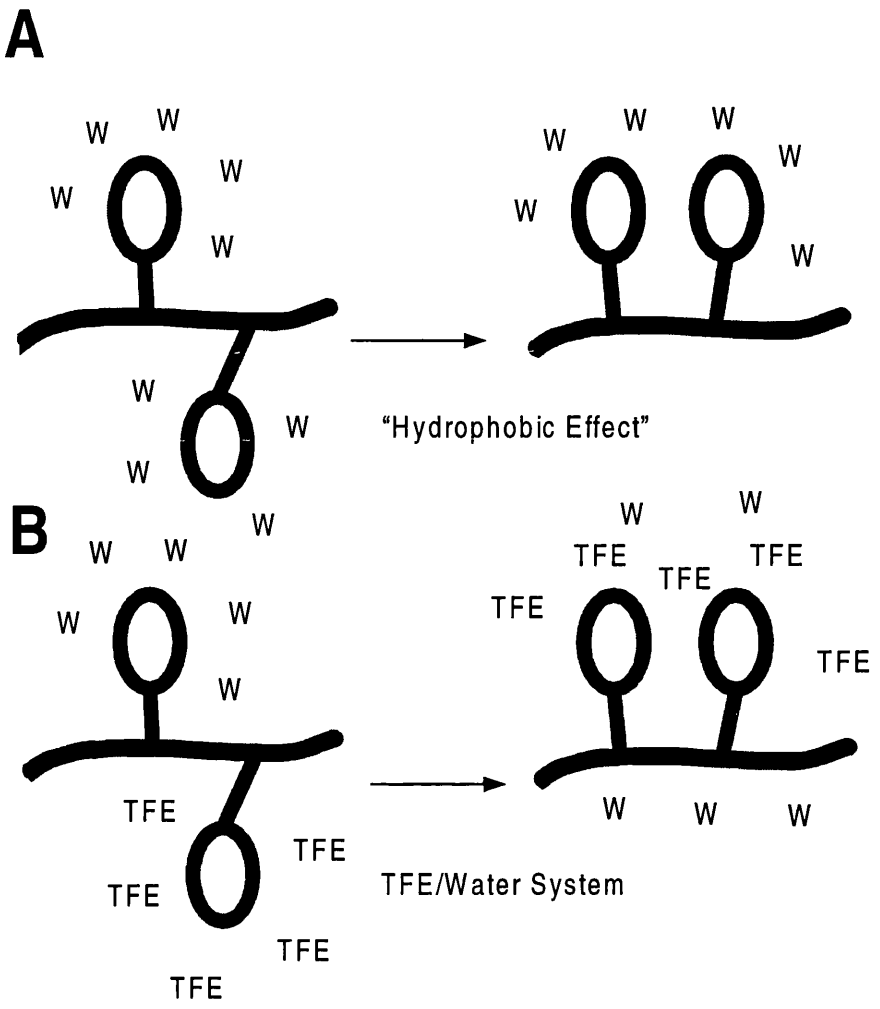

Figure 7.1 The Hydrophobic Collapse Model Supported in a TFE Mixture.

The figure is adapted from Bodkin & Goodfellow (1996). Panel **a)** shows the hydrophobic collapse of the apolar side-chains in water (W) and **b)** in the water/TFE (W/TFE) system. The low-energy conformation shown on the right-hand side is obtained by minimising the exposed hydrophobic surface area in **a),** or in **b)** where the hydrophobic groups are stabilised by the more hydrophobic solvent trifluoroethanol. TFE stabilises the folded form because the energy of TFE/water system is lower that of TFE or water alone.

Recent observations have focussed on the interaction of TFE with water molecules on the peptide, with two different interpretations. One view suggests that TFE behaves as an indirect chaotrope disrupting the solvent shell on α-helices (Luo & Baldwin, 1999; Walgers *et al.*, 1998), and thereby stabilising them. A second view casts TFE as a kosmotrope where its desolving effect destabilises the unfolded state (Kentsis & Sosnick, 1998). There are however several puzzling

contradictions. If TFE stabilises or strengthens local hydrophobic interactions in α-helices (Albert & Hamilton, 1995; Hirota *et al.*, 1998; Padmanabhan *et al.*, 1998), β-turn and β-hairpin (Reiersen *et al.*, 1998; Searle *et al.*, 1996), why is there lack of experimental evidence that TFE actually binds to hydrophobic groups? (Storrs *et al.*, 1992). Again, TFE disrupts tertiary interactions in proteins (by weakening non-polar interactions; Gast *et al.*, 1999; Luo & Baldwin, 1998) while preserving secondary structures.

Here the author proposes a structural model that may help to account for these observations. A temperature induced structural transition from random coil to type II β-turn in a elastin peptide in TFE solutions at different temperatures has been studied. The mechanism of contraction of elastin peptides derives from temperature induced folding, also seen in the folding of cold-denaturated alpha-helices in hexafluoro-2-propanol (Andersen *et al.*, 1996). For elastin this involves physical (temperature/pressure) or chemical (solvent composition) induced collapse of hydrophobically bound waters generating a positive entropy of bulk water and increased hydrophobic interactions, a phenomenon well known in protein folding (Cheng & Rossky, 1998; Dill, 1990; Livingstone *et al.*, 1991; Urry, 1993). Specifically, the elastin transition involves loss of hydrated water at higher temperatures from exposed valine side-chains inducing val-val interactions that fold the VPGVG sequence into a type II β-turn (Reiersen *et al.*, 1998; Urry, 1988a,b, 1993). In this study, increasing temperature induced a type II β-turn at low TFE concentrations. At higher concentrations of TFE (>30% v/v), however, the amount of β-turn structure decreased with increasing temperature. A model is proposed in which TFE associates with elastin side-chains in its *micellar* form and thus forms a mobile matrix which supports hydrophobic interactions.

7.2 Results

The peptide in this study, Ac-GVG(VPGVG)$_3$-NH_2, was synthesised, purified and analysed on circular dichroism as described previously (Chapter 6, Reiersen *et al.*, 1998). The elastin derived peptide Ac-GVG(VPGVG)$_3$-NH_2 incorporates a rather hydrophobic repeating (VPGVG)n sequence without any charged groups and is

thus a good model for studying the effect of temperature and trifluoroethanol (TFE) on intramolecular hydrophobic interactions. This peptide covers more than one turn of the suggested β-spiral in larger elastin polymers (Urry, 1988a,b), and its transition has previously been shown to be independent of concentration with reversible temperature scans (Chapter 6, Reiersen *et al.*, 1998). The effect of TFE at two different temperatures is shown in Figure 7.2a and b.

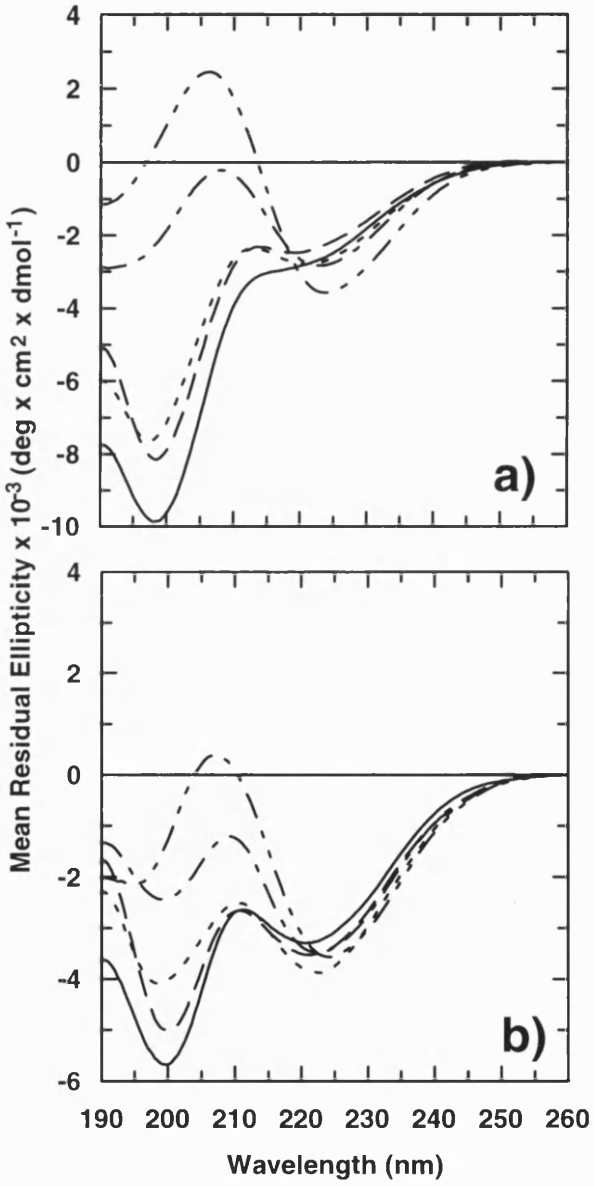

Figure 7.2 CD Scans of GVG(VPGVG)$_3$ at Different Temperatures in TFE/phosphate Buffer pH 7.0 Mixtures.

(legend continues on the next page).

Figure 7.2 continued.

Panel **a)** shows the melting of the peptide at 6.8° C and panel **b)** for 58.6° C. Peptide L (20.4 μM, Figure 6.1, chapter 6) was scanned in a 0.2 cm quartz cuvette integrating each 0.5 nm up to 260 nm for one second, and the average of four scans is displayed. The different TFE concentrations, diluted (v/v) in 10 mM phosphate buffer pH 7.0, are as follows (————) for 10 mM phosphate buffer alone; (— — —), 5 % TFE; (- - - - - -), 15 % TFE; (— - — -), 30 % TFE and (— - - —), for 98 % TFE.

By increasing the concentration of TFE there was a shift in the circular dichroic spectra from a global minimum at 199 nm typical for unordered peptides, to a global maximum at 206 nm with a near isodichroic point around 218 nm. This latter spectrum has previously been shown to be diagnostic of type II β-turns (Perczel *et al.*, 1993; Urry, 1988a,b; Woody, 1995). There was a significant effect on the proportion of type II β-turn at 6.8° C at elevated concentrations of TFE. The transition to type II β-turn in elastin results in a closer association of the two val-groups on the *cis*-face of the β-turn at higher temperatures (Reiersen *et al.*, 1998; Urry, 1988a, b; Wasserman & Salemme, 1990). Similarly, by increasing the temperature with phosphate buffer alone, the proportion of type II β-turn increased (Figure 7.2ab). This was also seen for concentrations of TFE below 30 %. However, by raising the temperature the amount of β-turn structure decreased for the two highest TFE concentrations (Figure 7.3ab). The mean residual ellipticity at 206 nm was lowered to within the same ellipticity range for 30 % and 98 % TFE as it was increased for the lower concentrations of TFE and phosphate buffer measured between 6.8° C and 58.6° C (Figure 7.3b).

7.3 Discussion

It is tantalising to suggest that the similar conformational effect on the elastin peptide by increasing concentrations of TFE and increasing temperature, as illustrated in Figures 7.2 - 7.3, derive from the same, or closely similar mechanism. No synergetic effect of low concentrations of TFE and increasing temperature was seen.

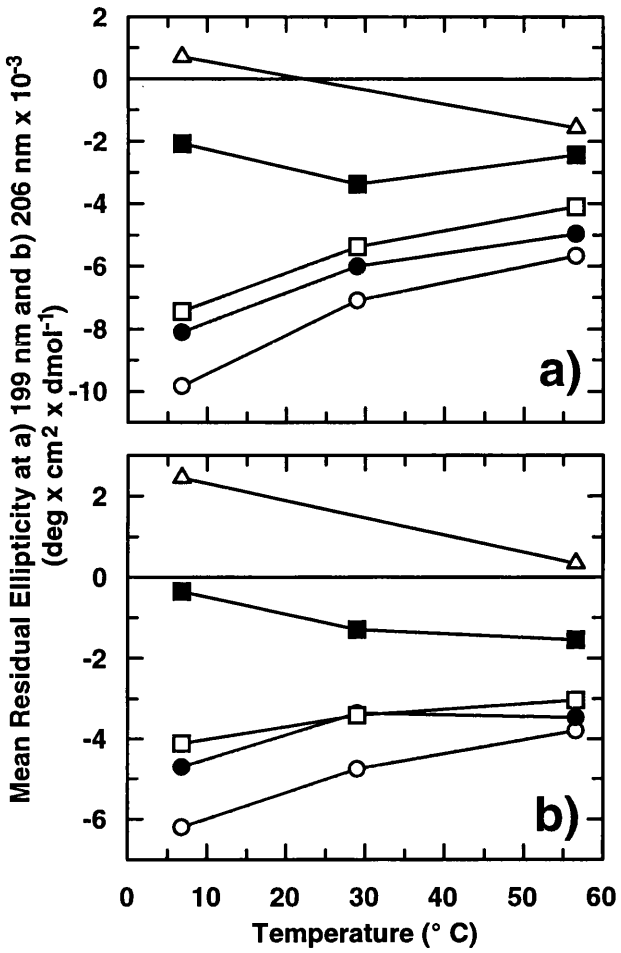

Figure 7.3 CD Wavelength Trends of GVG(VPGVG)$_3$ in TFE/phosphate Buffer at Different Temperatures. The mean residual ellipticity, taken from Figure 7.2ab, at the respective temperatures was followed at two wavelengths. Panel **a)** shows the temperature effect measured at 199 nm while **b)** is at 206 nm. The TFE concentrations in 10 mM phosphate buffer are as follows: (-○-), 0 %; (-●-), 5 %; (-□-), 15 %; (-■-), 30 %; and (-△-) 98 %.

Previously it has been shown that the amount of β-turn in elastin-like peptides increases for all TFE-concentrations up to 98 % (v/v) measured at 15.7° C (chapter 6 and Reiersen *et al.*, 1998), suggesting that the required val-val hydrophobic interactions are not inhibited but rather stimulated in TFE.

Some type II elastin β-turns also fold in TFE without forming the 4→1 hydrogen-bond (Bisaccia *et al.*, 1998, Dyson *et al.*, 1988, and references herein). In the sequence VPG-*Hiv*-G (*Hiv* is S-α-hydroxyvaleric acid, in which no

hydrogen bond is possible) the type II CD spectrum was seen in TFE and compared well with the wild type sequence VPGVG (Arad & Goodman, 1990).

Rajan & Balaram (1996) have argued that TFE binds through its fluoro-groups to hydrophobic side-chains on α-helices, although there is no experimental evidence from NMR for this (Storrs *et al.*, 1992). There have been observations that TFE strengthens intrahelical hydrogen-bonds (Luo & Baldwin, 1997) and weaken hydrogen-bonds to solvent (Cammers-Goodwin *et al.*, 1996). Contrariwise, D-H isotope partitioning in a GCN4 coil-coil showed that intramolecular peptide hydrogen-bonds are weakened by TFE (Kentsis & Sosnick, 1998). The foregoing suggests that the main driving force for chemical folding of VPGVG-peptides in TFE is not hydrogen-bond formation. Recently Luo & Baldwin (1999) suggested a role for hydrophobic residues in shielding polar groups from solvents in the helical state, thus stabilising the helix against thermal denaturation.

Some alcohols, in particular long-chain and halogenols, form micelles that are not homogenous in size but exist in different alcohol-water clathrate structures dependent on their concentration (Gast *et al.*, 1999; Hirota *et al.*, 1998; Kuprin *et al.*, 1995). This implies that the local concentration of TFE in these micelles may be many times larger than the bulk concentration of TFE. It is also a thermodynamic certainty that the effective TFE concentrations within the micelles will change as a function of temperature. This may affect thermodynamic calculations based on concentration and size of molecules.

TFE and hexafluoro-2-propanol (HFIP) have been shown to form clathrate starting from 10 % HFIP and around 20 % TFE (Gast *et al.*, 1999; Kuprin *et al.*, 1995). This implies that there are small micelles of TFE/HFIP in water with an intra-micellar alcohol concentration that is much higher than the average bulk concentration. The bell shaped profiles of the light scattering data show that the sizes of the micelles vary between 5-10 Å (Gast *et al.*, 1999). More recently, Hong *et al.* (1999) have shown by x-ray scattering that micellar clusters of alcohols such as TFE and HFIP are formed with a maximum scattering intensity at about 30 % (v/v) for HFIP, although the curve for TFE is weaker and much broader. This correlated well with the transitions seen for β-mellitin and β-lactoglobulin in various concentrations of HFIP and TFE. However, these authors

did not investigate the effect of temperature on the scattering behaviour of these cosolvent. These data, along with my observations may explain the effect of TFE in supporting local hydrophobic interactions in α-helices, β-hairpins and β-turns (Albert & Hamilton, 1995; Hirota *et al.*, 1998; Padmanabhan & Baldwin, 1994; Reiersen *et al.*, 1998; Searle *et al.*, 1996). The micelles may interact with local hydrophobic clusters by disrupting water structures around these groups, and additionally, may provide a mobile matrix for further assisted side-chain associations (Figure 7.4ab). The latter may be important to lower the side-chain conformational entropy, which is thought to be a key factor in the folding of α-helices (Aurora *et al.*, 1997).

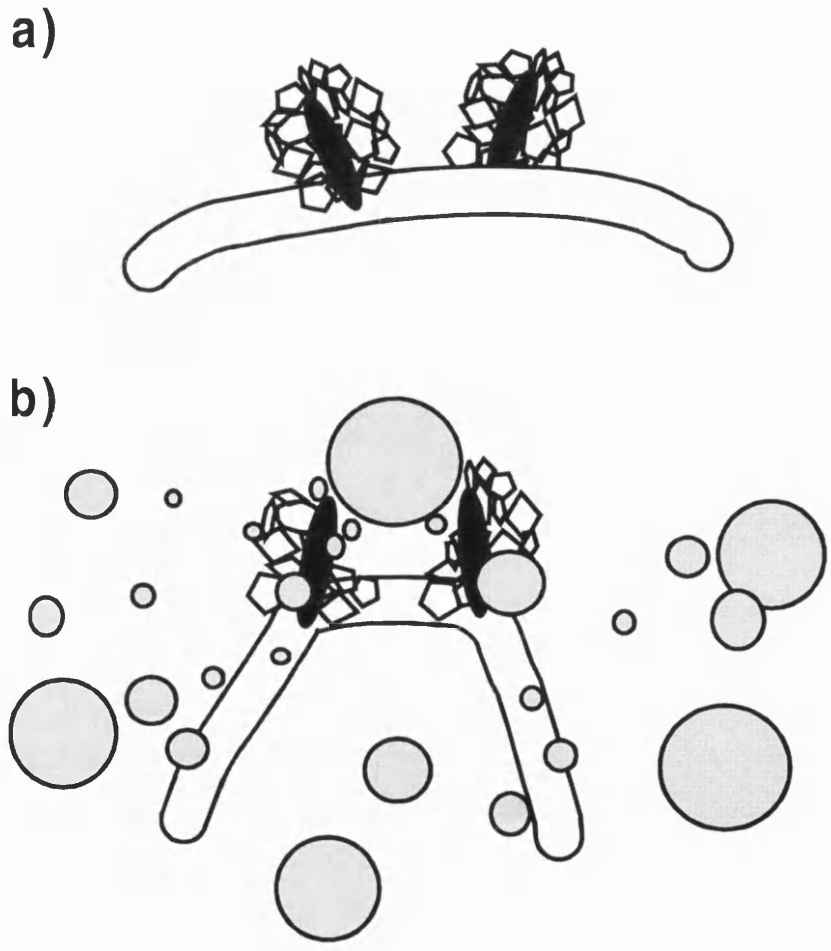

Figure 7.4 Model for the TFE Effect on Local Side-chains in a Short Peptide

A peptide backbone with two hydrophobic groups is illustrated in panel **a)**. Each group is hydrophobically hydrated with water molecules forming polygons. In panel **b)** the same peptide is shown after addition of TFE/water mixture. The TFE-micelles are shaded. In this snapshot the TFE-micelles are seen to have destroyed the water structure on the side-chains and to be supporting side-chain side-chain interactions by providing a mobile, structural matrix.

The differences in micelle size and composition, dependent on TFE-concentration, may explain why TFE switches secondary structure conformations at TFE-concentrations above 50 %. At elevated concentrations the TFE micelles are smaller, but have an higher local intra-micellar TFE concentration (Figure 7.5). This provides a better matrix to redirect non-local side-chain interactions in an existing structure to a more local folding nucleus. As the majority of TFE induced transitions occurs from a non-local (β-sheets; Otzen & Fersht, 1995) to a local folding contact (helices, turns and hairpins; Thomas & Dill, 1993), the TFE-induced transition can easily be explained by the micelle model (Figure 7.4ab). The destabilisation of tertiary and quaternary structures in proteins originates from the same phenomenon - by favouring the stabilisation of short-range hydrophobic contacts the long-range hydrophobic interactions are systematically disrupted, resulting in denaturation of the nonpolar core (Hirota *et al.*, 1998).

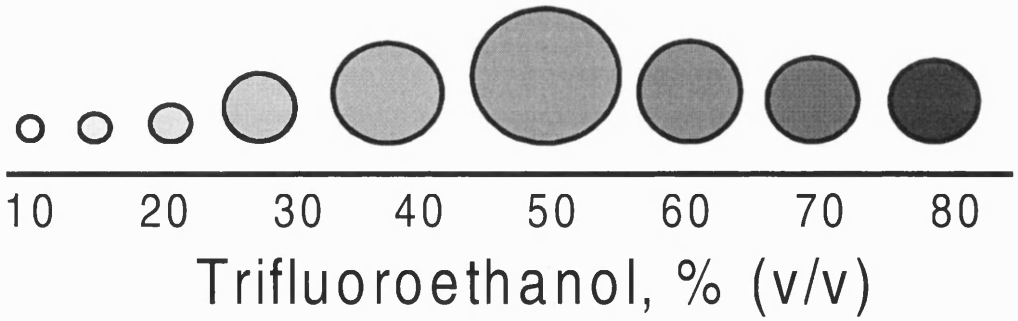

Figure 7.5 Model for the TFE Concentration Dependent Micelle Size.

The relative micelle size of trifluoroethanol as a function of concentration is shown. The micelle sizes are derived from light scattering intensity data at 20° C (Gast, *et al.*, 1999). The relative intra-micelle TFE concentrations are indicated by the grey intensity (feint to dark equals low to high). For further explanation, see text.

The observation in this study that concentrations of TFE at or above 30 % have the opposite effect to low concentrations of TFE at higher temperatures (Figure 7.3ab), suggests that the micelle structures are altered in composition and size at higher temperatures. At least for *tert*-butyl alcohol (Iwasaki & Fujiyama, 1979)

and hexafluoro-2-propanol (Kuprin *et al.*, 1995) both light scattering and low angle x-ray scattering, respectively, have been shown to increase with temperature, possibly due to the increased segregation of alcohol from water (Iwasaki & Fujiyama, 1979; Kuprin *et al.*, 1995). Interestingly, the scattering of micelles containing low concentrations of *tert*-butyl alcohol is lowered by increasing temperature (Iwasaki & Fujiyama, 1979). At higher temperatures it would be expected that the local TFE-concentration in the micelles will increase due to a more positive mixing enthalpy between alcohol and water, and that the micelle will become more hydrophobic, ultimately leading to a macroscopic phase separation (Iwasaki & Fujiyama, 1979). This provides an explanation for the thermo-stabilisation of helices whereby the TFE-micelle stabilises the helix side-chains by offering a mobile matrix which can interact with the helix surface.

What can be said about cold-denaturation? Cold-denaturation of alpha-helices in 8-10% hexafluoro-2-propanol has previously been described as a destabilisation of coil state (Andersen *et al.*, 1996). By reducing the temperature the density of HFIP-micelles will increase, as seen by Kuprin *et al.* (1995), and will therefore diminish the ability of the HFIP matrix to provide an effective local chaperoning environment for the helix side-chains.

The importance of having an external supporting interface in the folding and stability of proteins has been well addressed in the literature. An exposed hydrophobic surface is important for chaperone function and activity (Das & Surewicz, 1995), and α-helices are generally stabilised by tertiary hydrophobic contacts with other parts of the protein. The helix-stabilising effect by reducing the nonpolar surface-area has been stressed in several previous studies (Padmanabhan & Baldwin, 1994; Zhang *et al.*, 1995a and references herein; Butcher & Moe, 1996).

On the basis of the observations that TFE forms micelles in water solutions, the author has proposed a structural model in which TFE forms a mobile, temperature sensitive solvent matrix that locally chaperone hydrophobic side-chains of secondary structures. This model accounts for the various effect by TFE on hydrophobic groups in peptides and proteins, and may provide an explanation for the phenomenon of cold-denaturation.

Chapter 8. An Engineered Minidomain Containing an Elastin Turn Exhibits a Reversible Temperature-Induced IgG-binding[1].

8.1 Introduction.

One of the applications of protein engineering is the development of novel switch-mechanisms which can regulate and control protein folding and function. There are several naturally occurring mechanisms whereby the activity of a protein can be regulated by conformational change. For example, it may be allosterically modified by binding of a ligand, or as a direct consequence of rearrangements in structure due to covalent modification (e.g. phosphorylation), or as a result of changes in physical or chemical parameters, such as temperature, pH or degree of hydration (Daughdrill *et al.*, 1997; Uesugi *et al.*, 1997; van Stokkum *et al.*, 1995). The hydration or dehydration of hydrophobic surfaces is a particularly novel mechanism employed to drive conformational changes in elastomeric proteins (Urry, 1988a,b,1993).

In the classical hydrophobic model, water molecules associated with hydrophobic interfaces are structurally ordered and transitions involving hydrophobic hydrated surfaces involve the loss of bound water, or melting of clathrate-like water structures near hydrophobic groups. During protein folding the loss of water results in an increase in entropy of bulk water accompanied by an increase in protein hydrophobic interactions, providing the driving force for protein function, assembly, stability and folding (Dill, 1990; Head-Gordon, 1995; Livingstone *et al.*, 1991; Muller, 1993; Urry, 1993). Contrary to the behaviour of many globular proteins, the elastic muscle protein, elastin, undergoes an inverse temperature transition during hydrophobic dehydration. Polymers derived from elastin and containing repeating (VPGVG)n sequences (n up to150) are completely soluble in water below their transition temperatures (~25° C) but contract in length by more than 50 % with increasing temperature. The free energy released during this transition is sufficient for an elastin fibre to lift more than

[1] Note. This chapter contains additional material to that published by Reiersen & Rees (1999).

1000 times its own mass. The transition involves loss of hydrated water from exposed valine sidechains at the higher temperatures inducing val-val interactions that energise the formation of an ordered β-spiral with three VPGVG units per turn of the spiral, each VPGVG forming a type II β-turn (Reiersen *et al.*, 1998; Urry, 1988a, b, 1993).

Formation of the type II β-turn has been verified by different physical and spectroscopic studies, although the presence of other types of β-turns has also been reported (Arad & Goodman, 1990; Bhandary *et al.*, 1990; Urry, 1988a, b, 1993). The behaviour of the elastin polymers can be regulated by covalent modification such as phosphorylation, electrochemical reduction of prosthetic groups attached to the polymer, or by the replacement of residues in the sequence by residue types sensitive to pressure, temperature or pH. Recently it was shown that the behaviour of the polymeric elastin can be mimicked by small peptides of 8-28 residues containing the VPGVG sequence in single or multiple copies. This has opened up the possibility of using such sequences in a protein engineering context as molecular 'switches' (Chapter 3 and Reiersen *et al.*, 1998).

In this chapter the first attempt to introduce a temperature switch into a globular protein using the elastin fragment approach is described. The target protein was a biologically active fragment of protein A, a multi-domain protein from *Staphylococcus aureus* which binds to the Fc region of IgG. Protein A is found on the cell surface of the bacteria and contains a tandem repeat of five different but homologous binding domains, each of approximately 60 residues in a three-helix bundle and designated E, D, A, B, and C (Uhlén *et al.*, 1984). A synthetic version of the B-domain, the Z-domain, has been constructed for high-level protein expression (Nilsson & Abrahmsén, 1990), and recently has been minimised to two helices (33 residues) connected by a type I β-turn. This 2-helix fragment largely retains the binding affinity of the parent B-domain towards the Fc-portion of IgG (Braisted & Wells, 1996; Starovasnik *et al.*, 1997).

In this study the type I β-turn of this minidomain was replaced with an elastin β-turn. In this construction the elastin sequence acts as a temperature switch. The minidomain with the elastin-turn binds the Fc of mouse IgG2a with an improved affinity at higher temperatures. At the same temperatures, the wild type minidomain undergoes the expected decrease in affinity as it unfolds. This

demonstrates that short elastin sequences when inserted into globular proteins have the ability to induce structure at higher temperatures, opening up the possibility of a general method for introducing controlled temperature regulation of protein function.

8.2 Materials and Methods.

8.2.1 Peptide Synthesis.

The synthesis was carried out by Synt:em (Nîmes, France) on an Automated Multiple Peptide Synthesis instrument (AMS 422, ABIMED) using a Fmoc solid support protocol (polyethylene glycol grafted polystyrene support) as described by Reiersen & Rees (1999). The purity was confirmed by analytic HPLC and by mass spectroscopy analysis using a Maldi-tof spectrometer (Voyager DE Elite, PE Applied Biosystems) with dihydroxybenzoic acid as matrix at Synt:em, and also by amino acid analysis (chapter 5.3).

8.2.2 Circular Dichroism Studies.

The secondary structure of the minidomain constructs was analysed by recording CD spectra on Jobin-Yvon Model CD6 Dichrograph Instrument (Instruments S.A. UK Ltd., Stanmore, UK) as described in chapter 5.4.

8.2.3 Thermodynamic Analysis of CD-data.

The free energy for melting or folding of structure at 222 nm was fitted to a macroscopic, reversible, two-state model using the observed CD-data, $[\theta]^{222}$ and temperature, T. For folding (U→F) or melting (F→U) of structure, respectively equations (8.1) and (8.2) were used.

$$\Delta G_{U\rightarrow F} = -RT \ln[([\theta]^{222} - [\theta]^{U})/([\theta]^{F} - [\theta]^{222})] \quad (8.1)$$

$$\Delta G_{F\rightarrow U} = -RT \ln[([\theta]^{222} - [\theta]^{F})/([\theta]^{U} - [\theta]^{222})] \quad (8.2)$$

The pre and post-transitional slopes for melting in TFE, respectively mF and mU in equations (8.3) and (8.4) below, used the data from WtSS and MutSS minidomains. For folding (U→F) in buffer the respective slopes were similarly taken from MutOpen1 and MutOpen3 minidomains.

$$[\theta]^{F} = mF \times T + off1 \quad (8.3)$$

$$[\theta]^{U} = mU \times T + off2 \quad (8.4)$$

The offset values off1 and off2, together with ΔH and ΔS, were fitted for the melting curves of the minidomains. Where a mutant exhibited a less well defined transition startpoint, datapoints were extrapolated based on the pre-transitional region of the wild-type minidomain in the same solvent. The heat capacity was set to zero since all minidomains were of relatively low molecular weight (~ 4000 Da) (Chapter 6, Scholtz *et al.*1991a, and references herein). By replacing $[\theta]^{U}$ with $[\theta]^{F}$, and vice versa, in equations (8.1) and (8.2), and (8.5) and (8.6), the thermodynamic values for the inverse transition, $\Delta G_{U\rightarrow F}$, were found.

$$\Delta G_{F\rightarrow U} = \Delta H_{F\rightarrow U} - T\Delta S_{F\rightarrow U} \quad (8.5)$$

$$[\theta]^{222} = ([\theta]^{F} + [\theta]^{U} \times \exp-(\Delta G_{F\rightarrow U}/RT))/(1 + \exp-(\Delta G_{F\rightarrow U}/RT)) \quad (8.6)$$

The data were fitted to either equation (8.1) or (8.2), together with equations (8.3-8.6), using the least squares method in the Grafit software (Leatherbarrow, 1989).

8.2.4 Surface Plasmon Resonance Spectroscopy.

Interaction kinetics of the minidomains (analytes) with immobilised Fc (ligand) was monitored by surface plasmon resonance spectroscopy using either BIAcoreX™ or BIAcore2000™ (Biosensor, Sweden) as described in chapter 5.8. The BIAcore 2000 was used for analyses of WtSS and MutSS minidomains over the temperature range +5° to +37° C. Purified Fc prepared from the IgG2a mouse monoclonal antibody 561 (anti-CD34), a gift from Dynal A/S (Norway), and human serum albumin (HSA, Novo Nordisk, Denmark) were immobilised on a research grade CM-5 carboxymethylated sensor chip in 10 mM sodium acetate buffer pH 4.5 using the amine coupling kit with N-ethyl-N'-[(dimethylamino)propyl] carbodiimide (EDC) and N-Hydroxysuccinimide (NHS) provided by the manufacturer. The Fc of the mAb 561 (10 µl of 5 µg/ml) and HSA (10µl of 10 µg/ml) were immobilised at +25° C in the BIAcore2000 with a flow rate of 10µl Hepes buffered saline (HBS; 10 mM Hepes pH 7.4, 150 mM NaCl, 3.4 mM EDTA) containing 0.005 % (v/v) surfactant per minute. This gave 3100 and 3400 RUs respectively after blocking with 1M ethanolamine pH 8.5 and regeneration using 5 µl 10 mM glycine-HCl buffer pH 5.4. Interaction analyses were performed with a flow rate of 30 µl/min in HBS/P20 (running buffer). Each minidomain (100 µl) was injected, using the KINJECT command, over a range of concentrations - between 4 and 10 different concentrations, depending on the experiment. The binding of the minidomains to Fc-561 was corrected by subtracting the RU's at the HSA portion of the chip (due to bulk-effects). The surface was regenerated prior to each injection with glycine-HCl pH 2.4. The data for the association constant was sampled by diluting each minidomain in running buffer to obtain several low concentrations, and the dissociation constant was determined from the highest concentration to minimise rebinding.

8.2.5 Evaluation of BIAcore Data.

The k_{on} and k_{off} values were fitted by evaluating the sensorgram data as described in chapter 5.5.1. The relative differences in free energy of binding, $\Delta\Delta G$, between

the different minidomains over the temperature ranges examined were calculated from:

$$\Delta\Delta G = +RT_x \ln[K_D(\text{mutant minidomain}) \text{ at } T / K_D (\text{wild-type minidomain}) \text{ at } T] \quad (8.7)$$

Where R is the molar gas constant, T is the temperature (in Kelvin) and the K_D values are those based on the fast on- and off-rates.

8.3 Results

The engineering of the small binding protein selected for this study, so that it was capable of being reversibly modulated by temperature changes, used an inter-helix turn replacement strategy in which the wild type turn was replaced by the elastin sequence, GVGVPGVG (Chapter 6 and Reiersen *et al.*, 1998). The minidomain derived from the B-domain of Protein A (Braisted & Wells, 1996) was the model protein used (Figure 8.1, WtOpen). This minidomain is 33 residues long, is amenable to peptide synthesis and binds the Fc region of IgG.

WtOpen	NH_2-F^{6}NMQQQRRFYEALH^{19}DPNLNEE^{26}QRNAKIKSIRDD^{38}-COO$^-$
MutOpen1	NH_2-F^{6}NMQQQRRFYEALG^{19}VPGVGQQ^{26}QRNAKIKSIRDD^{38}-COO$^-$
MutOpen2	NH_2-F^{6}NMQQQRRFYEALG^{19}VPGVGEE^{26}QRNAKIKSIRDD^{38}-$CONH_2$
MutOpen3	NH_2-F^{6}NMQQQRRFYEALG^{19}VPGVGEE^{26}QRNAKIKSIRDD^{38}-COO$^-$
WtSS	NH_2-F^{6}NMQCQRRFYEALH^{19}DPNLNEE^{26}QRNAKIKSIRDDC^{39}-COO$^-$
MutSS	NH_2-F^{6}NMQCQRRFYEALG^{19}VPGVGQQ^{26}QRNAKIKSIRDDC^{39}-COO$^-$

Figure 8.1 Sequences of Short IgG-binding Minidomains Derived from Protein A.

The minimised IgG-binding B-domain of protein A (Braisted & Wells, 1996) was synthesised (WtOpen), and the turn-region mutants (residues 19-26) based on the elastin sequence GVPGVG are also shown (MutOpen 1-3). Minidomains with disulphur bond [17] were also synthesised. Both the wild-type minidomain, WtSS, and its mutant minidomain, MutSS, have an S-S bond between Cys10 and Cys39.

The wild type β-turn HDPNLN was replaced with the elastin sequence GVPGVG. The GV portion at the N-terminal start of the turn was omitted because it was flanked by the similar dipeptide AL (*AL*HDPNLN). However, the possibility was considered that the charge from the EE residues at the C-terminal end of the turn (HDPNLN*EE*) would elevate the transition temperature of the elastin sequence beyond 37° C (Chapter 6 and Reiersen *et al.*, 1998) and so EE was replaced with QQ in one construct (Figure 8.1, MutOpen1 and MutOpen3). Minidomains with a disulphide bond were also synthesised (Figure 8.1, WtSS and MutSS), since the wild-type S-S minidomain has been shown to be more thermostable and exhibit better Fc-binding than the open form (Starovasnik *et al.*, 1997). The minidomain purities and molecular masses (Syntem, France; see experimental section) were respectively: WtOpen (95 %, 4122.0 Da), MutOpen1 (95%, 3879.3 Da), MutOpen2 (98%, 3879.7 Da), MutOpen3 (95 %, 3881.5 Da), WtSS (97%, 4181.8 Da), and finally MutSS (96%, 3956.3 Da). The minidomains dissolved in deionised water were also examined by quantitative and qualitative amino acid analysis as described in Table 8.1 (chapter 5.3.3), and generally verified the composition although there were some deviations from the expected values.

Table 8.1 Amino Acid Analysis of Minidomains.

Minidomain	Amino acid composition: Amino acid type, experimental value [expected composition].
WtOpen	Asp + Asn, 6.16 [7]; Glu + Gln, 6.28 [7]; Ser, 0.94 [1]; Gly, 0.35 [0]; His, 1.04 [1]; Arg, 4.13 [4]; Ala, 2.28 [2]; Pro, 1.16 [1]; Tyr, 0.95 [1]; Thr, 0.14 [0]; Val 0.11, [0]; Met, 0.74 [1]; Ile, 2.21 [2]; Leu, 2.31 [2]; Phe, 2.18 [2]; Lys, 2.01 [2].
MutOpen1	Asp + Asn, 3.87 [4]; Glu + Gln, 6.58 [7]; Ser, 1.01 [1]; Gly, 3.06 [3]; Arg, 4.05 [4]; Ala, 2.09 [2]; Pro, 1.38 [1]; Tyr, 0.94 [1]; Val, 2.29 [2]; Met, 0.66 [1]; Ile, 1.93 [2]; Leu, 1.07 [1]; Phe, 2.00 [2]; Lys, 2.05 [2].

Table continues on the next page.

Table 8.1 continued.

Minidomain	Amino acid composition: Amino acid type, experimental value [expected composition].
MutOpen2	Asp + Asn, 3.73 [4]; Glu + Gln, 6.47 [7]; Ser, 0.95 [1]; Gly, 3.12 [3]; Arg, 4.41 [4]; Ala, 2.00 [2]; Pro, 1.15 [1]; Tyr, 0.95 [1]; Val, 2.18 [2]; Met, 0.38 [1]; Ile, 1.90 [2]; Leu, 1.02 [1]; Phe,1.85 [2]; Lys, 2.24 [2].
MutOpen3	Asp + Asn, 2.91 [4]; Glu + Gln, 6.00 [7]; Ser, 0.87 [1]; Gly, 3.36 [3]; Arg, 4.37 [4]; Ala, 1.78 [2]; Pro, 2.42 [1]; Tyr, 1.06 [1]; Val, 2.25 [2]; Met, 0.58 [1]; Ile, 1.99 [2]; Leu, 0.99 [1]; Phe,2.02 [2]; Lys, 2.32 [2].
WtSS	Asp + Asn, 7.27 [7]; Glu + Gln, 6.29 [6]; Ser, 0.40 [1]; Gly, 0.10 [0]; His, 1.09 [1]; Arg, 4.26 [4]; Ala, 2.21 [2]; Pro, 0.99 [1]; Tyr, 0.79 [1]; Met, 0.39 [1]; Ile, 2.00 [2]; Leu, 2.10 [2]; Phe,1.93 [2]; Lys, 2.15 [2].
MutSS	Asp + Asn, 4.11 [4]; Glu + Gln, 6.00 [6]; Ser, 0.49 [1]; Gly, 3.42 [3]; Arg, 4.23 [4]; Ala, 2.25 [2]; Pro, 1.11 [1]; Tyr, 0.80 [1]; Val, 2.19 [2]; Met, 0.28 [1]; Ile, 2.00 [2]; Leu, 1.00 [1]; Phe,1.87 [2]; Lys, 2.22 [2].

The values are the median of two independent amino acid analyses. Cysteines (and partly methionines and serines) are destroyed during hydrolysis (Blackburn, 1968).

8.3.1 Structural Characterisation of Minidomains by Circular Dichroism.

The minidomains were scanned by far-UV circular dichroism (chapter 5.4) in phosphate buffer at a low temperature in order to study the effect of mutations in the turn-region (Figure 8.2). Only the wild-type minidomains (WtOpen and WtSS, Figure 8.1) had characteristic alpha-helical CD-spectra with minima around 208 and 222 nm and a maximum around 190 nm. The relatively low CD-amplitude (MRE around -10,000 deg cm^2 $dmol^{-1}$) for WtOpen indicated that this existed only as a partially folded α-helical structure (Luo & Baldwin, 1997), and references herein). However, the WtSS minidomain had a higher helical content - probably due to the additional stabilisation introduced by the S-S bridge. More surprising was the observation that all mutants with the elastin β-turn were largely unstructured at the low temperature, although MutOpen2 with a protected C-

terminus, had a higher helix content in phosphate buffer (measured at 222 nm) than the other mutants.

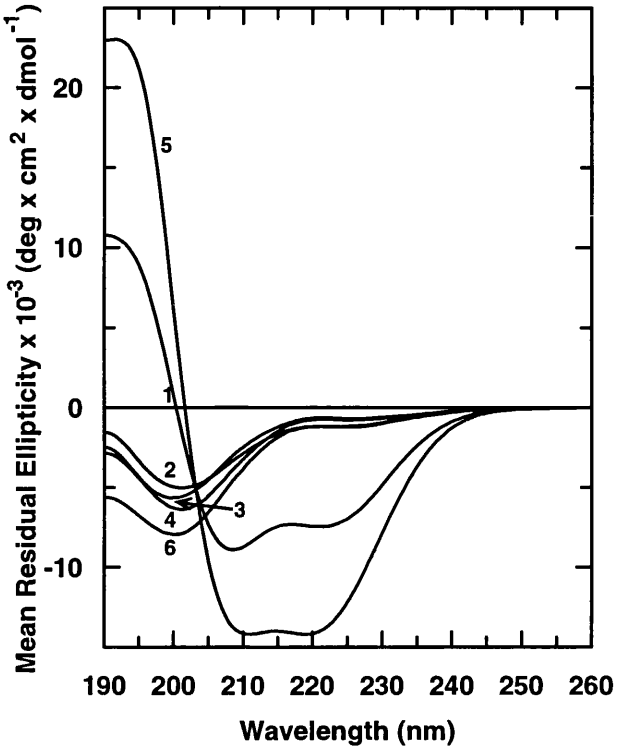

Figure 8.2 Circular Dichroic Wavelength Scans of Minidomains in Phosphate Buffer pH 7.0 or in Deionised Water. The minidomains were scanned once in 10 mM buffer at +6.4° C using a 0.2 cm stoppered cuvette with 5 s integration time (0.5 nm steps; slit: 2.0 nm). WtSS and MutSS were scanned in deionised water. The different spectra with their respective minidomain concentrations are respectively: WtOpen (1; 21.4 μM), MutOpen1 (2; 26.9 μM), MutOpen2 (3; 29.7 μM), MutOpen3 (4; 21.1 μM), WtSS (5; 24.3 μM) and MutSS (6; 25.1 μM).

The effect of TFE, known to have a stabilising effect on α-helices (Cammers-Goodwin *et al.*, 1996; Jasanoff & Fersht, 1994), was tested on all minidomains. It was observed that TFE stabilised or induced α-helix structure in all minidomains, illustrated for WtSS and MutSS in Figure 8.3. By increasing the concentration of TFE in phosphate buffer, a CD-transition from random coil to an α-helical spectrum was seen for MutSS, with a near isodichroic point around 204 nm (Figure 8.3b). Similar spectra were obtained for MutOpen1-3 (not shown). This demonstrated that all mutants possessed an α-helix propensity, even though they were largely unordered in phosphate buffer. The CD-spectra of the wild-type

minidomains in phosphate buffer reflected a greater α-helical content with increasing concentrations of TFE (Figure 8.3a and 8.3c).

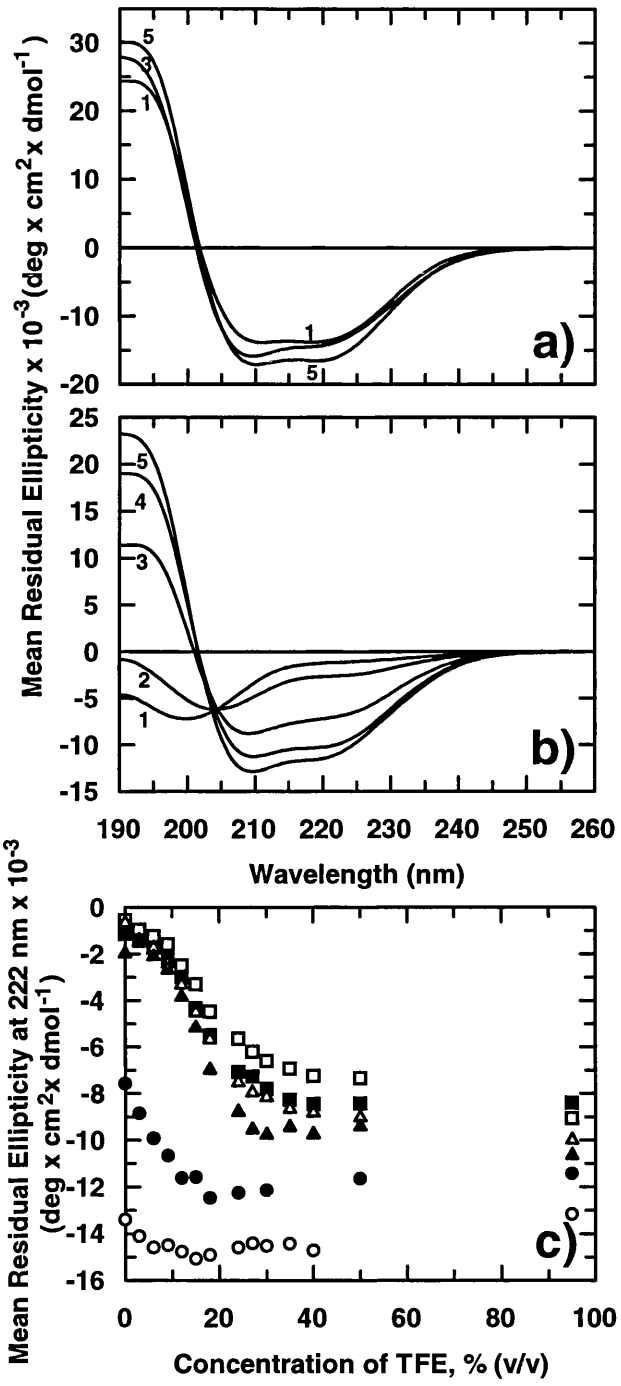

Figure 8.3 The Concentration Effect of Trifluoroethanol (TFE) on the Minidomains.

The effect of increasing concentrations of TFE in phosphate buffer on WtSS **(a)** and MutSS 6 **(b)** is shown. The numbers represent increasing concentrations of TFE: **1**, 0 % TFE; **2**, 9 % TFE; **3**, 18 % TFE; **4**, 27 % TFE; **5**, 95 % TFE. The minidomains were scanned once at +6.4° C and the experimental conditions and minidomain concentrations were the same as described in Figure 8.2. The effect on the mean residual ellipticity at 222 nm for WtOpen (●), MutOpen1 (□), MutOpen2 (■), MutOpen3 (▲), WtSS (○) and MutSS (▲) is illustrated in panel **(c)**.

At about 20 % (v/v) TFE the transition seemed to be complete, while for the mutant minidomains the maximum effect of TFE was seen at 30 %. However, when the concentration of TFE was increased above 20 % for wild-type minidomains (WtOpen and WtSS), the CD-signal at 222 nm was diminished. The sigmoid profiles of the CD-curves, with an inflection point at about 20 % TFE, suggest that cooperative interactions are involved in this transition. At 50% TFE, the helix content of the minidomains was in the order: WtSS > WtOpen > MutSS > MutOpen2=MutOpen3 > MutOpen1.

For all minidomains the temperature dependent CD scans in TFE were 95-100 % reversible after cooling as shown for MutSS and WtSS in Figure 8.4, and this is also reported by Starovasnik *et al.* (1997).

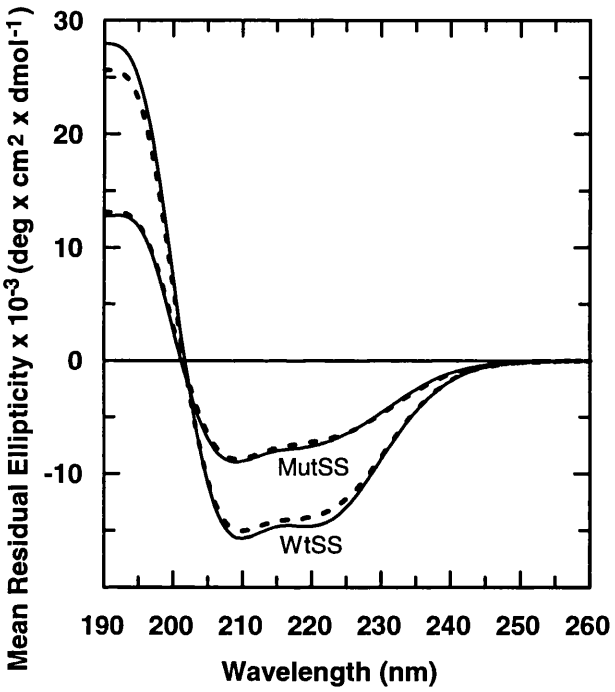

Figure 8.4 Reversibility After Melting of MutSS and WtSS in 30 % (v/v) TFE.

Minidomains MutSS (25.1 µM) and WtSS (24.3 µM) were stepwise heated in a 0.2 cm quartz cuvette from around 2° until 70° (MutSS) and until 90° C for WtSS. The minidomains were scanned once integrating at each 0.5 nm for 5 seconds. The thin lines are respectively the scans at +26.3° C and +23.7° C for WtSS and MutSS recorded at a rising temperature, and the bold dashed lines are the scans after the minidomains have been exposed to the high temperature and rapidly cooled down to 26.5° C and 23.4° C again.

The observed near isodichroic point at 204 nm for the effect of increasing concentrations of TFE (Figure 8.3b) and also for the temperature scans (not

shown), indicated that the melting of the α-helices in TFE for the minidomains followed a two-state reversible α-helix-coil transition. In order to quantify the effect of the mutations in the turn region, α-helix structure was first induced in all minidomains using TFE (30 % or 60 %, v/v) and their melting was then followed at 222 nm. However, two methods were first compared in order to optimise the best fit of the data to thermodynamic parameters (Figure 8.5).

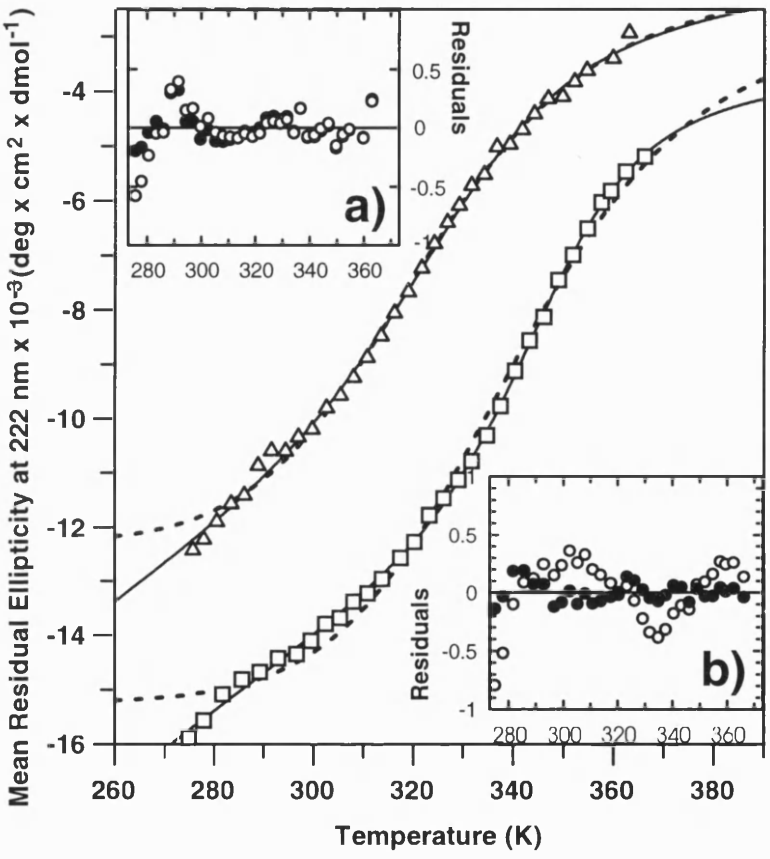

Figure 8.5 Optimising Methods of Fitting Raw CD Melting Data to the van't Hoff Equation. The raw data at 222 nm for melting of minidomains WtOpen (▵) and WtSS (□) in 30 % (v/v) TFE were fitted by two methods. One method set the folded state for WtOpen or the unfolded state for WtSS at a fixed value while fitting the other state to derive ΔH and ΔS (○ , - - - -). The other method fixes both the unfolded and unfolded states as two different slopes to derive ΔH and ΔS (● ,———). The differences between the fitted values for each method and the raw data (the residuals) are plotted for WtOpen in insert **a)** and for WtSS in insert **b)**. χ^2 (●) = 0.017 (WtOpen) and 0.0076 for WtSS, while χ^2 (○) = 0.031 (wtOpen) and 0.078 for WtSS.

One method set the unfolded or folded state as a fixed value and fitting the other state with ΔH and ΔS, the other fixing both the folded and unfolded state as slopes. It was acknowledged that for these minidomains the pre and post slopes were different. Comparing residuals of these fits, the latter method (the slope method) was the best and generally gave a best reduced chi squared (χ^2) (Figure 8.5). Nevertheless, the energies were not changed by more than 20-30 % (data not shown). The slope method was implemented for fitting the data from melting of all minidomains in 30 % (v/v)TFE (Figure 8.6) and in 60 % (v/v) TFE for the open minidomains (Figure 8.7).

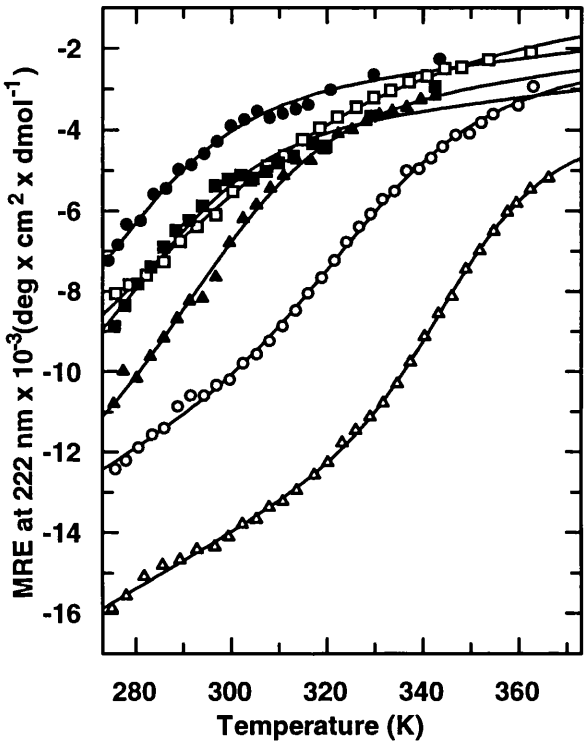

Figure 8.6 The Temperature Effect on Minidomains in 30 % Trifluoroethanol (TFE).

The melting of the minidomains was followed at 222 nm/260 nm using the average of three independent scans with an integration time of 5 s (in 0.2 cm cuvette, slit: 2.0), and the temperature effect on minidomains in 30 % (v/v) TFE are shown. Respectively, WtOpen (○), MutOpen1 (●), MutOpen2 (□), MutOpen3 (■), WtSS (△) and MutSS (▲). The data were fitted to a two-state transition with slopes (see methods). WtSS and MutSS were fitted with fixed pre- and posttransitional slopes.

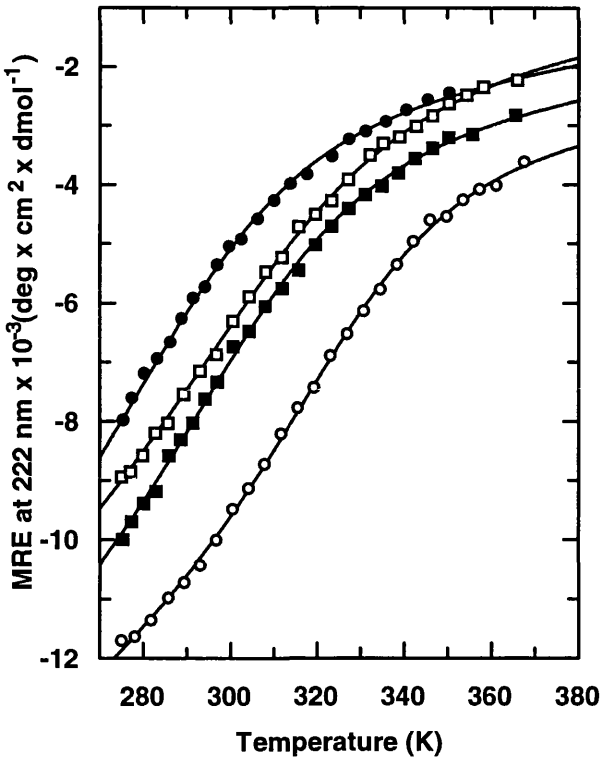

Figure 8.7 The Temperature Effect on Minidomains in 60 % Trifluoroethanol (TFE).

The melting of the minidomains was followed at 222 nm/260 nm using the average of three independent scans with an integration time of 5 s (in 0.2 cm cuvette, slit: 2.0), and the temperature effect on minidomains in 60 % (v/v) TFE are shown. Respectively, WtOpen (○), MutOpen1 (●), MutOpen2 (□) and MutOpen3 (■). The data were fitted to a two-state transition with fixed slopes (see methods).

Table 8.2 displays the thermodynamic data for the different minidomains in 30 % and 60 % TFE.

Table 8.2 Thermodynamic Values for Melting of Minidomains in Trifluoroethanol[a].

Minidomain	[TFE], % (v/v)	T_M (° C)	ΔH (kcal mol^{-1})	ΔS (kcal mol^{-1} K^{-1})
WtOpen	30 %	58	15.4 ± 1.0	0.046 ± 0.003
MutOpen1	"	10	12.0 ± 0.7	0.042 ± 0.003
MutOpen2	"	33	7.4 ± 0.4	0.024 ± 0.001
MutOpen3	"	16	12.9 ± 1.4	0.045 ± 0.005
WtSS	"	75	23.9 ± 1.0	0.069 ± 0.003
MutSS	"	26	12.8 ± 0.6	0.043 ± 0.002

Table continues on the next page.

Table 8.2 continued.

Minidomain	[TFE], % (v/v)	T_M (° C)	ΔH (kcal mol^{-1})	ΔS (kcal mol^{-1} K^{-1})
WtOpen	60 %	58	13.2 ± 0.8	0.040 ± 0.002
MutOpen1	"	22	9.3 ± 0.4	0.031 ± 0.001
MutOpen2	"	45	9.2 ± 0.5	0.029 ± 0.002
MutOpen3	"	37	10.0 ± 0.5	0.032 ± 0.002

[a] The Mean Residual Ellipticity was followed at 222 nm for each minidomain and then fitted to a reversible van't Hoff equation with ΔCp =O allowing ΔH and ΔS to float. The pre- and posttransitional slopes were fixed at the same values for all minidomains, and the pretransitional region for the mutants (MutOpen1-3 and MutSS) was extrapolated based on the observed data for their respective wild-type minidomains, WtOpen and WtSS.

Complete data for the stability of all minidomains were obtained only for 30 % TFE (Table 8.2). Compared to WtOpen the T_M was lowered by 25° C and 42° C for MutOpen2 and MutOpen3 respectively and by 48° C for MutOpen1 in 30 % TFE. The wild-type disulphide-stabilised minidomain WtSS was 49° C more stable than its mutant partner, MutSS. The difference in stability between WtOpen and MutOpen1 and between WtSS and MutSS shows that the GVPGVG-turn lowers the stability of the helices irrespective of the presence of a disulphide bond, notwithstanding the fact that the disulphide bonded minidomains were already 16-17° C more stable than the open forms. The stability difference between the open form and S-S stabilised wild type minidomains in tris buffer has previously been reported as 40° C (Starovasnik *et al.*, 1997), and for S-S stabilised laminin helices it was around 18° C (Antonsson *et al.*, 1995). These results confirmed that MutOpen1 was the least, while WtSS was the most thermostable.

There were no large differences in ΔH or ΔS values observed for the open form mutants and the corresponding S-S constructs, indicating that the thermodynamic effect of TFE was the same for both forms (both minidomains were initially melted in 0 % TFE). Interestingly, WtSS had larger values for ΔS and ΔH in TFE relative to WtOpen reflecting the influence of a stabilising S-S bond on the energetics of a helix-stabilising trifluoroethanol system.

For WtOpen and WtSS minidomains the CD-amplitude decreased with increasing temperature in HBS as shown for WtSS in Figure 8.8a.

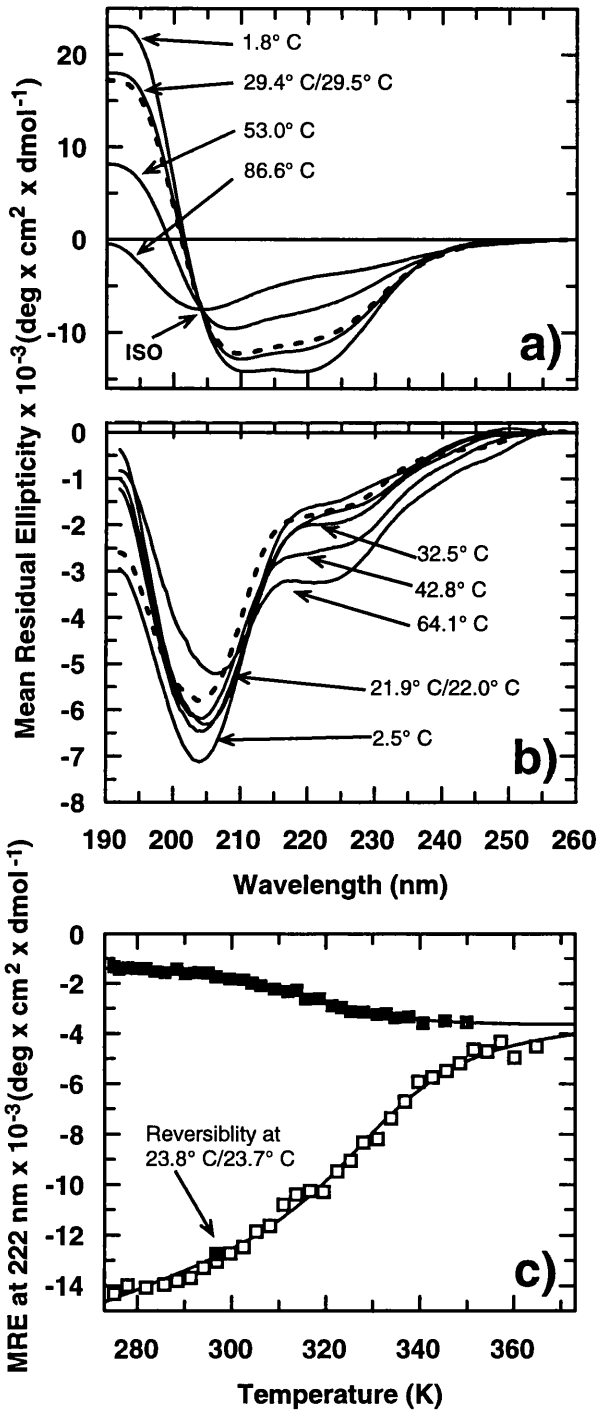

Figure 8.8 Temperature CD-wavelength Scans of WtSS and MutSS Minidomains in Deionised Water and in HBS with 0.005 % (v/v) P20.

WtSS (24.3 μM) in deionised water was scanned once from 190 nm to 260 nm (0.2 cm quartz cuvette with 5 s integration time; slit 2.0 nm; 0.5 nm step size) at different temperatures, as displayed in panel **a).** Similarly MutSS (350.7 μM) in Hepes Buffered Saline added 0.005 % surfactant P20 (panel **b**) was scanned from 192 nm to 260 nm at different temperatures using a 0.1 mm stoppered cuvette.

Figure legend continues on the next page.

Figure 8.8 continued.

The bold dashed lines (▪ ▪ ▪ ▪) illustrate the reversibility of the scans after being heated up to 60-80° C and then by rescanning the minidomains at the temperature x, (../x) given in the plots. Panel **c)** shows the melting of WtSS (□ ; 24.3 μM) and MutSS (■ ; 25.1 μM) in HBS buffer with P20. The melting was followed by measuring the CD-ellipticity at 222 nm/260 nm (in 0.2 cm cuvette, slit: 2.0 nm) at different temperatures averaging three independent scans with an integration time of 5 seconds.

The same behaviour was seen in TFE, phosphate buffer, micellar SDS and sodium sulphate at higher temperatures (Chapter 9). However, in contrast to the wild-type behaviour, the melting curves for the mutants in HBS, phosphate buffer or water had an increased CD-amplitude at 210-260 nm with increasing temperature and a near isodichroic point at 210 nm, as shown for MutSS in Figure 8.8b. All transitions were 90-100 % reversible as is illustrated in Figure 8.8abc. The MRE at 222 nm was followed for MutOpen1-3, MutSS and WtSS in 10 mM phosphate buffer and HBS with increasing temperature, and the melting curves for WtSS and MutSS in HBS are shown in Figure 8.8c. Their sigmoid profiles are consistent with the occurrence of a cooperative transition. The data were fitted to a two-state reversible transition in the direction folded to unfolded for WtSS, or to the reverse transition for MutOpen1, MutOpen3 and MutSS.

The concentration dependence of the spectra at 15.5° C and 48° C in phosphate buffer was also tested for selected minidomains (up to 620 μM; Figure 8.9). For MutSS the concentration was taken from 15 μM to 1.8 mM in the BIAcore running buffer (HBS with 0.005% (v/v) P20) at 25° C without any significant deviations at 222 nm. By equilibrium ultracentrifugation of WtSS and WtOpen it has previously been shown that they are monomeric and highly soluble (Starovasnik *et al.*, 1997). In addition, short to intermediate (8-23) GVPGVG-based peptides were also concentration independent at elevated temperatures (Chapter 6).

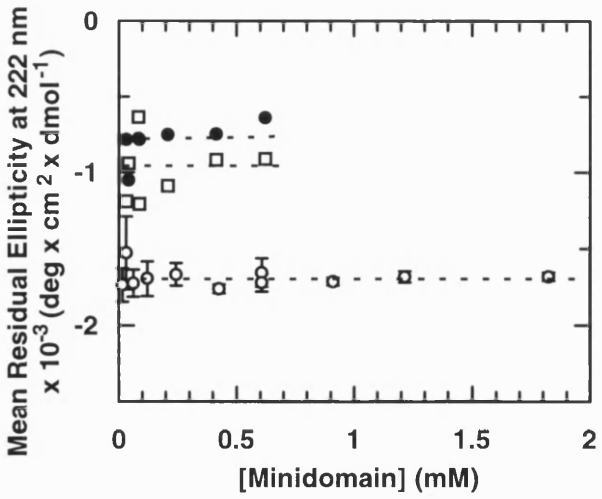

Figure 8.9 Concentration Dependence of Minidomains MutOpen1 and MutSS in Phosphate Buffer and HBS Respectively.

MutOpen1 in 10 mM phosphate buffer pH 7.0 was scanned one time (integrating for 5 s at each 0.5 nm) at different concentrations at 15.5° C (●) and 48° C (□) by varying cuvette sizes from 0.01 cm until 0.2 cm. MutSS (○) in HBS (BIAcore running buffer) was scanned at 25° C in 0.05 cm quartz cuvette at 222 nm. For MutSS, the average of 6 integrations at 222 nm with 10 s integration time was used. Standard deviation is thus given for MutSS at each point.

The melting of MutOpen2 exhibited unusual behaviour in which increased and decreased MREs at 222 nm as a function of temperature were seen (not shown). For this reason, only the thermodynamic data for MutOpen1, MutOpen3 and MutSS are given in Table 8.3.

Table 8.3 Thermodynamic Data for Inverse Thermal Transition at 222 nm for Mutant Minidomains in Buffers[a].

	T_M (° C)	ΔH (kcal mol^{-1})	ΔS (kcal mol^{-1} K^{-1})
MutOpen1 in phosphate buffer	21	16.5 ± 1.1	0.056 ± 0.004
MutOpen1 in HBS with P20	32	14.4 ± 1.8	0.047 ± 0.006
MutOpen3 in phosphate buffer	46	16.4 ± 1.2	0.051 ± 0.004
MutOpen3 in HBS with P20	43	12.1 ± 1.5	0.038 ± 0.005
MutSS in HBS with P20	42	18.4 ± 1.1	0.059 ± 0.003
GVG(VPGVG) peptides[b]	-	16.8	0.056

Table 8.3 continued.

[a] The melting data at 222 nm were fitted to a reversible van't Hoff equation allowing ΔS and ΔH to float. All data were fitted with fixed pre and posttransitional slopes. The heat capacity was fixed at 0. [b] From chapter 6, the values are the average of short $GVG(VPGVG)_n$ peptides (n=1 and 3) in 10 mM phosphate buffer pH 7.0.

The van't Hoff plots were linear with correlation coefficients (r) on the average of -0.98 (Figure 8.10), and there was a slightly better fit for the minidomains in HBS than in phosphate buffer.

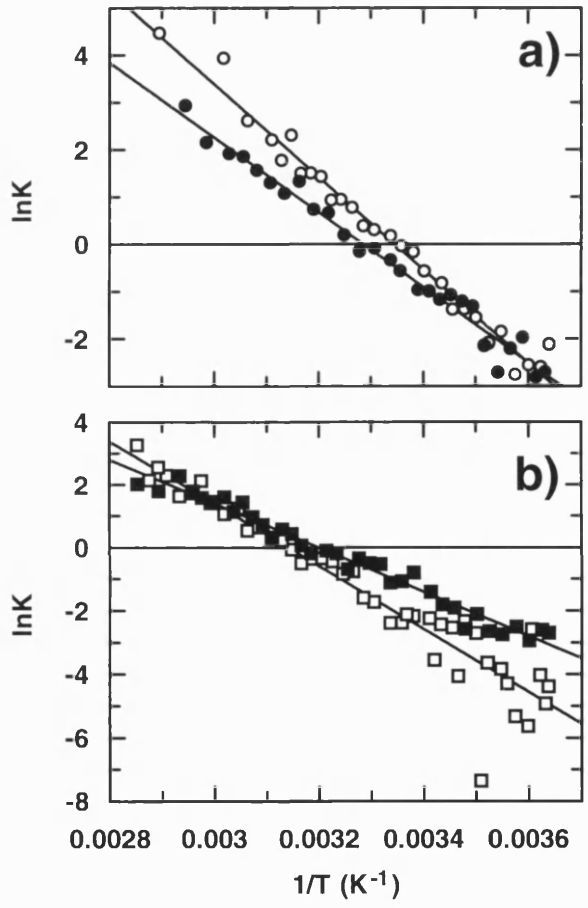

Figure 8.10 van't Hoff Plots of MutOpen1 and MutOpen3 for the Transition in HBS and Phosphate Buffer.

The plots are the fit of raw data to the two state van't Hoff transition (derived from equation 8.1) for MutOpen1 **a)** in respectively 10 mM phosphate buffer pH 7 (○) and in HBS (●). Similarly fittings are for MutOpen3 **b)** in 10 mM phosphate buffer pH 7 (□) and in HBS (■). Coefficients of correlation (r) varied between -0.95 to -0.99.

The energies involved in the transition (Table 8.3) were lower than for the melting of WtSS in HBS (ΔH = 20.8 kcal mol^{-1} and ΔS = 0.063 kcal mol^{-1} K^{-1}) and of similar magnitude to those observed for folding of individual GVGVPGVG-peptides (Chapter 6).

8.3.2 Evaluation of Minidomains by Surface Plasmon Resonance.

The kinetics of minidomain binding to immobilised Fc was studied using the BIAcoreX™ and BIAcore 2000™ (BIAcore, Sweden). The data generated were fitted both to a one-component model (equation 8.8) and to a two-component model (equation 8.9):

$$\text{Minidomain} + \text{Fc561} \leftrightarrow \text{Minidomain-Fc561} \qquad (8.8)$$

$$2\ \text{Minidomains} + \text{Fc561} + \text{Fc561*} \leftrightarrow \text{Minidomain-Fc561} + \text{Minidomain-Fc561*} \qquad (8.9)$$

where Fc561 and Fc561* represent two different epitopes on the ligand. The goodness of these fits is illustrated for WtSS at 20° C in Figure 8.11ab. There was generally a better fit (lower χ^2) to a two-component model over the temperature ranges tested, for both the association and dissociation phases. The on-rates were measured from the slope of a linear fit of the ks_A or ks_B values versus the lowest concentrations used, illustrated for WtSS and MutSS respectively in Figure 8.12a and 8.12b (inserts). The ks_A-values represent the fastest rate-constant relative to ks_B. The linear correlation coefficient (r) for the secondary fit of the fast on-rates was around 0.98. By contrast, the slower on-rates (k_{onB}) were approximately 50-fold lower in magnitude and generally exhibited much larger variability at the elevated temperatures. At the lower temperatures, however, both the fast and slow

off-rates were statistically determined for WtOpen and MutOpen, and also at all temperatures for WtSS and MutSS (not shown).

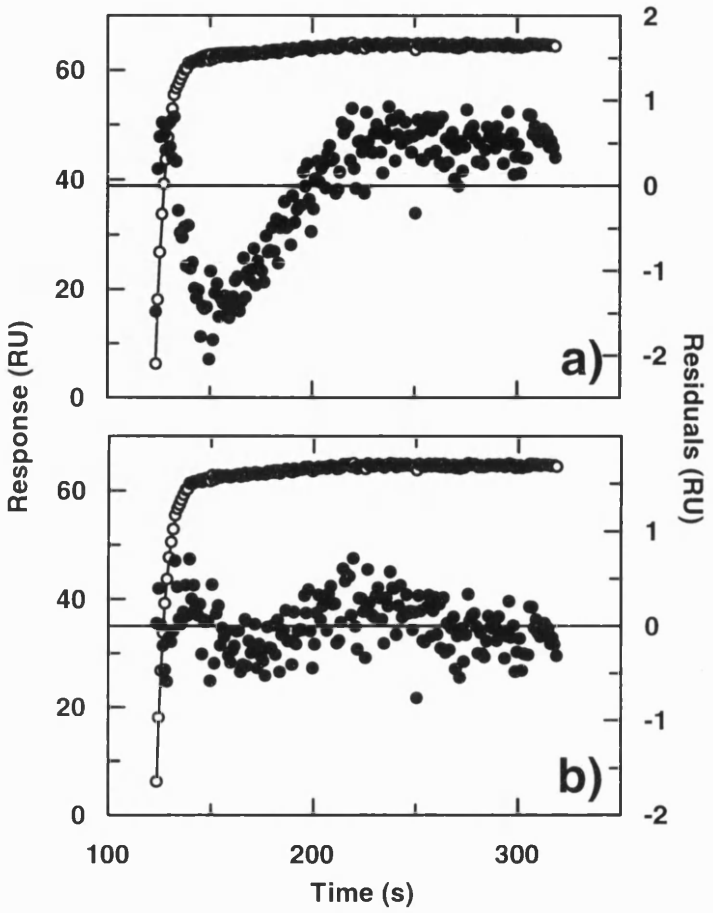

Figure 8.11 BIAcore Fits for WtSS and MutSS.

The association between 200 nM WtSS and immobilised Fc of 561 (mouse monoclonal IgG2a) at 20° C was fitted to a WtSS + Fc561 ← → WtSS-Fc561 model using BIAevaluation 2.1 software **a)**. The χ^2 for the fit was 0.556. Panel **b)** represents the fit to the model: 2 WtSS + Fc561 + Fc561* ← → WtSS-Fc561 + WtSS-Fc561*, where one WtSS minidomain reacts with 2 independent sites on Fc561. The χ^2 for this fit was 0.0795. The lines show the fit of raw-data (○), and residuals for the model (●).

The dissociation constants ~200 nM for WtOpen and ~100 nM WtSS using the slow off-rates (0.04 s^{-1} and 0.02 s^{-1} respectively at +10° C/+5° C) were very similar to those previously reported (Starovasnik *et al.*, 1997). However, it has to be stressed that the systems are different. In this report the association of the

minidomain to the Fc of a mouse IgG2a (561) was studied, while Starovasnik *et al* (1997) and Braisted and Wells (1996) studied binding to a human IgG1.

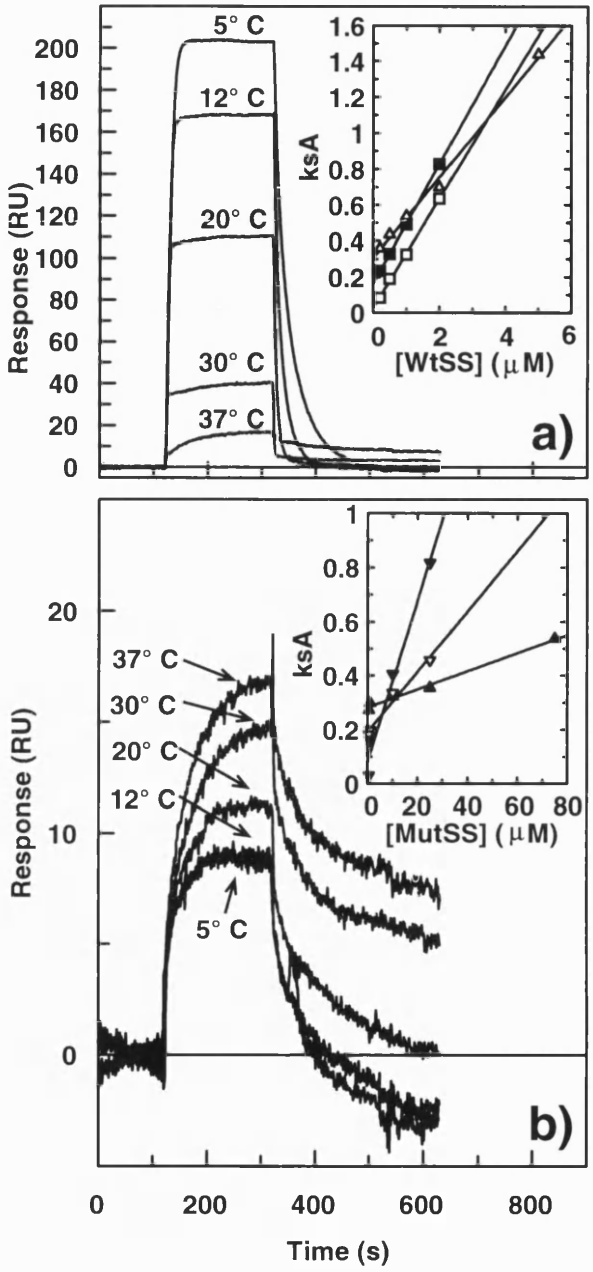

Figure 8.12 BIAcore Progress Curves for WtSS and MutSS.

The BIAcore progress curves for binding of minidomains to Fc561 at different temperatures are shown for 500 nM WtSS in **a)** and for 1 μM MutSS in **b)**. The plots of their respective fast on-rates, ksA (see methods), versus minidomain concentrations are illustrated in the inserted panels in **a)** for WtSS (□ , 12° C; ■ , 20° C and ▲ , 37° C) and in **b)** for MutSS (▲ , 12° C; ▽ , 25° C and ▼ , 37° C).

The temperature dependent progress curves for binding and dissociation of WtSS and MutSS to immobilised Fc of the mouse monoclonal IgG2a are shown in Figure 8.12a and Figure 8.12b, respectively. Interestingly, there was a reverse temperature effect for the binding of MutSS relative to WtSS (Figure 8.12ab and Figure 8.13abc).

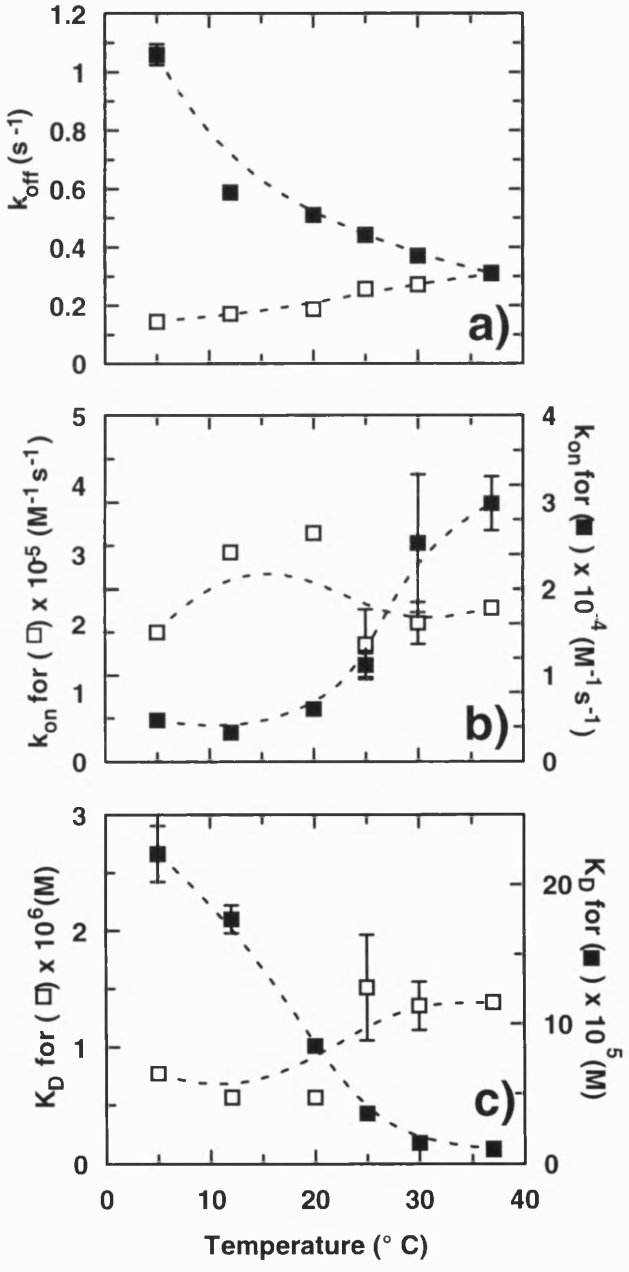

Figure 8.13 The Temperature Dependence of the Fast Kinetic Constants for WtSS and MutSS Minidomains.

Figure legend continues on the next page.

Figure 8.13 continued.

The respective kinetic constants for the S-S linked minidomains WtSS (□) and MutSS (■) are in panel a, b and c. Panel **a)** shows the fast off-rates, panel **b)** the fast on-rates and panel **c)** illustrates their respective fast dissociation constants (= k_{off}/k_{on}) at different temperatures. The k_{on}-rates were found from the slopes of the plots of ksA versus minidomain concentration, as is illustrated in Figure 8.12ab (inserts) for the model Minidomain + Fc561 + Fc561* ← → Minidomain-Fc561 + Minidomain-Fc561*. The off-rates were determined from the model $Minidomain_i$-$Fc561_i$ ← → $Minidomain_i$ + $Fc\text{-}561_j$ (parallel dissociation of two complexes). The off-rates were fitted using BIAevaluation 2.1 and the on-rates were fitted using both BIAevaluation 2.1 and GRAFIT (Leatherbarrow, 1989). Both the on-rates and off-rates display their fitted standard errors. The standard errors of the dissociation constant were manually calculated based on SE's for k_{on} and k_{off}.

The fast off-rates for WtOpen, MutOpen1 and WtSS increased with increasing temperature (Figure 8.13a and Figure 8.14a), while over the same temperature range the mutant MutSS had a lowered off-rate (Figure 8.13a). The slow off-rates did not vary much for the minidomains over the temperature range tested, but both the fast and slow off-rates decreased for MutSS from 5° to 37° C (not shown). The slow off-rates for the MutSS were also lower than for WtSS (respectively ~0.01 s^{-1} versus ~0.02 s^{-1}) which is surprising considering the lower residual structure in this minidomain. Again, there was only a small variation in the on-rates for WtSS over the temperature range applied. For MutSS however, the on-rate tripled on increasing the temperature from 5° to 37° C (Figure 8.13b). Similar effects were seen with WtOpen and MutOpen1 whose on-rates halved and doubled, respectively, over the temperature range 10° C to 30° C (Figure 8.14b). The overall effect of these changes is exemplified by the behaviour of the MutSS minidomain, whose increased fast on-rate and lowered fast off-rate at 37° C improved its affinity some 21-fold, compared with that observed at 5° C (K_D reduced from 222 μM to 10.4 μM) (Figure 8.13c). Using the slow off-rates, MutSS also improved its affinity by 8-fold (from 2.8 μM to 0.4μM) in the same temperature range.

In contrast, for the WtOpen minidomain (without S-S bridge) the K_D increased 8-fold over the same temperature range (Fig 8.14c), while for WtSS (with S-S bridge) the K_D was unchanged (using either the slow or fast off-rates).

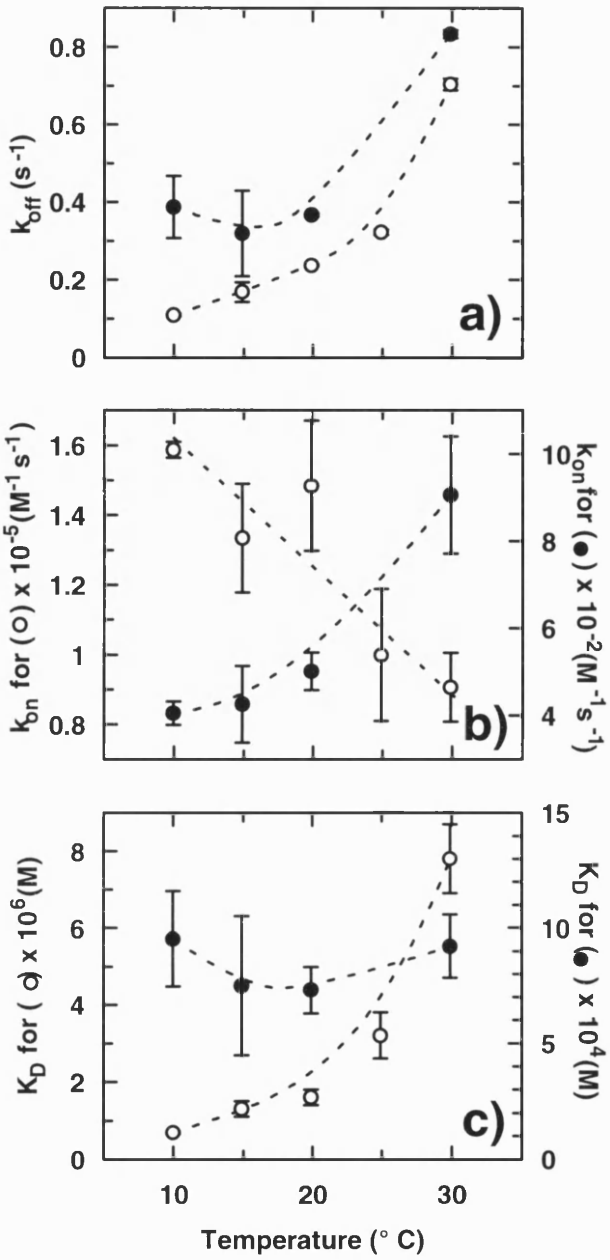

Figure 8.14 The Temperature Dependence of the Fast Kinetic Constants for WtOpen and MutOpen1 Minidomains. The respective kinetic constants for the 'open' minidomains WtOpen (□) and MutOpen1 (■) are in panel a, b and c. Panel **a)** shows the fast off-rates, panel **b)** the fast on-rates and panel **c)** illustrates their respective fast dissociation constants (= k_{off}/k_{on}) at different temperatures as described in Figure 8.13.

8.3.3 Free Energy Differences

The ΔΔG values vs. temperature had a better linear fit for WtOpen and MutOpen1 (correlation coefficient r = -0.99) than for WtSS and MutSS (r = -0.96, Figure 8.15).

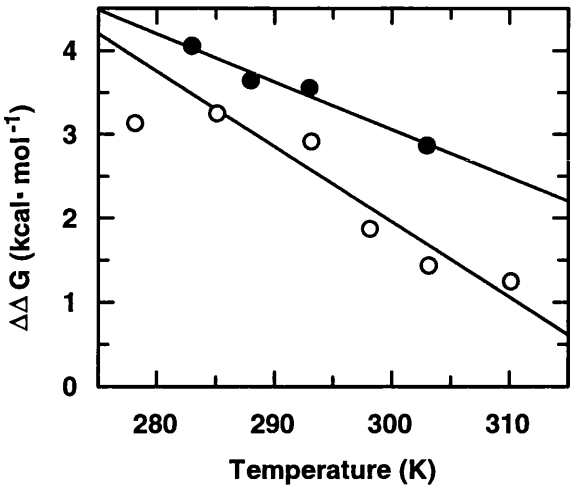

Figure 8.15 The Temperature Dependency of Binding Free Energy (ΔΔG) of MutOpen1 and MutSS Relative to Their Wildtype Minidomains.

The binding free energy at different temperatures was calculated as described in the methods, and the ΔΔG versus different temperatures is displayed (ΔΔG = $+RT_x$ ln[K_D (MutOpen1 at T_x)/K_D (WtOpen at T_x)] and ΔΔG = $+RT_x$ ln[K_D (MutSS at T_x)/K_D (WtSS at T_x)]. The linear fit of the data using GRAFIT (Leatherbarrow, 1989) gave a linear correlation coefficient (r) of -0.99, and a slope of -0.0570 ± 0.007 kcal mol^{-1} K^{-1} (intercept 20.2 ± 2.0) for MutOpen1 and likewise (r) of -0.96 with a slope of -0.0897 ± 0.016 kcal mol^{-1} K^{-1} (intercept 28.9 ± 4.8) for MutSS.

Over the temperature range measured, ΔΔG was positive for both minidomain pairs indicating that the binding of wild-type to Fc was tighter than that of the mutants. However, over the same temperature range ΔΔG decreased by 0.057 kcal mol^{-1} K^{-1} for MutOpen1 relative to WtOpen, and by 0.090 kcal mol^{-1} K^{-1} for MutSS relative to WtSS. The Δ(ΔΔG) was lowered respectively by 1.2 kcal mol^{-1} (from 283 K to 303K) for MutOpen1 or by 2.9 kcal mol^{-1} (from 278 K to 310 K) for MutSS relative to the wildtype partners. If this relationship were to hold over a wider temperature range it predicts that the affinity of MutOpen1

would exceed that of WtOpen beyond 81° C, while that of MutSS would exceed the affinity of WtSS beyond 49° C.

8.4 Discussion

The first example of the introduction of an elastin-like sequence into the primary structure of a globular protein has been described here. Previously it has been shown that short elastin peptides can undergo an entropically driven transition from an extended to a type II β-turn, mimicking the behaviour of the much longer, naturally occurring elastin molecule (Chapter 6, Reiersen *et al.*, 1998). By increasing the hydrophobicity in the turn-region the probability of formation of the turn containing the elastin GVPGVG sequence should increase with increasing temperature. In this design, the wild-type β-turn (type I) residues were replaced with the helix-destabilising Val, Gly, Pro residues, while the native Glu-Glu sequence adjacent to the turn was mutated to Gln-Gln in order to avoid an abnormally high transition temperature (Chapter 6, Reiersen *et al.*, 1998). Making such a change thus ran the risk of affecting the helix stability, since Val, Gly and Pro are known to have a low helix propensity although Gln is more stabilising than Glu (Chakrabartty *et al.*, 1994).

The substitution of the type I β-turn by the more hydrophobic elastin turn resulted in melting of the helical structure of the wild-type minidomain in phosphate buffer. However, even the wild-type minidomain is unstable *per se* and stabilisation by a disulphide-bridge at the termini was found to be necessary (Starovasnik *et al.*, 1997). Stabilising α-helices in TFE also offers a way of expressing the difference in intramolecular stability between mutant and wildtype α-helical minidomains where the helicity of the mutants is more or less lost. This is illustrated for MutOpen1 and MutSS whose melting temperatures were decreased by about 48° C in 30 % TFE compared to wild type WtOpen and WtSS minidomains (Table 8.2). MutOpen2 and MutOpen3, which retained the Glu25-Glu26 sequence close to the turn, were more helical in TFE than the Gln25-Gln26 sequences and their T_M's were lowered by 'only' 25-42° C. This unexpected effect may be due to stabilising interactions with positively charged residues

(Arg28 or Lys31) located close to the turn. A helix stabilising effect was seen for MutOpen2 which contained an amidated C-terminus (Table 8.2), an effect that has previously been shown for α-helices (Fairman *et al.*, 1989).

The CD-amplitudes for MutOpen1-3 and MutSS, in phosphate buffer or in HBS containing P20, increased at 222 nm with increasing temperature, signalling the formation of an α-helix or type I β-turn (Perczel *et al.*, 1993; Woody, 1995). The shift of the isodichroic point from 204 nm to 210 nm, and the lower intensities of the CD-signals at 222-nm for the melting curves in buffer, were more characteristic of a type I β-turn (Woody, 1995). Several other observations also argue that a type I β-turn was formed at the higher temperatures. Type I β-turn structures have also been found in elastin sequences (Arad & Goodman, 1990; Bhandary *et al.*, 1990) although the Pro-Gly type II β-turn is between 0.2 - 1.7 kcal mol^{-1} more stable than type I β-turn and is also more common in elastin (Urry, 1993; Yang *et al.*, 1996) and references therein). A conformational interconversion between type I and II β-turn in proteins is however quite common for Pro-Gly turns (Gunasekaran *et al.*, 1998).

The energies associated with the observed transitions for MutOpen1, MutOpen3 and MutSS (Table 8.3) were similar to those found for short (8-12 residue) elastin peptides (chapter 3). The melting of MutOpen1 over the temperature range 0-60° involved a free energy difference of 3.0 kcal mol^{-1} , within the range reported to be required for β-turn formation (2-4 kcal mol^{-1}) though just below that required for α-helix formation (4 kcal mol^{-1}; (Yang *et al.*, 1996 and references herein).

The better fit of the BIAcore data to a heterogeneous kinetic model may be due to several factors. The minidomains were initially selected by panning against a human monoclonal IgG1 (Braisted & Wells, 1996). In this system the binding to the Fc-region of a mouse monoclonal IgG2a was described. It is possible that the panning of a specific binder to human IgG1 has selected for a species whose binding to related IgG epitopes is less promiscuous than the parent domain. This selection seems to have resulted in a weaker, heterogeneous binding behaviour to IgG2a (the better fit to two Fc561 sites, Fc561 and Fc561*, is shown in Figure 8.11). This may have implications for further design of antibodies by phage

display - the choice between specificity or promiscuity. An alternative explanation is that the increased temperature may have generated different conformations of the epitopes on IgG2a due to structural instability, seen as a better fit of data to one-component kinetics at low temperatures and two-component kinetics at higher temperatures for some minidomains. Starovasnik *et al.* (1997) also suggest two $\chi 1$ rotamer conformations for Phe-14 in the binding-site of the wild-type minidomain. Thirdly, there may have been a mixed population of mutant domains, originating from the presence of multiple β-turns, although we think this unlikely.

The mutant minidomains MutOpen1 and MutSS in HBS showed a good correlation between on-rate and 2° structure content (measured by CD-amplitude at 222 nm) as temperature was increased. For MutSS a 21-fold improvement in K_D was obtained, due predominantly to the decrease in off-rate at the higher temperatures, an effect not seen for its open partner, MutOpen1. This was in stark contrast to the behaviour of wild-type WtSS which, although more thermostable, showed little variation in K_D over the same temperature range. This improvement in binding of the mutants with increasing temperature is, we believe, due to the formation of an entropy driven type I β-turn.

Other studies have shown a correlation between lowered α-helicity and lowered affinity (on-rates) of human insulin-like growth factor I (Jansson *et al.*, 1997). For Protein A Fc-binding domains, the residues involved in binding are known to be aligned on adjacent faces of two of the three helices (Starovasnik *et al.*, 1997). Any perturbation of these two helices will be likely to affect the affinity of the domain. This is clearly observed for the wild type domains where denaturation of the helices mirrors loss of binding. However, in the mutant domains, the temperature induced formation of a type I β-turn (Starovasnik *et al.*, 1997) may serve to stabilise the alignment of fluctuating helices (reducing its conformational entropy relative to the wild type), resulting in correctly positioned binding residues and a concomitant increase in affinity. As a matter of comparison, the formation of different turn conformations has also been shown to affect binding of the RGD-epitope to Integrins (Bach II *et al.*, 1996) and of inhibitor binding to HIV-1 protease (Nicholson *et al.*, 1995).

There have been several previous attempts to alter the stability of proteins in a predictable manner by mutating residues in turn regions. Longer loops have been inserted without any significant effect on protein stability and folding, and residue substitutions have also been made (Ladurner & Fersht, 1997; Predki *et al.*, 1996; Viguera & Serrano, 1997). However, mutations of structurally important turns may still affect the function of a protein (Bach II *et al.*, 1996). The ability to control binding of Protein A by a temperature switch is a challenging task since its triple-helical core is normally quite thermostable. A switch which turns off the activity at low temperatures and turns it on again at higher temperatures may have several industrial applications, and in the particular example described here, may offer a novel temperature regulation for protein A. It may also become a general method for regulating other globular proteins where lowering the on-rate at lower temperatures and increasing it at higher temperatures leads to regulation of binding or some other activity.

Chapter 9. Sodium Sulphate Refolds and Reactivates a Globular IgG-binding Minidomain with a Short Elastin Polymer β-turn[1].

9.1 Introduction

To develop novel switches in binding proteins in order to affect their affinity is of general interest. Protein A is a multi domain binding protein that is very frequently utilised for purification of antibodies and for production of fusion proteins (Hermanson *et al.*, 1992; Nilsson & Abrahmsén, 1990). According to data from Repligen's home page (www.repligen.com) the therapeutic market for monoclonal antibodies is estimated to be more than $1 billion in 1999, which stresses the need to develop simple IgG purification procedures which are easily adjusted to GMP demands. Protein A is found on the surface of *Staphylococcus aureus*, and the five ~58 residue domains, E, D, A, B, C are suggested to each exhibit a triple α-helical structure (Gouda *et al.*, 1992; Jendeberg *et al.*, 1996; Starovasnik *et al.*, 1996; Tashiro *et al.*, 1997; Uhlén *et al.*, 1984). The third helix is not necessary for Fc-binding, and it is possible to remove it by improving the packing of the two anti-parallel helices and selecting for binding using phage display technology (Braisted & Wells, 1996; Starovasnik *et al.*, 1997) This new minidomain with two helices additionally stabilised by a disulphide bridge, has now been a target for a selective turn mutation.

The water soluble hydrophobic muscle polymer protein elastin can be induced to contract by reducing its length by 50 % and as a consequence lift a mass greater than 1000 times its own mass, and in this context it may be a potential modulator of structural transitions also in globular proteins (Reiersen *et al.*, 1998; Urry, 1984, 1993). The ability for the muscle protein elastin to operate as a structural switch is dependent on the location of hydrophobic groups surrounding a proline-glycine type II β-turn interspersed with mobile glycinyl-valyl-glycinyl repeats (Urry, 1988a, b; Urry *et al.*,1998). In elastin fibres this is mainly based on the

[1] To be submitted for publication.

repeating sequence (VPGVG)n forming a β-spiral with three repeats for each turn of the spiral in its folded form. The two valines are hydrophobically hydrated at low temperatures (Urry, 1984; Urry *et al.*, 1997, 1998). Exposing hydrophobic groups on the surface of proteins is normally structurally destabilising (Schwehm *et al.*, 1998), and type II β-turns in globular proteins are usually very hydrated (Robert & Ho, 1995). However, by altering solvent conditions and temperature the unstructured hydrophobic turn region of elastin is dehydrated, and the valine groups across the turn mutually stabilise the β-turn (entropically driven folding with an inverse temperature transition) (Reiersen *et al.*, 1998; Urry, 1993). For example adding 1.0 M sodium chloride lowered the transition temperature for the inverse folding of (VPGVG)n polymers by more than 14° C, and kosmotropes such as ammonium sulphate are even better inducers (Urry, 1993). The ability of the short elastin peptide to undergo temperature and alcohol induced transitions has already been described (Reiersen *et al.*, 1998). It has also been shown that by replacing a native type I β-turn with an elastin β-turn, it is possible to induce IgG-binding of the minidomain by raising temperature (chapter 8). In this context it was of interest to test whether these sequences may alter the structure and function of a minidomain from Protein A as a function of solvent composition.

Water contributes to the stability of proteins by promoting a hydrogen-bonded network on the protein surface (Nakasako, 1999). Additionally, it may act as a modulator of protein folding where, during structural transitions, it can assume the role of a "foldase" (Sundaralingam & Sekharudu, 1989; Xu & Cross, 1999). Also, it may destabilise some secondary structures as is observed for cold-denaturated proteins (Antonino *et al.*, 1991). Sodium sulphate is frequently used for protein purification purposes. The kosmotropic salt is suggested to interact strongly with water molecules, exhibiting a structuring effect on the bulk water. Thus, it minimises the water exposed surface area in proteins and stabilises proteins (Collins & Washabaugh, 1985). For elastin sequences the salt has the potential to break down hydrophobically hydrated water molecules and promote folding. It has recently been shown that sodium sulphate is capable of inducing helical structure in staphylococcal nuclease, initially through intramolecular stabilisation, but by increasing protein concentration also intermolecular associations promote the α-helical folding (Uversky *et al.*, 1998a). Sodium sulphate also stimulates α-helix

formation in short peptides (Scholtz *et al.*, 1991b), and promotes the assembly of monomers to form the native tetrameric enzyme catalase, from bovine liver (Prajapati *et al.*, 1998).

In this chapter, an engineered Protein A minidomain which exhibited no detectable secondary structure by circular dichroism due to a hydrophobically hydrated elastin β-turn, is shown to regain its native β-turn and IgG-binding affinity by altering solvent condition with the kosmotrope sodium sulphate. This implies that it is possible to engineer the elastin muscle sequences into globular proteins in order to obtain a solvent-dependent switch that can modulate protein activity.

9.2 Materials and Methods.

The peptides were synthesised and analysed by HPLC, mass spectrometry and circular dichroism as described in chapter 8.3.

9.2.1 Surface Plasmon Resonance Spectroscopy.

The interaction of the minidomains (analytes) with immobilised Fc of the mouse mAb 561 (ligand) was followed over time by surface plasmon resonance spectroscopy using BIAcore2000^{TM} (Biosensor, Sweden) as described in chapter 8.3.4. Interaction analysis was performed by dissolving the minidomains in the different running buffers of HBS/P20 with Na_2SO_4 (0 to 0.6 M). To avoid rebinding of analytes a relatively high flow-rate of 30 µl/min in HBS/P20/Na_2SO_4 was applied, and the accuracy of the 100 µl analyte injections was obtained using the KINJECT command. The data was analysed as described previously (chapter 5.5.1 and chapter 8.3.2).

9.3 Results

The engineered minidomains in this study were based on the B-domain of Protein A (Braisted & Wells, 1996; Starovasnik *et al.*, 1997), where the native type I β-turn was replaced by an elastin β-turn, GVPGVG. Figure 8.1 (chapter 8.4) displays the primary structures of the minidomains in this study. The introduction of an extra disulphide-bridge stabilises the α-helical structure (Starovasnik *et al.*, 1997). However, the mutant minidomains, studied by circular dichroism, were unstructured in water or phosphate buffer (MutSS and MutOpen1), illustrating the destabilisation by the hydrophobic β-turn (Chapter 8.4.1, Reiersen & Rees, 1999). In contrast, the wild-type minidomains, WtOpen and WtSS, had an α-helical CD-spectra in buffer as observed previously (Braisted & Wells, 1996; Starovasnik *et al.*, 1997) but with a relatively low helical content, especially for the minidomain without S-S bridge (Figure 8.2, chapter 8.3.1).

In chapter 8 it was shown that it is possible to induce an α-helical structure in the unordered minidomains by dissolving them in TFE (Reiersen & Rees, 1999). Additionally, by varying the concentration of TFE it was possible to study the energetics of the temperature effect of increasing concentrations of TFE as described for WtOpen in Figure 9.1 and Table 9.1. The ΔH and ΔS values decreased by increasing concentrations of TFE although their T_Ms were quite similar.

Also micellar SDS (25 mM) induced CD-spectra which resembled α-helices for both WtOpen and MutOpen (Figure 9.2ab). However, these spectra exhibited a much larger 208/222 ratio than observed for the TFE-induced spectra. This is typical for an incomplete α-helix induction or a transition to a 3_{10}-helical structure (Hungerford *et al.*, 1996). Following the MRE's at 222 nm of the minidomains in different solvents as a function of temperature, it is possible to evaluate the stabilising effects of the solvents.

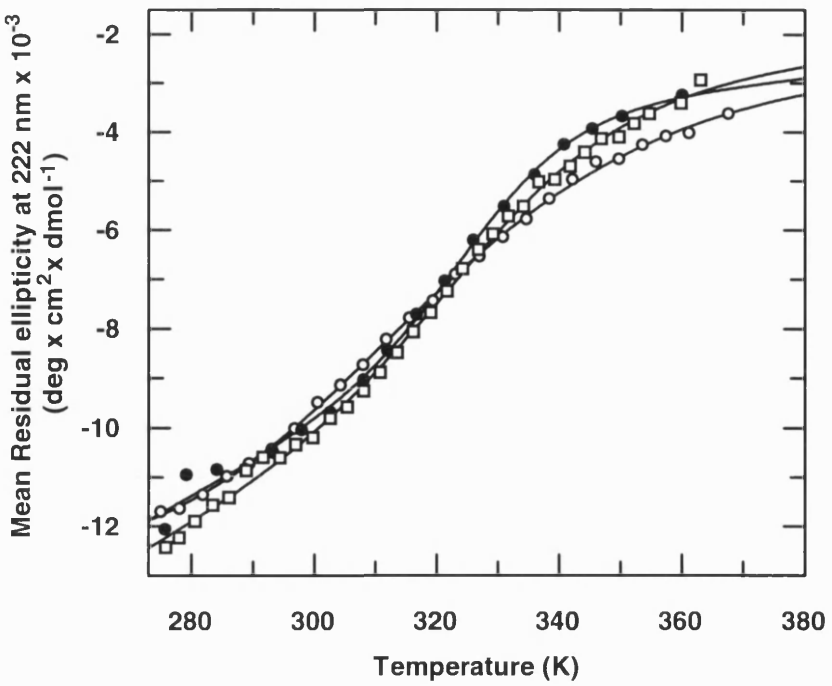

Figure 9.1 Melting Curves of WtOpen in Increasing Concentrations of TFE.

Minidomain WtOpen (21.4 μM) was scanned at 222 nm/260 nm in 20 % (v/v) TFE (●), 30 % TFE (□) and 60 % TFE (○) by averaging three scans of five second integration at each 0.5 nm step. The data were fitted to a two-state transition with fixed pre and post-transitional slopes as described in Figure 8.5.

Table 9.1 Thermodynamic Values for Melting of WtOpen in Trifluoroethanol[a].

% TFE (v/V)	T_M (° C)	ΔH (kcal mol^{-1})	ΔS (kcal mol^{-1} K^{-1})
20 % TFE	55	22.7 ± 2.7	0.069 ± 0.009
30 % TFE	58	15.4 ± 1.0	0.046 ± 0.003
60 % TFE	58	13.2 ± 0.8	0.040 ± 0.002

[a] The Mean Residual Ellipticity was followed at 222 nm for each minidomain and then fitted to a reversible van't Hoff equation with ΔCp =O allowing ΔH and ΔS to float. The pre- and posttransitional slopes were fixed.

Temperature melting of WtOpen in micellar SDS had a very shallow slope (Fig 9.2ab) intercepting the melting curve of WtOpen in phosphate buffer (the estimated T_M of melting in phosphate was 19° C).

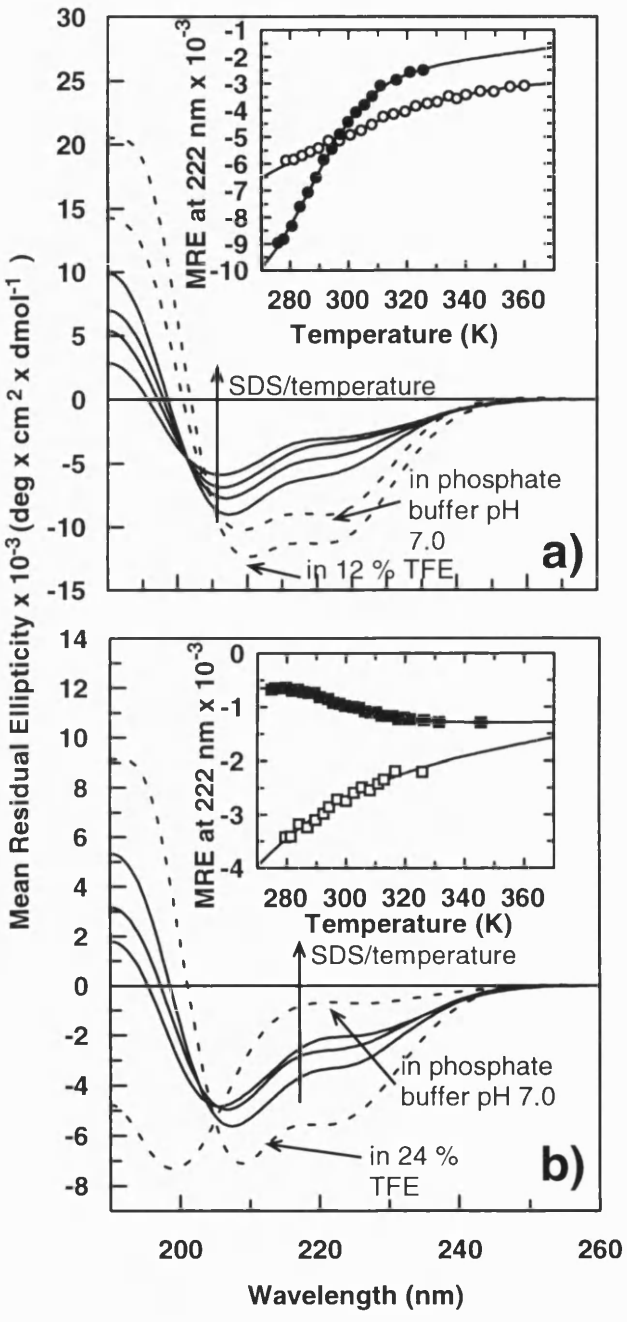

Figure 9.2 Circular Dichroic Scans of WtOpen and MutOpen1 in SDS, TFE and Phosphate Buffer.

The CD scans of WtOpen in 25 mM SDS, phosphate buffer (at 2.2° C) and 12 % (v/v) TFE (at 2.5° C) are displayed in panel **a)**. The arrow for SDS/temperature is in the direction of increasing temperature, respectively for each curve at 5.5° C, 35° C, 64° C and 87° C.

Figure legend continues on the next page

Figure 9.2 continued.

The MutOpen1 was also scanned in the similar solvents (Panel **b**) at 1.5° C and 6.4° C for respectively phosphate buffer and 24 % TFE, and the arrow for SDS/temperature is from 6.4° C, 23.9° C and 52.6° C. The inserted panels in **a)** and **b)** similarly illustrate respectively the melting of WtOpen in phosphate buffer (closed circles) and in 25 mM SDS (open circles), and melting of MutOpen1 in phosphate buffer (closed square) and 25 mM SDS (open square).

There was thus a complicated effect on the α-helical structure by SDS which was destabilising at the lower temperatures and stabilising at higher temperatures. This is probably correlated to the induction of the more unstable 3_{10}-helix. The melting curves in SDS had isodichroic points around 202 nm suggesting a two-state transition. However, relative to its structure in phosphate buffer, the mutant minidomain MutOpen was stabilised in SDS.

Figure 9.3ab illustrates the effect of sodium sulphate on the secondary structures of the disulphide stabilised minidomains, MutSS and WtSS. The kosmotrope sodium sulphate was applied to both MutSS and WtSS, and it induced structures in both minidomains. The largely unordered MutSS in water as observed by a CD-spectrum with a global minimum around 200 nm and a negative shoulder between 210-210 nm (Figure 9.3a), gradually transformed into an α-helical like CD-spectrum by increasing the sodium sulphate concentration. At 1.87 mM sodium sulphate the CD-spectrum for MutSS had a positive global maximum around 190 nm, and two negative minima around 208 and 222 nm. However, there was no single isodichroic point, and the cross-over points were generally observed varying between 206-210 nm. The low intensities of the amplitudes and the shift of the cross-over points argue that sodium sulphate induced structure that was more similar to a type I/III β-turn CD-spectrum (Perczel *et al.*, 1993; Woody, 1995). When sodium sulphate was added to WtSS peptide it also improved its α-helical structure as revealed by a larger CD-amplitude around 190 nm and 208/222 nm (Figure 9.3a). By increasing the concentration of the MutSS peptide from 122 μM to 1.82 mM and simultaneously lowering the sodium sulphate concentration from 0.9 M to 0.8 M, the positive amplitude increased while the negative amplitude at 208/222 nm decreased (Figure 9.3b). This suggests, in contrast to sodium sulphate induced structure in SNase (Uversky *et al.*, 1998a), that intermolecular interactions (aggregation) destroy the structure. The increased CD-

amplitude seen for concentrations up to 0.9 M for WtSS (and for MutSS) may on the other hand be due to stabilising intramolecular interactions.

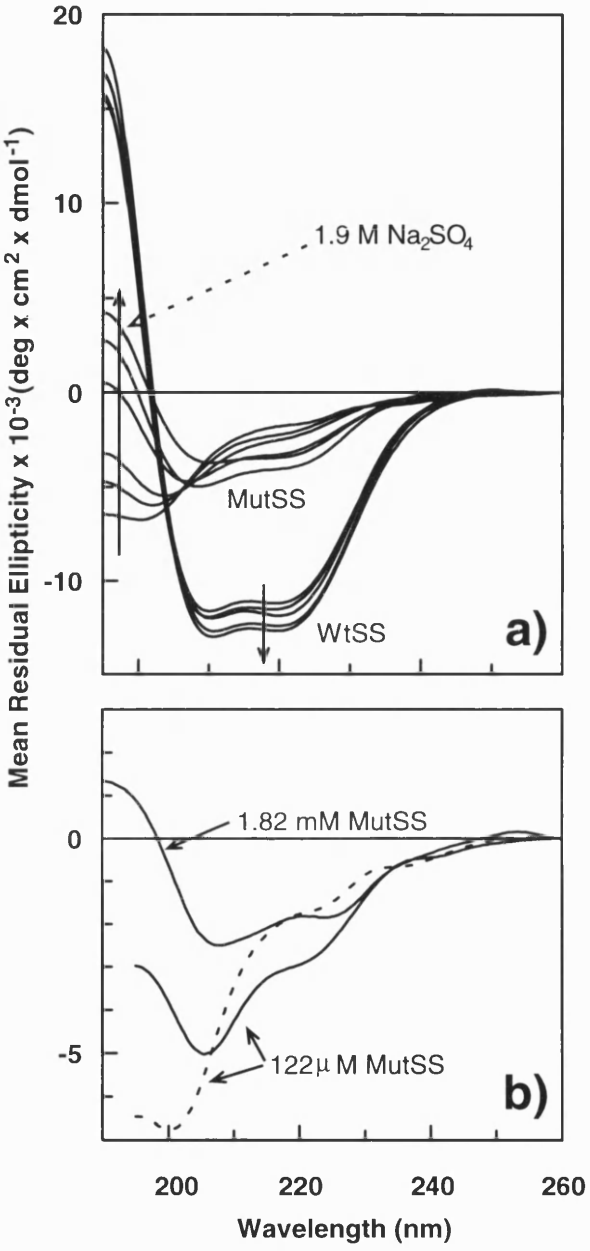

Figure 9.3 The Effect of Sodium Sulphate on WtSS and MutSS at 24.8° C. The CD scans of MutSS and WtSS in a 0.05 cm quartz cuvette (slit 2.0 nm; integration time of 5.0 s) at increasing concentrations of sodium sulphate are shown in panel **a)**. For MutSS (121.5 μM) it was increased in the direction of the arrow from 0 M, 0.30 M, 0.60 M, 1.2 M, 1.5 M and 1.87 M, and similarly for WtSS (125.5 μM) from 0 M, 0.15 M, 0.30 M., 0.60 M and 0.90 M. Panel **b)** shows the effect of increasing the concentration of MutSS while at the same time lowering the sodium sulphate concentration from 0.9 to 0.8 M (continuous lines) and in deionised water (dashed line). The scans were in a 0.01 cm quartz cuvette (integration time of 10 s).

The melting of WtSS and MutSS in 0.9 M sodium sulphate is illustrated in Figure 9.4. For MutSS and WtSS a near isodichroic point was observed around 204 nm by raising temperature. The reversibility is also illustrated in the figures.

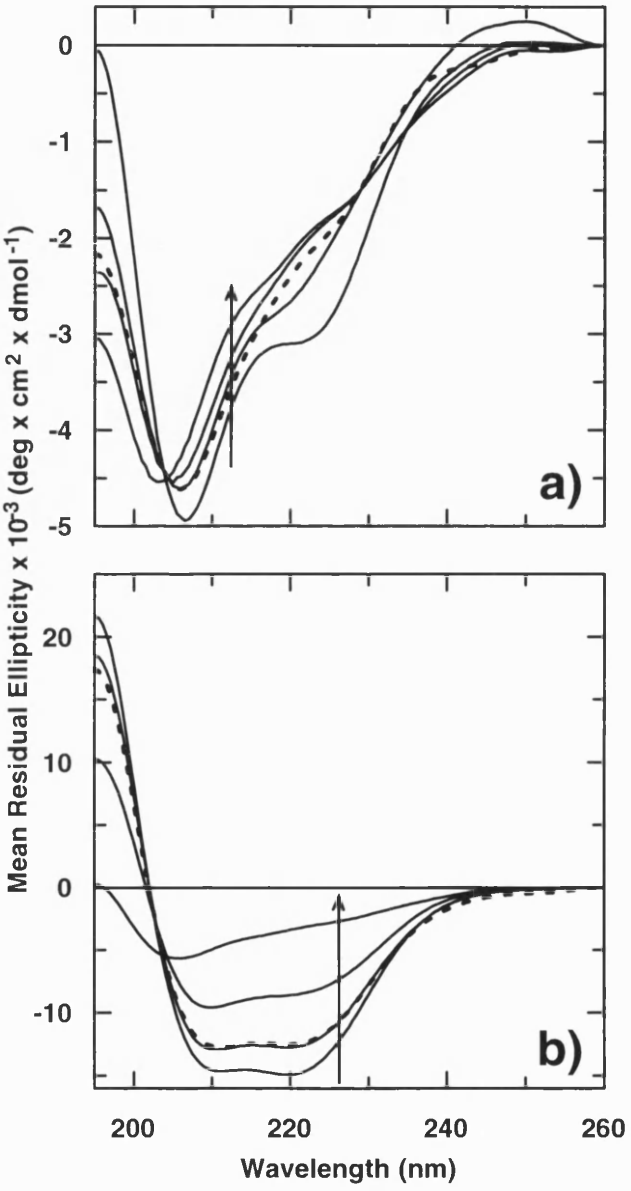

Figure 9.4 Temperature Scans of WtSS and MutSS in 0.9 M Sodium Sulphate.

Minidomains MutSS (121.5 µM, panel **a**) and WtSS (125.5 µM, panel **b**) were scanned one time in a 0.05 cm circular quartz cuvette by integrating each 0.5 nm wavelength step for 5 s (slit 2.0) from 195 nm until 260 nm. The temperature was raised in the direction of the arrow from 3.5° C (first intercepting curve) for MutSS **a)** through 23.7° C, 45.7° C until 70.2° C, and for WtSS **b)** through 28.6° C, 55.4° C until 86.4° C. The reversibility was tested by cooling down again until 23.6° C **a)** or 28.7° C **b)** and by rescanning again (- - - -).

The melting curves are displayed in Figure 9.5 and they all show that the thermostability is increased by adding sodium sulphate. For MutSS it regained some secondary structure, and WtSS increased its T_M by 13 ° C in 0.9 M sodium sulphate relative to its spectrum in deionised water (from 53° C in water to 66° C in 0.9 M Na_2SO_4).

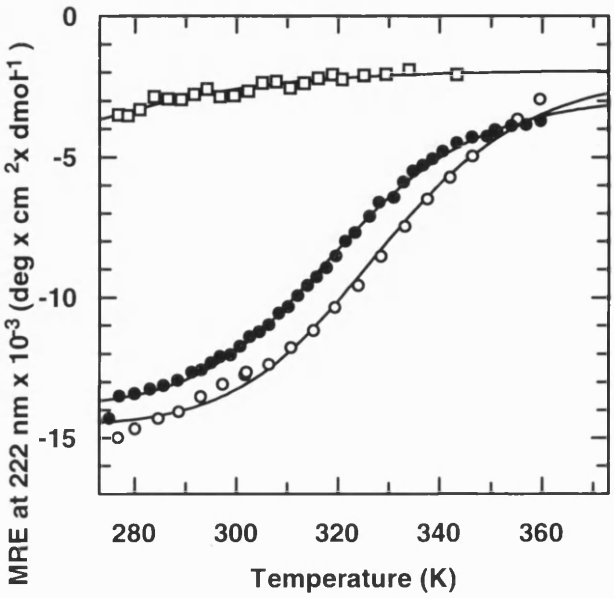

Figure 9.5 Melting Curves of WtSS and MutSS in 0.9 M Sodium Sulphate. The minidomains MutSS (121.5 µM) and WtSS (125.5 µM) were melted in a 0.05 cm stoppered quartz cuvette by recording the MRE at 222 nm using the average of three independent recordings at 222 nm and 260 nm with an integration time of 5 s (slit: 2.0), as described in chapter 5.4.3. The data were fitted to a two-state van't Hoff equation as described in chapter 8.3.3. WtSS (○) and MutSS (□) are in 0.9 M Na_2SO_4, and WtSS (●) is in deionised water.

There is some uncertainty whether a pure two-state transition can be implemented for the minidomains in sodium sulphate solution, due to their propensity for aggregation in this solvent, especially at elevated salt concentrations. However, the melting curves were fitted to a two-state transition by using the procedure described in chapter 8.3.3. The reported energies for WtSS which had a well-defined transition (Figure 9.5), were ΔH (water) = 21.2 ± 0.7 kcal mol^{-1}, ΔS (water) = 0.065 ± 0.002 kcal mol^{-1} K^{-1}, ΔH (0.9 M Na_2SO_4) = 17.7 ± 0.8 kcal mol^{-1} and ΔS (0.9 M Na_2SO_4) = 0.052 ± 0.003 kcal mol^{-1} K^{-1}.

The observations that sodium sulphate was able to induce a β-turn structure in MutSS was further studied by testing its affinity by surface plasmon resonance spectroscopy on BIAcore 2000 as displayed in Figure 9.6.

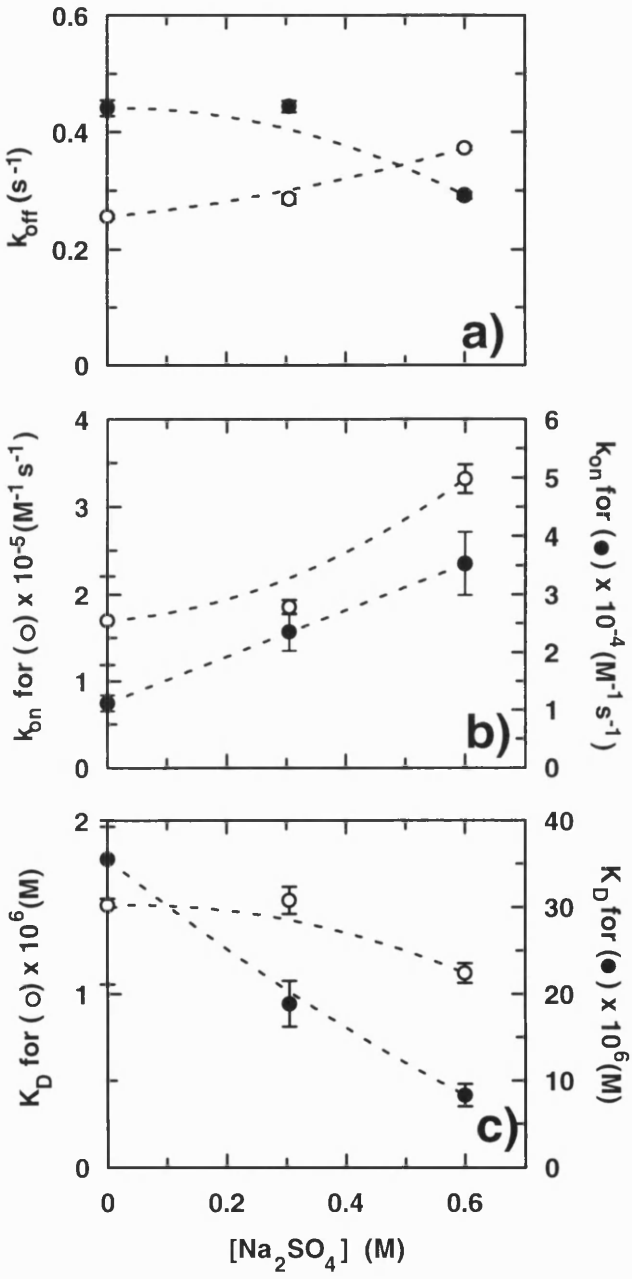

Figure 9.6 Effect of Sodium Sulphate on the Fast Kinetic Constants for MutSS and WtSS. Panels **a)**, **b)**, and **c)** show respectively the off-rates, on-rates and the dissociation constants (= k_{off}/k_{on}) for WtSS (○) and MutSS (●) interacting with immobilised Fc of the mAb 561 (mouse IgG2a) at different concentrations of sodium sulphate at 25° C. The data were fitted as described in Figure 8.13 and in chapter 8. Both the on-rates and off-rates display their fitted standard errors, and the standard errors of K_D were manually calculated based on SE's for k_{on} and k_{off}.

Figure 9.6 displays on-rates, off-rates and the dissociation constants as a function of sodium sulphate concentration for both WtSS and MutSS. The figures display the fast on- and off-rates because there was a better fit to a two-component kinetics model where there are either two different sites on the Fc that can bind the minidomains, or that there are different conformations of the minidomains (Reiersen & Rees, 1999). The off-rates for the WtSS and MutSS had opposite trends. While the off-rates for the MutSS dcreased they increased for WtSS. This indicated that the MutSS-Fc complex was more stable than the WtSS-Fc complex. However, the on-rates for both increased as a function of salt concentration. This is consistent with the observations that sodium sulphate induced α-helical structure in WtSS and turn structure in MutSS (Figure 9.3). Indeed, this was also reflected in a improved affinity for both (Figure 9.6). The dissociation constant of WtSS improved as a function of salt concentration, from 1.5 μM (buffer alone) to 1.1 μM (at 0.6 M Na_2SO_4). Similarly for MutSS it improved from 36 μM to 8 μM, respectively. Relative to WtSS the affinity of MutSS was about threefold greater which may originate in the better stabilisation of the mutant β-turn in the salt-solution.

9.4 Discussion

The apparent complete melting of secondary structure at lower temperatures is one of the characteristics of elastin peptides and polymers (Urry, 1993). The hydrophobic groups in elastin are hydrated at lower temperatures and do not contribute to stability by hydrophobic interactions. A proposed mechanism of elasticity of elastin in addition to the solvent entropy, is the librational entropy mechanism (Urry, 1988a,b). The mobility of the Gly-Val-Gly elastin sequences induces a large-amplitude rocking motion in the whole protein, as is seen by its coupled dihedral angles. By increasing temperature, or otherwise manipulating the hydrophobically hydrated structure, the elastin polymer contracts driven by an increase in the entropy of the system. This is due to the release of its bound water

molecules and an increase in the mobility of the GVG-segments (Urry, 1988a,b; Urry *et al.*, 1998). The combination of a glycine-rich sequence with a large mobility and a proline residue which restricts it, may very well melt secondary structures of a globular host protein. This property may also be responsible for the destabilisation of the helical minidomain in this study. The intramolecular hydrophobic Val-Val interactions that increase with temperature, or altered solvent conditions, additionally stabilise and guide the folding of this mobile sequence (Reiersen *et al.*, 1998).

The stabilising interactions can be enhanced in solvents such as micellar SDS, TFE and sodium sulphate. Micellar SDS was able to induce a 3_{10}-helical like structure in both WtOpen and MutOpen, although it destabilised the existing α-helical structure in WtOpen while it induced it in MutOpen. Trifluoroethanol was however a more powerful helical inducer for both MutOpen and WtOpen.

The lowered cooperativity of the melting of WtOpen in 25 mM SDS, seen as a swallower slope of its melting curve, indicates that it has a small ΔH value (Applequist, 1963). However, exact calculation of thermodynamic values for the SDS curve is a problem since the pre-transitional region was not well defined. On the other hand, there was a near isodichroic point and the minidomains exhibited reversible melting in SDS. Melting curves at increasing concentrations of TFE had a lowered cooperativity and ΔH and ΔS-values, as was also recently found by Luo & Baldwin (1997). The lowered ΔH may be linked with the hydrophobicity of the solvent and its interaction with the peptide and not only with the loss of H-bonded water-molecules associated with the peptide (chapter 7). However, the increased entropy from the loss of peptide H-bonded water molecules was not seen, probably because the water molecules were still indirectly associated with the peptide through TFE/water micelles (chapter 7). It is interesting to note that the energies for melting of WtSS on going from water to 0.9 M sodium sulphate also involved a reduction in ΔH and ΔS.

Sodium sulphate induced a type I β-turn structure in MutSS while it also stabilised and increased the amount of α-helicity in WtSS. There is reason to believe from the existence of isodichroic point and the reversibility of the melting curves, that a intramolecular two-state transition is working at least under low peptide and salt concentrations. There is now evidence these conditions only affect

the intramolecular folding of a protein, while larger concentrations promote intermolecular association of peptides/proteins. Uversky *et al.* (1998a) have proposed a phase diagram correlating protein versus salt concentration. Here, sodium sulphate partly folds staphylococcal nuclease which is a 'non-globular monomer' at salt concentrations below 0.8 M and for protein concentration below 0.4 mg/ml. It is therefore likely that the smaller and very soluble 4 kDa minidomain (Reiersen & Rees, 1999; Starovasnik *et al.*, 1997) is monomeric at peptide concentrations below 100 μM (0.4 mg/ml) in low concentrations of sodium sulphate, although by increasing the peptide concentration to 1.82 mM (7.3 mg/ml) there was a clear shift in the CD-spectrum indicating increasing intramolecular associations. In this study, the minidomain concentrations were generally below 30 μM for kinetic on-rate determinations and only 0.3 M and 0.6 M Na_2SO_4 were used as running buffers in the BIAcore 2000 apparatus.

The structure of the two minidomains differ in the turn region. The hydrophilic type I β-turn sequence in WtSS was replaced by the more hydrophobic elastin turn sequence in MutSS (Figure 8.1). MutSS has surface exposed valine residues which are probably solvated by clathrate water structures (Urry, 1993; Urry *et al.*, 1997). Thus, the induction of an active and folded minidomain from an 'unordered' state, guided by a interhelical disulphide bridge, would be expected to involve changes in water structure. The different residues may dictate the overall water structure associated with a sequence. The negative residues bind more water molecules than positive residues due to their charge transfer potential (Collins & Washabaugh, 1985; Kuhn *et al.*, 1993), and water on hydrophobic residues are organised into polygonal clathrates (Head-Gordon, 1995; Nakasako, 1999; Urry *et al.*, 1998). The hydrophobically associated water layer may be weaker than on charged residues (Collins & Washabaugh, 1985; Urry *et al.*, 1997), but nevertheless it is very important for specifying the balance between exposed and buried non-polar residues, and thus the folding of the protein. According to Collins & Washabaugh (1985) the valine residues in the elastin sequence can be classified as non-polar kosmotropes because they have a structuring effect on the water molecules (one layer) (Head-Gordon, 1995; Nakasako, 1999). Sodium sulphate is however a better kosmotrope because it has a structuring effect on up to 5-6 layers of water (15 Å). This is because the

sulphate groups have negative charges which are cumulatively transferred to interfacial water molecules, giving them a more covalent character. On the other hand, it has also been shown that even non-polar residues may induce structuring of several water-layers (Pertsemlidis *et al.*, 1999; Urry *et al.*, 1997). It has previously been shown that sodium sulphate exposes hydrophobic surface clusters leading to tetramerisation of an enzyme (Prajapati et al., 1998). The relatively larger gain in affinity for the unstructured MutSS relative to WtSS by adding sodium sulphate, may thus be explained by a hydrophobically stabilised type I β-turn (a switch to native conformation) which aligns the helices for binding. Further masking of unfavourable charges and stimulated intrahelical hydrophobic interactions by the salt, may structure the helices and slightly improve its affinity. That the wild-type minidomain increased its helical structure and affinity by sodium sulphate may be due to improved interhelical hydrophobic packing, masking of unfavourable electrostatic interactions, or even direct binding of the sulphate ion involved (Cacace *et al.*, 1997; Collins & Washabaugh, 1985; Goto *et al.*, 1990). The large number of ionic residues in the phage-selected minidomain is a compromise between solubility and affinity. Thirteen of 34 residues carry a charged group at pH 7, and seven of these are positively charged. Even one of the conserved residues in the active centre of the B-domain, Gln33, is replaced by Lys33 in the phage selected minidomain (Braisted & Wells, 1996; Gouda *et al.*, 1998).

Previously, several enzymes, protein-DNA and receptor interactions have been reported to exhibit increased affinity in sodium sulphate (Cacace *et al.*, 1997). Increased ionic strength is often used as a method to release protein-protein interactions (Hermanson *et al.*, 1992). Thus, the expected lowered affinity in a system involving sodium sulphate concentration up to 0.6 M may be compensated by the increased and stabilised secondary structure of the minidomains.

Here we have demonstrated that the salt refolds and turns on activity of an engineered minidomain with water exposed hydrophobic side chains. The loss of structural water molecules, either by raising temperature (Reiersen & Rees, 1999; Urry *et al.*, 1997), or in this study by adding a kosmotropic salt, affects the secondary structure of small engineered minidomain. This also suggests that

sodium sulphate precipitated antibodies may be purified directly on an immobilised protein A column. By using an immobilised engineered protein A minidomain with an elastin-turn, it may be possible to bind sodium or ammonium sulphate precipitated (and redissolved) IgGs. The elution is very simple since it only requires running water through the column to melt its secondary structure. Alternatively, it may also be possible to bind IgGs at room temperature and elute at low temperatures simply by storing the column in the refrigerator (Reiersen & Rees, 1999).

Chapter 10. Conclusions and Further Development.

10.1 Conclusions.

It has been demonstrated here by circular dichroism that short elastin-like peptides (8-18 mers) can undergo similar structural transitions to the longer elastin polymers (chapter 6). The short peptides formed a type II β-turn with increasing temperature or by the addition of solvents such as TFE and SDS. There was also an effect of charge and composition on this transition. Hydrophobic residues lowered the transition temperature while charges at the termini increased it. This has also been described for the longer polymer (Urry, 1993). Additionally, the mean residual ellipticities were followed over various temperatures (within the range 1° to 90° C) and data were fitted to a van't Hoff two-state transition. The positive ΔS terms of the transition energies for the 8 mer (1 VPGVG repeat) and the 18 mers (three repeats) were quite similar implying that the cooperative unit does not exceed 1 VPGVG repeat. Thus, the intra-monomeric hydrophobic val-val interactions may be sufficient to initiate folding of the larger elastin polymer. This suggests that is should be possible to utilise these sequences in the generation of switch-site structures in globular proteins.

In addition, a model has been suggested by the author for the effect of TFE on peptides and proteins (chapter 7). TFE-micelles interact with hydrophobic groups by forming a mobile matrix that chaperones or assists the folding of secondary structures. The model can explain how TFE (and other related alcohols) can break down non-local hydrophobic interactions while at the same time supporting local structures.

The encouraging results in chapter 6 were followed up by testing these sequences in a globular protein. A simple two-helical minidomain of the five-domain triple helical staphylococcal protein A was chosen as a model system (chapter 8 and 9). This short minidomain has been shown to retain the same affinity towards IgG as the parent Protein A domain. In this construct, the native type I β-turn was replaced with the elastin β-turn GVPGVG. The elastin-turn

mutant completely melted all helical structure in the minidomains and lowered the stability by about 50° C. However, by analysing the mutant minidomain in TFE by surface plasmon resonance spectroscopy, a 21-fold improvement in affinity on raising the temperature from 4° to 37° C was observed. This was in contrast to the wild-type which showed the expected loss in affinity over the same temperature range. The energy involved and the topology of the CD-spectra suggested that a type I β-turn was formed as the temperature was increased.

The elastin minidomain also responded in a similar way when sodium sulphate was present. Sodium sulphate is a common salt used for protein purification. Here this salt induced a type I β-turn structure in the minidomain and improved its IgG-binding. This further suggests that Na_2SO_4 can be used to regulate binding/ dissociation of this minidomain - presenting an alternative method of protein purification.

In this thesis it has been shown that a small fragment (8 residues) of the large elastin polymer is capable of forming a beta-turn structure at elevated temperatures and that it can also undergo structural modulation by pH (Reiersen, *et al.*, 1998). Similarly, it has been demonstrated that, when this sequence is inserted into a small binding protein, manipulation of the temperature can induce a structural change, and consequently the affinity of the protein (Reiersen & Rees, 1999). Thus, the molecule produced can be thought of as a reversible affinity material whose binding properties are modified over a physiologically relevant temperature range.

10.2 Future Work and Application.

The application of this technology in the field of protein purification is particularly attractive since novel products can rapidly penetrate what is a considerable market. For example, the separation product protein A, a large multi-domain protein that is involved in the affinity purification of antibodies for both diagnostic and therapeutic uses, has a market size approaching one billion US dollars.

Current affinity chromatographic methods using protein A require relatively harsh conditions (pH 2-3) to reverse the binding of the target protein during purification. The "ideal" affinity purification process though should permit protein recovery under mild conditions. The harsh binding and elution conditions may also lead to leakage of the protein A ligand from the chromatographic support. For example, at the high elution pH values, alkaline hydrolysis of the matrix occurs: thus exposure of adsorbents to pH extremes should be avoided. When protein A affinity methods are applied to the separation of cells (relevant to a number of therapeutic domains) these extreme pH values are unacceptable and other, less effective methods must be used. The development of a novel derivative of protein A in which an elastomeric switch has been incorporated, would move the normal purification conditions of protein A into the physiological range (pH 5-7), thus considerably improving the viability of the purified product. Similarly, separation by moderate temperature changes (4° to 37° C) will provide a simple and gentle procedure and reduce reagent costs.

There is also considerable industrial interest in finding new biotechnological methods to obtain gentle reversal of antigen-antibody binding. Typically, this type of binding can be reversed by use of chaotropic salts, low pH-buffers or high ionic strength. For the immuno-isolation of cells for use in human subjects, these relatively harsh methods can damage cells adversely. Even enzymatic digestion can affect further manipulation of cells. As an example of the scale of interest in this problem, the Norwegian company Dynal® A/S, the world's largest supplier of magnetic particles, has developed a method for cell isolation which uses a double antibody protocol, known as DETACHaBEAD™. However, the mechanism of this detachment is poorly understood and thus not predictable, and the company is actively looking for alternative strategies.

An elastin sequence has also recently been introduced into the linker region of a single chain Fv fragment of an antibody. The design has been cloned, expressed in *E. coli* and purified. Characterisation of this scFv is in progress, but we expect to be able to modulate antibody binding in the same manner as with the Protein A construct (Reiersen *et al.* (2000), unpublished results).

Bibliography

Adzhubei, A. A. & Sternberg, M. J. E. (1993). Left-Handed Polyproline II Helices Commonly Occur in Globular Proteins. *J. Mol. Biol.* **229**(2), 472-493.

Albericio, F. & Carpino, L. A. (1997). Coupling Reagents and Activation. *Meth. Enzymol.* **289**, 104-126.

Albericio, F., Kneib-Cordonier, N., Biancalana, S., Gera, L., Masada, R. I., Hudson, D. & Barany, G. (1990). Preparation and Application of the 5-(4-(9-Fluorenylmethyloxycarbonyl)aminomethyl-3,5-dimethoxyphenoxy)-valeric Acid (PAL) Handle for the Solid-Phase Synthesis of C-terminal Peptide Amides under Mild Conditions. *J. Org. Chem.* **55**, 3730-3743.

Albert, J. S. & Hamilton, A. D. (1995). Stabilization of Helical Domains in Short Peptides Using Hydrophobic Interactions. *Biochemistry* **34**(3), 984-990.

Alexandropoulos, K., Cheng, G. & Baltimore, D. (1995). Proline-rich Sequences That Bind to Src Homology 3 Domains With Individual Specificities. *Proc. Natl. Acad. Sci. USA* **92**, 3110-3114.

Altamirano, M. M., Blackburn, J. M., Aguayo, C. & Fersht, A. R. (2000). Directed Evolution of New Catalytic Activity Using the Alpha/Beta-barrel Scaffold. *Nature* **403**, 617-622.

Ames, J. B., Ishima, R., Tanaka, T., Gordon, J. I., Stryer, L. & Ikura, M. (1997). Molecular Mechanics of Calcium-myristoyl Switches. *Nature* **389**, 198-202.

Andersen, N. H., Cort, J. R., Liu, Z., Sjöberg, S. J. & Tong, H. (1996). Cold Denaturation of Monomeric Peptide Helices. *J. Am. Chem. Soc.* **118**(42), 10309-10310.

Antonino, L. C., Kautz, R. A., Nakano, T., Fox, R. O. & Fink, A. L. (1991). Cold Denaturation and ^2H_2O Stabilization of a Staphylococcal Nuclease Mutant. *Proc. Natl. Acad. Sci. USA* **88**(17), 7715-7718.

Antonsson, P., Kammerer, R. A., Schulthess, T., Hänisch, G. & Engel, J. (1995). Stabilization of the Alpha-Helical Coiled-Coil Domain in Laminin by C-terminal Disulfide Bonds. *J. Mol. Biol.* **250**, 74-79.

Antonyraj, K. J., Karunakaran, T. & Raj, P. A. (1998). Bacterial Activity and Poly-L-proline II Conformation of the Tandem Repeat Sequence of Human Salivary Mucin Glycoprotein (MG2),. *Arch. Biochem. Biophys.* **356**(2), 197-206.

Applequist, J. (1963). On the Helix-coil Equilibrium in Polypeptides. *J. Chem. Phys.* **38**(4), 934-941.

Arad, O. & Goodman, M. (1990). Depsipeptide Analogues of Elastin Repeating Sequences: Conformational Analysis. *Biopolymers* **29**(12-1), 1651-1668.

Atherton, E., Cameron, L. R. & Sheppard, R. C. (1988a). Peptide Synthesis. Part 10. Use of Pentafluorophenyl Esters of Fluorenyl Methoxycarbonyl Amino Acids in Solid Phase Peptide Synthesis. *Tetrahedron* **44**(3), 843-857.

Atherton, E., Holder, J. L., Meldal, M., Sheppard, R. C. & Valerio, R. M. (1988b). Peptide Synthesis. Part 12. 3,4-Dihydro-4-oxo-1,2,3-benzotriazin-3-yl Esters of Fluorenylmethoxycarbonyl Amino Acids as Self-indicating Reagents for Solid Phase Peptide Synthesis. *J. Chem. Soc. Perkin Trans.* **I**, 2887-2894.

Atkins, A. R., Brereton, I. M., Kroon, P. A., Lee, H. T. & Smith, R. (1998). Calcium is Essential for the Structural Integrity of the Cysteine-rich Ligand-

binding Repeat of the Low-density Lipoprotein Receptor. *Biochemistry* **37**(6), 1662-1670.

Aurora, R., Creamer, T. P., Srinivasan, R. & Rose, G. D. (1997). Local Interactions in Protein Folding: Lessons From the α-Helix. *J. Biol. Chem.* **272**(3), 1413-1416.

Ayato, H., Tanaka, I. & Ashida, T. (1980). The Crystal Structure of the Repeating Pentapeptide of Elastin: Boc-Val-Pro-Gly-Val-Gly-OH·H_2O. In *Peptide Chemistry* (Okawa, K., ed.), pp. 107-112. Protein Research Foundation, Osaka.

Bach II, A. C., Espina, J. R., Jackson, S. A., Stouten, P. F. W., Duke, J. L., Mousa, S. A. & DeGrado, W. F. (1996). Type II' to Type I Beta-turn Swap Changes Specificity for Integrin. *J. Am. Chem. Soc.* **118**, 293-294.

Baim, S. B., Labow, M. A., Levine, A. J. & Shenk, T. (1991). A Chimeric Mammalian Transactivator Based on the *lac* Repressor That is Regulated by Temperature and Isopropyl β-D-Thiogalactopyranoside. *Proc. Natl. Acad. Sci. USA* **88**, 5072-5076.

Baldwin, R. L., Stolowitz, M. L., Hood, L. & Wisnieski, B. J. (1996). Structural Changes of Tumor Necrosis Factor Alpha Associated With Membrane Insertion and Channel Formation. *Proc. Natl. Acad. Sci. USA* **93**, 1021-1026.

Barbas III, C. F. & Wagner, J. (1995). Synthetic Human Antibodies: Selecting and Evolving Functional Proteins. *Methods: Comp. Methods Enzymol.* **8**, 94-103.

Barford, D. & Johnson, L. N. (1989). The Allosteric Transition of Glycogen Phosphorylase. *Nature* **340**, 609-616.

Barron, L. D., Hecht, L. & Wilson, G. (1997). The Lubricant of Life: A Proposal That Solvent Water Promotes Extremely Fast Conformational Fluctations in Mobile Heteropolypeptide Structure. *Biochemistry* **36**(43), 13143-13147.

Baudin-Chich, V., Pagnier, J., Marden, M., Bohn, B., Lacaze, N., Kister, J., Schaad, O., Edelstein, S. J. & Poyart, C. (1990). Enhanced Polymerization of Recombinant Human Deoxyhemoglobin β6 Glu--> Ile. *Proc. Natl. Acad. Sci. USA* **87**, 1845-1849.

Bayer, E. (1991). Towards the Chemical Synthesis of Proteins. *Angew. Chem. Int. Ed. Engl.* **30**(2), 113-129.

Bedford, M. T., Reed, R. & Leder, P. (1998). WW Domain-mediated Interactions Reveal a Spleiceosome-associated Protein That Binds a Third Class of Proline-rich Motif: The Proline, Glycine and Methionine-rich Motif. *Proc. Natl. Acad. Sci. USA* **95**, 10602-10607.

Bello, J. (1993). Helix Promotion in Polypeptides by Polyols. *Biopolymers* **33**, 491-495.

Bellsolell, L., Prieto, J., Serrano, L. & Coll, M. (1994). Magnesium Binding to the Bacterial Chemotaxis Protein CheY Results in Large Conformational Changes Involving Its Functional Surface. *J. Mol. Biol.* **238**(4), 489-495.

Beste, G., Schmidt, F. S., Stibora, T. & Skerra, A. (1999). Small Antibody-like Proteins With Prescribed Ligand Specificities Derived From the Lipocain Fold. *Proc. Natl. Acad. Sci. USA* **96**, 1898-1903.

Bhandary, K. K., Senadhi, S. E., Prasad, K. U., Urry, D. W. & Vijay-Kumar, S. (1990). Conformation of a Cyclic Decapeptide Analog of a Repeat Pentapeptide Sequence of Elastin: Cyclo-bis(valyl-prolyl-alanyl-valyl-glycyl). *Int. J. Pept. Protein Res.* **36**, 122-127.

Bhat, T. N., Bentley, G. A., Boulot, G., Greene, M. I., Tello, D., Dall'Acqua, W., Souchon, H., Schwarz, F. P., Mariuzza, R. A. & Poljak, R. J. (1994). Bound Water Molecules and Conformational Stabilization Help Mediate an Antigen-antibody Association. *Proc. Natl. Acad. Sci. USA* **91**, 1089-1093.

Biosensor, AB (1995). BIAevaluation 2.1 Software Handbook. .

Biosensor, AB (1996). Chapter 2. Description. *BIACORE 2000 Instrument Handbook*, 1-14.

Bisaccia, F., Castiglione-Morelli, M. A., Spisani, S., Ostuni, A., Serafini-Fracassini, A., Bavoso, A. & Tamburro, A. M. (1998). The Amino Acid Sequence Coded by the Rarely Expressed Exon 26A of Human Elastin Contains a Stable Beta-turn with Chemotactic Activity for Monocytes. *Biochemistry* **37**(31), 11128-11135.

Bisang, C., Weber, C., Inglis, J., Schiffer, C. A., van Gunsteren, W. F., Jelesarov, I., Bosshard, H. R. & Robinson, J. A. (1995). Stabilization of Type-I Beta-Turn Conformations in Peptides Containing the NPNA-Repeat Motif of the *Plasmodium falciparum* Circumsporozoite Protein by Substituting Proline for (S)-Alpha-Methylproline. *J. Am. Chem. Soc.* **117**, 7904-7915.

Blackburn, S. (1968). Hydrolytic Procedures. In *Amino Acid Determination. Methods and Techniques*, pp. 11-29. Edward Arnold (publishers) Ltd & Marcel Dekker Inc., London, New York.

Blake, C. & Serpell, L. (1996). Synchrotron X-ray Studies Suggest That the Core of the Transthyretin Amyloid Fibril Is a Continuous Beta-Sheet Helix. *Structure* **4**, 989-998.

Blokzijl, W. & Engberts, J. B. F. N. (1993). Hydrophobic Effects. Opinions and Facts. *Angew. Chem. Int. Ed. Engl.* **32**, 1545-1579.

Blundell, T. L. (1994). Problems and Solutions in Protein Engineering - Towards Rational Design. *Trends Biotechnol.* **12**, 145-148.

Bodkin, M. J. & Goodfellow, J. M. (1996). Hydrophobic Solvation in Aqueous Trifluoroethanol Solution. *Biopolymers* **39**, 43-50.

Bogin, O., Peretz, M., Hacham, Y., Korkhin, Y., Frolow, F., Kalb(Gilboa), A. J. & Burstein, Y. (1998). Enhanced Thermal Stability of *Clostridium beijerinckii* Alcohol dehydrogenase After Strategic Substitution of Amino Acid Residues with Prolines from the Homologous Thermophilic *Thermoanaerobacter brockii* Alcohol Dehydrogenase. *Protein Sci.* **7**, 1156-1163.

Booth, D. R., Sunde, M., Bellotti, V., Robinson, C. V., Hutchinson, W. L., Fraser, P. E., Hawkins, P. N., Dobson, C. M., Radford, S. E., Blake, C. F. & Pepys, M. B. (1997). Instability, Unfolding and Aggregation of Human Lysozyme Variants Underlying Amyloid Fibrillogenesis. *Nature* **385**, 787-793.

Bork, P., Schultz, J. & Ponting, C. P. (1997). Cytoplasmic Signalling Domains: The next Generation. *Trends Biochem. Sci.* **22**, 296-298.

Borza, D. -B., Tatum, F. M. & Morgan, W. T. (1996). Domain Structure and Conformation of Histidine-Proline-Rich Glycoprotein. *Biochemistry* **35**(6), 1925-1934.

Borza, D.-B. & Morgan, W. T. (1998). Histidine-Proline-rich Glycoprotein as a Plasma pH Sensor. *J. Biol. Chem.* **273**(10), 5493-5499.

Bradbury, A. F. & Smyth, D. G. (1991). Peptide Amidation. *Trends Biochem. Sci.* **16**, 112-115.

Braisted, A. C. & Wells, J. A. (1996). Minimizing a Binding Domain From Protein A. *Proc. Natl. Acad. Sci. USA* **93**(12), 5688-5692.

Broch, H., Moulabbi, M., Vasilescu, D. & Tamburro, A. M. (1996). Conformational and Electrostatic Properties of V-G-G-V-G, a Typical Sequence of the Glycine-Rich Regions of Elastin - an Ab-Initio Quantum Molecular Study. *Int. J. Pept. Protein Res.* **47**(5), 394-404.

Brown, D. R., Qin, K., Herms, J. W., Madlung, A., Manson, J., Strome, R., Fraser, P. E., Kruck, T., von Bohlen, A., Schulz-Schaeffer, W., Giese, A., Westaway, D. & Kretzschmar, H. (1997). The Cellular Prion Protein Binds Copper *In Vivo*. *Nature* **390**, 684-686.

Bruch, M., Weiss, V. & Engel, J. (1988). Plasma Serine Proteinase Inhibitors (Serpins) Exhibit Major Conformational Changes and a Large Increase in Conformational Stability Upon Cleavage at Their Reactive Sites. *J. Biol. Chem.* **263**(32), 16626-16630.

Bryson, J. W., Betz, S. F., Lu, H. S., Suich, D. J., Zhou, H. X., O'Neil, K. T. & DeGrado, W. F. (1995). Protein Design: A Hierarchic Approach. *Science* **270**, 935-941.

Buchner, J. (1999). Hsp90 & Co. - A Holding for Folding. *Trends Biochem. Sci.* **24**, 136-141.

Bullough, P. A., Hughson, F. M., Skehel, J. J. & Wiley, D. C. (1994). Structure of Influenza Haemagglutinin at the pH of Membrane Fusion. *Nature* **371**, 37-43.

Bülow, L. & Mosbach, K. (1991). The Oligopeptide $(Gly\text{-}Pro)_2$-Ala-$(Gly\text{-}Pro)_2$ Increases the Internal Proline Level and Improves NaCl Tolerance when Produced in *Escherichia coli*. *Gene* **109**, 125-129.

Burdick, D. J. & Stults, J. T. (1997). Analysis of Peptide Synthesis Products by Electrospray Ionization Mass Spectrometry. *Meth. Enzymol.* **289**, 499-519.

Burnette, W. N. (1994). AB_5 ADP-ribosylating Toxins: Comparative Anatomy and Physiology. *Structure* **2**, 151-158.

Bush, A. I., Pettingell, W. H., Multhaup, G., d.Paradis, M., Vonsattel, J.-P., Gusella, J. F., Beyreuther, K., Masters, C. L. & Tanzi, R. E. (1994). Rapid Induction of Alzheimer Aβ Amyloid Formation by Zinc. *Science* **265**, 1464-1467.

Butcher, D. J. & Moe, G. R. (1996). Role of Hydrophobic Interactions and Desolvation in Determining the Structural Properties of a Model Alpha-Beta Peptide. *Proc. Natl. Acad. Sci. USA* **93**(3), 1135-1140.

Butcher, D. J., Nedved, M. L., Neiss, T. G. & Moe, G. R. (1996). Proline Pipe Helix: Structure of the Tus Proline Repeat Determined by ^{1}H NMR. *Biochemistry* **35**(3), 698-703.

Cacace, M. G., Landau, E. M. & Ramsden, J. J. (1997). The Hofmeister Series: Salt and Solvent Effects on Interfacial Phenomena. *Quart. Rev. Biophys.* **30**(3), 241-277.

Cagas, P. M. & Corden, J. L. (1995). Structural Studies of a Synthetic Peptide Derived From the Carboxy-Terminal Domain of RNA Polymerase II. *Proteins: Struct. Funct. Genet.* **21**, 149-160.

Cammers-Goodwin, A., Allen, T. J., Oslick, S. L., McClure, K. F., Lee, J. H. & Kemp, D. S. (1996). Mechanism of Stabilization of Helical Conformations of Polypeptides by Water Containing Trifluoroethanol. *J. Am. Chem. Soc.* **118**(13), 3082-3090.

Canziani, G., Zhang, W., Cines, D., Rux, A., Willis, S., Cohen, G., Eisenberg, R. & Chaiken, I. (1999). Exploring Biomolecular Recognition Using Optical Biosensors. *Methods: Comp. Methods Enzymol.* **19**, 253-269.

Carell, R. W., Evans, D. L. & Stein, P. E. (1991). Mobile Reactive Centre of Serpins and the Control of Thrombosis. *Nature* **353**, 576-578.

Carpino, L. A. & Han, G. Y. (1970). The 9-Fluorenylmethoxycarbonyl Function, a New Base-sensitive Amino-protecting group. *J. Am. Chem. Soc.* **92**(19), 5748-5749.

Carr, C. M. & Kim, P. S. (1993). A Spring-loaded Mechanism for the Conformational Change of Influenza Hemagglutinin. *Cell* **73**, 823-832.

Cedergren, L., Andersson, R., Jansson, B., Uhlèn, M. & Nilsson, B. (1993). Mutational Analysis of the Interaction Between Staphylococcal Protein A an Human IgG1. *Protein Eng.* **6**(4), 441-448.

Chakrabarti, P. & Chakrabarti, S. (1998). C-H $\cdots$ O Hydrogen Bond Involving Proline Residues in Alpha-Helices. *J. Mol. Biol.* **284**, 867-873.

Chakrabartty, A., Kortemme, T. & Baldwin, R. L. (1994). Helix Propensities of the Amino Acids Measured in Alanine-based Peptides Without Helix-stabilizing Side-chain Interactions. *Protein Sci.* **3**, 843-852.

Chan, D. C., Bedford, M. T. & Leder, P. (1996). Formin Binding Proteins Bear WWP/WW Domains That Bind Proline-rich Peptides and Functionally Resemble SH3 Domains. *EMBO J.* **15**(5), 1045-54.

Chang, D. K. & Urry, D. W. (1988). Molecular Dynamics Calculations On Relaxed and Extended States of the Polypentapeptide of Elastin. *Chem. Phys. Lett.* **147**(4), 395-400.

Chen, H. I. & Sudol, M. (1995). The WW Domain of Yes-associated Protein Binds a Proline-rich Ligand That Differs From the Concensus Established

For Src Homology 3 -binding Modules. *Proc. Natl. Acad. Sci. USA* **92**, 7819-7823.

Cheng, Y.-K. & Rossky, P. J. (1998). Surface Topography Dependence of Biomolecular Hydrophobic Hydration. *Nature* **392**, 696-699.

Chiou, J.-S., Tatara, T., Sawamura, S., Kaminoh, Y., Kamaya, H., Shibata, A. & Ueda, I. (1992). The α-Helix to β-Sheet Transition in Poly(L-Lysine): Effects of Anestehetics and High Pressure. *Biochim. Biophys. Acta* **1119**, 211-217.

Chou, P. Y. & Fasman, G. D. (1977). β-Turns in Proteins. *J. Mol. Biol.* **115**, 135-175.

Cohen, F. E. & Prusiner, S. B. (1998). Pathologic Conformations of Prion Proteins. *Annu. Rev. Biochem.* **67**, 793-819.

Collins, K. D. & Washabaugh, M. W. (1985). The Hofmeister Effect and The Behaviour of Water at Interfaces. *Quart. Rev. Biophys.* **18**(4), 323-422.

Cook, W. J., Einspahr, H., Trapane, T. L., Urry, D. W. & Bugg, C. E. (1980). Crystal Structure and Conformation of the Cyclic Trimer of a Repeat Pentapeptide of Elastin, cyclo-(L-Valyl-L-Prolylglycyl-L-Valylglycyl)$_3$. *J. Am. Chem. Soc.* **102**(17), 5502-5505.

Corden, J. L. & Patturajan, M. (1997). A CTD Function Linking Transcription to Splicing. *Trends Bioch. Sci.* **22**, 413-416.

Cordes, M. H. J., Walsh, N. P., McKnight, C. J. & Sauer, R. T. (1999). Evolution of a Protein Fold In Vitro. *Science* **284**, 325-327.

Corey, D. R. & Schultz, P. G. (1989). Introduction of a Metal-dependent Regulatory Switch into an Enzyme. *J. Biol. Chem.* **264**(7), 3666-3669.

Cormack, B. P., Ghori, N. & Falkow, S. (1999). An Adhesin of the Yeast Pathogen *Candida glabrata* Mediating Adherance to Human Epithelial Cells. *Science* **285**, 578-582.

Coyne, K. J., Qin, X.-X. & Waite, J. H. (1997). Extensible Collagen in Mussel Byssus: A Natural Block Polymer. *Science* **277**, 1830-1832.

Creighton, T. E. (1984). *Proteins. Structures and Molecular Properties.* 1st edit, W. H. Freeman and Company, New York.

daSilva, A. C. R. & Reinach, F. C. (1991). Calcium Binding Induces Conformational Changes in Muscle Regulatory Proteins. *Trends Biochem. Sci.* **16**, 53-57.

Dahiyat, B. I. & Mayo, S. L. (1997). De Novo Protein Design: Fully Automated Sequence Selection. *Science* **278**, 82-87.

Dalal, S., Balasubramanian, S. & Regan, L. (1997). Protein Alchemy: Changing Beta-Sheet into Alpha-Helix. *Nature Struct. Biol.* **4**(7), 548-552.

Das, K. P. & Surewicz, W. K. (1995). Temperature-Induced Exposure of Hydrophobic Surfaces and its Effect on the Chaperone Activity of Alpha-Crystallin. *FEBS Lett.* **369**, 321-325.

Daughdrill, G. W., Chadsey, M. S., Karlinsey, J. E., Hughes, K. T. & Dahlquist, F. W. (1997). The C-Terminal Half of the Anti-Sigma Factor, FlgM, Becomes Structured when Bound to Its Target, Sigma28. *Nature Struct. Biol.* **4**(4), 285-291.

DeGrado, W. F., Summa, C. M., Pavone, V., Nastri, F. & Lombardi, A. (1999). De Novo Design and Structural Characterization of Proteins and Metalloproteins. *Annu. Rev. Biochem.* **68**, 779-819.

Deisenhofer, J. (1981). Crystallographic Refinement and Atomic Models of a Human Fc Fragment and Its Complex with Fragment B of Protein A from *Staphylococcus aureus* at 2.9- and 2.8-Å Resolution. *Biochemistry* **20**(9), 2361-2370.

Denisov, V. P., Jonsson, B.-H. & Halle, B. (1999). Hydration of Denaturated and Molten Globule Proteins. *Nature Struct. Biol.* **6**(3), 253-260.

Di Cera, E., Guinto, E. R., Vindigni, A., Dang, Q. D., Ayala, Y. M., Wuyi, M. & Tulinsky, A. (1995). The Na^+ binding Site of Thrombin. *J. Biol. Chem.* **270**(38), 22089-22092.

Dill, K. A. (1990). Dominant Forces in Protein folding. *Biochemistry* **29**(31), 7133-7155.

Dobbins, J. R., Murali, N. & Long, E. C. (1996). Structural Redesign and Stabilization of the Overlapping Tandem β-turns of RNA-polymerase. *Int. J. Pept. Protein Res.* **47**, 260-268.

Dyson, H. J., Rance, M., Houghten, R. A., Lerner, R. A. & Wright, P. E. (1988). Folding of Immunogenic Peptide Fragments of Proteins in Water Solution. I. Sequence Requirements for the Formation of a Reverse Turn. *J. Mol. Biol.* **201**, 161-200.

Einbond, A. & Sudol, M. (1996). Towards Prediction of Cognate Complexes Between the WW Domain and Proline-rich Ligands. *FEBS Lett.* **384**, 1-8.

El Hawrani, A. S., Moreton, K. M., Sessions, R. B., Clarke, A. R. & Holbrook, J. J. (1994). Engineering Surface Loops of Proteins - a Preferred Strategy for Obtaining New Enzyme Function. *Trends Biotechnol.* **12**, 207-211.

Emsley, P., Charles, I. G., Fairweather, N. F. & Isaacs, N. W. (1996). Structure of *Bordetella Pertussis* Virulence Factor P.69 Pertactin. *Nature* **381**, 90-92.

Facchiano, F., Ragone, R., Porcelli, M., Cacciapuoti, G. & Colonna, G. (1992). Effect of Temperature on the Propylamine Transferase From *Sulfolobus solfataricus*, an Extreme Thermophilic Acheabacterium. I: Conformational Behaviour of the Oligomeric Enzyme in Solution. *Eur. J. Biochem.* **204**, 473-482.

Fairman, R., Shoemaker, K. R., York, E. J., Steward, J. M. & Baldwin, R. L. (1989). Further Studies of the Helix Dipole Model: Effects of a Free α-NH_3^+ or α-COO^- Group on Helix Stability. *Proteins: Struct. Funct. Genet.* **5**, 1-7.

Fedorov, A. A., Fedorov, E., Gertler, F. & Almo, S. C. (1999). Structure of EVH1, a Novel Proline-rich Ligand-binding Module Involved in Cytoskeletal Dynamics and Neural Function. *Nature Struct. Biol.* **6**(7), 661-665.

Feng, S., Chen, J. K., Yu, H., Simon, J. A. & Schreiber, S. L. (1994). Two Binding Orientations for Peptides to the Src SH3 Domain: Development of a General Model for SH3-ligand Interactions. *Science* **266**, 1241-1247.

Ferrell, J., J. E. (1998). How Regulated Proteins Translocation Can Produce Switch-like Responses. *Trends Biochem. Sci.* **23**, 461-465.

Fischer, S. & Verma, C. S. (1999). Binding of Buried Structural Water Increases the Flexibility of Proteins. *Proc. Natl. Acad. Sci. USA* **96**, 9613-9615.

Frankel, A. D. (1992). The Importance of Being Flexible. *Proc. Natl. Acad. Sci. USA* **89**, 11653.

Freifelder, D. M. (1982). Optical Rotary Dispersion and Circular Dichroism. In *Physical Biochemistry. Applications to Biochemistry and Molecular Biology* 2 edit., pp. 573-601. W. H. Freeman and Company, New York.

Freund, C., Dötsch, V., Nishizawa, K., Reinherz, E. L. & Wagner, G. (1999). The GYF Domain is a Novel Structural Fold That is Involved in Lymphoid Signaling Through Proline-rich Sequences. *Nature Struct. Biol.* **6**(7), 656-660.

Gast, K., Zirwer, D., Müller-Frohne, M. & Damaschun, G. (1999). Trifluoroethanol-induced Conformational Transitions of Proteins: Insights Gained From the Differences Between Alpha-lactalbumine and Ribonuclease A. *Protein Sci.* **8**, 625-634.

Gavish, M., Popovitz-Biro, R., Lahav, M. & Leiserowitz, L. (1990). Ice Nucleation by Alcohols Arranged in Monolayers at the Surface of Water Drops. *Science* **250**, 973-975.

Gerstein, M. & Chothia, C. (1991). Analysis of Protein Loop Closure. Two Types of Hinges Produce One Motion in Lactate Dehydrogenase. *J. Mol. Biol.* **220**, 133-149.

Gerstein, M., Lesk, A. M. & Chothia, C. (1994). Structural Mechanisms for Domain Movements in Proteins. *Biochemistry* **33**(22), 6739-6749.

Gerstein, M., Schulz, G. & Chotia, C. (1993). Domain Closure in Adenylate Kinase. Joints on Either Side of Two Helices Close Like Neighboring Fingers. *J. Mol. Biol.* **229**, 494-501.

Gettins, P. & Harten, B. (1988). Properties of Thrombin- and Elastase-Modified Human Antithrombin III. *Biochemistry* **27**(10), 3634-3639.

Gonzalez Jr., L., Plecs, J. J. & Alber, T. (1996). An Engineered Allosteric Switch in Leucine-zipper Oligomerization. *Nature Struct. Biol.* **3**(6), 510-515.

Gosline, J. M. (1978). Hydrophobic Interaction and a Model for the Elasticity of Elastin. *Biopolymers* **17**, 677-695.

Goto, Y., Takahashi, N. & Fink, A. L. (1990). Mechanism of Acid-induced Folding of Proteins. *Biochemistry* **29**, 3480-3488.

Gouda, H., Shiraishi, M., Takahashi, H., Kato, K., Torigoe, H., Arata, Y. & Shimada, I. (1998). NMR Study of the Interaction Between the B Domain of Staphylococcal Protein A and the Fc Portion of Immunoglobulin G. *Biochemistry* **37**, 129-136.

Gouda, H., Torigoe, H., Saito, A., Sato, M., Arata, Y. & Shimada, I. (1992). Three-Dimensional Solution Structure of the B Domain of Staphylococcal Protein A: Comparisons of the Solution and Crystal Structures. *Biochemistry* **31**(40), 9665-9672.

Goward, C. R., Scawen, M. D., Murphy, J. P. & Atkinson, T. (1993). Molecular Evolution of Bacterial Cell-surface Proteins. *Trends Biochem. Sci.* **18**, 136-140.

Graf von Stosch, A., Jiménez, M. A., Kinzel, V. & Reed, J. (1995a). Solvent Polarity-Dependent Structural Refolding: A CD and NMR Study of a 15 Residue Peptide. *Proteins: Struct. Funct. Genet.* **23**, 196-203.

Graf von Stosch, A., Kinzel, V., Pipkorn, R. & Reed, J. (1995b). Investigation of the Structural Components Governing the Polarity-dependent Refolding of a CD4-binding Peptide From gp120. *J. Mol. Biol.* **250**, 507-513.

Gray, W. R., Sandberg, L. B. & Foster, J. A. (1973). Molecular Model for Elastin Structure and Function. *Nature* **246**, 461-466.

Green, H. (1993). Human Genetic Diseases Due to Codon Reiteration: Relationship to an Evolutionary Mechanism. *Cell* **74**, 955-956.

Greenfield, N. J. (1996). Methods to Estimate the Conformation of Proteins and Polypeptides from Circular Dichroism Data. *Anal. Biochem.* **235**, 1-10.

Guda, C., Zhang, X., McPherson, D. T., Xu, J., Cherry, J. H., Urry, D. W. & Daniell, H. (1995). Hyper Expression of an Environmentally Friendly Synthetic Polymer Gene. *Biotechnol. Lett.* **17**(7), 745-750.

Guerette, P. A., Ginzinger, D. G., Weber, B. H. F. & Gosline, J. M. (1996). Silk Properties Determined by Gland-Specific Expression of a Spider Fibroin Gene Family. *Science* **272**, 112-114.

Guinto, E. R. & Di Cera, E. (1996). Large Heat-Capacity Change in a Protein-Monovalent Cation Interaction. *Biochemistry* **35**(27), 8800-8804.

Gunasekaran, K., Gomathi, L., Ramakrishnan, C., Chandrasekhar, J. & Balaram, P. (1998). Conformational Interconversions in Peptide Beta-turns: Analysis of Turns in Proteins and Computational Estimates of Barriers. *J. Mol. Biol.* **284**, 1505-1516.

Guss, B., Uhlén, M., Nilsson, B., Lindberg, M., Sjöquist, J. & Sjödahl, J. (1984). Region X, The Cell-wall-attachment Part of Staphylococcal Protein A. *Eur. J. Biochem.* **138**, 413-420.

Guy, C. A. & Fields, G. B. (1997). Trifluoroacetic Acid Cleavage and Deprotection of Resin-bound Peptides Following Synthesis by Fmoc Chemistry. *Meth. Enzymol.* **289**, 67-83.

Hagestedt, T., Lichtenberg, B., Wille, H., Mandelkow, E.-M. & Mandelkow, E. (1989). Tau Protein Becomes Long and Stiff Upon Phosphorylation: Correlation between Paracrystalline Structure and Degree of Phosphorylation. *J. Cell. Biol.* **109**, 1643-1651.

Halford, N. G., Tatham, A. S., Sui, E., Daroda, L., Dreyer, T. & Shewry, P. R. (1992). Identification of a Novel Beta-Turn-Rich Repeat Motif in the D Hordeins of Barley. *Biochim. Biophys. Acta* **1122**, 118-122.

Harada, M., Sisido, M., Hirose, J. & Nakanishi, M. (1991). Photoreversible Antigen-antibody Reactions. *FEBS Lett.* **286**(1-2), 6-8.

Hare, P. D. & Cress, W. A. (1997). Metabolic Implications of Stress-induced Proline Accumulation in Plants. *Plant Growth Regul.* **21**, 79-102.

Harpaz, Y., Elmasry, N., Fersht, A. R. & Henrick, K. (1994). Direct Observation of Better Hydration at the N-terminus of an Alpha-Helix With Glycine Rather Alanine as The N-cap Residue. *Proc. Natl. Acad. Sci. USA* **91**, 311-315.

Haupts, U., Tittor, J., Bamberg, E. & Oesterhelt, D. (1997). General Concept for Ion Translocation by Halobacterial Retinal Proteins: The Isomerization/Switch/Transfer (IST) Model. *Biochemistry* **36**(1), 2-7.

Head-Gordon, T. (1995). Is Water Structure Around Hydrophobic Groups Clathrate-like? *Proc. Natl. Acad. Sci. USA* **92**, 8308-8312.

Hermanson, G. T., Mallia, A. K. & Smith, P. K. (1992). Immunoglobulin Binding Proteins. In *Immobilized Affinity Ligand Techniques* 1st edit., pp. 244-252, 333-336. Academic Press Inc., San Diego, New York, Boston, London, Sydney, Tokyo, Toronto.

Higaki, J. N., Fletterick, R. J. & Craik, C. S. (1992). Engineered Metalloregulation in Enzymes. *Trends Biochem. Sci.* **17**, 100-104.

Hillson, J. L., Karr, N. S., Oppliger, I. R., Mannik, M. & Sasso, E. H. (1993). The Structural Basis of Germline-encoded V_H3 Immunoglobulin Binding to Staphylococcal Protein A. *J. Exp. Med.* **178**, 331-336.

Hirota, N., Mizuno, K. & Goto, Y. (1998). Group Additive Contributions to the Alcohol-induced Alpha-helix Formation of Melittin: Implications for the Mechanism of the Alcohol Effects on Proteins. *J. Mol. Biol.* **275**, 365-378.

Hoh, J. H. (1998). Functional Protein Domains From the Thermally Driven Motion of Polypepide Chains: A Proposal. *Proteins: Struct. Funct. Genet.* **32**, 223-228.

Homola, J., Yee, S. S. & Gauglitz, G. (1999). Surface Plasmon Resonance Sensors: Review. *Sensors Actuators* **54**(B), 3-15.

Hong, D.-P., Hoshino, M., Kuboi, R. & Goto, Y. (1999). Clustering of Fluorine-substituted Alcohols as a Factor Responsible for Their Marked Effects on Proteins and Peptides. *J. Am. Chem. Soc.* **121**(37), 8427-8433.

Hornshaw, M. P., McDermott, J. R., Candy, J. M. & Lakey, J. H. (1995). Copper Binding to the N-terminal Tandem Repeat Region of Mammalian and Avian Prion Protein: Structural Studies Using Synthetic Peptides. *Biochem. Biophys. Res. Comm.* **214**(3), 993-999.

Hosszu, L. L. P., Baxter, N. J., Jackson, G. S., Power, A., Clarke, A. R., Waltho, J. P., Craven, J. & Collinge, J. (1999). Structural Mobility of the Human Prion Protein Probed by Backbone Hydrogen Exchange. *Nature Struct. Biol.* **6**(8), 740-743.

Hudson, D. (1990). Methodological Implications of Simultaneous Solid-phase Peptide Synthesis: A Comparison of Active Esters. *Peptide Res.* **3**(1), 51-55.

Hungerford, G., Martinez-Insua, M., Birch, D. J. S. & Moore, B. D. (1996). A Reversible Transition Between an Alpha-Helix and a 3_{10}-Helix in a Fluorescence-Labeled Peptide. *Angew. Chem. Int. Ed. Engl.* **35**(3), 326-329.

Huston, J. S., Cohen, C., Maratea, D., Fields, F., Tai, M.-S., Cabral-Denison, N., Juffras, R., Rueger, D. C., Ridge, R. J., Oppermann, H., Keck, P. & Baird, L. G. (1992). Multisite Association by Recombinent Proteins Can Enhance Binding Selectively. *Biophys. J.* **62**, 87-91.

Hutchinson, E. G. & Thornton, J. M. (1994). A Revised Set of Potentials for Beta-turn Formation in Proteins. *Protein Sci.* **3**, 2207-2216.

Ibrahim, S. (1993). Immunoglobulin Binding Specificities of the Homology Regions (Domains) of Protein A. *Scand. J. Immunol.* **38**, 368-374.

Ikura, M. (1996). Calcium Binding and Conformational Response in EF-hand Proteins. *Trends Biochem. Sci.* **21**, 14-17.

Ikura, T., Tsurupa, G. P. & Kuwajima, K. (1997). Kinetic Folding and *Cis/Trans* Prolyl Isomerization of Staphylococcal Nuclease. A Study by Stopped-flow Absorption, Stopped-flow Circular Dichroism, and Molecular Dynamics Simulations. *Biochemistry* **36**(21), 6529-6538.

Imperiali, B. & Ottesen, J. J. (1999). Uniquely Folded Mini-protein Motifs. *J. Peptide Res.* **54**, 177-184.

Instruments S.A. (1990). Instruction Manual of CD6 Dichrograph. Instruments, S. A. & Jobin-Yvon. NP/INSTRCD6/0590.

Israelachvili, J. & Wennerström, H. (1996). Role of Hydration and Water Structure in Biological and Colloidal Interactions. *Nature* **379**, 219-225.

Iwasaki, K. & Fujiyama, T. (1979). Light-scattering Study of Clathrate Hydrate Formation in Binary Mixtures of tert-Butyl Alcohol and Water. 2. Temperature Effect. *J. Phys. Chem.* **83**(4), 463-468.

Jäger, M. & Plückthun, A. (1999). Domain Interactions in Antibody Fv and ScFv Fragments: Effects on Unfolding Kinetics and Equilibria. *FEBS Lett.* **462**, 307-312.

Janknecht, R., Sander, C. & Pongs, O. (1991). (HX)n Repeats: A pH-controlled Protein-protein Interaction Motif of Eukaryotic Transcription Factors? *FEBS Lett.* **295**(1-3), 1-2.

Jansson, B., Palmcrantz, C., Uhlèn, M. & Nilsson, B. (1989). A Dual-affinity Gene Fusion System to Express Small Recombinant Proteins in a Soluble Form: Expression and Characterization of Protein A Deletion Mutants. *Protein Engin.* **2**, 555-561.

Jansson, B., Uhlén, M. & Nygren, P.-Å. (1998). All Individual Domains of Staphylococcal Protein A Show Fab Binding. *FEMS Immunol. Med. Microbiol.* **20**, 69-78.

Jansson, M., Uhlen, M. & Nilsson, B. (1997). Structural Changes in Insulin-like Growth Factor (IGF) I Mutant Proteins Affecting Binding Kinetic Rates to IGF Binding Protein 1 and IGF-I Receptor. *Biochemistry* **36**(14), 4108-4117.

Jasanoff, A. & Fersht, A. R. (1994). Quantitative Determination of Helical Propensities from Trifluoroethanol Titration Curves. *Biochemistry* **33**(8), 2129-2135.

Jayaraman, G., Kumar, T. K. S., Arunkumar, A. I. & Yu, C. (1996). 2,2,2-Trifluoroethanol Induces Helical Conformation in an All β-sheet Protein. *Biochem. Biophys. Res. Comm.* **222**(1), 33-37.

Jendeberg, L., Persson, B., Andersson, R., Karlsson, R., Uhlèn, M. & Nilsson, B. (1995). Kinetic Analysis of the Interaction Between Protein A Domain Variants and Human Fc Using Plasmon Resonance Detection. *J. Mol. Recog.* **8**, 270-278.

Jendeberg, L., Tashiro, M., Tejero, R., Lyons, B. A., Uhlén, M., Montelione, G. T. & Nilsson, B. (1996). The Mechanism of Binding Staphylococcal Protein A to Immunoglobin G Does Not Involve Helix Unwinding. *Biochemistry* **35**, 22-31.

Johnson Jr., W. C. (1985). Circular Dichroism and Its Empirical Application to Biopolymers. In *Methods of Biochemical Analysis* (Glick, D., ed.), Vol. 31, pp. 61-163. John Wiley & Sons, New York, Chichester, Brisbane, Toronto, Singapore.

Johnson Jr., W. C. (1990). Protein Secondary Structure and Circular Dichroism: A Practical Guide. *Proteins Struct. Funct. Genet.* **7**, 205-214.

Johnson, L. N. & Barford, D. (1994). Electrostatic Effects In the Control of Glycogen Phosphorylase By Phosphorylation. *Protein Sci.* **3**, 1726-1730.

Johnson, N. P., Lindstrom, J., Baase, W. A. & von Hippel, P. H. (1994). Double-stranded DNA Templates can Induce α-helical Conformation in Peptides Containing Lysine and Alanine: Functional Implications for Leucine Zipper and Helix-loop-helix Transcription Factors. *Proc. Natl. Acad. Sci. USA* **91**, 4840-4844.

Kakizuka, A. (1998). Protein Precipitation: A Common Etiology in Neurodegenerative Disorders? *Trends. Genet.* **14**(10), 396-402.

Kamada, K., Horiuchi, T., Ohsumi, K., Shimamoto, N. & Morikawa, K. (1996). Structure of a Replication-terminator Protein Complexed With DNA. *Nature* **383**, 598-603.

Karlsson, R., Michaelsson, A. & Mattsson, L. (1991). Kinetic Analysis of Monoclonal Antibody-antigen Interactions With a New Biosensor Based Analytical System. *J. Immunol. Meth.* **145**, 229-240.

Karlsson, R. & Ståhlberg, R. (1995). Surface Plasmon Resonance Detection and Multispot Sensing for Direct Monitoring of Interactions Involving Low-molecular-weight Analytes and for Determination of Low Affinities. *Anal. Biochem.* **228**, 274-280.

Karpuj, M. V., Garren, H., Slunt, H., Price, D. L., Gusella, J., Becher, M. W. & Steinman, L. (1999). Transglutaminase Aggregates Huntingtin Into Nonamyloidogenic Polymers, and Its Enzymatic Activity Increases in Huntington's Disease Brain Nuclei. *Proc. Natl. Acad. Sci. USA* **96**, 7388-7393.

Kayed, R., Bernhagen, J., Greenfield, N., Sweimeh, K., Brunner, H., Voelter, W. & Kapurniotu, A. (1999). Conformational Transitions of Islet Amyloid Polypeptide (IAPP) in Amyloid Formation *in Vitro*. *J. Mol. Biol.* **287**, 781-796.

Kentsis, A. & Sosnick, T. R. (1998). Trifluoroethanol Promotes Helix Formation by Destabilizing Backbone Exposure: Desolvation Rather than Native Hydrogen Bonding Defines the Kinetic Pathway of Dimeric Coiled Coil Folding. *Biochemistry* **37**, 14613-14622.

Khaled, M. A., Urry, D. W. & Okamoto, K. (1976). The Gamma-turn as an Independent Conformational Feature in Solution. *Biochem. Biophys. Res. Comm.* **72**(1), 162-169.

Kitakuni, E., Kuroda, Y., Oobatake, M., Tanaka, T. & Nakamura, H. (1993). Thermodynamic Characterization of an Artificially Designed Amphiphilic Alpha-helical Peptide Containing Periodic Prolines. Abstracts of the 5th Annual Meeting of the Protein Engineering Society of Japan. *Protein Engin.* **6**(8), 1024.

Kitakuni, E., Kuroda, Y., Oobatake, M., Tanaka, T. & Nakamura, H. (1994). Thermodynamic Characterization of an Artificially Designed Amphiphilic Alpha-helical Peptide Containing Periodic Prolines: Observations of High Thermal Stability and Cold Denaturation. *Protein Sci.* **3**, 831-837.

Kobayashi, M. & Shimizu, S. (1998). Metalloenzyme Nitrile Hydratase: Structure, Regulation, and Application to Biotechnology. *Nature Biotechnol.* **16**, 733-736.

Kobe, B. & Kemp, B. E. (1999). Active Site-directed Protein Regulation. *Nature* **402**, 373-376.

Kohn, W. D., Kay, C. M., Sykes, B. D. & Hodges, R. S. (1998). Metal Ion Induced Folding of a de Novo Designed Coiled-coil Peptide. *J. Am. Chem. Soc.* **120**, 1124-1132.

Koide, A., Bailey, C. W., Huang, X. & Koide, S. (1998). The Fibronectin Type III Domain as a Scaffold for Novel Binding Proteins. *J. Mol. Biol.* **284**, 1141-1151.

Kraulis, P. J. (1991). MOLSCRIPT: A Program to Produce Both Detailed and Schematic Plots of Protein Structures. *J. Appl. Crystallog.* **24**, 946-950.

Kuhn, L. A., Swanson, C. A., Siani, M. A., Tainer, J. A. & Getzoff, E. D. (1993). Amino Acid Hydrophobicity in the Context of Folded Proteins: A Crystallographic Hydration Scale. *Protein Engin.* **6**(Suppl.), 129.

Kuprin, S., Gräslund, A., Ehrenberg, A. & Koch, M. H. J. (1995). Nonideality of Water-Hexafluoropropanol Mixtures as Studied by X-Ray Small Angle Scattering. *Biochem. Biophys. Res. Comm.* **217**(3), 1151-1156.

Kuwahara, C., Takeuchi, A. M., Nishimura, T., Haraguchi, K., Kubosaki, A., Matsumoto, Y., Saeki, K., Matsumoto, Y., Yokoyama, T., Itohara, S. & Onodera, T. (1999). Prions Prevent Neuronal Cell-line Death. *Nature* **400**, 225-226.

Kuwata, K., Hoshino, M., Era, S., Batt, C. A. & Goto, Y. (1998). Alpha to Beta Transition of Beta-lactoglobulin as Evidenced by Heteronuclear NMR. *J. Mol. Biol.* **283**, 731-739.

Labeit, S. & Kolmerer, B. (1995). Titins: Giant Proteins in Charge of Muscle Ultrastructure and Elasticity. *Science* **270**, 293-296.

Lacassie, E., Delmas, A., Meunier, C., Sy, D. & Trudelle, Y. (1996). High Thermal Stability and Cold-denaturation of an Artificial Polypeptide. *Int. J. Pept. Protein Res.* **48**, 249-258.

Ladurner, A. G. & Fersht, A. R. (1997). Glutamine, Alanine or Glycine Repeats Inserted into the Loop of a Protein Have Minimal Effects on Stability and Folding Rates. *J. Mol. Biol.* **273**, 330-337.

Langone, J. J., Boyle, M., D. P. & Borsos, T. (1978). Studies on The Interaction Between Protein A and Immunoglobulin G. II. Composition and Activity of Complexes Formed Between Protein A and IgG. *J. Immunol.* **121**(1), 333-338.

Lazo, N. D. & Downing, D. T. (1998). Amyloid Fibrils May be Assembled From Beta-helical Protofibrils. *Biochemistry* **37**(7), 1731-1735.

Leatherbarrow, R. J. (1989). Grafit 3.01 edit. Erithacus Software Ltd.

Lee, M. S. & Cao, B. (1996). Nuclear Magnetic Resonance Chemical Shift: Comparison of Estimated Secondary Structures in Peptides By Nuclear Magnetic Resonance and Circular Dichroism. *Protein Engin.* **9**(1), 15-25.

Lee, S., Iwata, T., Oyagi, H., Aoyagi, H., Ohno, M., Anzai, K., Kirino, Y. & Sugihara, G. (1993). Effects of Salts on Conformational Change of Basic Amphipathic Peptides From Beta-structure to Alpha-helix in the Presence of Phospholipid Liposomes and Their Channel-forming Ability. *Biochim. Biophys. Acta* **1151**, 76-82.

Lesk, A. M. & Chothia, C. (1984). Mechanisms of Domain Closure in Proteins. *J. Mol. Biol.* **174**, 175-191.

Lesk, A. M. & Chothia, C. (1988). Elbow Motion in the Immunoglobulins Involves a Molecular Ball-and-socket Joint. *Nature* **335**, 188-190.

Li, D. Y., Brooke, B., Davis, E. C., Mecham, R. P., Sorensen, L. K., Boak, B. B., Eichwald, E. & Keating, M. T. (1998). Elastin is an Essential Determinant of Arterial Morphogenesis. *Nature* **393**, 276-280.

Li, S.-C. & Deber, C. M. (1993). Peptide Environment Specifies Conformation. *J. Biol. Chemistry* **268**(31), 22975-22978.

Li, S.-C., Goto, N. K., Williams, K. A. & Deber, C. M. (1996). Alpha-Helical, But Not Beta-Sheet, Propensity of Proline Is Determined By Peptide Environment. *Proc. Natl. Acad. Sci. USA* **93**(13), 6676-6681.

Lichtenberg, B., Mandelkow, E.-M., Hagestedt, T. & Mandelkow, E. (1988). Structure and Elasticity of Microtubule-associated Protein Tau. *Nature* **334**, 359-362.

Liemann, S., Bringemeier, I., Benz, J., Göttig, P., Hofmann, A., Huber, R., Noegel, A. A. & Jacob, U. (1997). Crystal Structure of the C-terminal Tetrad Repeat from Synexin (Annexin VII) of *Dictyostelium discoideum*. *J. Mol. Biol.* **270**, 79-88.

Lim, W. A., Richards, F. M. & Fox, R. O. (1994). Structural Determinants of Peptide-binding Orientation and of Sequence Specificity in SH3 Domains. *Nature* **372**, 375-379.

Lin, K., Rath, V. L., Dai, S. C., Fletterick, R. J. & Hwang, P. K. (1996). A Protein Phosphorylation Switch at the Conserved Allosteric Site in GP. *Science* **273**, 1539-1541.

Linder, M. E., Middleton, P., Hepler, J. R., Taussig, R., Gilman, A. G. & Mumby, S. M. (1993). Lipid Modifications of G Proteins: α Subunits are Palmitoylated. *Proc. Natl. Acad. Sci. USA* **90**, 3675-3679.

Linke, W. A., Ivemeyer, M., Mundel, P., Stockmeier, M. R. & Kolmerer, B. (1998). Nature of PEVK-titin Elasticity in Skelatal Muscle. *Proc. Natl. Acad. Sci. USA* **95**, 8052-8057.

Linke, W. A., Ivemeyer, M., Olivieri, N., Kolmerer, B., Rüegg, J. C. & Labeit, S. (1996). Towards a Molecular Understanding of the Elasticity of Titin. *J. Mol. Biol.* **261**(1), 62-71.

Liu, J.-J. & Lindquist, S. (1999). Oligopeptide-repeat Expansions Modulate 'Protein-only' Inheritance in Yeast. *Nature* **400**, 573-576.

Livingstone, J. R., Spolar, R. S. & Record, M. T., Jr. (1991). Contribution to the Thermodynamics of Protein Folding from the Reduction in Water-Accessible Nonpolar Surface Area. *Biochemistry* **30**(17), 4237-4244.

Ljungberg, U. K., Jansson, B., Niss, U., Nilsson, R., Sandberg, B. E. B. & Nilsson, B. (1993). The Interaction Between Different Domains of Staphylococcal Protein A and Human Polyclonal IgG, IgA, IgM and $F(ab)_2$: Separation of Affinity from Specificity. *Mol. Immunol.* **30**(14), 1279-1285.

Long, M. M., Rapaka, R. S., Volpin, D., Pasquali-Ronchetti, I. & Urry, D. W. (1980). Spectroscopic and Electron Micrographic Studies on the Repeat Tetrapeptide of Tropoelastin: (Val-Pro-Gly-Gly)n. *Arch. Biochem. Biophys.* **201**(2), 445-452.

Lu, P.-J., Wulf, G., Zhou, X. Z., Davies, P. & Lu, K. P. (1999a). The Prolyl Isomerase Pin1 Restores the Function of Alzheimer-associated Phosphorylated Tau Protein. *Nature* **399**, 784-788.

Lu, P.-J., Zhou, X. Z., Shen, M. & Lu, K. P. (1999b). Function of WW Domains as Phosphoserine- or Phosphothreonine-Binding Modules. *Science* **283**, 1325-1328.

Lu, Z.-X., Fok, K.-F., Erickson, B. W. & Hugli, T. E. (1984). Conformational Analysis of COOH-terminal Segments of Human C3a. *J. Biol. Chem.* **259**(12), 7367-7370.

Luan, C. -H., Harris, R. D., Prasad, K. U. & Urry, D. W. (1990). Differential Scanning Calorimetry Studies of the Inverse Temperature Transition of the Polypentapeptide of Elastin and Its Analogs. *Biopolymers* **29**(14), 1699-1706.

Luo, P. & Baldwin, R. L. (1997). Mechanism of Helix Induction by Trifluoroethanol: A Framework for Extrapolating the Helix-Forming Properties of Peptides from Trifluoroethanol/Water Mixtures Back to Water. *Biochemistry* **36**(27), 8413-8421.

Luo, P. & Baldwin, R. L. (1999). Interaction Between Water and Polar Groups of the Helix Backbone: An Important Determinant of Helix Propensities. *Proc. Natl. Acad. Sci. USA* **96**, 4930-4935.

Luo, Y. & Baldwin, R. L. (1998). Trifluoroethanol Stabilizes the pH 4 Folding Intermediate of Sperm Whale Apomyoglobin. *J. Mol. Biol.* **279**, 49-57.

MacArthur, M. W. & Thornton, J. M. (1991). Influence of Proline Residues On Protein Conformation. *J. Mol. Biol.* **218**(2), 397-412.

MacBeath, G., Kast, P. & Hilvert, D. (1998). Redesigning Enzyme Topology by Directed Evolution. *Science* **279**, 1958-1961.

Maccallum, P. H., Poet, R. & Milner-White, E. J. (1995). Coulombic Attractions Between Partially Charged Main-Chain Atoms Stabilise the Right-Handed Twist Found in Most Beta-Strands. *J. Mol. Biol.* **248**(2), 374-384.

MacDonald, M. E., Ambrose, C. M., Duyao, M. P., Myers, R. H., Lin, C., Srinidhi, L., Barnes, G., Taylor, S. A. & 50 other authors. (1993). A Novel Gene Containing a Trinucleotide Repeat That is Expanded and Unstable on Huntington's Disease Chromosomes. *Cell* **72**, 971-983.

Macias, M. J., Hyvönen, M., Baraldi, E., Schultz, J., Sudol, M., Saraste, M. & Oschkinat, H. (1996). Structure of the WW Domain of a Kinase-associated Protein Complexed with a Proline-rich Peptide. *Nature* **382**, 646-649.

Mahoney, N. M., Rozwarski, D. A., Fedorov, E., Fedorov, A. A. & Almo, S. C. (1999). Profilin Binds Proline-rich Ligands in two Distinct Amide Backbone Orientations. *Nature Struct. Biol.* **6**(7), 666-671.

Makarov, A. A., Lobachov, V. M., Adzhubei, I. A. & Esipova, N. G. (1992). Natural Polypeptides in Left-handed Helical Conformation. A Circular

Dichroism Study of the Linker Histones' C-terminal Fragments and β-endorphin. *FEBS Letters* **306**(1), 63-65.

Malakaukas, S. M. & Mayo, S. L. (1998). Design, Structure and Stability of a Hyperthermophilic Protein Variant. *Nature Struct. Biol.* **5**(6), 470-475.

Mann, M. & Wilm, M. (1995). Electrospray Mass Spectrometry for Protein Characterization. *Trends Biochem. Sci.* **20**, 219-224.

Manning, M. C., Illangasekare, M. & Woody, R. W. (1988). Circular Dichroism Studies of Distorted Alpha-helices, Twisted Beta-sheets, and Beta-turns. *Biophys. Chem.* **31**, 77-86.

Marcotte, E. M. & Eisenberg, D. (1999). Chicken Prion Tandem Repeats Form a Stable, Protease-Resistant Domain. *Biochemistry* **38**, 667-676.

Martenson, R. E., Park, J. Y. & Stone, A. L. (1985). Low-ultraviolet Circular Dichroism Spectroscopy of Sequential Peptides 1-63, 64-95, 96-128, and 129-168 Derived from Myelin Basic Protein of Rabbit. *Biochemistry* **24**, 7689-7695.

Maruya, M., Sameshima, M., Nemoto, T. & Yahara, I. (1999). Monomer Arrangement in Hsp90 dimer as Determined by Decoration with N and C-Terminal Region Specific Antibodies. *J. Mol. Biol.* **285**, 903-907.

Maruyama, K. (1997). Connectin/Titin, Giant Elastic Protein of Muscle. *FASEB J.* **11**, 341-345.

Matsushima, N., Creutz, C. E. & Kretsinger, R. H. (1990). Polyproline, Beta-turn Helices, Novel Secondary Structures Proposed for the Tandem Repeats Within Rhodopsin, Synaptophysin, Synexin, Gliadin, RNA Polymerase II, Hordein, and Gluten. *Proteins: Struct. Funct. Genet.* **7**, 125-155.

Mattos, C., Petsko, G. A. & Karplus, M. (1994). Analysis of Two-Residue Turns in Proteins. *J. Mol. Biol.* **238**(5), 733-747.

McIlhinney, R. A. J. (1990). The Fats of Life: The Importance and Function of Protein Acylation. *Trends Biochem. Sci.* **15**, 387-391.

McIntire, W. E., Schey, K. L., Knapp, D. R. & Hildebrandt, J. D. (1998). A Major G Protein α_o Isoform in Bovine Brain is Deamidated at Asn346 and Asn347, Residues Involved in Receptor Coupling. *Biochemistry* **37**(42), 14651-14658.

McKean, P. G., Trenholme, K. R., Rangarajan, D., Keen, J. K. & Smith, D. F. (1997). Diversity of Repeat-containing Surface Proteins of *Leishmania major*. *Mol. Biochem. Parasitol.* **86**, 225-235.

McLaughlin, S. & Aderem, A. (1995). The Myristoyl-electrostatic Switch: A Modulator of Reversible Protein-membrane Interactions. *Trends Biochem. Sci.* **20**, 272-276.

McPherson, D. T., Morrow, C., Minehan, D. S., Wu, J., Hunter, E. & Urry, D. W. (1992). Production and Purification of a Recombinant Elastomeric Polypeptide G-$(VPGVG)_{19}$-VPGV, from *Eschericia coli*. *Biotechnol. Prog.* **8**(4), 347-352.

McPherson, D. T., Xu, J. & Urry, D. W. (1996). Product Purification By Reversible Phase Transition Following *Escherichia Coli* Expression of Genes Encoding Up to 251 Repeats of the Elastomeric Pentapeptide GVGVP. *Protein Expr. Purific.* **7**(1), 51-57.

Meredith, G. D., Chang, W.-H., Li, Y., Bushnell, D. A., Darst, S. T. & Kornberg, R. D. (1996). The C-terminal Domain Revealed in the Structure of RNA Polymerase II. *J. Mol. Biol.* **258**, 413-419.

Merrifield, B. (1997). Concept and Early Development of Solid-phase Peptide Synthesis. *Meth. Enzymol.* **289**, 3-13.

Merrifield, R. B. (1963). Solid Phase Peptide Synthesis. I. The Synthesis of a Tetrapeptide. *J. Am. Chem. Soc.* **85**, 2149-2154.

Meyer, D. E. & Chilkoti, A. (1999). Purification of Recombinant Proteins By Fusion With Thermally-responsive Polypeptides. *Nature Biotechnol.* **17**, 1112-1115.

Mezei, M. (1998). Chameleon Sequences in the PDB. *Protein Engin.* **11**(6), 411-414.

Miles, M. J., Carr, H. J., McMaster, T. C., I'Anson, K. J., Belton, P. S., Morris, V. J., Field, J. M., Shewry, P. R. & Tatham, A. S. (1991). Scanning Tunneling Microscopy of a Wheat Seed Storage Protein Reveals Details of an Unusual Supersecondary Structure. *Proc. Natl. Acad. Sci. USA* **88**(1), 68-71.

MilliGen/Biosearch. (1990). 9050 Peptide Syntheziser Manual. .

Minor Jr., D. L. & Kim, P. S. (1996). Context-dependent Secondary Structure Formation of a Designed Protein Sequence. *Nature* **380**, 730-734.

Miranda, L. P. & Alewood, P. F. (1999). Accelerated Chemical Synthesis of Peptides and Small Proteins. *Proc. Natl. Acad. Sci. USA* **96**, 1181-1186.

Mitchell, D. C. & Litman, B. J. (1999). Effect of Protein Hydration on Receptor Conformation: Decreased Levels of Bound Water Promote Metarhodopsin II Formation. *Biochemistry* **38**, 7617-7623.

Mitsui, A. & Sharp, P. A. (1999). Ubiquitination of RNA Polymerase II Large Subunit Signaled by Phosphorylation of Carboxy-terminal Domain. *Proc. Natl. Acad. Sci. USA* **96**, 6054-6059.

Miura, T., Hori-i, A. & Takeuchi, H. (1996). Metal-dependent Alpha-helix Formation Promoted by the Glycine-rich Octapeptide Region of Prion Protein. *FEBS Lett.* **396**, 248-252.

Moks, T., Abrahmsén, L., Nilsson, B., Hellman, U., Sjöquist, J. & Uhlén, M. (1986). Staphylococcal Protein A Consists of Five IgG-binding Domains. *Eur. J. Biochem.* **156**, 637-643.

Moriarty, D. F. & Raleigh, D. P. (1999). Effects of Sequential Proline Substitutions on Amyloid Formation by Human $Amylin_{20-29}$. *Biochemistry* **38**(6), 1811-1818.

Mourey, L., Samama, J.-P., Delarue, M., Petitou, M., Choay, J. & Moras, D. (1993). Crystal Structure of Cleaved Bovine Antithrombin III at 3.2 Å Resolution. *J. Mol. Biol.* **232**, 223-241.

Mukohata, Y., Ihara, K., Tamura, T. & Sugiyama, Y. (1999). Halobacterial Rhodopsins. *J. Biochem.* **125**, 649-657.

Muller, N. (1993). Hydrophobicity and Stability For a Family of Model Proteins. *Biopolymers* **33**(8), 1185-1193.

Murray, N. J. & Williamson, M. P. (1994). Conformational Study of a Salvary Proline-rich Protein Repeat Sequence. *Eur. J. Biochem.* **219**, 915-921.

Musacchio, A., Wilmanns, M. & Saraste, M. (1994). Structure and Function of the SH3 Domain. *Prog. Biophys. Mol. Biol.* **61**, 283-297.

Nagashima, S., Nakasako, M., Dohmae, N., Tsujimura, M., Takio, K., Odaka, M., Yohda, M., Kamiya, N. & Endo, I. (1998). Novel Non-heme Iron Center of Nitrile Hydratase With a Claw Setting of Oxygen Atoms. *Nature Struct. Biol.* **5**(5), 347-351.

Nakamura, S., Tanaka, T., Yada, R. Y. & Nakai, S. (1997). Improving the Thermostability of *Baciullus stearothermophilus* Neutral Protease by Introducing Proline into the Active Site Helix. *Protein Engin.* **10**(11), 1263-1269.

Nakasako, M. (1999). Large-Scale Networks of Hydration Water Molecules Around Bovine Beta-Trypsin Revealed by Cryogenic X-Ray Crystal Structure Analysis. *J. Mol. Biol.* **289**, 547-564.

Nakasako, M., Odaka, M., Yohda, M., Dohmae, N., Takio, K., Kamiya, N. & Endo, Y. (1999). Tertiary and Quarternary Structures of Photoreactive Fe-type Nitrile Hydratase from *Rhodococcus* sp. N-771: Roles of Hydration Water Molecules in Stabilizing the Structures and the Structural Origin of the Substrate Specificity of the Enzyme. *Biochemistry* **38**(31), 9887-9898.

Nanzer, A. P., Torda, A. E., Bisang, C., Weber, C., Robinson, J. A. & van Gunsteren, W. F. (1997). Dynamic Studies of Peptide Motifs in the *Plasmodium falciparum* Circumsporozoite Surface Protein by Restrained and Unrestrained MD Simulations. *J. Mol. Biol.* **267**, 1012-1025.

Narayanaswami, V., Wang, J., Schieve, D., Kay, C. M. & Ryan, R. O. (1999). A Molecular Trigger of Lipid Binding-induced Opening of a Helix Bundle Exchangeable Apolipoprotein. *Proc. Natl. Acad. Sci. USA* **96**, 4366-4371.

Narhi, L. O., Philo, J. S., Li, T., Zhang, M., Samal, B. & Arakawa, T. (1996a). Induction of Alpha-Helix in the Beta-Sheet Protein Tumor Necrosis Factor-Alpha: Acid-Induced Denaturation. *Biochemistry* **35**(35), 11454-11460.

Narhi, L. O., Philo, J. S., Li, T., Zhang, M., Samal, B. & Arakawa, T. (1996b). Induction of Alpha-Helix in the Beta-Sheet Protein Tumor Necrosis Factor-Alpha: Thermal- and Trifluoroethanol-Induced Denaturation At Neutral pH. *Biochemistry* **35**(35), 11447-11453.

Nave, R., Fürst, D. O. & Weber, K. (1989). Visualization of the Polarity of Isolated Titin Molecules: A Single Globular Head on a Long Thin Rod As the M Band Anchoring Domain? *J. Cell. Biol.* **109**, 2177-2187.

Nedved, M. L., Gottlieb, P. A. & Moe, G. R. (1994). CD and DNA Binding Studies of a Proline Repeat-containing Segment of the Replication Arrest Protein Tus. *Nucl. Acids Res.* **22**(23), 5024-5030.

Ng, K. K.-S. & Weis, W. I. (1998). Coupling of Prolyl Peptide Bond Isomerization and Ca(II) Binding in a C-type Mannose-binding Protein. *Biochemistry* **37**(51), 17977-17989.

Nguyen, J. T., Turck, C. W., Cohen, F. E., Zuckermann, R. N. & Lim, W. A. (1998). Exploiting the Basis of Proline Recognition by SH3 and WW Domains: Design of N-substituted Inhibitors. *Science* **282**, 2088-2092.

Nicholson, L. K., Yamazaki, T., Torchia, D. A., Grzesiek, S., Bax, A., Stahl, S. J., Kaufman, J. D., Wingfield, P. T., Lam, P. Y. S., Jadhav, P. K., Hodge, C. N., Domaille, P. J. & Chang, C.-H. (1995). Flexibility and Function in HIV-1 Protease. *Nature Struct. Biol.* **2**(4), 274-280.

Nilsson, B. & Abrahmsén, L. (1990). Fusions to Staphylococcal Protein A. *Methods Enzymol.* **185**, 144-161.

Nilsson, B., Moks, T., Jansson, B., Abrahmsèn, L., Elmblad, A., Holmgren, E., Henrichson, C., Jones, T. A. & Uhlèn, M. (1987). A Synthetic IgG-binding Domain Based on Staphylococcal Protein A. *Protein Engin.* **1**(2), 107-113.

Nilsson, I. & von Heijne, G. (1998). Breaking the Camel's Back: Proline-induced Turns in a Model Transmembrane Helix. *J. Mol. Biol.* **284**, 1185-1189.

Nishi, N., Ohiso, I., Sakairi, N., Tokura, S., Tsunemi, M. & Oka, M. (1995). Synthesis and Conformational Investigation of Tandem Repeat Sequence in RNA Polymerase II. *Biochem. Biophys. Res. Comm.* **206**(3), 981-987.

Nishizawa, K., Freund, C., Li, J., Wagner, G. & Reinherz, E. L. (1998). Identification of a Proline-binding Motif Regulating CD2-triggered T Lymphycyte Activation. *Proc. Natl. Acad. Sci. USA* **95**, 14897-14902.

Noelken, M. E., Wisdom Jr., B. J. & Hudson, B. G. (1981). Estimation of the Size of Collagenous Polypeptides by Sodium Dodecyl Sulfate-Polyacrylamide Gel Electrophoresis. *Anal. Biochem.* **110**, 131-136.

Noguti, T. & Gö, N. (1989a). Structural Basis of Hierarchical Multiple Substates of a Protein. I: Introduction. *Proteins: Struct. Funct. Genet.* **5**, 97-103.

Noguti, T. & Gö, N. (1989b). Structural Basis of Hierarchical Multiple Substates of a Protein. V: Nonlocal Deformations. *Proteins: Struct., Funct. Genet.* **5**, 132-138.

Nord, K., Nilsson, J., Nilsson, B., Uhlén, M. & Nygren, P.-Å. (1995). A Combinatorial Library of an Alpha-Helical Bacterial Receptor Domain. *Protein Engin.* **8**(6), 601-608.

Nugent, P. G., Albert, A., Orprayoon, P., Wilsher, J., Pitts, J. E., Blundell, T. L. & Dhanaraj, V. (1996). Protein Engineering Loops in Aspartic Proteinases: Site-Directed Mutagenesis, Biochemical Characterization and X-Ray Analysis of Chymosin With a Replaced Loop From Rhizopuspepsin. *Protein Engin.* **9**(10), 885-893.

Nuttall, S. D., Rousch, M. J. M., Irving, R. A., Hufton, S. E., Hoogenboom, H. R. & Hudson, P. J. (1999). Design and Expression of Soluble CTLA-4 Variable Domain as a Scaffold for the Display of Functional Polypeptides. *Proteins: Struct. Funct. Genet.* **36**, 217-227.

Oas, T. G. & Endow, S. A. (1994). Springs and Hinges: Dynamic Coiled Coils and Discontinuities. *Trends Biochem. Sci.* **19**, 51-54.

O'Shannessy, D. J., Brigham-Burke, M., Soneson, K. K., Hensley, P. & Brooks, I. (1993). Determination of Rate and Equilibrium Binding Constants for Macromolecular Interactions Using Surface Plasmon Resonance: Use of Nonlinear Least Squares Analysis Methods. *Anal. Biochem.* **212**, 457-468.

Otzen, D. E. & Fersht, A. R. (1995). Side-chain Determinants of Beta-sheet Stability. *Biochemistry* **34**, 5718-5724.

Ozols, J. (1990). Amino Acid Analysis. *Methods Enzymol.* **182**, 587-601.

Padmanabhan, S. & Baldwin, R. L. (1994). Helix-stabilizing Interaction Between Tyrosine and Leucine or Valine when the Spacing is i, i+4. *J. Mol. Biol.* **241**, 706-713.

Padmanabhan, S., Jiménez, M. A., Laurents, D. V. & Rico, M. (1998). Helix-Stabilizing Nonpolar Interactions between Tyrosine and Leucine in Aqueous and TFE Solutions: 2D-^{1}H NMR and CD Studies in Alanine-Lysine Peptides. *Biochemistry* **37**(49), 17318-17330.

Pappenheimer Jr., A. M. (1977). Diphtheria Toxin. *Annu. Rev. Biochem.* **46**, 69-94.

Perczel, A., Foxman, B. M. & Fasman, G. D. (1992). How Reverse Turns May Mediate the Formation of Helical Segments in Proteins: An X-ray Model. *Proc. Natl. Acad. Sci. USA* **89**, 8210-8214.

Perczel, A., Hollósi, M., Sándor, P. & Fasman, G. D. (1993). The Evaluation of Type I and Type II Beta-Turn Mixtures. Circular Dichroism, NMR and Molecular Dynamics Studies. *Int. J. Pept. Protein Res.* **41**(3), 223-236.

Pertsemlidis, A., Saxena, A. M., Soper, A. K., Head-Gordon, T. & Glaeser, R. M. (1996). Direct Evidence For Modified Solvent Structure Within the Hydration Shell of a Hydrophobic Amino Acid. *Proc. Natl. Acad. Sci. USA* **93**(20), 10769-10774.

Pertsemlidis, A., Soper, A. K., Sorenson, J. M. & Head-Gordon, T. (1999). Evidence for Microscopic, Long-Range Hydration Forces for a Hydrophobic Amino Acid. *Proc. Natl. Acad. Sci. USA* **96**, 481-486.

Perutz, M. F. (1999). Glutamine Repeats and Neurodegenerative Diseases: Molecular Aspects. *Trends Biochem. Sci.* **24**, 58-63.

Perutz, M. F., Johnson, T., Suzuki, M. & Finch, J. T. (1994). Glutamine Repeats as Polar Zippers: Their Possible Role in Inherited Neurodegenerative Diseases. *Proc. Natl. Acad. Sci. USA* **91**, 5355-5358.

Plaxco, K. W., Spitzfaden, C., Campbell, I. D. & Dobson, C. M. (1996). Rapid Refolding of a Proline-rich All Beta-sheet Fibronectin Type III Module. *Proc. Natl. Acad. Sci. USA* **93**, 10703-10706.

Potter, K. N., Li, Y. & Capra, D. (1996). Staphylococcal Protein A Simultaneously Interacts with Framework Region 1, Complementarity-Determining Region 2, and Framework Region 3 on Human VH3-Encoded Igs. *J. Immunol.* **157**, 2982-2988.

Prajapati, S., Bhakuni, V., Babu, K. R. & Jain, S. K. (1998). Alkaline Unfolding and Salt-induced Folding of Bovine Liver Catalase at High pH. *Eur. J. Biochem.* **255**, 178-184.

Predki, P. F., Agrawal, V., Brünger, A. T. & Regan, L. (1996). Amino-Acid Substitutions In a Surface Turn Modulate Protein Stability. *Nature Struct. Biol.* **3**(1), 54-58.

Prince, R. C. & Gunson, D. E. (1998). Prions are Copper-binding Proteins. *Trends Biochem. Sci.* **23**, 197-198.

Privalov, P. L.. & Makhatadze, G. I. (1993). Contribution of Hydration to Protein Folding Thermodynamics. II. The Entropy and Gibbs Energy of Hydration. *J. Mol. Biol.* **232**, 660-679.

Privalov, P. L. (1992). Physical Basis of the Stability of the Folded Conformations of Proteins. In *Protein Folding* (Creighton, T. H., ed.), pp. 83-126. W. H. Freeman and Company, New York.

Prusiner, S. B., McKinley, M. P., Bowman, K. A., Bolton, D. C., Bendheim, P. E., Groth, D. F. & Glenner, G. G. (1983). Scrapie Prions Aggregate to Form Amyloid-like Birefringent Rods. *Cell* **35**, 349-358.

Quinn, T. P., Tweedy, N. B., Williams, R. W., Richardson, J. S. & Richardson, D. C. (1994). Betadoublet: De Novo Design, Synthesis, and Characterization of a Beta-Sandwich Protein. *Proc. Natl. Acad. Sci. USA* **91**(19), 8747-8751.

Rajan, R. & Balaram, P. (1996). A Model For the Interaction of Trifluoroethanol With Peptides and Proteins. *Int. J. Pept. Protein Res.* **48**, 328-336.

Randen, I., Potter, K. N., Li, Y., Thompson, K. M., Pascual, V., Førre, Ø., Natvig, J. B. & Capra, J. D. (1993). Complementarity-determining Region 2 Is

Implicated in the Binding of Staphylococcal Protein A to Human Immunoglobulin V_H3 Variable Regions. *Eur. J. Immunol.* **23**, 2682-2686.

Reed, J. & Kinzel, V. (1991). A Conformational Switch Is Associated with Receptor Affinity in Peptides Derived from the CD4-Binding Domain of gp120 from HIV I. *Biochemistry* **30**(18), 4521-4528.

Reed, J. & Kinzel, V. (1993). Primary Structure Elements Responsible For the Conformational Switch In the Envelope Glycoprotein gp120 From Human Immunodefieciency Virus Type 1: LPCR Is a Motif Governing Folding. *Proc. Natl. Acad. Sci. USA* **90**, 6761-6765.

Reed, J. & Reed, T. A. (1997). A Set of Constructed Type Spectra for the Practical Estimation of Peptide Secondary Structure from Circular Dichroism. *Anal. Biochem.* **254**, 36-40.

Rees, A. R., Staunton, D., Webster, D. M., Searle, S. J., Henry, A. H. & Pedersen, J. T. (1994). Antibody Design: Beyond the Natural Limits. *Trends Biotechnol.* **12**, 199-206.

Reiersen, H., Clarke, A. R. & Rees, A. R. (1998). Short Elastin-Like Peptides Exhibit the Same Temperature Induced Structural Transitions as Elastin Polymers: Implications for Protein Engineering. *J. Mol. Biol.* **283**(1), 255-264.

Reiersen, H. & Rees, A. R. (1999). An Engineered Minidomain Containing an Elastin Turn Exhibits a Reversible Temperature-Induced IgG binding. *Biochemistry* **38**(45), 14897-14905.

Reimer, U., Scherer, G., Drewello, M., Kruber, S., Schutkowski, M. & Fischer, G. (1998). Side-chain Effects on Peptidyl-prolyl *cis/trans* Isomerisation. *J. Mol. Biol.* **279**, 449-460.

Reiter, Y., Schuck, P., Boyd, L. F. & Plaskin, D. (1999). An Antibody Single-domain Phage Display Library of a Native Heavy Chain Variable Region: Isolation of Functional Single-domain VH Molecules with a Unique Interface. *J. Mol. Biol.* **290**, 685-698.

Renugopalakrishnan, V., Khaled, M. A., Rapaka, R. S. & Urry, D. W. (1978a). Proton Magnetic Resonance and Conformational Energy Calculations of Repeat Peptides of Tropoelastin. A Permutation of The Hexapeptide. *Biochim. Biophys. Acta* **536**, 421-428.

Renugopalakrishnan, V., Khaled, M. A. & Urry, D. W. (1978b). Proton Magnetic Resonance and Conformational Energy Calculations of Repeat Peptides of Tropoelastin: the Pentapeptide. *J. Chem. Soc. Perkin II*, 111-119.

Richardson, J. S. (1981). The Anatomy and Taxonomy of Protein Structure. *Adv. Protein Chem.* **34**, 167-253.

Richman, D. D., Cleveland, P. H., Oxman, M. N. & Johnson, K. M. (1982). The Binding of Staphylococcal Protein A By The Sera of Different Animal Species. *J. Immunol.* **128**(5), 2300-2305.

Roben, P. W., Salem, A. N. & Silverman, G. J. (1995). V_H3 Family Antibodies Bind Domain D of Staphylococcal Protein A. *J. Immunol.* **154**, 6437-6445.

Robert, C. H. & Ho, P. S. (1995). Significance of Bound Water to Local Chain Conformations in Protein Crystals. *Proc. Natl. Acad. Sci. USA* **92**, 7600-7604.

Robinson, A. B. & Robinson, L. R. (1991). Distribution of Glutamine and Aspargine Residues and Their Near Neighbors in Peptides and Proteins. *Proc. Natl. Acad. Sci. USA* **88**, 8880-8884.

Robson, K. J. H., Naitza, S., Barker, G., Sinden, R. E. & Crisanti, A. (1997). Cloning and Expression of the Thrombospondin Related Adhesive Protein Gene of *Plasmodium berghei*. *Mol. Biochem. Parasitol.* **84**, 1-12.

Roditi, I., Schwarz, H., Pearson, T. W., Beecroft, R. P., Liu, M. K., Richardson, J. P., Bühring, H.-J., Pleiss, J., Bülow, R., Williams, R. O. & Overath, P. (1989). Procyclin Gene Expression and Loss of the Variant Surface Glycoprotein During Differentiation of *Trypanosom Brucei*. *J. Cell. Biol.* **108**, 737-746.

Rose, G. D. (1978). Prediction of Chain Turns in Globular Proteins on a Hydrophobic Basis. *Nature* **272**, 586-590.

Ruben, G. C., Iqbal, K., Grundke-Iqbal, I., Wisniewski, H. M., Ciardelli, T. L. & Johnson, J. E., Jr. (1991). The Microtubule-associated Protein Tau Forms a Triple-stranded Left-hand Helical Polymer. *J. Biol. Chem.* **266**(32), 22019-22027.

Safar, J., Roller, P. P., Gajdusek, D. C. & Gibbs Jr., C. J. (1994). Scrapie Amyloid (Prion) Protein Has the Conformational Characteristics of an Aggregated Molten Globule Folding Intermediate. *Biochemistry* **33**, 8375-8383.

Sagermann, M., Baase, W. A. & Matthews, B. W. (1999). Structural Characterization of an Engineered Tandem Repeat Contrasts the Importance of Context and Sequence in Protein Folding. *Proc. Natl. Acad. Sci. USA* **96**, 6078-6083.

Sakashita, H., Ohkubo, T., Sakuma, T., Kainosho, M., Sekiguchi, M. & Morikawa, K. (1994). Methylation-Dependent Switch Mechanism of the *Escherichia Coli* Ada Protein. *Protein Engin.* **7**(9), 1153.

Sandberg, L. B., Leslie, J. G., Leach, C. T., Alvarez, V. L., Torres, A. R. & Smith, D. W. (1985). Elastin Covalent Structure as Determined by Solid Phase Amino Acid Sequencing. *Pathol. Biol.* **33**(4), 266-274.

Sandberg, L. B., Weissman, N. & Smith, D. W. (1969). The Purification and Partial Characterization of a Soluble Elastin-like Protein from Copper-deficient Porcine Aorta. *Biochemistry* **8**(7), 2940-2945.

Scherzinger, E., Sittler, A., Schweiger, K., Heiser, V., Lurz, R., Hasenbank, R., Bates, G. P., Lehrach, H. & Wanker, E. E. (1999). Self-assembly of Polyglutamine-containing Huntingtin Fragments Into Amyloid-like Fibrils: Implications for Huntington's Disease Pathology. *Proc. Natl. Acad. Sci. USA* **96**, 4604-4609.

Schleif, R. (1999). Arm-domain Interactions in Proteins: A Review. *Proteins: Struct. Funct. Genet.* **34**, 1-3.

Scholtz, J. M., Marqusee, S., Baldwin, R. L., York, E. J., Stewart, J. M., Santoro, M. & Bolen, D. W. (1991a). Calorimetric Determination of the Enthalpy Change For the Alpha-Helix to Coil Transition of an Alanine Peptide in Water. *Proc. Natl. Acad. Sci. USA* **88**(7), 2854-2858.

Scholtz, J. M., York, E. J., Stewart, J. M. & Baldwin, R. L. (1991b). A Neutral, Water-Soluble, Alpha-Helical Peptide: The Effect of Ionic Strength on the Helix-Coil Equilibrium. *J. Am. Chem. Soc.* **113**(13), 5102-5104.

Schwehm, J. M., Kristyanne, E. S., Biggers, C. C. & Stites, W. E. (1998). Stability Effects of Increasing the Hydrophobicity of Solvent-exposed Side Chains in Staphylococcal Nuclease. *Biochemistry* **37**, 6939-6948.

Searle, M. S., Zerella, R., Williams, D. H. & Packman, L. C. (1996). Native-Like Beta-Hairpin Structure in an Isolated Fragment From Ferredoxin: NMR and

CD Studies of Solvent Effects On the N-Terminal 20 Residues. *Protein Engin.* **9**(7), 559-565.

Selkoe, D. J. (1999). Translating Cell Biology into Therapeutic Advances in Alzheimer's Disease. *Nature* **399**(Suppl), A23-A31.

Sibanda, B. L. & Thornton, J. M. (1985). β-Hairpin Families in Globular Proteins. *Nature* **316**, 170-174.

Siedlecka, M., Goch, G., Ejchart, A., Sticht, H. & Bierzynski, A. (1999). Alpha-helix Nucleation by a Calcium-binding Peptide Loop. *Proc. Natl. Acad. Sci. USA* **96**, 903-908.

Simanek, E. E., Huang, D.-H., Pasternack, L., Machajewski, T. D., Seitz, O., Millar, D. S., Dyson, H. J. & Wong, C.-H. (1998). Glycosylation of Threonine of the Repeating Unit of RNA Polymerase II with β-Linked N-Acetylglycosame Leads to a Turnlike Structure. *J. Am. Chem. Soc.* **120**, 11567-11575.

Skoog, D. A., West, D. M. & Holler, F. J. (1988). High-Performance Liquid Chromatography. In *Fundamentals of Analytical Chemistry* 5 edit., pp. 644-666. Sauders College Publishing, New York, Chicago, San Fransico, Philadelphia, Montreal, Toronto, London, Sydney, Tokyo.

Smith, D. F. & Rangarajan, D. (1995). Cell Surface Components of *Leishmania*: Identification of a Novel Parasite Lectin? *Glycobiology* **5**(2), 161-166.

Smith, D. W., Weissman, N. & Carnes, W. H. (1968). Cardiovascular Studies on Copper Deficent Swine. XII. Partial Purification of a Soluble Protein Resembling Elastin. *Biochem. Biophys. Res. Comm.* **31**(3), 309-315.

Smith, G. (1998). Patch Engineering: A General Approach for Creating Proteins That Have New Binding Activities. *Trends Biochem. Sci.* **23**, 457-460.

Smith, S. P., Barber, K. R., Dunn, S. D. & Shaw, G. S. (1996). Structural Influence of Cation Binding to Recombinant Human Brain S100b: Evidence For Calcium-Induced Exposure of a Hydrophobic Surface. *Biochemistry* **35**(27), 8805-8814.

Sommer-Knudsen, J., Bacic, A. & Clarke, A. E. (1998). Hydroxyproline-rich Plant Glycoproteins. *Phytochemistry* **47**(4), 483-497.

Sönnichsen, F. D., Van Eyk, J. E., Hodges, R. S. & Sykes, B. D. (1992). Effect of Trifluoroethanol on Protein Secondary Structure: An NMR and CD Study Using a Synthetic Actin Peptide. *Biochemistry* **31**(37), 8790-8798.

Soto, C., Castaño, E. M., Frangione, B. & Inestrosa, N. C. (1995). The Alpha-Helical to Beta-Strand Transition in the Amino-terminal Fragment of the Amyloid Beta-Peptide Modulates Amyloid Formation. *J. Biol. Chem.* **270**(7), 3063-3067.

Sotriffer, C. A., Liedl, K. R., Linthicum, D. S., Rode, B. M. & Varga, J. M. (1998). Ligand-induced Domain Movement in an Antibody Fab: Molecular Dynamics Studies Confirm the Unique Domain Movement Observed Experimentally for Fab NC6.8 Upon Complexation and Reveal its Segmental Flexibility. *J. Mol. Biol.* **278**, 301-306.

Sprang, S. R., Acharya, K. R., Goldsmith, E. J., Stuart, D. I., Varvill, K., Fletterick, R. J., Madsen, N. B. & Johnson, L. N. (1988). Structural Changes in Glycogen Phosphorylase Induced by Phosphorylation. *Nature* **336**, 215-221.

Sreerama, N. & Woody, R. W. (1994). Poly(Pro)II Helices in Globular-Proteins - Identification and Circular Dichroic Analysis. *Biochemistry* **33**(33), 10022-10025.

Sreerama, N. & Woody, R. W. (1999). Molecular Dynamics Simulations of Polypeptide Conformations in Water: A Comparison of α, β, and Poly(Pro)II Conformations. *Proteins: Struct. Funct. Genet.* **36**, 400-406.

Stadtman, E. R. & Ginsburg, A. (1974). The Glutamine Synthetase of *Escherichia coli*: Structure and Control. In *The Enzymes* 3 edit. (Boyer, P. D., ed.), Vol. X, pp. 755-807. Academic Press Inc., New York.

Stanfield, R. L. & Wilson, I. A. (1994). Antigen-induced Conformational Changes in Antibodies: A Problem for Structural Prediction and Design. *Trends Biotech.* **12**, 275-279.

Starovasnik, M. A., Braisted, A. C. & Wells, J. A. (1997). Structural Mimicry of a Native Protein by a Minimized Binding Domain. *Proc. Natl. Acad. Sci. USA* **94**, 10080-10085.

Starovasnik, M. A., O'Connell, M. P., Fairbrother, W. J. & Kelley, R. F. (1999). Antibody Variable Region Binding by Staphylococcal Protein A: Thermodynamic Analysis and Location of the Fv Binding Site on E-domain. *Protein Sci.* **8**, 1423-1431.

Starovasnik, M. A., Skelton, N. J., O'Connell, M. P., Kelley, R. F., Reilley, D. & Fairbrother, W. J. (1996). Solution Structure of the E-domain of Staphylococcal Protein A. *Biochemistry* **35**, 15558-15569.

Starzyk, R. M., Burbaum, J. J. & Schimmel, P. (1989). Insertion of New Sequences into the Catalytic Domain of an Enzyme. *Biochemistry* **28**, 8479-8484.

Stayton, P. S., Shimoboji, T., Long, C., Chilkoti, A., Chen, G., Harris, J. M. & Hoffman, A. S. (1995). Control of Protein-ligand Recognition Using a Stimuli-responsive Polymer. *Nature* **378**, 472-474.

Stenberg, E., Persson, B., Roos, H. & Urbaniczky, C. (1991). Quantitative Determination of Surface Concentration of Protein with Surface Plasmon Resonance Using Radiolabeled Proteins. *J. Colloid Interface Sci.* **143**(2), 513-526.

Stöckel, J., Safar, J., Wallace, A. C., Cohen, F. E. & Prusiner, S. B. (1998). Prion Protein Selectively Binds Copper(II) Ions. *Biochemistry* **37**, 7185-7193.

Storrs, R. W., Truckses, D. & Wemmer, D. E. (1992). Helix Propagation in Trifluoroethanol Solutions. *Biopolymers* **32**, 1695-1702.

Stroud, R. M. (1991). Mechanisms of Biological Control By Phosphorylation. *Curr. Opin. Struct. Biol.* **1**, 826-835.

Su, Y., Yamashita, M. M., Greasley, S. E., Mullen, C. A., Shim, J. H., Jennings, P. A., Benkovic, S. J. & Wilson, I. A. (1998). A pH-dependent Stabilization of an Active Site Loop Observed from Low and High pH Crystal Structures of Mutant Monomeric Glycinamide Ribonucleotide Transformylase at 1.8 to 1.9 Å. *J. Mol. Biol.* **281**, 485-499.

Sundaralingam, M. & Sekharudu, Y. C. (1989). Water-inserted Alpha-helical Segments Implicate Reverse Turns as Folding Intermediates. *Science* **244**, 1333-1337.

Suñé, C., Hayashi, T., Liu, Y., Lane, W. S., Young, R. A. & Garcia-Blanco, M. A. (1997). CA150, a Nuclear Protein Associated with the RNA Polymerase II Holoenzyme, Is Involved in Tat-Activated Human Immunodeficiency Virus Type I Transcription. *Mol. Cell. Biol.* **17**(10), 6029-6039.

Suzuki, M. (1989). SPKK, A New Nucleic Acid-binding Unit of Protein Found in Histone. *EMBO J.* **8**(3), 797-804.

Suzuki, M., Neuhaus, D., Gerstein, M. & Aimoto, S. (1994). Solution Structure of the DNA Binding Octapeptide Repeat of the *K10* Gene Product. *Protein Engin.* **7**(4), 461-470.

Suzuki, M. & Yagi, N. (1991). Structure of the SPXX Motif. *Proc. R. Soc. Lond.* **B246**, 231-235.

Szilàk, L., Moitra, J., Krylov, D. & Vinson, C. (1997). Phosphoylation Destabilizes Alpha-Helices. *Nature Struct. Biol.* **4**(2), 112-114.

Takahashi, Y., Ueno, A. & Mihara, H. (1998). Design of a Peptide Undergoing Alpha-Beta Structural Transition and Amyloid Fibrillogenesis by the Introduction of a Hydrophobic Defect. *Chem. Eur. J.* **4**(12), 2475-2484.

Talay, S. R., Valentin-Weigand, P., Timmis, K. N. & Chhatwal, G. S. (1994). Domain Structure and Conserved Epitopes of Sfb Protein, the Fibronectin-binding Adhesin of *Streptococcus pyogenes*. *Mol. Microbiol.* **13**(3), 531-539.

Tashiro, M. & Montelione, G. T. (1995). Structures of Bacterial Immunoglobulin-binding Domains and Their Complexes With Immunoglobulins. *Curr. Opin. Struct. Biol.* **5**, 471-481.

Tashiro, M., Tejero, R., Zimmermann, D. E., Celda, B., Nilsson, B. & Montelione, G. T. (1997). High-resolution Solution NMR Structure of the Z Domain of Staphylococcal Protein A. *J. Mol. Biol.* **272**, 573-590.

Tawfik, D. S., Chap, R., Eshhar, Z. & Green, B. S. (1994). pH On-off Switching of Antibody-hapten Binding by Site-specific Chemical Modification of Tyrosine. *Protein Engin.* **7**(3), 431-434.

Teeter, M. M. (1984). Water Structure of a Hydrophobic Protein at Atomic Resolution: Pentagon Rings of Water Molecules in Crystals of Crambin. *Proc. Natl. Acad. Sci. USA* **81**, 6014-6018.

Templeton, T. J. & Kaslow, D. C. (1997). Cloning and Cross-species Comparison of the Thrombospondin-related Anonymous Protein (TRAP) Gene From *Plasmodium knowlesi*, *Plasmodium vivax* and *Plasmodium gallinaceum*. *Mol Biochem. Parasitol.* **84**, 13-24.

Thomas, P. D. & Dill, K. A. (1993). Local and Nonlocal Interactions in Globular Proteins and Mechanisms of Alcohol Denaturation. *Protein Sci.* **2**, 2050-2065.

Thompson, M. J. & Eisenberg, D. (1999). Transproteomic Evidence of a Loop-Deletion Mechanism for Enhanching Protein Thermostability. *J. Mol. Biol.* **290**, 595-604.

Thornton, J. M., Sibanda, B. L., Edwards, M. S. & Barlow, D. J. (1988). Analysis, Design and Modification of Loop Regions in Proteins. *BioEssays* **8**(2), 63-69.

Tilburn, J., Sarkar, S., Widdick, D. A., Espeso, E. A., Orejas, M., Mungroo, J., Peñalva, M. A. & Arst Jr., H. N. (1995). The *Asparagillus* PacC Zinc Finger Transcription Factor Mediates Regulation of Both Acid- and Alkaline Expressed Genes by Ambient pH. *EMBO J.* **14**(4), 779-790.

Tobias, D. J., Mertz, J. E. & Brooks III, C. L. (1991). Nanosecond Time Scale Folding Dynamics of a Pentapeptide in Water. *Biochemistry* **30**(24), 6054-6058.

Treumann, A., Zitzmann, N., Hülsmeier, A., Prescott, A. R., Almond, A., Sheehan, J. & Ferguson, M. A. J. (1997). Structural Characterisation of Two

Forms of Procyclic Acidic Repetitive Protein Expressed by Procyclic Forms of *Trypanosoma brucei*. *J. Mol. Biol.* **269**, 529-547.

Trkola, A., Dragic, T., Arthos, J., Binley, J. M., Olson, W. C., Allaway, G. P., Cheng-Mayer, C., Robinson, J., Maddon, P. J. & Moore, J. P. (1996). CD4-Dependent, Antibody-Sensitive Interactions Between HIV-I and its Co-Receptor CCR-5. *Nature* **384**, 184-187.

Tseng, H.-C., Lu, Q., Henderson, E. & Graves, D. J. (1999). Phosphorylated Tau can Promote Tubulin Assembly. *Proc. Natl. Acad. Sci. USA* **96**, 9503-9508.

Tskhovrebova, L., Trinick, J., Sleep, J. A. & Simmons, R. M. (1997). Elasticity and Unfolding of Single Molecules of the Giant Muscle Protein Titin. *Nature* **387**, 308-312.

Tsujimura, M., Dohmae, N., Odaka, M., Chijimatsu, M., Takio, K., Yohda, M., Hoshino, M., Nagashima, S. & Endo, I. (1997). Structure of the Photoreactive Iron Center of the Nitrile Hydratase from *Rhodococcus* sp. N-771. *J. Biol. Chem.* **272**(47), 29454-29459.

Ueda, T., Tamura, T., Maeda, Y., Hashimoto, Y., Miki, T., Yamada, H. & Imoto, T. (1993). Stabilization of Lysozyme By the Introduction of Gly-Pro Sequence. *Protein Engin.* **6**(2), 183-187.

Uesugi, M., Nyanguile, O., Lu, H., Levine, A. J. & Verdine, G. L. (1997). Induced Alpha-Helix in the VP16 Activation Domain upon Binding to a Human TAF. *Science* **277**, 1310-1313.

Uhlén, M., Guss, B., Nilsson, B., Gatenbeck, S., Philipson, L. & Lindberg, M. (1984). Complete Sequence of the Staphylococcal Gene Encoding Protein A, a Gene Evolved Through Multiple Duplications. *J. Biol. Chem.* **259**, 1695-1702 (Correction, ibid. p. 13628).

Urry, D. W. (1984). Protein Elasticity Based On Conformations of Sequential Polypeptides: The Biological Elastic Fiber. *J. Protein Chem.* **3**(5-6), 403-436.

Urry, D. W. (1988a). Entropic Elastic Processes in Protein Mechanisms .II. Simple (Passive) and Coupled (Active) Development of Elastic Forces. *J. Protein Chem.* **7**(2), 81-114.

Urry, D. W. (1988b). Entropic Elastic Processes in Protein Mechanisms. I. Elastic Structure Due to an Inverse Temperature Transition and Elasticity Due to Internal Chain Dynamics. *J. Protein Chem.* **7**(1), 1-34.

Urry, D. W. (1993). Molecular Machines: How Motion and Other Functions of Living Organisms Can Result From Reversible Chemical Changes. *Angew. Chem. Int. Ed. Eng.* **32**(6), 819-841.

Urry, D. W., Harris, R. D., Long, M. M. & Prasad, K. U. (1986). Polytetrapeptide of Elastin: Temperature-correlated Elastomeric Force and Structure Development. *Int. J. Pept. Protein Res.* **28**, 649-660.

Urry, D. W. & Long, M. M. (1976). Conformations of the Repeat Peptides of Elastin in Solution: An Application of Proton and Carbon-13 Magnetic Resonance to the Determination of Polypeptide Secondary Structure. In *CRC Crit. Rev. Biochem.* (Fasman, G. D., ed.), pp. 2-45. CRC Press Inc., Waltham.

Urry, D. W., Long, M. M., Ohnishi, T. & Jacobs, M. (1974). Circular Dichroism and Absorption of the Polytetrapeptide of Elastin: A Polymer Model for the β-turn. *Biochem. Biophys. Res. Comm.* **61**(4), 1427-1433.

Urry, D. W., Nicol, A., Gowda, D. C., Hoban, L. D., McKee, A., Williams, T., Olsen, D. B. & Cox, B. A. (1993). Medical Applications of Bioelastic

Materials. In *Biotechnological Polymers. Medical, Pharmaceutical and Industrial Applications - A Conference in Print* (Gebelein, C. G., ed.), pp. 82-103. Technomic Publishing Company Inc., Lancaster.

Urry, D. W., Peng, S., Xu, J. & McPherson, D. T. (1997). Characterization of Waters of Hydrophobic Hydration by Microwave Dielectric Relaxation. *J. Am. Chem. Soc* **119**(5), 1161-1162.

Urry, D. W., Peng, S. Q., Hayes, L. C., McPherson, D., Xu, J., Woods, T. C., Gowda, D. C. & Pattanaik, A. (1998). Engineering Protein-based Machines to Emulate Key Steps of Metabolism (Biological Energy Conversion). *Biotech. Bioeng.* **58**(2-3), 175-190.

Urry, D. W., Shaw, R. G. & Prasad, K. U. (1985). Polypentapeptide of Elastin: Temperature Dependence of Ellipticity and Correlation with Elastomeric Force. *Biochem. Biophys. Res. Comm.* **130**(1), 50-57.

Urry, D. W., Trapane, T. L., Long, M. M. & Prasad, K. U. (1983). Test of the Librational Entropy Mechanism of Elasticity of the Polypentapeptide of Elastin - Effect of Introducing a Methyl Group At Residue 5. *J. Chem. Soc. Faraday Trans. I* **79**(P4), 853-868.

Urry, D. W., Trapane, T. L., Sugano, H. & Prasad, K. U. (1981). Sequential Polypeptides of Elastin: Cyclic Conformational Correlates of the Linear Polypentapeptide. *J. Am. Chem. Soc.* **103**(8), 2080-2089.

Uversky, V. N., Segel, D. J., Doniach, S. & Fink, A. L. (1998a). Association-induced Folding of Globular Proteins. *Proc. Natl. Acad. Sci. USA* **95**, 5480-5483.

Uversky, V. N., Winter, S., Galzitskaya, O. V., Kittler, L. & Lober, G. (1998b). Hyperphosphorylation Induces Structural Modification of Tau-protein. *FEBS Lett.* **439**, 21-25.

van Stokkum, I. H. M., Lindsell, H., Hadden, J. M., Haris, P. I., Chapman, D. & Bloemendal, M. (1995). Temperature-Induced Changes in Protein Structures Studied by Fourier Transform Infrared Spectroscopy and Global Analysis. *Biochemistry* **34**(33), 10508-10518.

Venkatachalam, C. M. (1968). Stereochemical Criteria for Polypeptides and Proteins. V. Conformation of a System of Three Linked Peptide Units. *Biopolymers* **6**, 1425-1436.

Venkatachalam, C. M. & Urry, D. W. (1981). Development of a Linear Helical Conformation From Its Cyclic Correlate. Beta-spiral Model of the Elastin Poly(pentapeptide)(VPGVG)n. *Macromolecules* **14**, 1225-1229.

Viguera, A.-R. & Serrano, L. (1997). Loop Length, Intramolecular Diffusion and Protein folding. *Nature Struct. Biol.* **4**(11), 939-946.

Viles, J. H., Cohen, F. E., Prusiner, S. B., Goodin, D. B., Wright, P. E. & Dyson, H. J. (1999). Copper Binding to the Prion Protein: Structural Implications of Four Identical Cooperative Binding Sites. *Proc. Natl. Acad. Sci. USA* **96**, 2042-2047.

Volpin, D., Urry, D. W., Cox, B. A. & Gotte, L. (1976). Optical Diffraction of Tropoelastin and Alpha-Elastin Coacervates. *Biochim. Biophys. Acta* **439**, 253-258.

Walgers, R., Lee, T. C. & Cammers-Goodwin, A. (1998). An Indirect Chaotropic Mechanism for the Stabilization of Helix Conformation of Peptides in Aqueous Trifluoroethanol and Hexafluoro-2-propanol. *J. Am. Chem. Soc.* **120**(20), 5073-5079.

Walker, B., Kasianowicz, J., Krishnasastry, M. & Bayley, H. (1994). A Pore-forming Protein with a Metal-actuated Switch. *Protein Engin.* **7**(5), 655-662.

Wang, L., Voloshin, O. N., Stasiak, A., Stasiak, A. & Camerini-Otero, R. D. (1998). Homologous DNA Pairing Domain Peptides of RecA Protein: Intrinsic Propensity to Form Beta-Structures and Filaments. *J. Mol. Biol.* **277**, 1-11.

Wasserman, Z. R. & Salemme, F. R. (1990). A Molecular Dynamics Investigation of the Elastomeric Restoring Force in Elastin. *Biopolymers* **29**(12-1), 1613-1631.

Waterhous, D. V. & Johnson, W. C., Jr. (1994). Importance of Environment in Determining Secondary Structure in Proteins. *Biochemistry* **33**(8), 2121-2128.

Wellings, D. A. & Atherton, E. (1997). Standard Fmoc Protocols. *Meth. Enzymol.* **289**, 44-66.

Wille, H., Zhang, G.-F., Baldwin, M. A., Cohen, F. E. & Prusiner, S. B. (1996). Separation of Scrapie Prion Infectivity from PrP Amyloid Polymers. *J. Mol. Biol.* **259**, 608-621.

Williams, J. C., Wierenga, R. K. & Saraste, M. (1998). Insights Into Src Kinase Functions: Structural Comparisons. *Trends Biochem. Sci.* **23**, 179-184.

Williamson, M. P. (1994). The Structure and Function of Proline-rich Regions in Proteins. *Biochem. J.* **297**, 249-260.

Willner, I. & Rubin, S. (1996). Control of the Structure and Functions of Biomaterials by Light. *Angew. Chem. Int. Ed. Engl.* **35**(4), 367-385.

Wilmot, C. M. & Thornton, J. M. (1990). Beta-turns and Their Distortions: A Proposed New Nomenclature. *Protein Engin.* **3**(6), 479-493.

Wilmot, C. M. & Thornton, J. M. (1988). Analysis and Prediction of the Different Types of β-Turn in Proteins. *J. Mol. Biol.* **203**, 221-232.

Wilson, D. R. & Finlay, B. B. (1997). The 'Asx-Pro turn' as a Local Structural Motif Stabilized by Alternative Patterns of Hydrogen Bonds and a Concensus-derived Model of the Sequence Asn-Pro-Asn. *Protein Engin.* **10**(5), 519-529.

Winkler, G., Wolschann, P., Briza, P., Heinz, F. X. & Kunz, C. (1985). Spectral Properties of Trifluoroacetic Acid - Acetonitrile Gradient Systems for Separation of Picomole Quantities of Peptides by Reversed-phase High-performance Liquid Chromatography. *J. Chromatogr.* **347**, 83-88.

Wishner, B. C., Ward, K. B., Lattman, E. E. & Love, W. E. (1975). Crystal Structure of Sickle-cell Deoxyhemoglobin at 5 Å Resolution. *J. Mol. Biol.* **98**, 179-194.

Wolber, P. & Warren, G. (1989). Bacterial Ice-nucleation Proteins. *Trends Biochem. Sci.* **14**, 179-182.

Wood, S. J., Wetzel, R., Martin, J. D. & Hurle, M. R. (1995). Prolines and Amyloidogenicity in Fragments of the Alzheimers's Peptide β/A4. *Biochemistry* **34**(3), 724-730.

Woody, R. W. (1995). Circular Dichroism. *Methods Enzymol.* **246**, 34-71.

Wopfner, F., Weidenhöfer, G., Schneider, R., von Brunn, A., Gilch, S., Schwarz, T. F., Werner, T. & Schätzl, H. M. (1999). Analysis of 27 Mammalian and 9 Avian PrPs Reveals High Conservation of Flexible Regions of the Prion Protein. *J. Mol. Biol.* **289**, 1163-1178.

Wrigley, C. W. (1996). Gigant Proteins With Flour Power. *Nature* **381**, 738-739.

Wu, L., Gerard, N. P., Wyatt, R., Choe, H., Parolin, C., Ruffing, N., Borsetti, A., Cardoso, A. A., Desjardin, E., Newman, W., Gerard, C. & Sodroski, J. (1996). CD4-Induced Interaction of Primary HIV-1 gp120 Glycoproteins with the Chemokine Receptor CCR-5. *Nature* **384**, 179-183.

Xiong, H., Buckwalter, B. L., Shieh, H.-M. & Hecht, M. H. (1995). Periodicity of Polar and Nonpolar Amino Acids is the Major Determinant of Secondary Structure in Self-assembling Oligomeric Peptides. *Proc. Natl. Acad. Sci. USA* **92**, 6349-6353.

Xu, F. & Cross, T. A. (1999). Water: Foldase Activity in Catalyzing Polypeptide Conformational Rearrangements. *Proc. Natl. Acad. Sci. USA* **96**, 9057-9061.

Yang, A.-S., Hitz, B. & Honig, B. (1996). Free Energy Determinants of Secondary Structure Formation: III. Beta-Turns and Their Role in Protein Folding. *J. Mol. Biol.* **259**(4), 873-882.

Yang, J. J., Pitkeathly, M. & Radford, S. E. (1994). Far-UV Circular Dichroism Reveals a Conformational Switch in a Peptide Fragment from the Beta-sheet of Hen Lyzozyme. *Biochemistry* **33**(23), 7345-7353.

Yao, J., Feher, V. A., Espejo, B. F., Reymond, M. T., Wright, P. E. & Dyson, H. J. (1994). Stabilization of a Type-VI Turn in a Family of Linear Peptides in Water Solution. *J. Mol. Biol.* **243**(4), 736-753.

Yeh, H., Ornstein-Goldstein, N., Indik, Z., Sheppard, P., Anderson, N., Rosenbloom, J. C., Cicila, G., Yoon, K. & Rosenbloom, J. (1987). Sequence Variation of Bovine Elastin m-RNA Due to Alternative Splicing. *Collagen Rel. Res.* **7**(4), 235-247.

Yu, B., Blaber, M., Gronenborn, A. M., Clore, G. M. & Caspar, D. L. D. (1999). Disordered Water Within a Hydrophobic Protein Cavity Visualized by X-ray Crystallography. *Proc. Natl. Acad. Sci. USA* **96**, 103-108.

Yu, H., Chen, J. K., Feng, S., Dalgarno, D. C., Brauer, A. W. & Schreiber, S. L. (1994). Structural Basis for the Binding of Proline-rich Peptides to SH3 Domains. *Cell* **76**, 933-945.

Zhang, H., Kaneko, K., Nguyen, J. T., Livshits, T. L., Baldwin, M. A., Cohen, F. E., James, T. L. & Prusiner, S. B. (1995a). Conformational Transitions in Peptides Containing Two Putative α-Helices of the Prion Protein. *J. Mol. Biol.* **250**, 514-526.

Zhang, J. & Corden, J. L. (1991). Phosphorylation Causes a Conformational Change in the Carboxyl-terminal Domain of the Mouse RNA Polymerase II Largest Subunit. *J. Biol. Chem.* **266**(4), 2297-2302.

Zhang, L., Benz, R. & Hancock, R. E. W. (1999). Influence of Proline Residues on the Antibacterial and Synergistic Activites of the Alpha-Helical Peptides. *Biochemistry* **38**(25), 8102-8111.

Zhang, L. & Hermans, J. (1996). Hydrophilicity of Cavities in Proteins. *Proteins: Struct. Funct. Genet.* **24**(4), 433-438.

Zhang, S. & Rich, A. (1997). Direct Conversion of an Oligopeptide From a Beta-sheet to an Alpha-helix: A Model for Amyloid Formation. *Proc. Natl. Acad. Sci. USA* **94**, 23-28.

Zhang, X., Guda, C., Datta, R., Dute, R., Urry, D. W. & Daniell, H. (1995b). Nuclear Expression of an Environmentally Friendly Synthetic Protein Based Polymer Gene in Tobacco Cells. *Biotechnol. Lett.* **17**(12), 1279-1284.

Zhong, L. & Johnson, W. C., Jr. (1992). Environment Affects Amino Acid Preference For Secondary Structure. *Proc. Natl. Acad. Sci. USA* **89**, 4462-4465.

Zimmerman, S. S. & Scheraga, H. A. (1977). Local Interactions in Bends of Proteins. *Proc. Natl. Acad. Sci. USA* **74**(10), 4126-4129.

Appendix

A

Herald Reiersen, Anthony R. Clarke, and Anthony R. Rees (1998).
Short Elastin-like Peptides Exhibit the Same Temperature-induced Structural Transitions as Elastin Polymers: Implications for Protein Engineering.

J. Mol. Biol. **283**, 255-264.

B

Herald Reiersen and Anthony Rees (1999).
An Engineered Minidomain Containing an Elastin Turn Exhibits a Reversible Temperature-Induced IgG Binding.

Biochemistry **38**(45), 14897-14905.

Reprinted from *J. Mol. Biol.* (1998) **283**, 255–264

JMB

Short Elastin-like Peptides Exhibit the Same Temperature-induced Structural Transitions as Elastin Polymers: Implications for Protein Engineering

Herald Reiersen, Anthony R. Clarke and Anthony R. Rees

Article No. mb982067 J. Mol. Biol. (1998) 283, 255–264

JMB

Short Elastin-like Peptides Exhibit the Same Temperature-induced Structural Transitions as Elastin Polymers: Implications for Protein Engineering

Herald Reiersen[1], Anthony R. Clarke[2] and Anthony R. Rees[1]*

[1]*Department of Biology & Biochemistry, University of Bath, Claverton Down, Bath BA2 7AY, UK*

[2]*Department of Biochemistry University of Bristol, School of Medical Sciences, Bristol BS8 1TD, UK*

**Corresponding author*

Elastin is a major protein component of the vascular wall and is responsible for its unusual elastic properties. Polymers of its repeating VPGVG sequences have been synthesised and shown to exhibit an inverse temperature transition where, as temperature rises, the polymer collapses from an extended chain to a β-spiral structure with three VPGVG units per turn, each pentamer adopting a type II β-turn conformation. These studies, however, have not established whether the temperature-driven conformational change is an intrinsic property of the individual pentameric sequences or a global, co-operative effect of many pentamers within the β-spiral structure. Here, we examine by circular dichroism the behaviour of elastin-like peptides $(VPGVG)_n$, where n varies between 1 and 5. Remarkably, we find that all lengths of peptide undergo an extended $\longleftrightarrow$ β-turn transition with increasing temperature, suggesting that the induction of the β-spiral occurs at the level of single pentameric units. The origin of this effect is a positive ΔS term for the transition. At 35°C, the average transition midpoint temperature, the value of $T\Delta S$ is about 15 kcal mol^{-1}. With larger oligomers ($n = 3$), there is only a modest rise in ΔS, suggesting that the dominant entropic effect resides within the monomer and that interactions between these units make only a small contribution to the energetics of the transition. Charges at the termini, and residue replacements or additions, regulate the transitions for the short peptides in a manner similar to that observed for the longer polymers. The behaviour of the same peptides in trifluoroethanol and SDS solutions is consistent with formation of the β-turn being driven by interactions between non-polar groups. The significance of this behaviour for the rational design of temperature-induced responses in proteins is discussed.

Keywords: elastin; peptide; temperature; transition; hydrophobicity

Introduction

Elasticity of the vascular cell wall is mediated by polymeric peptide sequences that are capable of undergoing viscoelastic transitions. Several repeating sequences have been described for the elastin precursor protein, tropoelastin. In order of their frequency of occurrence they are the pentapeptide VPGVG, the hexapeptide APGVGV, the nonapeptide VPGFGVGAG and the tetrapeptide VPGG (Sandberg *et al.*, 1985; Yeh *et al.*, 1987). In elastin, the most frequent pentapeptide sequence, VPGVG, recurs up to 50 times in a single molecule. Synthetic polymers of $(VPGVG)_n$, where n can be as high as 150, are soluble in water below 25°C but above 25°C undergo a phase transition to a visco-

Abbreviations used: CD, circular dichroism; ESP/MS, positive electrospray mass spectrometry; Fmoc, N^{α}-9-fluorenylmethyloxycarbonyl; Fmoc-PAL, 5- [4-(9-fluorenylmethyloxycarbonyl)-aminomethyl-3,5-dimethoxyphenoxy)] valeric acid; HOBT, 1-hydroxybenzotriazole hydrate; HPLC, high-performance liquid chromatography; $[\theta]_M$, MRE, mean residual ellipticity; PEG, polyethylene glycol; PS, polystyrene; TFA, trifluoroacetic acid; TFE, trifluoroethanol; T_M, transition temperature midpoint.

E-mail address of the corresponding author: arrees@compuserve.com

0022-2836/98/410255–10 $30.00/0

elastic state consisting of about 50% peptide and 50% water by mass. This transition is accompanied by a contraction to less than one half the extended length of the polymer, releasing sufficient energy in the process to lift a mass 1000 times the mass of the polymer itself (Urry, 1993). The presently accepted mechanism of this contraction involves a transition from an extended state at temperatures below the transition temperature, T_M, to an ordered β-spiral above the T_M with three VPGVG units, each forming a type II β-turn, per turn of the spiral (Urry, 1988a,b). This is a rare example of an inverse temperature transition during which a protein becomes more ordered at the higher temperature. The transition and the structural features of the ordered, higher-temperature form have been studied by CD (Urry *et al.*, 1985), NMR (Renugopalakrishnan *et al.*, 1978), and X-ray crystallography (Cook *et al.* (1980) studied a cyclic tri-repeat of VPGVG). These physical studies are consistent with the proposed type II β-turn in which the collapse to the spiral state is driven by dehydration of the hydrophobic valine side-chains. The temperature at which this transition occurs can be manipulated by varying the composition of the polymer $(VPGXG)_n$ and the value of T_M depends both on the nature of residue X and the value of n. In addition, T_M has been shown to be sensitive to pH, ionic strength, pressure and covalent modifications such as phosphorylation (Urry, 1993).

Despite extensive characterisation of such polymers the minimum viscoelastic unit has not been defined. In particular, the relative contributions to the viscoelastic state of the intrinsic propensity of VPGVG units to form type II β-turns, and any co-operative interactions between the β-spiral turns ($n = 3$), have not been determined.

In this study, we examine the thermodynamic behaviour of single and multiple units of the VPGVG sequence using CD to monitor the previously well characterised formation of the type II β-turn structure, and we demonstrate that the polymer behaviour surprisingly can be reproduced by a single VPGVG unit. This has opened up the exciting possibility of engineering temperature and pH switch sequences of non-disruptive lengths into existing proteins.

Results

Design of short elastin peptides

In this study, short elastin peptides were designed to test the effect of sequence variations on the conformational transitions observed. Of specific interest was the effects of charge adjacent to the elastomeric units, studied using both uncapped peptides at various pH values and capped peptides carrying *N*-acetylation or *C*-amidation, or both. In these short peptides, the effect of adding an extra glycine residue at the N termini of 8-mers was investigated (Figure 1A to H). In order to test if there was any correlation between the number of elastomeric (-VPGVG-) units present and the T_M for turn formation, we synthesised an 18-mer peptide (three VPGVG units) and a 28-mer peptide (five VPGVG units: Figure 1L and O). To measure the influence on T_M of increased hydrophobicity adjacent to the elastomeric unit, additional leucine and isoleucine residues were introduced stepwise at the C terminus of the 18-mer peptides (Figure 1I–K, M and N). The effects of internal charged residues adjacent to, or within, the elastomeric sequences were studied. In one design, a lysine residue flanked by a leucine residue was placed close to the N terminus (Figure 1J), while in a second design a glutamic acid residue was added also, replacing one of the two valine residues of an elastomeric unit (Figure 1K).

A: *H*-GVG(VPGVG)-NH_2 **E:** Ac-GVG(VPGVG)-NH_2

B: *H*-GVG(VPGVG)-*OH* **F:** Ac-GVG(VPGVG)-*OH*

C: *H*-*G*GVG(VPGVG)-NH_2 **G:** Ac-*G*GVG(VPGVG)-NH_2

D: *H*-*G*GVG(VPGVG)-*OH* **H:** Ac-*G*GVG(VPGVG)-*OH*

I: Ac-GVG(VPGVG)(VPGVG)(VPGVG)*ILG*-NH_2

J: Ac-G*KL*(VPGVG)(VPGVG)(VPGVG)*ILG*-NH_2

K: Ac-G*KL*(VPG*E*G)(VPGVG)*ILG*-NH_2

L: Ac-GVG(VPGVG)(VPGVG)(VPGVG)-NH_2

M: Ac-GVG(VPGVG)(VPGVG)(VPGVG)*L*-NH_2

N: Ac-GVG(VPGVG)(VPGVG)(VPGVG)*IL*-NH_2

O: Ac-GVG(VPGVG)(VPGVG)(VPGVG)(VPGVG)(VPGVG)-NH_2

Figure 1. Sequences of short homologous elastin based peptides. Sequences of short elastin peptides with different composition were synthesised by solid-phase Fmoc chemistry. Deviations from the sequence Ac-GVG(VPGVG)$_n$-NH_2 ($n = 1$, 3, 5) are highlighted in italics. Ac-, acetyl; -NH_2, amide.

CD analysis of peptides

CD spectra of the 9-mer peptide D at various temperatures are shown in Figure 2a. For comparison, spectra of the 18-mer peptide L are shown in Figure 2b. All other short and longer peptides showed a similar CD profile (data not shown). The global minimum varied slightly with pH but was typically within the range 198 to 200 nm, as has been found for unordered peptides (Woody, 1995). For the short peptides, at +1°C the minimum mean residual ellipticity was −7000 to −10,000 deg cm^2 dmol^{-1} compared to −40,000 deg cm^2 dmol^{-1} for an ideal random coil. This is within the same range (−5000 to −16,000 deg cm^2 dmol^{-1}) previously seen for the longer $(VPGG)_n$ and the $(VPGVG)_n$ elastin polymers (Urry *et al.*, 1985, 1986). The corresponding values for the 18 to 21-mer peptides (I to O) were −17,000 to −19,000 deg

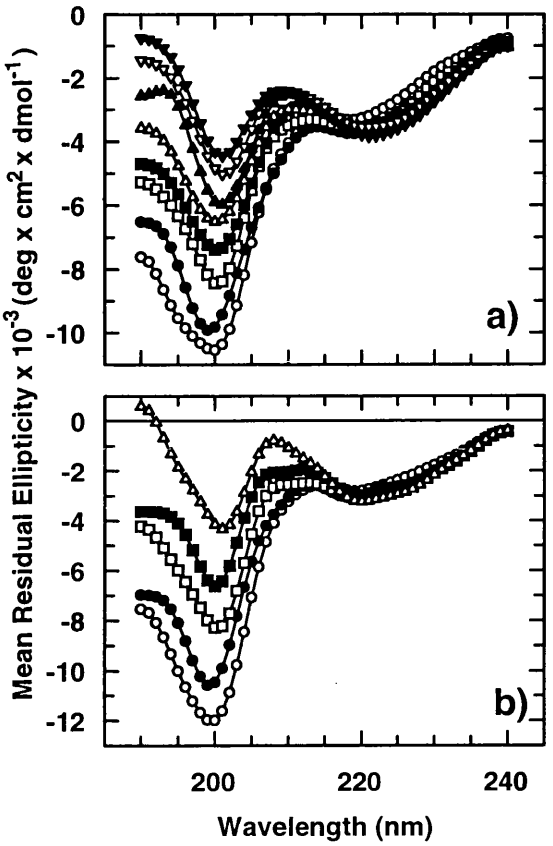

Figure 2. CD wavelength scans of peptides D and L at different temperatures. The peptides were scanned in 10 mM phosphate buffer (pH 7.0). a) Peptide D (49.1 μM) was recorded at (○) 1.1°C, (●) 15.4°C, (□) 25.0°C, (■) 34.5°C, (△) 43.8°C, (▲) 53.0°C, (▽) 63.0° C, and (▼) 81.5°C. b) Peptide L (20.7 μM) was scanned at (○) 1.3°C, (●) 15.4°C, (□) 34.0°C, (■) 48.4° C and (△) 76.6°C.

cm^2 $dmol^{-1}$. This suggests, somewhat surprisingly, that the shorter peptides are less disordered at low temperatures than the longer peptides. The MRE values of the short peptides are, in fact, within the range expected from an equimolar mixture of random coil and type II β-turns (Perczel *et al.*, 1993).

For all peptides, the CD amplitudes at 195 to 205 nm decreased with increasing temperature, with a smaller decrease in amplitude at 206 to 212 nm. A positive peak in this latter region is characteristic of type II β-turns (Perczel *et al.*, 1993; Urry *et al.*, 1985; Woody, 1995). A near isodichroic point around 218 nm was found for the short peptides in the reported transition. This was seen both for the effect of increasing concentrations of TFE (data not shown), which induces a type II β-turn, and for the temperature effect described in Figure 2a and b. A near isodichroic point for melting of the larger elastin polymer has been detected by Urry *et al.* (1988a) around 220 nm. However, some peptides showed little change in the position of minima/maxima when the temperature is varied and the spectroscopic changes in these are dominated by changes in intensity. For peptide K, which has the most heterogeneous composition (Figure 1), an increase in amplitude at 210 to 230 nm was observed with a local minimum at 222 nm (with an approximate isodichroic point at 208 nm). These were found also at higher temperatures for some short peptides with the N-terminal GGVG sequence (see Figure 1c, d and g). These spectra resemble class C-spectra associated with helical or type I/III β-turn structures.

The transition curves of the short peptides D, E and H in phosphate buffer, peptides C, D and G in different buffers, and for the longer peptides J, L and N at pH 7 are shown in Figure 3a to c. The start of the transition was initially fitted for each melting curve, although well-defined transitions were obtained for the majority of peptides. The transition range for all the 8/9-mer peptides (A to H) was 3000 to 5000 MRE units increasing to 5000 to 10,000 for the longer peptides I to O (data not shown). These values are similar to those reported for the longer elastin polytetrapeptide $(VPGG)_n$, though a little lower than for the polypentapeptide $(VPGVG)_n$, which undergoes a change of 16,000 MRE units during a transition (Urry *et al.*, 1985, 1986).

Thermodynamic analysis

In order to obtain thermodynamic data from the melting curves, a selection of short and longer peptides (C, E, L and N) was tested for reversibility by incubation for 30 minutes at +70° C and then rapid cooling to +20°C. All were found to be fully reversible (Figure 4a). The concentration-dependence was tested on peptide L (18-mer) and on the most hydrophobic short peptide E (8-mer) at two different temperatures (Figure 4b and c). In all cases ellipticities were found, within the limit of experimental error, to be independent of peptide concentration over this temperature range. This observation shows that the temperature-induced formation of the β-turn is due to intramolecular interactions rather than intermolecular associations. The melting curves reported here were obtained at peptide concentrations 10 to 20 times lower than the maximum concentrations shown in Figure 4c (around 18 μM for the longer peptides and below 50 μM for the shorter peptides).

Data were fitted to van't Hoff plots and were linear. Where a low signal-to-noise ratio in the CD measurements resulted in a larger spread of data, a better fit was obtained by fixing one or both endpoints for the transition (Figure 5).

Fitting of the CD data to the van't Hoff equation allowed calculation of ΔH, ΔS and T_M values for the transitions of most peptides. However, due to the uncertainty of the start of the transition for some short peptides (Figure 3b) only those with well-defined transition curves are reported (Table 1). It was not possible to determine melting temperatures for two of the longer peptides, K and O.

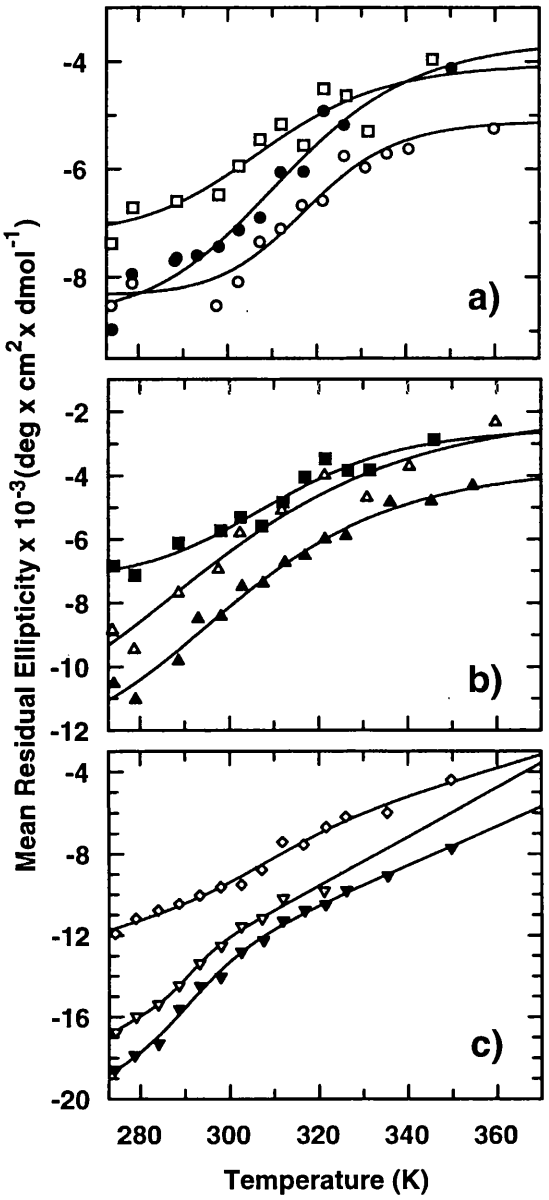

Figure 3. Melting of short and long elastin peptides. The 8 or 9-mer peptides C (37.1 μM), D (49.1 μM), E (38.5 μM), G (41.8 μM) and H (31.3 μM) and the longer peptides J (16.4 μM), L (20.7 μM) and N (17.9 μM) were scanned from 190 to 240/260 nm at different temperatures in (a) 10 mM acetate or borate buffers, or (b and c) in 10 mM phosphate buffer, and the mean residual ellipticity at or close to 200 nm was plotted *versus* temperature. The van't Hoff fits are also shown. a) Melting of the 9-mer peptides C (○, at 201 nm, pH 4.0), D (●, at 200 nm, pH 9.5) and G (□, at 201 nm, pH 9.5); b) melting of the 8-9-mer peptides H (■, 202 nm), E (△, 199 nm) and D (▲, 200 nm); c) melting of the 18-21-mer peptides N (▽), J (▼) and L (◇) at 199 nm.

All peptides studied exhibited positive ΔH and ΔS, supporting the model of an entropy-driven folding transition. The ΔH and ΔS values for the 8/9-mer and 21-mer peptides (Table 1) were closely similar, suggesting that each VPGVG repeat behaves as a thermodynamically independent unit (see Discussion).

Melting temperatures for short peptides that had N and C termini in the same state were well correlated (Table 2 and Fig. 6). Acetylation of α-amino or amidation of α-carboxy groups (or both) lowered the transition temperatures by an average of 13°C for both 8 and 9-mers compared to free N and/or C termini. However, there was no significant difference in melting temperature for peptides where the terminal charges differed in sign (Table 2, compare peptides A and B at pH 4 *versus* B and F at pH 9.5 for the 8-mers, and peptides C and D at pH 4 *versus* D and H at pH 9.5 for the 9-mers), indicating that the presence of either one or the other charge had a similar effect on the structural transition for the short peptides. The melting temperatures for the peptides at pH 7.0 were lowered compared to those with high T_M values (Figure 6), and the effect was larger for the 9-mer peptides compared to the 8-mers. This suggests that there may be an additive stabilising effect through N and C-terminal interactions; the lower melting temperatures found for some of the 8-mers compared to the larger 18-mer may be explained by this.

The presence of an extra glycine residue at the N termini of the smaller peptides increased the melting temperatures by about 6°C for both low T_M and high T_M peptides (Figure 6). An opposite effect was seen by the addition of a hydrophobic residue (or residues) near the C terminus, which resulted in a lowering of the melting temperature by 20 to 23°C (compare peptide L with M and N, Table 1).

Peptide K, a 21-mer containing a glutamic acid replacement in the central VPGVG unit, was more disordered at lower temperatures than the other peptides (MRE value of −20,000 deg cm^2 dmol^{-1} at 1.4°C; see Perczel *et al.*, 1993; Urry *et al.*, 1985) and thermodynamic analysis was not possible. Thermodynamic data were obtained however with peptide J, which has the same residue insertions at the N and C termini as peptide K but lacks the internal glutamic acid residue. Interestingly, in this peptide the presence of a charged lysine residue did not elevate the melting temperature, probably due to the more dominant hydrophobic effect of an adjacent leucine residue (compare I with J, Table 1).

Effects of SDS and TFE

The effects of the detergent SDS were tested on the short (B, E and G) and the longer (K, L, N and O) peptides. For 8 and 9-mers, micellar SDS (25 mM) induced an increase in MRE at 210 nm for both peptides, and for the 8-mers this was observed also in non-micellar (2 mM) SDS (Figure 7a). For the longer peptides, this effect was seen only with micellar SDS (Figure 7b). The increase in MRE at 200 nm and the more gradual increase at 206 to 212 nm, characteristic of a transition to a type II β-turn (Perczel *et al.*, 1993; Urry *et al.*, 1985; Woody, 1995), indicated that all pep-

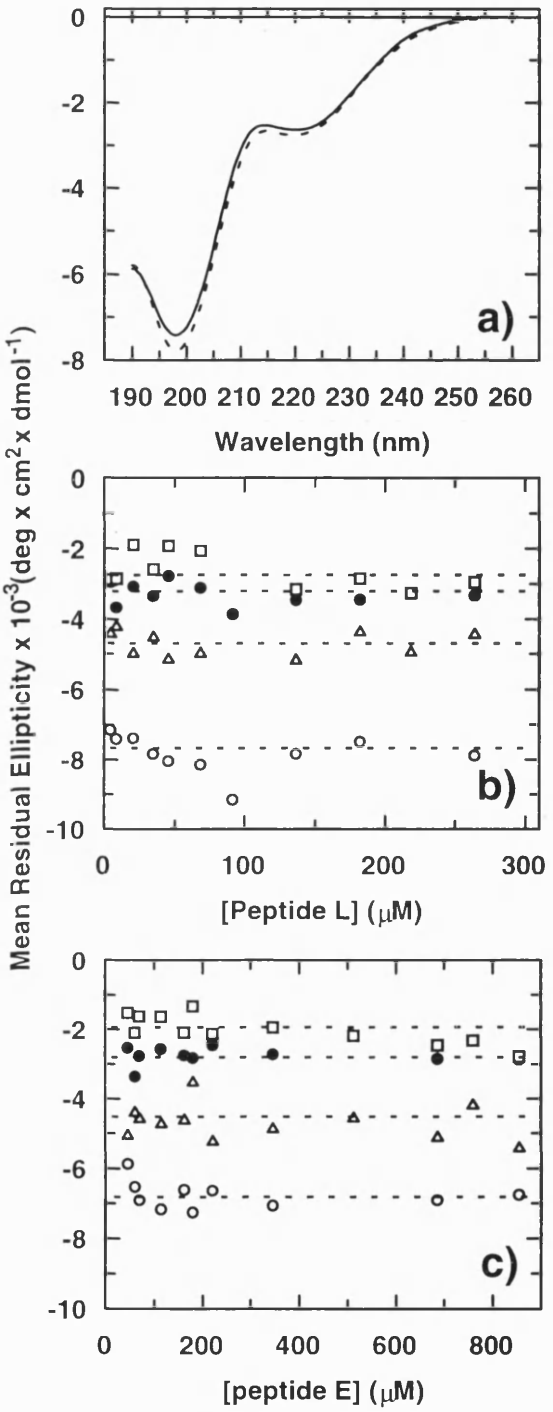

Figure 4. Test of reversibility and concentration dependence at pH 7.0. a) Scans of the 18-mer peptide L (91 μM in 10 mM phosphate buffer; 0.5 mm cuvette; spacing 0.5 nm; four scans each with one second integration time) at 20.6°C before heating (——) and after incubation at 70°C for 30 minutes with rapid cooling back to 20.6°C (- - - -). The concentration-dependence of MRE is shown in b and c. The concentration of peptide L was varied from 4.6 μM to 264 μM (b) using different quartz cuvettes (0.5 mm, 2 mm and 10 mm), and similarly the 8-mer peptide E was varied between 45 μM and 855 μM (c). The variation of mean residual ellipticity for peptide L at 15.5°C or peptide E at 15.6°C (at 199 nm, ○; and at 210 nm, ●) and for peptide L at 62.5°C or peptide E at 48.3°C (at 199 nm, △; and at 210 nm, □) is shown.

tides were becoming more ordered in the presence of SDS.

Induction of the type II β-turn was more pronounced in 87 to 92 % (v/v) TFE than in SDS for the 8, 9, 18 and 28-mer peptides (Figure 7a and b). For peptide L, the concentration of TFE was varied from 0 to 97%, and at about 35% TFE the gradients of the MRE values at 198 nm, 206 nm and 213 nm *versus* TFE concentration shifted markedly, suggesting the presence of a structural transition (Figure 7c).

Discussion

All of the peptides studied here exhibited an increase in MRE at 195 to 205 nm and at 206 to 212 nm, a signature of type II β-turn formation, with increasing temperature, supporting the notion that the folding of these sequences is a consequence of hydrophobic interactions that are driven by positive entropies of dehydration (Privalov & Makhatadze, 1993). The type of turn structure formed is critically dependent on both the flanking sequences and the solvent conditions. At low temperature (~0°C) the short peptides showed evidence of partial structure, as has been seen with the larger polymers (Urry *et al.*, 1985, 1986). In addition, most peptides showed an increase in MRE at 210 nm, typical of type II β-turn formation in VPGVG polymers (Urry *et al.*, 1985). Evidence for the formation of type I/III β-turns (increase in amplitude at 210 to 230 nm) was seen in the CD spectra of some peptides at high temperatures, suggesting that an equilibrium of different β-turn populations may exist for many of these sequences. Peptides having a GGVG N-terminal region (C, D, G and H in this study) are thought to preferentially adopt the type II′ β-turn (Broch *et al.*, 1996). Interconversion between type I and type II β-turns has been estimated to require +0.2 to −1.7 kcal mol^{-1} (Yang *et al.*, 1996, and references therein), a small enough change to be affected by flanking sequences or buffer composition (TFE, SDS, etc.). Previous crystallographic studies on the linear pentapeptide Boc-VPGVG-OMe showed the absence of any β-turn structure, while the structure of a cyclic decapeptide analogue of VPGVG exhibited a type III turn for one VPGVG unit followed by a type I turn for the second unit (Bhandary *et al.*, 1990). Here, we have clearly demonstrated that, when suitable flanking sequences are present, the VPGVG monomer is able to form the type II β-turn structure (within the discrimination capacity of CD) identical with that formed by the elastin-like polymer $(VPGVG)_n$. We have also confirmed that, when particular types of flanking residue are present, the transition temperature can be altered in the same direction as seen for the polymers (Urry, 1993). For example, the addition of extra hydro-

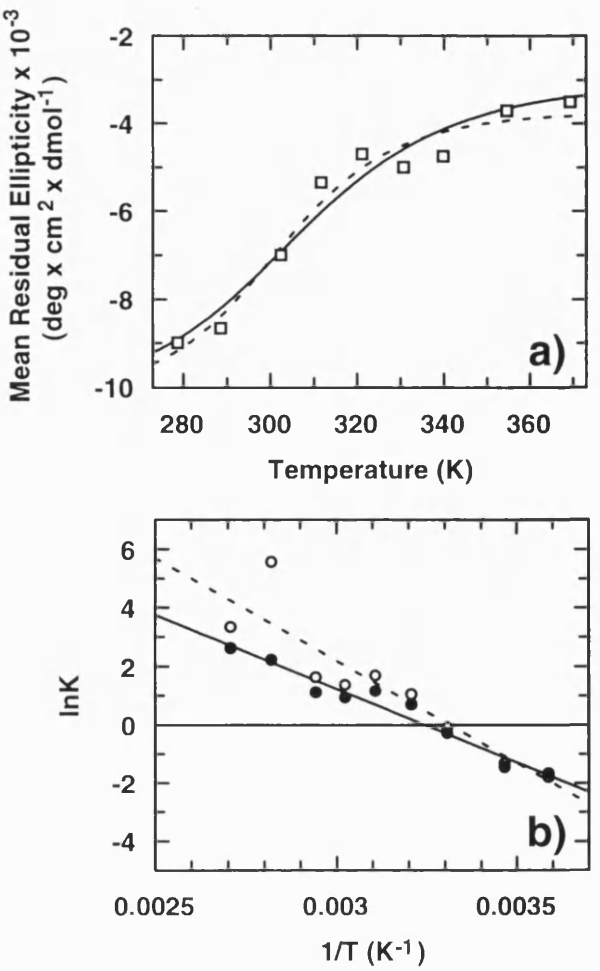

Figure 5. Fitting of the melting curve of peptide B in 10 mM phosphate buffer pH 7.0. The CD data at 199 nm (□) were fitted to a macroscopic, reversible, two-state model by optimising the linearity of the correlated van't Hoff plot. By using the fitted endpoints for the transition, $[\theta]^F$ and $[\theta]^U$, from the initial model (a), - - - -) the corresponding van't Hoff plot was constructed (b), ○, - - - -) and gave a linear correlation coefficient (r) of −0.91. After fixing $[\theta]^F$, the correlation coefficient for the van't Hoff plot improved to −0.98. The data with the correlation line (●, ——) and its corresponding fit for data of MRE against temperature with fixed $[\theta]^F$ (——) are shown in b) and a), respectively. Energies from fits: model with free $[\theta]^F$ and $[\theta]^U$ (- - - -), $\Delta H = 13.7 \pm 6.6$, $\Delta S = 0.045 \pm 0.021$; model with fixed $[\theta]^F$ (——), $\Delta H = 10.4 \pm 1.4$, $\Delta S = 0.034 \pm 0.004$.

phobic residues adjacent to the VPGVG turn sequence lowered the melting temperature by up to 20°C and an additional glycine residue increased T_M by 6°C. It seems quite remarkable that these large temperature effects could be produced by adding a single residue (compare the 8-mers *versus* 9-mers (Figure 6) and peptides L and M, Table 1), although when multiple additions were made the effect was not necessarily additive (compare peptides M and N, Table 1). Further, when a charged residue was inserted in the presence of these additional hydrophobic residues, the expected increase in melting temperature was not seen (compare peptides I and J, Table 1). This suggests that the melting temperature for an elastomeric sequence flanked by different non-elastomeric residues may be found by averaging the balance of hydrophobic and hydrophilic residues in the flanking regions.

The dramatic effect of charged residues on T_M is illustrated by the behaviour of the shorter peptides. A net charge at either the N or C terminus increased the melting temperature by as much as 20°C (compare peptides C and H at pH 4 and 9.5, Table 1). The thermodynamic effect of charged groups at the termini is likely to derive from an increased stability of the water shell surrounding the peptide.

For the amidated and acetylated VPGVG peptides of different lengths (peptides E and L), transition temperatures varied from those observed for the much longer VPGVG polymers (Luan *et al.*, 1990; Urry *et al.*, 1985).

Table 1. Thermodynamic values for thermal transitions in elastin peptides

Peptide	pH	T_M (°C)	$\Delta H_{U \to F}$ (kcal mol^{-1})	$\Delta S_{U \to F}$ (kcal mol^{-1} K^{-1})
A	7.0	41	11.0 ± 2.7	0.035 ± 0.009
B	9.5	35	14.9 ± 4.9	0.048 ± 0.016
C	4.0	45	20.0 ± 2.9	0.063 ± 0.009
D	9.5	40	13.0 ± 4.8	0.042 ± 0.016
G	9.5	35	13.7 ± 2.8	0.047 ± 0.009
H	9.5	47	14.4 ± 2.3	0.045 ± 0.007
I	7.0	20	26.0 ± 10.6	0.089 ± 0.036
J	7.0	18	25.3 ± 2.5	0.087 ± 0.009
L	7.0	37	18.9 ± 4.7	0.061 ± 0.015
M	7.0	14	15.9 ± 10.7	0.055 ± 0.036
N	7.0	17	12.1 ± 2.4	0.042 ± 0.008

Peptides A to H (8 and 9-mers) at their specific pH values were chosen because these melting curves had a well-defined transition (Figure 3a). The longer 18 to 21-mer peptides (I to N) were fitted with free endpoints, $\Delta H_{U \to F}$ and $\Delta S_{U \to F}$ specifying only the slope of the pre- and post-transition curves.

Table 2. Melting temperatures for transitions in short elastin peptides

Peptide	pH 4.0	pH 7.0	pH 9.5
A	35	41	30
B	40	34	35
C	45	37	24
D	39	27	40
E	22	21	20
F	23	34	39
G	33	26	35
H	26	36	47

The MRE for each peptide was followed at one wavelength for each pH value and plotted against temperature. Dependent on buffer, pH and type of peptide, the wavelength ranged from 197 to 202 nm. Values were obtained by fitting data to the van't Hoff equation with $\Delta C_p = 0$, allowing initially ΔH, ΔS and endpoints for transition to float. T_M was found from the relation $\Delta H / \Delta S$.

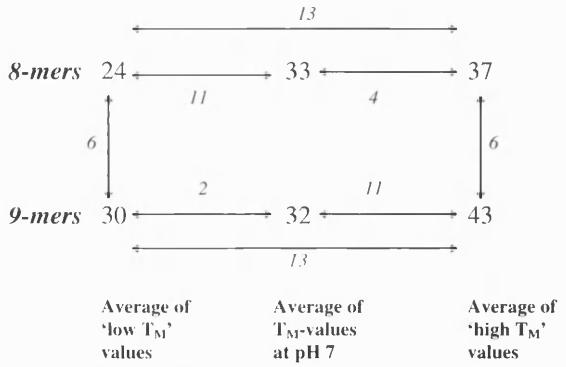

Figure 6. Average melting temperatures for thermal transitions of 8 and 9-mer elastin peptides. The large numbers represent the average of T_M values for the 8-mers (peptides A, B, E and F) and 9-mers (peptides C, D, G and H) from Table 1. The low T_M value is the average of the lowest melting temperatures at pH 4.0 or pH 9.5 for peptide A and F (or C and H for the 9-mer) and at pH 4 and 9.5 for peptide E (G for the 9-mer), the pH value that gives an uncharged molecule. Similarly, high T_M represents the average of high T_M values for peptide A and F (C and H), and at both pH 4 and pH 9.5 for peptide B (D for the 9-mer), the pH value that gives a charged molecule. The smaller numbers in italics represent the difference between average T_M values.

The effect of SDS on short elastin-sequences supports the hydrophobic collapse model of stabilisation. In this study, low concentrations of SDS (up to 25 mM) induced β-turn formation (Figure 7a). If SDS is able to bridge the two valine residues spanning each side (*cis*-face) of the PG-turn, it would disrupt their hydration and facilitate the closer interaction necessary for induction of a type II β-turn. Models extracted from an MD simulation of longer elastin peptides (Wasserman & Salemme, 1990) of a single GVGVPGVG unit in both the extended and contracted states (Figure 8), predict that the distance between the two valine residues in the high-temperature form is approximately 2 Å shorter than in the low-temperature form. The larger effect of SDS on the longer peptides (more than one VPGVG monomer) is consistent with the shielding hypothesis. The effects of TFE, studied on peptide L (Figure 7c), are consistent with a hydrophobic model of β-turn formation at high temperature. The largest effect was seen below 35% TFE, where hydrophobic interactions within the peptide are likely to be important. Since the total free energy is lower for the TFE/water mixture than for water alone, the preferred form for the TFE-mixture will be where the valine side-chains are closely packed. Bodkin & Goodfellow (1996) have discussed this as a general model for TFE-induced folding of secondary structures. Above 30% TFE, the electrostatic interactions become more dominant, reflected by the more reluctant formation of type II β-turn structures.

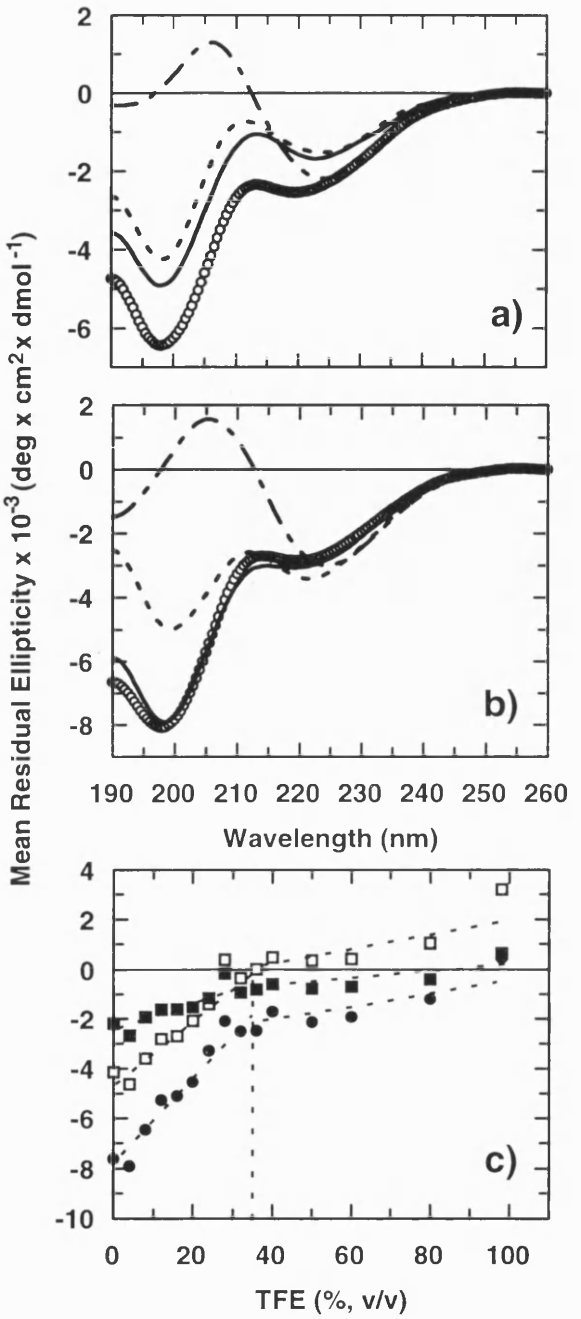

Figure 7. Effect of SDS and TFE on peptides E and L. a) Peptide E (218 μM) and b) peptide L (91 μM) were scanned in water (–○–), in 2 mM SDS (——), in 25 mM SDS (- - - -), and in 87% (v/v) TFE (– · –) at 20.5°C using 0.5 mm quartz cuvettes (four scans; 0.5 nm spacing; one second integration time). c) Peptide L (20.7 μM) was tested at different concentrations of TFE at 15.7°C in a 2 mm cuvette, and the variation of mean residual ellipticity *versus* TFE concentration at 198 nm (●), at 206 nm (□) and at 213 nm (■) is shown.

This study has demonstrated that short, elastin-like peptides can undergo structural transitions identical with those that have been observed in neutral and modified elastomeric polymers. In

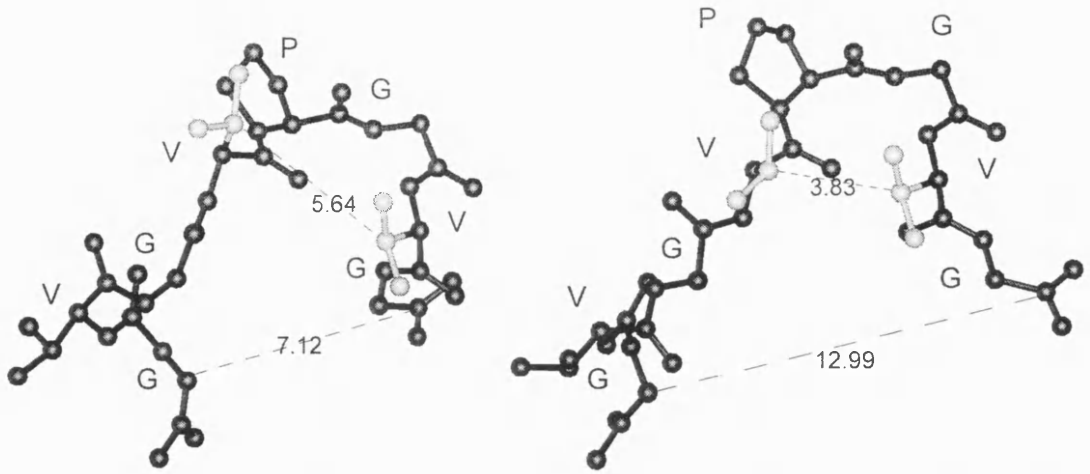

Figure 8. Molecular models of peptide Ac-GVGVPGVG-NH_2 in expanded and contracted conformations. Dihedral angles for the expanded and contracted form of the peptide in this study were extracted from the average ϕ and ψ angles in a published molecular dynamics simulation of $(VPGVG)_{18}$ in relaxed and stretched forms. At the left is shown the low-temperature expanded form and at the right the high-temperature contracted form. The distances between the valine C^{β} atoms and the N and C termini are shown.

elastin polymers, $(VPGVG)_n$, the identical pentamer sequences all contribute to form a β-spiral with type II turns (Pro^2-Gly^3 with a Val^1 C=O ··· H–N Val^4 hydrogen bond). Intramolecular hydrophobic contacts are thought to drive the transition within this spiral (Urry, 1988a). However, the only stabilising hydrogen bonds reside within each of the monomers, VPGVG. Even so, it is plausible that formation of the spiral is a cooperative transition, driven by hydrophobic collapse and stabilised by intra-pentamer H-bonds. We find no evidence for such a cooperative effect. The ΔH and ΔS values for an 8-mer (one VPGVG unit) and an 18-mer (three VPGVG units) are the same, indicating that a "cooperative unit" does not exceed one repeat. The contribution of configurational entropy to the total entropy on going from an 8-mer to an 18-mer can be shown to be minimal; the difference in conformational entropy, ΔS_{conf}, between the number of states for the relaxed (764) and extended (58) conformations of a single VPGVG peptide has been calculated to be 1.024 cal mol^{-1} K^{-1} per residue (one entropic unit per residue). The increased conformational entropy change between an 8-mer and an 18-mer would then be just 0.010 kcal mol^{-1} K^{-1}, assuming that the entropy derives from internal chain dynamics without random chain networks (Urry, 1988a). This shows that ΔS through the transition (Table 1) cannot be balanced by such small increases in ΔS_{conf} as the chain length increases.

These results lead to the intriguing possibility of engineering short, elastin-like peptide sequences into globular proteins. The presence of an elastic switch within a structurally sensitive region of a protein would enable the triggering of an "allosteric" response to temperature or pH (Noguti & Gō, 1989a,b). Is this energetically feasible? The free-energy change for the transition of the VPGVG-containing 8-mer (peptide B, pH 9.5) from 0° to 60°C was −2.9 kcal mol^{-1}, more than enough energy to fuel such a change.

Where such elastomeric sequences are introduced into enzymes or binding proteins, this will offer a novel method for modulating their activities, thermostabilities or labilities. Ultimately, such sequences will undoubtedly find use in the *de novo* design of proteins.

Materials and Methods

Materials

Reagent-grade Fmoc amino acids and Fmoc-PEG-PS resins (Perseptive Biosystems) were used for peptide synthesis. Acetic anhydride and methanol were of peptide-synthesis grade (Perkin Elmer).

Peptide synthesis and purification

Peptides were synthesised on Fmoc-PAL-PEG-PS resin (amidated C-terminal peptide) or Fmoc-Gly-PEG-PS resin (free C terminus) using a MilliGen/Biosearch 9050 PepSynthesizer (Millipore) with solid-phase Fmoc chemistry using HOBT-activation on an 0.1 mmol scale. The crude peptides from the TFA-cleavage were analysed on an analytical HPLC (LKB) using a gradient of 4.5 to 54% (v/v) acetonitrile in 0.1% (v/v) TFA over 91 minutes at +20°C on a C_{18} column (Vydac; 250 mm × 5 mm; 10 μm pore size). Peptides A to O were detected at 214 nm and eluted (0.7 ml min^{-1}), respectively, with A to H 18 to 20.5% acetonitrile, and I to O 29 to 36% acetonitrile. Large-scale purification using HPLC (Waters) at 20°C was performed using a shallower gradient elution; for peptides A to H a gradient of 13.5% to 22.5% acetonitrile in 0.1% TFA over 90 minutes was applied. Peptides were chromatographed at 10 ml min^{-1} from a preparative 240 mm × 24 mm Vydac C_{18} column (10 μm pore size) with detection at 214 nm and then freeze-dried. The purified peptides were dissolved in 50% (v/v) aqueous

methanol with 1.0 % (v/v) acetic acid at a concentration of 10 ng μl^{-1} and analysed by ESP/MS (VG Autospec with VG Analytical Electrospray). The expected molecular mass was obtained for all 15 peptides synthesised. Quantitative amino acid analysis was carried out. Samples were hydrolysed in 6 M HCl at 110°C for 24 hours under N_2 gas and then freeze-dried, dissolved in citrate buffer (pH 2.2), and analysed on a Pharmacia AlphaPlus II amino acid analyser. All peptides had the expected composition (data not shown).

Circular dichroism studies

CD spectra were recorded on a Jobin-Yvon Model CD6 Dichrograph instrument. Temperature CD scans were performed by cooling the samples to +1°C and then stepwise increasing temperature from +1 up to +85°C, allowing samples to equilibrate at each temperature for five minutes. The cuvette temperature was measured with a Fluke 51 K/J digital thermometer. The scans were collected using a spectral acquisition spacing of 0.5 or 1.0 nm (with 2.0 nm bandwidth) with an integration time of one second from 190 up to 260 nm. Scans were processed on a computer and the average of 4 to 15 runs were smoothed using the Sabitzky-Golay algorithm in the Dichrograph Software version 1.1 (Jobin-Yvon/Instruments SA). Stock peptide concentrations were determined by quantitative amino acid analysis. Data points at each wavelength were converted from peptide molar ellipticity to mean residual ellipticity ([θ], deg cm^2 $dmol^{-1}$) by dividing by the number of residues in the peptide. A single wavelength from the wavelength scans (190 to 240/260 nm) was graphed *versus* different temperatures.

Thermodynamic analysis

The free energy of the transition into the folded form at higher temperatures was fitted to a macroscopic, reversible, two-state model (equation (1)) using the observed CD data, $[\theta]^{obs}$ and temperature, T:

$$\Delta G_{U\rightarrow F} = -RT \ln[([\theta]^{obs} - [\theta]^{U})/([\theta]^{F} - [\theta]^{obs})] \quad (1)$$

The endpoints for the transition (high-temperature folded form, $[\theta]^{F}$, and low-temperature unfolded form $[\theta]^{U}$) together with ΔH and ΔS, were initially fitted using equations (2) and (3), or (2) and (4) for the 18 to 28-mer peptides. Equation (4) takes into account the slope effect (m) and off-axis adjustment (*off*) for transitions that have a slope in the pre- and postfolding base-lines:

$$\Delta G_{U\rightarrow F} = \Delta H_{U\rightarrow F} - T\Delta S_{U\rightarrow F} \quad (2)$$

$$[\theta]^{obs} = ([\theta]^{U} + [\theta]^{F} \times \exp -(\Delta G_{U\rightarrow F}/RT))/(1 + \exp -(\Delta G_{U\rightarrow F}/RT)) \quad (3)$$

$$[\theta]^{obs} = ([\theta]^{U} + [\theta]^{F} \times \exp -(\Delta G_{U\rightarrow F}/RT))/(1 + \exp -(\Delta G_{U\rightarrow F}/RT)) + m\,T + off \quad (4)$$

The data were further analysed using Grafit software (Leatherbarrow, 1989), and van't Hoff plots were constructed (plot of $\ln K$ *versus* $1/T$ where $K = ([\theta]^{obs} - [\theta]^{U})/([\theta]^{F} - [\theta]^{obs})$ utilising the data from CD, $[\theta]^{obs}$, and the previously fitted endpoints for transition $[\theta]^{U}$ and $[\theta]^{F}$. In some cases where the initial free fit gave a lower linear correlation coefficient ($r < -0.90$ to -0.93) for the van't Hoff plot, the data were refitted using the initial fitted values for endpoints and starting points and fixing either $[\theta]^{U}$ or $[\theta]^{F}$, or both $[\theta]^{U}$ and $[\theta]^{F}$. This resulted in correlation coefficients closer to -1. A new fit of ΔH and ΔS was found from equations (2) to (4) by fixing $[\theta]^{U}$ and $[\theta]^{F}$ from the best vant't Hoff plot. The transition temperature, T_M, for all peptides was calculated using the relation $T_M = \Delta H/\Delta S$.

Acknowledgements

We thank The Research Council of Norway (110859/410), DYNAL A/S, Oslo, Norway and the Wellcome Trust for equipment funding. A.R.C. is a Lister Senior Fellow. Mrs S. Phillips (School of Biology) and Dr R. Kinsman (School of Chemistry, University of Bath) are gratefully acknowledged for help with peptide synthesis. We thank Mr C. Cryer (School of Chemistry, University of Bath) for recording ESP/MS spectra and Dr G. Bloomberg (School of Medical Sciences, University of Bristol) for amino acid analysis. Dr G. Siligardi (Kings College, London) is acknowledged for help in reproducing some of the spectra. Finally, we thank Dr Alexei Finkelstein for helpful comments on the thermodynamic interpretation.

References

Bhandary, K. K., Senadhi, S. E., Prasad, K. U., Urry, D. W. & Vijay-Kumar, S. (1990). Conformation of a cyclic decapeptide analog of a repeat pentapeptide sequence of elastin: cyclo-bis(valyl-prolyl-alanyl-valyl-glycyl). *Int. J. Pept. Protein Res.* **36**, 122–127.

Bodkin, M. J. & Goodfellow, J. M. (1996). Hydrophobic solvation in aqueous trifluoroethanol solution. *Biopolymers*, **39**, 43–50.

Broch, H., Moulabbi, M., Vasilescu, D. & Tamburro, A. M. (1996). Conformational and electrostatic properties of V-G-G-V-G, a typical sequence of the glycine-rich regions of elastin – an *ab-initio* quantum molecular study. *Int. J. Pept. Protein Res.* **47**, 394–404.

Cook, W. J., Einspahr, H., Trapane, T. L., Urry, D. W. & Bugg, C. E. (1980). Crystal structure and conformation of the cyclic trimer of a repeat pentapeptide of elastin, cyclo-(L-valyl-L-prolylglycyl-L-valylglycyl)$_3$. *J. Am. Chem. Soc.* **102(17)**, 5502–5505.

Leatherbarrow, R. J. (1989). Grafit, 3.01 edit, Erithacus Software Ltd.

Luan, C. H., Harris, R. D., Prasad, K. U. & Urry, D. W. (1990). Differential scanning calorimetry studies of the inverse temperature transition of the polypentapeptide of elastin and its analogs. *Biopolymers*, **29**, 1699–1706.

Noguti, T. & Gō, N. (1989a). Structural basis of hierarchical multiple substates of a protein. I. Introduction. *Proteins: Struct. Funct. Genet.* **5**, 97–103.

Noguti, T. & Gō, N. (1989b). Structural basis of hierarchical multiple substates of a protein. V. Nonlocal deformations. *Proteins: Struct. Funct. Genet.* **5**, 132–138.

Perczel, A., Hollósi, M., Sándor, P. & Fasman, G. D. (1993). The evaluation of type I and type II beta-turn mixtures. Circular dichroism, NMR and mol-

ecular dynamics studies. *Int. J. Pept. Protein Res.* **41**, 223–236.
Privalov, P. A. & Makhatadze, G. I. (1993). Contribution of hydration to protein folding thermodynamics. II. The entropy and Gibbs energy of hydration. *J. Mol. Biol.* **232**, 660–679.
Renugopalakrishnan, V., Khaled, M. A. & Urry, D. W. (1978). Proton magnetic resonance and conformational energy calculations of repeat peptides of tropoelastin: the pentapeptide. *J. Chem. Soc. Perkin II*, 111–119.
Sandberg, L. B., Leslie, J. G., Leach, C. T., Alvarez, V. L., Torres, A. R. & Smith, D. W. (1985). Elastin covalent structure as determined by solid-phase amino-acid sequencing. *Pathol. Biol.* **33**, 266–274.
Urry, D. W. (1988a). Entropic elastic processes in protein mechanisms. I. Elastic structure due to an inverse temperature transition and elasticity due to internal chain dynamics. *J. Protein Chem.* **7**, 1–34.
Urry, D. W. (1988b). Entropic elastic processes in protein mechanisms. II. Simple (passive) and coupled (active) development of elastic forces. *J. Protein Chem.* **7**, 81–114.
Urry, D. W. (1993). Molecular machines: how motion and other functions of living organisms can result from reversible chemical changes. *Angew. Chem. Int. Ed. Engl.* **32**, 819–841.
Urry, D. W., Shaw, R. G. & Prasad, K. U. (1985). Polypentapeptide of elastin: temperature dependence of ellipticity and correlation with elastomeric force. *Biochem. Biophys. Res. Commun.* **130**, 50–57.
Urry, D. W., Harris, R. D., Long, M. M. & Prasad, K. U. (1986). Polytetrapeptide of elastin: temperature-correlated elastomeric force and structure development. *Int. J. Pept. Protein Res.* **28**, 649–660.
Wasserman, Z. R. & Salemme, F. R. (1990). A molecular dynamics investigation of the elastomeric restoring force in elastin. *Biopolymers*, **29**, 1613–1631.
Woody, R. W. (1995). Circular dichroism. *Methods Enzymol.* **246**, 34–71.
Yang, A.-S., Hitz, B. & Honig, B. (1996). Free energy determinants of secondary structure formation. III. Beta-turns and their role in protein folding. *J. Mol. Biol.* **259**, 873–882.
Yeh, H., Ornstein-Goldstein, N., Indik, Z., Sheppard, P., Anderson, N., Rosenbloom, J. C., Cicila, G., Yoon, K. G. & Rosenbloom, J. (1987). Sequence variation of bovine elastin messenger-RNA due to alternative splicing. *Collagen Relat. Res.* **7**, 235–247.

Edited by A. R. Fersht

(Received 2 April 1998; received in revised form 11 July 1998; accepted 13 July 1998)

An Engineered Minidomain Containing an Elastin Turn Exhibits a Reversible Temperature-Induced IgG Binding

Herald Reiersen and Anthony R. Rees

Department of Biology and Biochemistry, University of Bath, Claverton Down, Bath BA2 7AY, United Kingdom

Biochemistry®

Reprinted from
Volume 38, Number 45, Pages 14897–14905

An Engineered Minidomain Containing an Elastin Turn Exhibits a Reversible Temperature-Induced IgG Binding†

Herald Reiersen and Anthony R. Rees*

Department of Biology and Biochemistry, University of Bath, Claverton Down, Bath BA2 7AY, United Kingdom

Received June 1, 1999; Revised Manuscript Received September 1, 1999

ABSTRACT: A two-helix version of the triple α-helical staphylococcal Protein A, previously shown to retain the Fc binding properties of protein A, has been engineered to contain an elastin sequence, GVPGVG, within the inter-helix turn. The original type I β-turn was replaced with a β-turn from the muscle protein elastin, which has an inverse temperature-induced folding transition. These "elastin mutants" had lost their helical structure, as measured by circular dichroism (CD), and exhibited a lower stability than the wild-type domains (T_m reduced by about 48 °C) in 30% trifluoroethanol. For the wild-type domains, the amount of α-helix and the binding affinity for Fc decreased as the temperature was increased. In contrast, although the starting affinity was lower for the disulfide elastin-turn mutant, it exhibited a 21-fold improvement in affinity over the same temperature range. The melting curve for the elastin-turn minidomain showed cooperative behavior, as measured by the increase in CD-amplitude at 222 nm. The observed CD behavior is consistent with the formation of a type I β-turn, exhibiting similar ΔH and ΔS values to those seen previously for short elastin peptides [Reiersen, H., Clarke, A. R., and Rees, A. R. (1998) *J. Mol. Biol. 283,* 255−264], and accounting for the increase in on-rate. This demonstrates that, when inserted into a stable globular protein, short elastin sequences have the ability to modify local structure and activity, by operating as temperature modulated switches.

One[1] of the applications of protein engineering is the development of novel switch-mechanisms that can regulate and control protein folding and function. There are several naturally occurring mechanisms whereby the activity of a protein can be regulated by conformational change. For example, it may be allosterically modified by binding of a ligand, or as a direct consequence of rearrangements in structure due to covalent modification (e.g., phosphorylation), or as a result of changes in physical or chemical parameters, such as temperature, pH, or degree of hydration (*1*−*3*). The hydration or dehydration of hydrophobic surfaces is a particularly novel mechanism employed to drive conformational changes in elastomeric proteins (*4*−*6*).

In the classical hydrophobic model, water molecules associated with hydrophobic interfaces are structurally ordered and transitions involving hydrophobic hydrated surfaces involve the loss of bound water, or melting of clathrate-like water structures near hydrophobic groups. During protein folding, the loss of water results in an increase in entropy of bulk water accompanied by an increase in protein hydrophobic interactions, providing the driving force for protein function, assembly, stability, and folding (*6*−*10*). Contrary to the behavior of many globular proteins, the elastic muscle protein, elastin, undergoes an inverse temperature transition during hydrophobic dehydration. Polymers derived from elastin and containing repeating $(VPGVG)_n$ sequences ($n \geq 150$) are completely soluble in water below their transition temperatures (~25 °C) but contract in length by more than 50% with increasing temperature. The free energy released during this transition is sufficient for an elastin fiber to lift more than 1000 times its own mass. The transition involves loss of hydrated water from exposed valine side chains at the higher temperatures, inducing val−val interactions that energize the formation of an ordered β-spiral with three VPGVG units per turn of the spiral, each VPGVG forming a type II β-turn (*4*−*6, 11*).

Formation of the type II β-turn has been verified by different physical and spectroscopic studies, although the presence of other types of β-turns has also been reported (*4*−*6, 12*−*13*). The behavior of the elastin polymers can be regulated by covalent modification, such as phosphorylation, electrochemical reduction of prosthetic groups attached to the polymer, or by the replacement of residues in the sequence by residue types sensitive to pressure, temperature, or pH. Recently, we showed that the behavior of the polymeric elastin can be mimicked by small peptides of 8−28 residues containing the VPGVG sequence in single or multiple copies. This has opened up the possibility of using such sequences in a protein engineering context as molecular "switches" (*11*).

We describe in this paper the first attempt to introduce a temperature switch into a globular protein using the elastin

* Corresponding author. Telephone: +33 466 048666. Fax: +33 466 048667. E-mail:arrees@compuserve.com.

† This work was supported by grants from The Research Council of Norway (No. 110859/410) and DYNAL A/S, Oslo, Norway.

[1] Abbreviations: CD, circular dichroism; DMF (*N,N*-dimethylformamide); EDC, *N*-ethyl-*N'*-[(dimethylamino)propyl]carbodiimide; HBS, Hepes buffered saline; HSA, human serum albumin; MRE, $[\theta]_M$, mean residual ellipticity; NHS, *N*-Hydroxysuccinimide; P20, Polysorbate 20; RU, resonance units; SDS, sodium dodecyl sulfate; T_M, transition temperature midpoint; TFA, trifluoroacetic acid; TFE, trifluoroethanol.

10.1021/bi991243a CCC: $18.00
Published on Web 10/21/1999

fragment approach. The target protein was a biologically active fragment of protein A, a multidomain protein from *Staphylococcus aureus* that binds to the Fc region of IgG. Protein A is found on the cell surface of the bacteria and contains a tandem repeat of five different but homologous binding domains, each of approximately 60 residues in a three-helix bundle and designated E, D, A, B, and C (*14*). A synthetic version of the B-domain, the Z-domain, has been constructed for high-level protein expression (*15*) and, recently, has been minimized to two helices (33 residues) connected by a type I β-turn. This 2-helix fragment largely retains the binding affinity of the parent B-domain toward the Fc-portion of IgG (*16*−*17*).

In this study, we have replaced the type I β-turn of this minidomain with an elastin β-turn and have shown that the elastin sequence acts as a temperature switch. The minidomain with the elastin-turn binds the Fc of mouse IgG2a with an improved affinity at higher temperatures. At the same temperatures, the wild-type minidomain undergoes the expected decrease in affinity as it unfolds. This demonstrates that short elastin sequences when inserted into globular proteins have the ability to induce structure at higher temperatures, opening up the possibility of a general method for introducing controlled temperature regulation of protein function.

EXPERIMENTAL PROCEDURES

Peptide Synthesis. The synthesis was carried out by Synt:em (Nîmes, France) on an Automated Multiple Peptide Synthesis instrument (AMS 422, ABIMED) using a Fmoc solid support protocol (poly(ethylene glycol) grafted polystyrene support). The Fmoc amino acids were activated in situ by diisopropylcarbodiimide and 1-hydroxybenzotriazole in DMF with a standard 4-fold excess. An acetylation step was carried out after each amino acid incorporation to cap possible remaining amine groups and to ensure the absence of deletion peptides. The Fmoc protecting groups were removed by a solution of piperidine in DMF (20%) prior to each coupling, and after synthesis the peptide was cleaved from the support by a standard TFA cocktail, ether-precipitated, and purified on a Waters Prep LC 4000 System using Waters PrepPak Cartridge column C18, 6 μM, 60 Å (40 × 100 mm) and a gradient from A (0.1% TFA in water) to 60% B (0.08% v/ TFA in acetonitrile) in 60 min (flow 20 mL/min). Peptides were detected at 215 and 280 nm. The purity was confirmed using a Beckman LC126 HPLC system, with a Kromasil column C18, 5 μm, 100 Å (250 × 4.6 mm) applying a gradient from 95% A to 100% B in 15 min (flow 3.0 mL/min). The purity was further evaluated by mass spectroscopy analysis using a Maldi-tof spectrometer (Voyager DE Elite, PE Applied Biosystems) with dihydroxybenzoic acid as matrix.

Circular Dichroism Studies. The secondary structure of the minidomain constructs was analyzed by recording CD spectra on Jobin-Yvon Model CD6 Dichrograph Instrument (Instruments S. A. UK Ltd., Stanmore, UK). The instrument was iso-andosterone calibrated according to the manufacturers instructions, and it was temperature-controlled and N_2 purged during analysis. The minidomains were dissolved in sterile filtered (0.22 μm) solutions prior to analysis. Spectra were recorded from 190 to 260 nm with a step resolution of 0.5 nm (2.0 nm bandwidth), using an integration time of 1−5 s. The average of up to 4 runs were smoothed using the Sabitzky−Golay algorithm in the Dichrograph Software version 1.1 (Jobin-Yvon/Instruments S. A., France). Temperature CD scans were performed by a stepwise increase in temperature, from +1 °C and up, using a five minute equilibration time. The melting of the minidomains was monitored by integrating the molar ellipticity at 222 and 260 nm at each temperature for 10 s. The average of 3−6 measurements at each wavelength was used. The peptide stock concentrations (in deionized water) were determined by quantitative amino acid analysis. Data points at each wavelength were expressed as mean residual ellipticity ([θ], degree cm^2/dmol) by dividing the measured molar ellipticity by the number of residues in the minidomain.

Thermodynamic Analysis of CD-Data. The free energy for melting or folding of structure at 222 nm was fitted to a macroscopic, reversible, two-state model using the observed CD-data, $[\theta]^{222}$ and temperature, T. For folding (U→F) or melting (F→U) of structure, respectively, eqs 1 and 2 were used.

$$\Delta G_{U\rightarrow F} = -RT \ln[([\theta]^{222} - [\theta]^{U})/([\theta]^{F} - [\theta]^{222})] \quad (1)$$

$$\Delta G_{F\rightarrow U} = -RT \ln[([\theta]^{222} - [\theta]^{F})/([\theta]^{U} - [\theta]^{222})] \quad (2)$$

The pre- and post-transitional slopes for melting in TFE, respectively, mF and mU in eqs 3 and 4 below, used the data from WtSS and MutSS minidomains. For folding (U→F) in buffer, the respective slopes were similarly taken from WtOpen1 and WtOpen3 minidomains.

$$[\theta]^{F} = m\mathrm{F} \times T + \mathrm{off1} \quad (3)$$

$$[\theta]^{U} = m\mathrm{U} \times T + \mathrm{off2} \quad (4)$$

The offset values off1 and off2, together with ΔH and ΔS, were fitted for the melting curves of the minidomains. Where a mutant exhibited a less well-defined transition startpoint, datapoints were extrapolated based on the pre-transitional region of the wild-type minidomain in the same solvent. The heat capacity was set to zero since all minidomains were of relatively low molecular weight (~4000Da) [*11*, *18*, and references herein]. By replacing $[\theta]^{U}$ with $[\theta]^{F}$, and vice versa, in eqs 1 and 2, and 5 and 6, the thermodynamic values for the inverse transition, $\Delta G_{U\rightarrow F}$, were found.

$$\Delta G_{F\rightarrow U} = \Delta H_{F\rightarrow U} - T\Delta S_{F\rightarrow U} \quad (5)$$

$$[\theta]^{222} = ([\theta]^{F} + [\theta]^{U} \times \exp -(\Delta G_{F\rightarrow U}/RT))/(1 + \exp -(\Delta G_{F\rightarrow U}/RT)) \quad (6)$$

The data were fitted to either eq 1 or 2, together with eqs 3−6, using the least-squares method in the Grafit software (*19*).

Surface Plasmon Resonance Spectroscopy. Interaction kinetics of the minidomains (analytes) with immobilized Fc (ligand) was monitored by surface plasmon resonance spectroscopy using either BIAcoreX or BIAcore2000 (Biosensor, Sweden). The BIAcore 2000 was used for analyses of WtSS and MutSS minidomains over the temperature range +5° to +37 °C. Purified Fc prepared from the IgG2a mouse

monoclonal antibody 561 (antiCD34), a gift from Dynal A/S (Norway), and human serum albumin (HSA, Novo Nordisk, Denmark) were immobilized on a research grade CM-5 carboxymethylated sensor chip in 10 mM sodium acetate buffer pH 4.5 using the amine coupling kit with *N*-ethyl-*N*′-[(diimethylamino)propyl] carbodiimide (EDC) and *N*-Hydroxysuccinimide (NHS) provided by the manufacturer. The Fc of the mAb 561 (10 μL of 5 μg/mL) and HSA (10 μL of 10 μg/mL) were immobilized at +25 °C in the BIAcore2000 with a flow rate of 10 μL Hepes buffered saline (HBS;; 10 mM Hepes pH 7.4, 150 mM NaCl, 3.4 mM EDTA) containing 0.005% (v/v) surfactant per minute. This gave 3100 and 3400 Ru's respectively after blocking with 1M ethanolamine pH 8.5 and regeneration using 5 μL 10 mM glycine•HCl buffer pH 2.4. Interaction analyses were performed with a flow rate of 30 μL/min in HBS/P20 (running buffer;). Each minidomain (100 μL) was injected, using the KINJECT command, over a range of concentrations − between 4 and 10 different concentrations, depending on the experiment. The binding of the minidomains to Fc-561 was corrected by subtracting the RU's at the HSA portion of the chip (due to bulk-effects). The surface was regenerated prior to each injection with glycine•HCl pH 2.4. The data for the association constant was sampled by diluting each minidomain in running buffer to obtain several low concentrations, and the dissociation constant was determined from the highest concentration to minimize rebinding.

Evaluation of BIAcore Data. The k_{on} and k_{off} values were fitted by evaluating the sensorgram data using the BIAevaluattion 2.1 software (Pharmacia Biosensor). By nonlinear fitting of two exponentials, the two-component association phase for the model: 2 Minidomains + Fc561 + Fc561* → Minidomain−Fc561 + Minidomain−Fc561* (Fc561 and Fc561* are two independent epitopes on Fc561), was found from eq 7,

$$R = R_A(1 - \exp(-ks_A t)) + R_B(1 - \exp(-ks_B t)) \quad (7)$$

where R is the response at time, t, and R_A and R_B are steady-state response levels for the two events. To determine the on-rates, the fitted values for ks_A and ks_B were plotted against minidomain concentration C. By using the relations $ks_A = k_{onA}C' + k_{offA}$ and $ks_B = k_{onB}C + k_{offB}$, the k_{on}-rates for the parallel associations were found from the slope of a linear fit of ks_A or ks_B against C. The k_{on} - rate, which had its largest value,, i.e., the fastest rate-constant (k_{onA} extracted from ks_A), was used for further calculation. The off-rates were determined for the two component interaction (parallel dissociation of two complexes) from the following:

$$R = R_D \exp(-k_{offA} t) + R_E \exp(-k_{offB} t) \quad (8)$$

R_D and R_E are the contributions of each component to the total response at the start of dissociation. However, only the fitted k_{offA} and k_{offB} were further used by specifying the start of dissociation at $t = t_0$. Again, the k_{off} - rate, which had its largest value, i.e., the fastest off-rate (k_{offA}), was used for further calculation. The dissociation constants were determined from the relation $K_D = k_{off}/k_{on}$. The relative differences in free energy of binding, $\Delta\Delta G$, between the different minidomains over the temperature ranges examined were calculated from:

$$\Delta\Delta G = +RT_x \ln[K_D(\text{mutant minidomain}) \text{ at } T/K_D(\text{wild-type minidomain}) \text{ at } T] \quad (9)$$

where R is the molar gas constant, T is the temperature (in Kelvin) and the K_D values are those based on the fast on- and off-rates.

RESULTS

The engineering of the small binding protein selected for this study, so that it was capable of being reversibly modulated by temperature changes, used an inter-helix turn replacement strategy in which the wild-type turn was replaced by the elastin sequence, GVGVPGVG (*11*). The minidomain derived from the B-domain of Protein A (*16*) was the model protein used (Figure 1, WtOpen). This minidomain is 33 residues long, is amenable to peptide synthesis, and binds the Fc region of IgG. We replaced the wild-type β-turn HDPNLN with the elastin sequence GVPGVG. We omitted the GV portion at the N-terminal start of the turn because it was flanked by the similar dipeptide AL (*AL*HDPNLN). However, we were concerned that the charge from the EE residues at the C-terminal end of the turn (HDPNLN*EE*) would elevate the transition temperature of the elastin sequence beyond 37 °C (*11*) and so we replaced EE with QQ in one construct (Figure 1, MutOpen1 and MutOpen3). Minidomains with a disulfide bond were also synthesized (Figure 1, WtSS and MutSS), since the wild-type S−S minidomain has been shown to be more thermostable and exhibit better Fc-binding than the open form (*17*). The minidomain purities and molecular masses (Syntem, France; see Experimental Section) were respectively: WtOpen (95%, 4122.0 Da), MutOpen1 (95%, 3879.3 Da), MutOpen2 (98%, 3879.7 Da), MutOpen3 (95%, 3881.5 Da), WtSS (97%, 4181.8 Da), and finally MutSS (96%, 3956.3 Da).

Structural Characterization of Minidomains by Circular Dichroism. The minidomains were scanned by far-UV circular dichroism in phosphate buffer at a low temperature in order to study the effect of mutations in the turn-region (Figure 2). Only the wild-type minidomains (WtOpen and WtSS, Figure 1) had characteristic α-helical CD-spectra with minima around 208 and 222 nm and a maximum around 190 nm. The relatively low-CD-amplitude (MRE around −10 000 deg cm^2 dmol^{-1}) for WtOpen indicated that this existed only as a partially folded α-helical structure (20, and references herein). However, the WtSS minidomain had a higher helical content—probably due to the additional stabilization introduced by the S−S bridge. More surprising was the observation that all mutants with the elastin β-turn were largely unstructured at the low temperature, although MutOpen2 with a protected C-terminus, had a higher helix content in phosphate buffer (measured at 222 nm) than the other mutants.

The effect of TFE, known to have a stabilizing effect on α-helices (*21*−*22*), was tested on all minidomains. It was observed that TFE stabilized or induced α-helix structure in all minidomains, illustrated for WtSS and MutSS in Figure 3. By increasing the concentration of TFE in phosphate buffer, a CD-transition from random coil to an α-helical spectrum was seen for MutSS, with a near isodichroic point around 204 nm (Figure 3B). Similar spectra were obtained

WtOpen	NH_2-F^{6}NMQQQRRFYEAL**H^{19}DPNLNEE^{26}**QRNAKIKSIRDD^{38}-COO$^-$
MutOpen1	NH_2-F^{6}NMQQQRRFYEAL**G^{19}VPGVGQQ^{26}**QRNAKIKSIRDD^{38}-COO$^-$
MutOpen2	NH_2-F^{6}NMQQQRRFYEAL**G^{19}VPGVGEE^{26}**QRNAKIKSIRDD^{38}-$CONH_2$
MutOpen3	NH_2-F^{6}NMQQQRRFYEAL**G^{19}VPGVGEE^{26}**QRNAKIKSIRDD^{38}-COO$^-$
WtSS	NH_2-F^{6}NMQ**C**QRRFYEAL**H^{19}DPNLNEE^{26}**QRNAKIKSIRDD**C**^{39}-COO$^-$
MutSS	NH_2-F^{6}NMQ**C**QRRFYEAL**G^{19}VPGVGQQ^{26}**QRNAKIKSIRDD**C**^{39}-COO$^-$

FIGURE 1: Sequences of short IgG-binding minidomains derived from Protein A. The minimized IgG-binding B-domain of protein A (*16*) was synthesized (WtOpen), and the turn-region mutants (residues 19−26) based on the elastin sequence GVPGVG are also shown (MutOpen 1−3). Minidomains with disulfur bond (*17*) were also synthesized. Both the wild-type minidomain, WtSS, and its mutant minidomain, MutSS, have an S−S bond between Cys10 and Cys39.

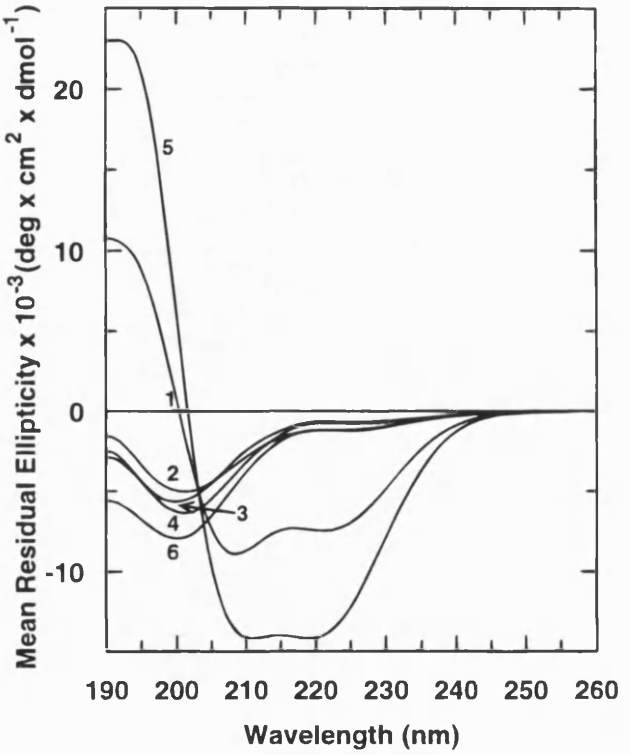

FIGURE 2: Circular Dichroic wavelength scans of minidomains in phosphate buffer pH 7.0 or in deionized water. The minidomains were scanned once in 10 mM buffer at +6.4 °C using a 0.2 cm stoppered cuvette with 5 s integration time (0.5 nm steps; slit: 2.0 nm). WtSS and MutSS were scanned in deionized water. The different spectra with their respective minidomain concentrations are respectively: WtOpen (1; 21.4 μM), MutOpen1 (2; 26.9 μM), MutOpen2 (3; 29.7 μM), MutOpen3 (4; 21.1 μM), WtSS (5; 24.3 μM) and MutSS (6; 25.1 μM).

for MutOpen1−3 (not shown). This demonstrated that all mutants possessed an α-helix propensity, even though they were largely unordered in phosphate buffer. The CD-spectra of the wild-type minidomains in phosphate buffer reflected a greater α-helical content with increasing concentrations of TFE (Figure 3A and 3C). At about 20% (v/v) TFE, the transition seemed to be complete, while for the mutant minidomains the maximum effect of TFE was seen at 30%. However, when the concentration of TFE was increased above 20% for wild-type minidomains (WtOpen and WtSS), the CD-signal at 222 nm was diminished. The sigmoid profiles of the CD-curves, with an inflection point at about 20% TFE, suggests that cooperative interactions are involved

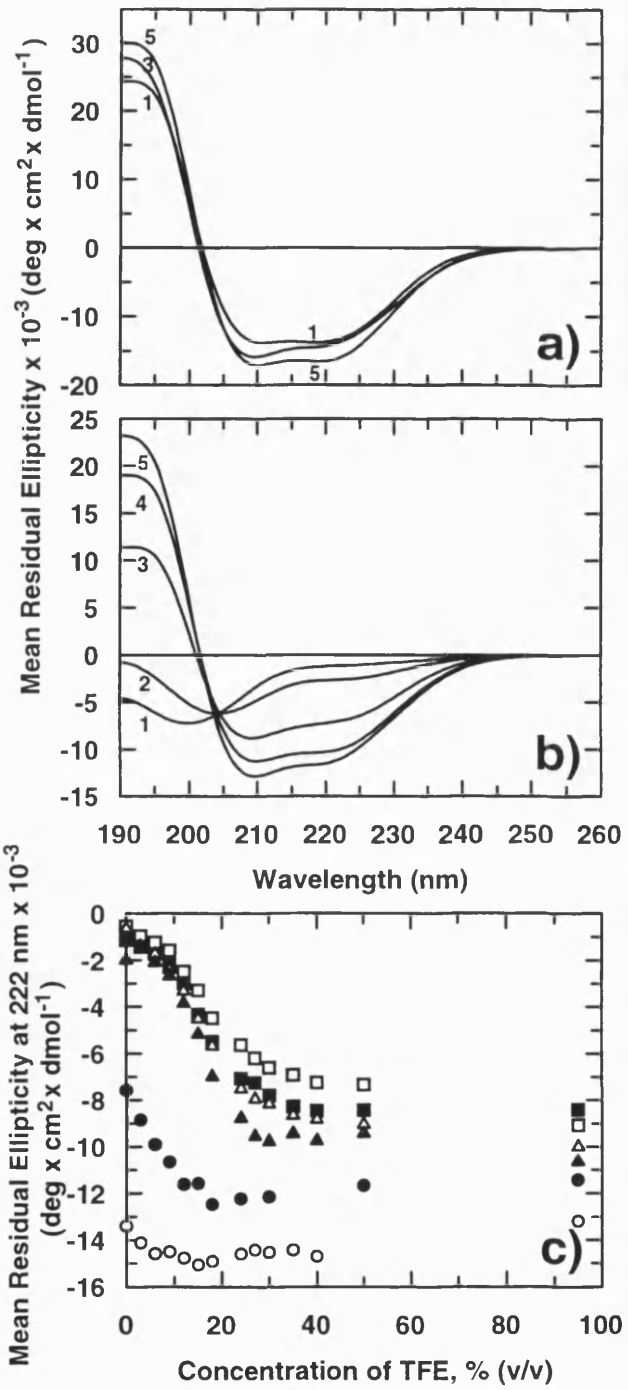

FIGURE 3: The concentration effect of Trifluoroethanol (TFE) on the minidomains. The effect of increasing concentrations of TFE in phosphate buffer on WtSS (a) and MutSS 6 (b) is shown. The numbers represent increasing concentrations of TFE: 1, 0% TFE; 2, 9% TFE; 3, 18% TFE; 4, 27% TFE; 5, 95% TFE. The minidomains were scanned once at +6.4 °C and the experimental conditions and minidomain concentrations were the same as described in Figure 2. The effect on the mean residual ellipticity at 222 nm for WtOpen (●), MutOpen1 (□), MutOpen2 (■), MutOpen3 (△), WtSS (○), and MutSS (▲) is illustrated in panel c.

in this transition. At 50% TFE, the helix content of the minidomains was in the order: WtSS > WtOpen > MutSS > MutOpen2 = MutOpen3 > MutOpen1.

For all minidomains the temperature-dependent CD scans in TFE were 95−100% reversible after cooling (not shown, but see ref *17*). The observed near isodichroic point at 204 nm also indicated that the melting of the α-helices in TFE

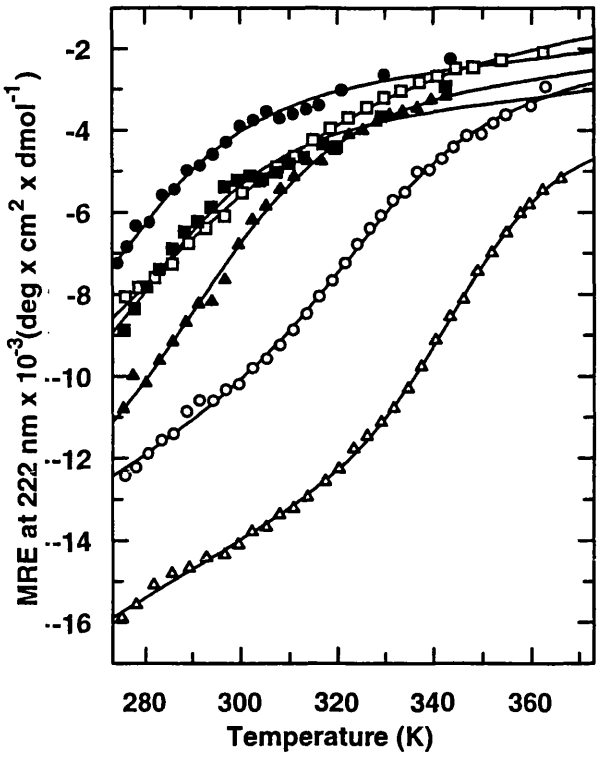

FIGURE 4: The temperature effect on minidomains in 30% trifluorroethanol (TFE). The melting of the minidomains was followeed at 222 nm using the average of three independent scans with am integration time of 5 s (in 0.2 cm cuvette, slit: 2.0), and the temperature effect on minidomains in 30% (v/v) TFE are shown. Respectively, WtOpen (○), MutOpen1 (●), MutOpen2 (□), MutOpen3 (■), WtSS (△), and MutSS (▲). The data were fitted to a two-sstate transition with slopes (see methods). WtSS and MutSS were fiitted with fixed pre and posttransitional slopes.

Table 1: Thermodynamic Values for Melting of Minidomains in 30% (v/v) Trifluoroethanol[a]

minidomain	T_M (°C)	ΔH (kcal mol^{-1})	ΔS (kcal mol^{-1} K^{-1})
WtOpen	58	15.4 ± 1.0	0.046 ± 0.003
MutOpen1	10	12.0 ± 0.7	0.042 ± 0.003
MutOpen2	33	7.4 ± 0.4	0.024 ± 0.001
MutOpen3	16	12.9 ± 1.4	0.045 ± 0.005
WtSS	75	23.9 ± 1.0	0.069 ± 0.003
MutSS	26	12.8 ± 0.6	0.043 ± 0.002

[a] The mean residual ellipticity was followed at 222 nm for each minidomain and then fitted to a reversible van't Hoff equation with $\Delta Cp = 0$ allowing ΔH and ΔS to float. The pre- and posttransitional slopes were fixed at the same values for all minidomains, and the pretransitional region for the mutants (MutOpen1-3 and MutSS) was extrapolated, based on the observed data for their respective wild-type minidomains, WtOpen and WtSS.

for the minidomains followed a two-state reversible α-helix-coil transition (Figure 3B). To quantify the effect of the mutations in the turn region, α-helix structure was first induced in all minidomains using TFE (30%) and their melting was then followed at 222 nm (Figure 4).

Further analysis of the melting curves was performed by fitting the data to a reversible van't Hoff two-state transition. Table 1 displays the thermodynamic data for the different minidomains in 30% TFE. Compared to WtOpen the T_M was lowered by 25 °C and 42 °C for MutOpen2 and MutOpen3, respectively and by 48 °C for MutOpen1. The wild-type disulfide-stabilized minidomain WtSS was 49 °C more stable than its mutant partner, MutSS. The difference in stability between WtOpen and MutOpen1 and between WtSS and MutSS shows that the GVPGVG-turn lowers the stability of the helices irrespective of the presence of a disulfide bond, notwithstanding the fact that the disulfide bonded minidomains were already 16−17 °C more stable than the open forms. The stability difference between the open form and S−S stabilized wild-type minidomains in Tris buffer has previously been reported as 40 °C (*17*), and for S−S stabilized laminin helices it was around 18 °C (*23*). These results confirmed that MutOpen1 was the least, while WtSS was the most thermostable.

There were no large differences in ΔH or ΔS values observed for the open form mutants and the corresponding S−S constructs, indicating that the thermodynamic effect of TFE was the same for both forms (both minidomains were initially melted in 0% TFE). Interestingly, WtSS had larger values for ΔS and ΔH in TFE relative to WtOpen reflecting the influence of a stabilizing S−S bond on the energetics of a helix-stabilizing trifluorethanol system.

For WtOpen and WtSS minidomains, the CD-amplitude decreased with increasing temperature in HBS as shown for WtSS in Figure 5A. The same behavior was seen in TFE, phosphate buffer, micellar SDS, and sodium sulfate at higher temperatures (not shown). However, in contrast to the wild-type behavior, the melting curves for the mutants in HBS, phosphate buffer or water had an increased CD-amplitude at 210−260 nm with increasing temperature and a near isodichroic point at 210 nm, as shown for MutSS in Figure 5B. All transitions were 90−100% reversible as is illustrated in Figure 5. A, B, and C. The MRE at 222 nm was followed for MutOpen1−3, MutSS and WtSS in 10 mM phosphate buffer, and HBS with increasing temperature, and the melting curves for WtSS and MutSS in HBS are shown in Figure 5C. Their sigmoid profiles are consistent with the occurrence of a cooperative transition. The data were fitted to a two-state reversible transition in the direction folded to unfolded for WtSS, or to the reverse transition for MutOpen1, MutOpen3, and MutSS.

The concentration dependence of the spectra at 15.5 and 48 °C in phosphate buffer was also tested for selected minidomains (up to 620 μM; data not shown). For MutSS the concentration was taken from 15 μM to 1.8 mM in the BIAcore running buffer (HBS with 0.005% (v/v) P20) at 25 °C without any significant deviations at 222 nm (not shown). By equilibrium ultracentrifugation of WtSS and WtOpen, it has previously been shown that they are monomeric and highly soluble (*17*). In addition, short to intermediate (8−23) GVPGVG-based peptides have also been shown to be concentration independent at elevated temperatures (*11*).

The melting of MutOpen2 exhibited unusual behavior in which increased and decreased MREs at 222 nm were seen (not shown). For this reason, only the thermodynamic data for MutOpen1, MutOpen3, and MutSS are given in Table 2. The van't Hoff plots were linear with correlation coefficients on the average of −0.98 (not shown). The energies involved in the transition (Table 2) were lower than for the melting of WtSS in HBS (ΔH = 20.8 kcal mol^{-1} and ΔS = 0.063 kcal mol^{-1} K^{-1}) and of similar magnitude to those observed for folding of individual GVGVPGVG-peptides (*11*).

Evaluation of Minidomains by Surface Plasmon Resonance. The kinetics of minidomain binding to immobilized

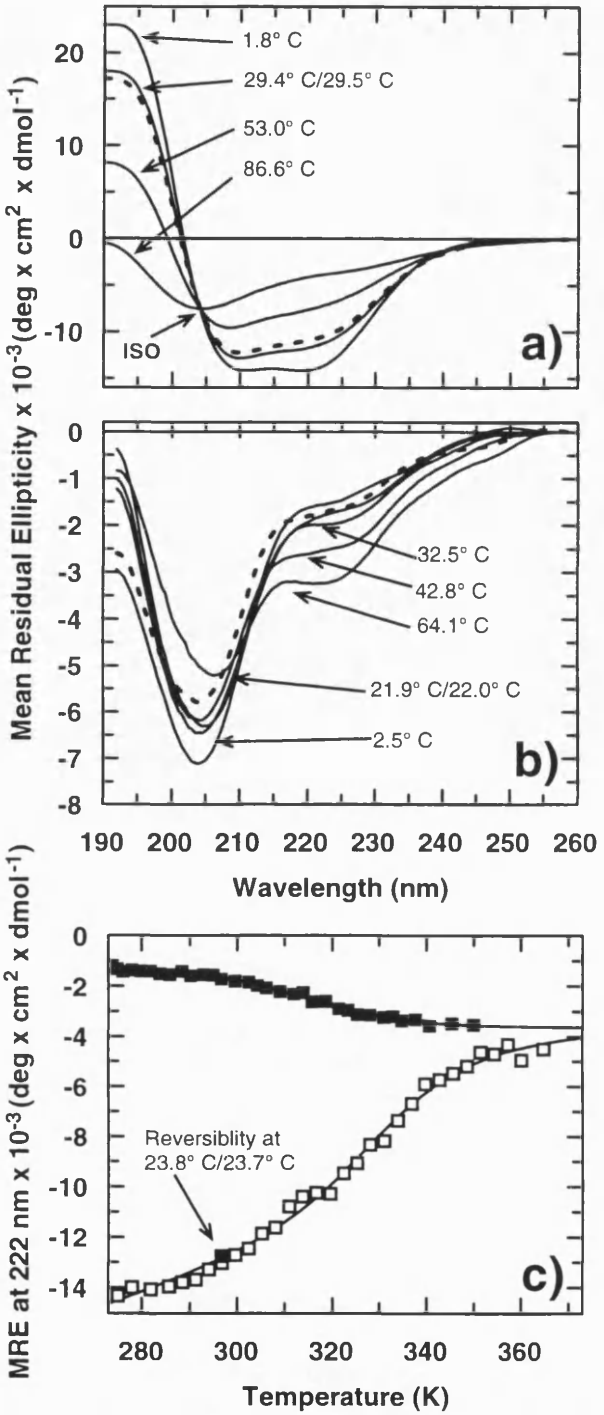

FIGURE 5: Temperature CD-wavelength scans of WtSS and MutSS minidomains in deionized water and in HBS with 0.005% (v/v) P20. WtSS (24.3 μM) in deionized water was scanned once from 190 to 260 nm (0.2 cm quartz cuvette with 5 s integration time; slit 2.0 nm; 0.5 nm step size) at different temperatures, as displayed in panel a. Similarly MutSS (350.7 μM) in Hepes-buffered saline added 0.005% surfactant P20 (panel b) was scanned from 192 to 260 nm at different temperatures using a 0.1 mm stoppered cuvette. The bold dashed lines (---) illustrate the reversibility of the scans after being heated to 60−80 °C and then by rescanning the minidomains at the temperature *x*, (../*x*) given in the plots. Panel c shows the melting of WtSS (□; 24.3 μM) and MutSS (■; 25.1 μM) in HBS buffer with P20. The melting was followed by measuring the CD-ellipticity at 222/260 nm (in 0.2 cm cuvette, slit: 2.0 nm) at different temperatures averaging three independent scans with an integration time of 5 s.

Fc was studied using the BIAcoreX and BIAcore 2000 (BIAcore, Sweden). The data generated were fitted both to

Table 2: Thermodynamic Data for Inverse Thermal Transition at 222 nm for Mutant Minidomains in Buffers[a]

	T_M (°C)	ΔH (kcal mol^{-1})	ΔS (kcal mol^{-1} K^{-1})
MutOpen1 in phosphate buffer	21	16.5 ± 1.1	0.056 ± 0.004
MutOpen1 in HBS with P20	32	14.4 ± 1.8	0.047 ± 0.006
MutOpen3 in phosphate buffer	46	16.4 ± 1.2	0.051 ± 0.004
MutOpen3 in HBS with P20	43	12.1 ± 1.5	0.038 ± 0.005
MutSS in HBS with P20	42	18.4 ± 1.1	0.059 ± 0.003
GVG(VPGVG) peptides[b]		16.8	0.056

[a] The melting data at 222 nm was fitted to a reversible van't Hoff equation allowing ΔS and ΔH to float. All data were fitted with fixed pre- and posttransitional slopes. The heat capacity was fixed at 0. [b] (*11*); the values are the average of short GVG(VPGVG)$_n$ peptides (n = 1 and 3) in 10 mM phosphate buffer pH 7.0.

a one-component model:

$$\text{Minidomain} + \text{Fc561} \rightleftarrows \text{Minidomain}-\text{Fc561}$$

and to a two-component model:

$$2\ \text{Minidomains} + \text{Fc561} + \text{Fc561*} \rightleftarrows \text{Minidomain}-\text{Fc561} + \text{Minidomain}-\text{Fc561*}$$

where Fc561 and Fc561* represent two different epitopes on the ligand. The goodness of these fits is illustrated for WtSS at 20 °C in Figure 6, A and B. There was generally a better fit (lower χ^2) to a two-component model over the temperature ranges tested, for both the association and dissociation phases. The on-rates were measured from the slope of a linear fit of the ks_A or ks_B values vs the lowest concentrations used, illustrated for WtSS and MutSS, respectively, in Figure 6C and 6D (inserts). The ks_A-values represent the fastest rate-constant relative to ks_B. The linear correlation coefficient (r) for the secondary fit of the fast on-rates was around 0.98. By contrast, the slower on-rates (k_{onB}) were approximately 50-fold lower in magnitude and generally exhibited much larger variability at the elevated temperatures. At the lower temperatures, however, both the fast and slow off-rates were statistically determined for WtOpen and MutOpen, and also at all temperatures for WtSS and MutSS (not shown). The dissociation constants ~200 nM for WtOpen and ~100 nM WtSS using the slow off-rates (0.04 s^{-1} and 0.02 s^{-1} respectively at +10 °C/+5 °C) were very similar to those previously reported (*17*). However, it has to be stressed that the systems are different. In this report, the association of the minidomain to the Fc of a mouse IgG2a (561) was studied, while Starovasnik et al. (*17*) and Braisted and Wells (*16*) studied binding to a human IgG1.

The temperature-dependent progress curves for binding and dissociation of WtSS (Figure 6C) and MutSS (Figure 6D) to immobilized Fc of the mouse monoclonal IgG2a are shown in Figure 6C and Figure 6D, respectively. Interestingly, there was a reverse temperature effect for the binding of MutSS relative to WtSS (Figure 6, C and D and Figure 7, A, B, and C). The fast off-rates for WtOpen, MutOpen1 and WtSS increased with increasing temperature (only shown for WtSS), while over the same temperature range the mutant MutSS had a lowered off-rate (Figure 7A). The slow off-rates did not vary much for the minidomains over the temperature range tested, but both the fast and slow off-rates decreased for MutSS from 5 to 37 °C (not shown). The slow off-rates for the MutSS were also lower than for

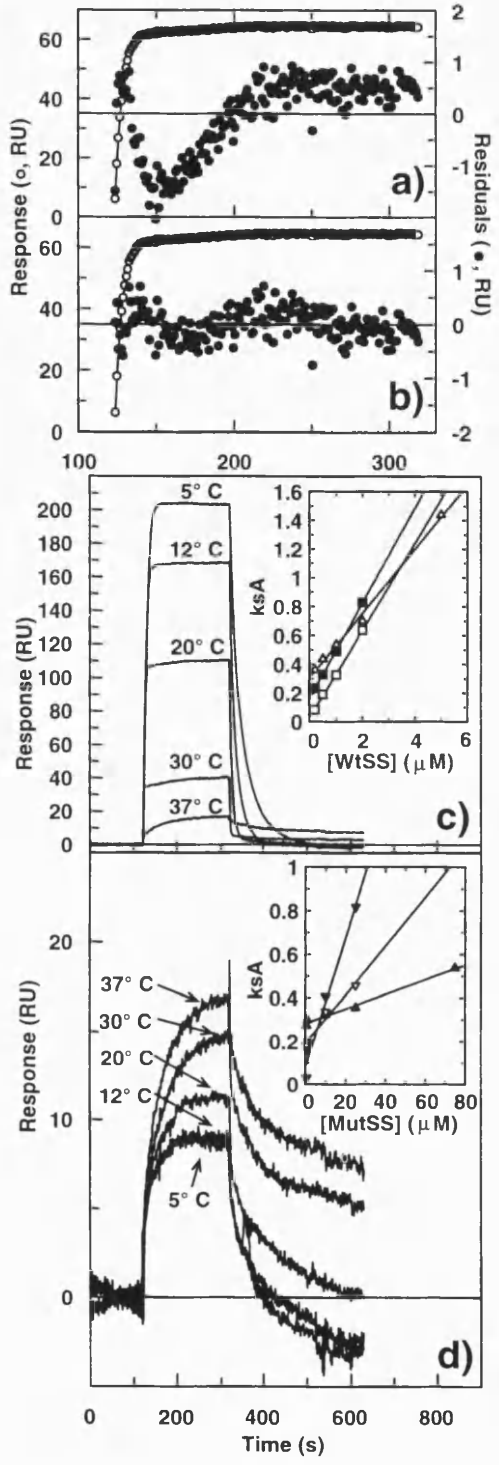

FIGURE 6: BIAcore fits and progress curves for WtSS and MutSS. The association between 200 nM WtSS and immobilized Fc of 5611 (mouse monoclonal IgG2a) at 20 °C was fitted to a WtSS + Fc5561 ⇄ WtSS−Fc561 model using BIAevaluation 2.1 software (panel a). The χ^2 for the fit was 0.556. Panel b represents the fit to the model: 2 WtSS + Fc561 + Fc561* ⇄ WtSS−Fc561 + WtSS−Fc561* where one WtSS minidomain reacts with 2 independent sites on Fc561. The χ^2 for this fit was 0.0795. The lines show the fit of raw-data (○), and residuals for the model (●). The BIAcore progress curves for binding of minidomains to Fc561 at diffferent temperatures are shown for 500 nM WtSS in (panel c) and 1 for 1 μM MutSS in d. The plots of their respective fast on-rates, ks_A (see methods) vs minidomain concentrations are illustrated in the inserted panels in c for WtSS (□, 12 °C; ■, 20 °C and △, 37 °C) and in d for MutSS (▲, 12 °C; △, 25 °C and ▼, 37 °C).

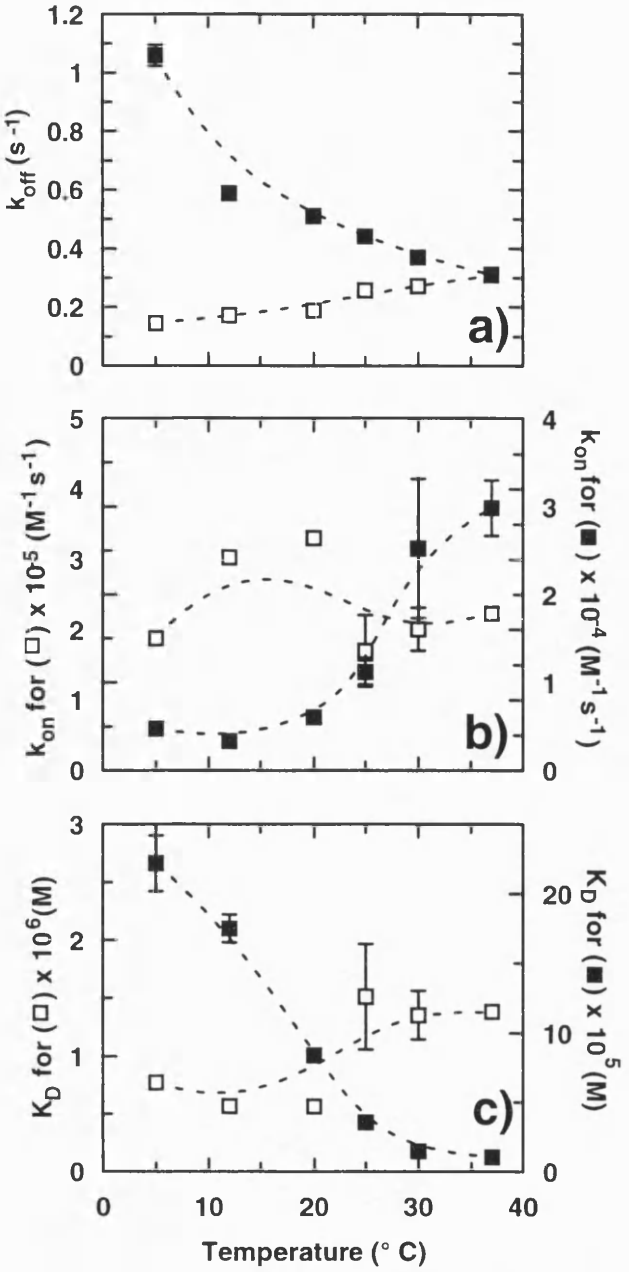

FIGURE 7: The temperature dependence of the fast kinetic constants for WtSS and MutSS minidomains. The respective kinetic constants for the S−S linked minidomains WtSS (□) and MutSS (■) are in panel a, b and c. Panel a shows the fast off-rates, panel b the fast on-rates and panel c illustrates their respective fast dissociation constants ($=k_{off}/k_{on}$) at different temperatures. The k_{on}-rates were found from the slopes of the plots of ks_A vs minidomain concentration, as is illustrated in Figure 6, C and D (inserts) for the model Minidomain + Fc561 + Fc561* ⇄ Minidomain−Fc561 + Minidomain−Fc561*. The off-rates were determined from the model $MinidomainiFc561_i \rightleftarrows Minidomain_i + Fc\text{-}561_j$ (parallel dissociation of two complexes). The off-rates were fitted using BIAevaluation 2.1 and the on-rates were fitted using both BIAevaluation 2.1 and GRAFIT (*19*). Both the on-rates and off-rates display their fitted standard errors. The standard errors of the dissociation constant were manually calculated based on SEs for k_{on} and k_{off}.

WtSS (respectively ~0.01 s^{-1} versus ~0.02 s^{-1}), which is surprising considering the lower residual structure in this minidomain. Again, there was only a small variation in the on-rates for WtSS over the temperature range applied. For MutSS however, the on-rate tripled on increasing the temperature from 5 to 37 °C (Figure 7B). Similar effects

were seen with WtOpen and MutOpen1 whose on-rates halved and doubled, respectively, over the temperature range 10−30 °C (data not shown). The overall effect of these changes is exemplified by the behavior of the MutSS minidomain, whose increased fast on-rate and lowered fast off-rate at 37 °C improved its affinity some 21-fold, compared with that observed at 5 °C (K_D reduced from 222 to 10.4 μM) (Figure 7C). Using the slow off-rates, MutSS also improved its affinity by 8-fold (from 2.8 to 0.4 μM) in the same temperature range.

In contrast, for the WtOpen minidomain (without S−S bridge) the K_D increased 8-fold over the same temperature range, while for WtSS (with S−S bridge) the K_D was unchanged (using either the slow or fast off-rates).

Free-Energy Differences. The $\Delta\Delta G$ values vs temperature had a better linear fit for WtOpen and MutOpen1 (correlation coefficient $r = -0.99$) than for WtSS and MutSS ($r = -0.96$). Over the temperature range measured, $\Delta\Delta G$ was positive for both minidomain pairs, indicating that the binding of wild-type to Fc was tighter than that of the mutants. However, over the same temperature range $\Delta\Delta G$ decreased by 0.057 kcal mol^{-1} K^{-1} for MutOpen1 relative to WtOpen, and by 0.090 kcal mol^{-1} K^{-1} for MutSS relative to WtSS. The $\Delta(\Delta\Delta G)$ was lowered, respectively, by 1.2 kcal mol^{-1} (20 K) for MutOpen1 or by 2.9 kcal mol^{-1} (32 K) for MutSS relative to the wild-type partners. If this relationship were to hold over a wider temperature range, then it predicts that the affinity of MutOpen1 would exceed that of WtOpen beyond 81 °C, while that of MutSS would exceed the affinity of WtSS beyond 49 °C.

DISCUSSION

We report here the first example of the introduction of an elastin-like sequence into the primary structure of a globular protein. Previously, we have shown that short elastin peptides can undergo an entropically driven transition from an extended to a type II β-turn, mimicking the behavior of the much longer, naturally occurring elastin molecule (*11*). By increasing the hydrophobicity in the turn-region, the probability of formation of the turn containing the elastin GVPGVG sequence should increase with increasing temperature. In this design, the wild-type β-turn (type I) residues were replaced with the helix-destabilizing Val, Gly, and Pro residues, while the native Glu−Glu sequence adjacent to the turn was mutated to Gln−Gln in order to avoid an abnormally high transition temperature (*11*). Making such a change, thus, ran the risk of affecting the helix stability, since Val, Gly, and Pro are known to have a low helix propensity although Gln is more stabilizing than Glu (*24*).

The substitution of the type I β-turn by the more hydrophobic elastin turn resulted in melting of the helical structure of the wild-type minidomain in phosphate buffer. However, even the wild-type minidomain is unstable per se and stabilization by a disulfide-bridge at the termini was found to be necessary (*17*). Stabilizing α-helices in TFE also offers a way of expressing the difference in intramolecular stability between mutant and wild-type α-helical minidomains where the helicity of the mutants is more or less lost. This is illustrated for MutOpen1 and MutSS whose melting temperatures were decreased by about 48 °C in 30% TFE compared to wild-type WtOpen and WtSS minidomains (Table 1). MutOpen2 and MutOpen3, which retained the Glu25−Glu26 sequence close to the turn, were more helical in TFE than the Gln25−Gln26 sequences and their T_M's were lowered by only 25−42 °C. This unexpected effect may be due to stabilizing interactions with positively charged residues (Arg28 or Lys31) located close to the turn.

A helix stabilizing effect was seen for MutOpen2 that contained an amidated C-terminus (Table 1), an effect that has previously been shown for α-helices (*25*). The CD-amplitudes for MutOpen1−3 and MutSS, in phosphate buffer or in HBS containing P20, increased at 222 nm with increasing temperature, signaling the formation of an α-helix or type I β-turn (*26*−*27*). The shift of the isodichroic point from 204 to 210 nm, and the lower intensities of the CD-signals at 222-nm for the melting curves in buffer, were more characteristic of a type I β-turn (*27*). Several other observations also argue that a type I β-turn was formed at the higher temperatures. Type I β-turn structures have also been found in elastin sequences (*12*−*13*) although the Pro−Gly type II β-turn is between 0.2 and 1.7 kcal mol^{-1} more stable than type I β-turn and is also more common in elastin (*6*, *28* and references therein). A conformational interconversion between type I and II β-turn in proteins is, however, quite common for Pro−Gly turns (*29*).

The energies associated with the observed transitions for MutOpen1, MutOpen3, and MutSS (Table 2) were similar to those found for short (8−12 residue) elastin peptides (*11*). The melting of MutOpen1 over the temperature range 0−60 °C involved a free energy difference of 3.0 kcal mol^{-1}, within the range reported to be required for β-turn formation (2−4 kcal mol^{-1}) though just below that required for α-helix formation (4 kcal mol^{-1}; *28* and references herein).

The better fit of the BIAcore data to a heterogeneous kinetic model may be due to several factors. The minidomains were initially selected by panning against a human monoclonal IgG1 (*16*). In this system, we have studied the binding to the Fc-region of a mouse monoclonal IgG2a. It is possible that the panning of a specific binder to human IgG1 has selected for a species whose binding to related IgG epitopes is less promiscuous than the parent domain. This selection seems to have resulted in a weaker, heterogeneous binding behavior to IgG2a (the better fit to two Fc561 sites, Fc561, and Fc561*, is shown in Figure 6B). This may have implications for further design of antibodies by phage display—the choice between specificity or promiscuity. An alternative explanation is that the increased temperature may have generated different conformations of the epitopes on IgG2a due to structural instability, seen as a better fit of data to one-component kinetics at low temperatures and two-component kinetics at higher temperatures for some minidomains. Starovasnik et al. (*17*) also suggest two χ^1 rotamer conformations for Phe14 in the binding-site of the wild-type minidomain. Third, there may have been a mixed population of mutant domains, originating from the presence of multiple β-turns, although we think this unlikely.

The mutant minidomains MutOpen1 and MutSS in HBS showed a good correlation between on-rate and 2° structure content (measured by CD-amplitude at 222 nm) as temperature was increased. For MutSS a 21-fold improvement in K_D was obtained, due predominantly to the decrease in off-rate at the higher temperatures, an effect not seen for its open partner, MutOpen1. This was in stark contrast to the behavior

of wild-type WtSS which, although more thermostable, showed little variation in K_D over the same temperature range. This improvement in binding of the mutants with increasing temperature is, we believe, due to the formation of an entropy driven type I β-turn.

Other studies have shown a correlation between lowered α-helicity and lowered affinity (on-rates) of human insulin-like growth factor I (*30*). For Protein A Fc-binding domains, the residues involved in binding are known to be aligned on adjacent faces of two of the three helices (*17*). Any perturbation of these two helices will be likely to affect the affinity of the domain. This is clearly observed for the wild-type domains where denaturation of the helices mirrors loss of binding. However, in the mutant domains, the temperature induced formation of a type I β-turn (*17*) may serve to stabilize the alignment of fluctuating helices (reducing its conformational entropy relative to the wild-type), resulting in correctly positioned binding residues and a concomitant increase in affinity. As a matter of comparison, the formation of different turn conformations has also been shown to affect binding of the RGD-epitope to Integrins (*31*) and of inhibitor binding to HIV-1 protease (*32*).

There have been several previous attempts to alter the stability of proteins in a predictable manner by mutating residues in turn regions. Longer loops have been inserted without any significant effect on protein stability and folding, and residue substitutions have also been made (*33*−*35*). However, mutations of structurally important turns may still affect the function of a protein (*31*). The ability to control binding of Protein A by a temperature switch is a challenging task since its triple-helical core is normally quite thermostable. A switch that turns off the activity at low temperatures and turns it on again at higher temperatures may have several industrial applications, and in the particular example described here, may offer a novel temperature regulation for protein A. It may also become a general method for regulating other globular proteins where lowering the on-rate at lower temperatures and increasing it at higher temperatures leads to regulation of binding or some other activity.

ACKNOWLEDGMENT

We thank Dr. A. R. Clarke and the Department of Biochemistry, School of Medical Sciences, University of Bristol, for giving us access to a CD-machine. We also gratefully acknowledge Mrs. A. K. Lindgaard and Mrs. H. T. Trømborg at Dynal Core Tech. R & D for start-up help with BIAcoreX and BIAcore2000 measurements. Finally, we thank Dr. G. Bloomberg at School of Medical sciences, University of Bristol for amino acid analysis.

REFERENCES

1. Daughdrill, G. W., Chadsey, M. S., Karlinsey, J. E., Hughes, K. T., and Dahlquist, F. W. (1997) *Nat. Struct. Biol. 4*, 285−291.
2. Uesugi, M., Nyanguile, O., Lu, H., Levine, A. J., and Verdine, G. L. (1997) *Science 277*, 1310−1313.
3. van Stokkum, I. H. M., Lindsell, H., Hadden, J. M., Haris, P. I., Chapman, D., and Bloemendal, M. (1995) *Biochemistry 34*, 10508−10518.
4. Urry, D. W. (1988) *J. Protein Chem. 7*, 1−34.
5. Urry, D. W. (1988) *J. Protein Chem. 7*, 81−114.
6. Urry, D. W. (1993) *Angew. Chem. Int. Ed. Engl. 32*, 819−841.
7. Dill, K. A. (1990) *Biochemistry 29*, 7133−7155.
8. Head-Gordon, T. (1995) *Proc. Natl. Acad. Sci. U.S.A. 92*, 8308−8312.
9. Livingstone, J. R., Spolar, R. S., and Record, M. T., Jr. (1991) *Biochemistry 30*, 4237−4244.
10. Muller, N. (1993) *Biopolymers 33*, 1185−1193.
11. Reiersen, H., Clarke, A. R., and Rees, A. R. (1998) *J. Mol. Biol. 283*, 255−264.
12. Arad, O., and Goodman, M. (1990) *Biopolymers 29*, 1651−1668.
13. Bhandary, K. K., Senadhi, S. E., Prasad, K. U., Urry, D. W., and Vijay-Kumar, S. (1990) *Int. J. Pept. Protein Res. 36*, 122−127.
14. Uhlén, M., Guss, B., Nilsson, B., Gatenbeck, S., Philipson, L., and Lindberg, M. (1984) *J. Biol. Chem. 259*, 1695−1702 (Correction, ibid. p 13628).
15. Nilsson, B., and Abrahmsén, L. (1990) *Methods Enzymol. 185*, 144−161.
16. Braisted, A. C., and Wells, J. A. (1996) *Proc. Natl. Acad. Sci. U.S.A. 93*, 5688−5692.
17. Starovasnik, M. A., Braisted, A. C., and Wells, J. A. (1997) *Proc. Natl. Acad. Sci. U.S.A. 94*, 10080−10085.
18. Scholtz, J. M., Marqusee, S., Baldwin, R. L., York, E. J., Stewart, J. M., Santoro, M., and Bolen, D. W.(1991) *Proc. Natl. Acad. Sci. U.S.A. 88*, 2854−2858.
19. Leatherbarrow, R. J. (1989), Erithacus Software Ltd.
20. Luo, P., and Baldwin, R. L. (1997) *Biochemistry 36*, 8413−8421.
21. Cammers-Goodwin, A., Allen, T. J., Oslick, S. L., McClure, K. F., Lee, J. H., and Kemp, D. S. (1996) *J. Am. Chem. Soc. 118*, 3082−3090.
22. Jasanoff, A., and Fersth, A. R. (1994) *Biochemistry 33*, 2129−2135.
23. Antonsson, P., Kammerer, R. A., Schulthess, T., Hänisch, G., and Engel, J. (1995) *J. Mol. Biol. 250*, 74−79.
24. Chakrabartty, A., Kortemme, T., and Baldwin, R. L. (1994) *Protein Sci. 3*, 843−852.
25. Fairman, R., Shoemaker, K. R., York, E. J., Steward, J. M., and Baldwin, R. L. (1989) *Proteins: Struct., Funct., Genet. 5*, 1−7.
26. Perczel, A., Hollósi, M., Sándor, P., and Fasman, G. D. (1993) *Int. J. Pept. Protein Res. 41*, 223−236.
27. Woody, R. W. (1995) *Methods Enzymol. 246*, 34−71.
28. Yang, A.-S., Hitz, B., and Honig, B. (1996) *J. Mol. Biol. 259*, 873−882.
29. Gunasekaran, K., Gomathi, L., Ramakrishnan, C., Chandrasekhar, J., and Balaram, P. (1998) *J. Mol. Biol. 284*, 1505−1516.
30. Jansson, M., Uhlén, M., and Nilsson, B. (1997) *Biochemistry 36*, 4108−4117.
31. Bach, A. C., II, Espina, J. R., Jackson, S. A., Stouten, P. F. W., Duke, J. L., Mousa, S. A., and DeGrado, W. F. (1996) *J. Am. Chem. Soc. 118*, 293−294.
32. Nicholson, L. K., Toshimasa, Y., Torchia, D. A., Bax, S. H., Stahl, S. J., Kaufman, D., Wingfield, P. T., Lam, P. Y. S., Jadhav, P. K., Hodge, N., Domaille, P. J., and Chang, C.-H. (1995) *Nature Struct. Biol. 2*, 274−280.
33. Ladurner, A. G., and Fersth, A. R. (1997) *J. Mol. Biol. 273*, 330−337.
34. Predki, P. F., Agrawal, V., Brünger, A. T., and Regan, L. (1996) *Nature Struct. Biol. 3*, 54−58.
35. Viguera, A.-R., and Serrano, L. (1997) *Nature Struct. Biol. 4*, 939−946.

BI991243A